



Strål  
säkerhets  
myndigheten

Swedish Radiation Safety Authority

Research

# APRI-11 – Final Report

## 2025:03

**Author:** Patrick Isaksson, SSM, Henrik Glänneskog, Vattenfall  
Sevostian Bechta, KTH, Weimin Ma, KTH  
Andrei Komlev, KTH, Yucheng Deng, KTH  
Boshen Bian, KTH, Wanhong Wang, KTH  
Hongdi Wang, KTH, Lu Zhao, KTH  
Yan Xiang, KTH, Christian Ekberg, CTH  
Anna-Elina Pasi, CTH, Fredrik Börjesson Sandén, CTH  
Pavel Kudinov, KTH, Govatsa Acharya, KTH  
Dmitry Grishchenko, KTH, Xicheng Wang, KTH

**Date:** Mars 2025

**Report number:** 2025:03

**ISSN:** 2000-0456

**Available at** [www.ssm.se](http://www.ssm.se)





Strålsäkerhetsmyndigheten

Swedish Radiation Safety Authority

Author: Patrick Isaksson, SSM  
Henrik Glänneskog, Vattenfall  
Sevostian Bechta, KTH  
Weimin Ma, KTH  
Andrei Komlev, KTH  
Yucheng Deng, KTH  
Boshen Bian, KTH  
Wanhong Wang, KTH  
Hongdi Wang, KTH  
Lu Zhao, KTH  
Yan Xiang, KTH  
Christian Ekberg, CTH  
Anna-Elina Pasi, CTH  
Fredrik Börjesson Sandén, CTH  
Pavel Kudinov, KTH  
Govatsa Acharya, KTH  
Dmitry Grishchenko, KTH  
Xicheng Wang, KTH

# 2025:03

## APRI-11 – Final Report

Date: Mars 2025

Report number: 2025:03

ISSN: 2000-0456

Available at [www.stralsakerhetsmyndigheten.se](http://www.stralsakerhetsmyndigheten.se)

This report was commissioned by the Swedish Radiation Safety Authority (SSM). The conclusions and viewpoints presented in the report are those of the author(s) and do not necessarily coincide with those of SSM.

## SSM perspektiv

### Bakgrund

Strålsäkerhetsmyndigheten (SSM) har tillsammans med de svenska kraftbolagen som driver kärnkraftsreaktorer i Sverige sedan början av 1990-talet finansiellt stöttat forskning inom svåra haverier vid KTH och Chalmers inom ramen för ett samarbete kallat APRI. APRI-finansieringen inleddes efter installationen av de konsekvenslindrande systemen på de svenska kärnkraftverken för att vidare studera och verifiera de antaganden som gjordes när haverihanteringsstrategin utvecklades. Forskningsmålen har på en strategisk nivå varit inriktade på att minska osäkerheterna i de olika ingående fenomenen och bidra till en mer fysikalisk förståelse för de fenomen som ingår i ett svårt haveriförlopp.

### Projektets syfte

Det övergripande målet med APRI-finansieringen är att erhålla och förbättra kunskapen om svåra haverier med inriktning på haverihanteringen som den implementeras i de befintliga svenska reaktorerna samt verifiera den svenska haverihanteringen som den har tillämpas. Forskningens konkreta fokus och inriktning är fenomen som bedöms vara av risksignifikans för den valda haverihanteringsstrategin. I målen för APRI-II var studierna vid KTH inriktats på dels in-vessel fenomen och dels en fortsatt forskning kring kylbarhet av härdrester i inneslutningen, dvs ex-vessel fasen av haveriförloppet. Mer specifikt har följande fem ämnesområden undersökts i APRI-II: i) återsmältning av härdrester vid sen in-vessel fas, ii) felmod för genomsmältning av reaktortanken, iii) växelverkan mellan härdsmälta och kylmedel, iv) växelverkan mellan smälta och strukturer under reaktortanken, v) reaktortillämpningar och säkerhetsanalyser. Vid CTH har forskningen fokuserat på den grundläggande förståelsen av tellurkemi under svåra haveriförhållanden.

### Författarsammanfattning

APRI-II har bidragit till en ökad förståelse av flera svåra haverifenomen och -processer, inklusive:

- Återsmältningfenomen av härdrester i reaktortanken: detta avser nedsmältningförloppet i reaktortankens botten och specifikt hur härdrester smälter och interagerar med andra material. Detta är viktigt för att kunna bedöma förutsättningarna i reaktortanken då genomträngning av reaktortanken sker.
- Reaktortankens felmod: förståelsen för hur genombrott av reaktortanken uppträder, vilket är väsentligt för förståelsen haverifenomen i inneslutningen.
- Växelverkan mellan smält material och kylmedel: detta involverar studier av hur smält material uppträder i kontakt med vatten, vilket är avgörande för förståelsen av fenomen i inneslutningen såsom ångexplosioner och kylbarhet av härdrester.
- Växelverkan mellan smält material och strukturer under reaktortanken: studien fokuserar på hur smält material påverkar strukturer (som serviceplattformar etc.) som är belägna under reaktortanken, vilket är betydelsefullt för att förstå förutsättningarna för ångexplosion och kylbarhet av härdrester i inneslutningen.
- Reaktortillämpningar och säkerhetsanalyser: detta avser studier av reaktortillämpningar för de svenska befintliga reaktorerna för att demonstrera metodutvecklingens betydelse för reaktorsäkerheten.
- Tellurkemi under svåra haveriförhållanden: detta forskningsområde handlar om hur tellur uppträder kemiskt under svåra haveriförhållanden, vilket ger data för modellutveckling och uppskattning av tellurutsläpp vid ett svårt haveri.

Resultaten har uppnåtts genom experimentella undersökningar, modellutveckling och simuleringar.

### Projektinformation

Kontaktperson på SSM: Patrick Isaksson  
Diarienummer: SSM2020-5601  
Aktivitetsnummer: 4530365

## SSM perspective

### Background

The Swedish Radiation Safety Authority together with the Swedish Power companies operating nuclear power reactors in Sweden have since early 1990's provided financial support for severe accident research at KTH and Chalmers. The research was initiated almost directly after the installation of severe accident management system and strategy, as filtered containment venting system and preflooding of the containment, to further study and verify the assumptions that was made when the accident management strategy was developed. The research objectives has on a strategic level continuously been focused on reducing uncertainties in the different phenomena and contributing to a more physical understanding on the phenomena involved in the severe accident progression in a Swedish BWR.

### Objectives of the project

The overall objective of APRI is to gain and improve knowledge in severe accident with a focus on the severe accident management as it is implemented in the current operating Swedish BWR's and PWR's and ultimately confirm the Swedish accident management as it is applied. The focus and orientation of the research are phenomena considered to be of risk importance for the Swedish accident management strategy. In the objectives for APRI-II, the study at KTH was focused on a few in-vessel phenomena and a continued research on ex-vessel core debris coolability. More specifically the following five topical areas have been investigated in APRI-II: i) in-vessel debris behavior, ii) vessel failure mode, iii) melt-coolant interactions, iv) ex-vessel corium-structure interactions, v) reactor applications and safety analyses. At CTH the research have been focused on the basic understanding of Tellurium chemistry during severe accident conditions.

### Summary by the author

APRI-II has provided an additional understanding of several phenomena and processes, including:

- Re-melting phenomena of core debris in the reactor vessel: this refers to the behavior of solid materials that may be present in the reactor during extreme conditions, specifically how they melt and interact with other materials.
- Failure modes in the reactor vessel: understanding the different ways in which the reactor vessel can fail which is crucial for the understanding of the ex-vessel behavior.
- Interaction between molten material and coolant: this involves studying how molten materials (like melted fuel) behave in contact with the coolant, which is crucial for the understanding of ex-vessel phenomena as steam explosion and debris coolability.
- Interaction between molten material and structures beneath the reactor vessel: this focuses on how molten materials affect the structural integrity of components located beneath the reactor, which is essential for the understanding of the conditions for steam explosion and debris coolability in the containment.
- Reactor applications and safety analyses: This refers to the study of practical applications for the Swedish reactors.
- Tellurium chemistry under severe accident conditions: this area of study concerns how tellurium behaves chemically during severe accident scenarios, providing data for model development.

The results have been achieved through experimental investigations, model development, and simulations. These methods allow for a comprehensive understanding of complex interactions and behaviors under various conditions.

### Project information

Contact person at SSM: Patrick Isaksson

**APRI**





The research project APRI-11 has been a cooperation between the following organisations:

Strålsäkerhetsmyndigheten (SSM)  
Forsmarks Kraftgrupp AB (FKA)  
OKG Aktiebolag (OKG)  
Ringhals AB (RAB)

The project has been supervised by a steering committee with representatives from SSM and the power companies as follows:

Roberta Concilio, FKA  
Staffan Dittmer, RAB  
Henrik Glänneskog, Vattenfall AB (project leader)  
Patrick Isaksson, SSM (chairman)  
Ola Jonsson, OKG  
Christian Linde, SSM  
Johan Olofsson, RAB  
Eric Ramenblad, FKA

The research activities has been carried out with participation from the APRI partners and from Swedish universities.

Editor:

Patrick Isaksson, SSM

Authors which has contributed to different sections of this report;

APRI partners:

Henrik Glänneskog, Vattenfall  
Patrick Isaksson, SSM

Kungliga Tekniska Högskolan, Department of Nuclear Power Safety (KTH-NPS):

Sevostian Bechta  
Weimin Ma  
Andrei Komlev  
Yucheng Deng  
Boshen Bian  
Wanhong Wang  
Hongdi Wang  
Lu Zhao  
Yan Xiang

Chalmers Tekniska Högskola, Department of Nuclear Chemistry (CTH-NC)

Christian Ekberg  
Anna-Elina Pasi  
Fredrik Börjesson Sandén

Kungliga Tekniska Högskolan, Department of Nuclear Engineering (KTH-NE):

Pavel Kudinov

Govatsa Acharya  
Dmitry Grishchenko  
Xicheng Wang

## SAMMANFATTNING

Denna rapport presenterar resultaten som erhållits från forskningsaktiviteterna rörande svåra haverier inom forskningsprogrammet APRI-11. APRI är ett finansiellt samarbete mellan Strålsäkerhetsmyndigheten (SSM) och svenska kärnkraftsföretag som ekonomiskt stödjer forskning inom svåra haverier vid Kungliga Tekniska Högskolan (KTH) och Chalmers Tekniska Högskola (CTH).

Det övergripande målet med APRI är att utveckla och förbättra förståelsen och kunskapen rörande svåra haverier med fokus på den haverihantering som implementeras i de svenska reaktorer som är i drift. Inriktningen på arbetet inom APRI är fenomen som bedöms vara risksignifikant för den svenska haverihanteringsstrategin. Kunskap i detta sammanhang innefattar bland annat data, modeller, koder, insikter och metoder och forskningen har generellt sett inriktats mot att studera konkreta utestående säkerhetsfrågor, fenomen eller haverihanteringsstrategier.

Målsättningen med APRI-samarbetet uppnås genom att finansiera specifika forskningsaktiviteter vid två svenska universitet, genom deltagande i internationell forskning inom svåra haverier samt genom att följa upp observationer och slutsatser från Fukushimaolyckan.

Den svenska haverihanteringsstrategin för svåra haverier med en stor vattenmassa under reaktortanken för kylning av härdrester var länge en tämligen unik ansats, där det fanns få kunskaper och erfarenhet att hämta från den internationella forskningen inom området. Avsikten med haverihanteringsstrategin är att avsluta smältförloppet, stabilisera härdrester i inneslutningen och upprätthålla integriteten i inneslutningen. Speciellt de svenska kokvattenreaktorerna bedöms vara känsliga för angrepp från härdsmälta på betongplattan vilket har varit motivet till den valda strategin. Denna strategi medför dock också potentiella negativa effekter genom växelverkan mellan härdsmälta och vatten, vilket kan ge upphov till högenergetiska ångexplosioner och laster på inneslutningen. Detta motiverade tidigare APRI-program att mer specifikt studera och undersöka den valda haverihanteringsstrategin och eventuella utmaningar. Betydande forskningsinsatser har utförts vid KTH:s avdelning för kärnkraftsäkerhet inom projekten APRI-6 till 9 för att studera frågeställningar rörande kylning av härdrester i inneslutningen och ångexplosioner.

I APRI-11 projektet fortsatte KTH:s avdelning för kärnkraftsäkerhet arbetet med att studera några centrala in-vessel fenomen tillsammans med fortsatt forskning kring kylning av härdrester ex-vessel i inneslutningen. Studierna av in-vessel fenomen påbörjades i APRI-10 och är ett nytt forskningsområde som motiveras av att ex-vesselfenomenen inte kan studeras separat utan att beakta fenomenen i nedre tankbotten innan frigörelse av smälta till inneslutningen. Mer specifikt har följande fem ämnesområden undersökts inom APRI-11: i) härdrester i reaktortanken, ii) reaktortankens felmod, iii) växelverkan mellan smälta-kylmedel iv) växelverkan mellan härdrester och strukturer utanför reaktortanken, v) reaktortillämpningar och säkerhetsanalyser. Resultaten från APRI-11 presenteras i denna rapport. Några nyckelresultat som noteras är:

### *(i) Härdrester i reaktortanken*

En pilotstudie har genomförts i SIMECO-2-anläggningen för att undersöka torrtrorkning och relokering av härdrester. Anläggningen har en hög arbetstemperatur, en transparent visualisering och avancerad instrumentering, vilket sammantaget gör uppställningen till en unik infrastruktur för att studera förloppet och värmeöverföringen av härdrester i reaktortankbotten. I MRSPOD-anläggningen har infiltration av smälta i härdrester studerats

och då vätningen hos partiklars yta i smälta bedöms påverka infiltrationen genomfördes ytterligare studier för att kvantifiera fenomenet.

(ii) *Felmod i reaktortanken*

Under flera år har simuleringar med kopplade termo-mekaniska analyser av reaktortankbotten utförts inom APRI med målet att förbättra metoderna att förutse tankgenombrott och spridningen av smälta i inneslutningen. För studierna i APRI-11 har den termiska lasten från smälta i tankbotten getts av MELCOR och den strukturmekaniska analysen har gjorts i ANSYS.

(iii) *Växelverkan mellan smälta-kylmedel*

Syftet med denna studie är att få grundläggande förståelse för hur härdrester bildas från smälta i kontakt med vattenmassan under reaktortanken genom experiment i DEFOR-anläggningen. I APRI-11 har studien inriktats mot studier med metalliska material, då oxidmaterial har undersökts i tidigare APRI-projekt. Några observationer är att metallisk smälta med högre smältpunkt (jämfört med oxid) vid samma överhettning ger ökad värmeöverföring till vatten och en högre grad av fragmentering. De andra testerna med metallsmälta uppvisar en snabb stelning vilket resulterar i ofullständig finfördelning av smältstrålen och infrusna "jetstrålar".

(iv) *Växelverkan mellan härds smälta och strukturer under reaktortanken*

Eftersom strukturerna som finns under reaktortanken i kokvattenreaktorerna inte har inkluderats i tidigare analyser rörande risken för potentiella ångexplosioner påbörjades en studie i APRI-11 som inkluderar strukturernas påverkan på smältstrålen och förutsättningarna för växelverkan mellan smälta och vatten. Baserat på en litteraturstudie har tre intressanta fenomen identifierats - stänkning av smälta, ablation av strukturer orsakat av angrepp från smälta samt påverkan genom stelning av smälta på strukturer.

(v) *Reaktortillämpningar och säkerhetsanalyser*

Målet med denna ämnesstudie är att utföra säkerhetsanalyser för reaktorapplikationer genom att tillämpa forskningsresultaten (till exempel modeller, datorprogram) i ett svenskt reaktorsammanhang. En metodik har utvecklats under APRI-11 för att undersöka härdresternas kylbarhet i inneslutningen för både svenska kok- och tryckvattenreaktorer. För simulering av svårt haveri med härdrester i nedre primärutrymmet i en kokvattenreaktor har COCOMO-koden kopplats med MELCOR-koden för att simulera haveriförloppet inklusive kylning och stabilisering av härdrester i inneslutningen. För att minska beräkningstiden för den kopplade MELCOR/COCOMO-simuleringen har surrogatmodeller utvecklats (baserat på COCOMO-koden) och kopplats med MELCOR för att möjliggöra snabbare beräkningar. Jämfört med enbart MELCOR-simuleringar påvisar både de kopplade simuleringarna av MELCOR/COCOMO och MELCOR/SM en tidigare tryckavlastning av inneslutningen.

Ett annat ämnesområde som har varit i fokus under ett antal APRI-projekt är förståelsen för fissionsprodukternas kemiska reaktioner under svåra haveriförhållanden, vilka har påverkan på den potentiella källtermen. Denna forskning har genomförts vid Chalmers avdelning för kärnkemi. Chalmers forskning har under många år fokuserat på haverikemi med tonvikt på flyktiga, medel- och långlivade fissionsprodukter som jod, cesium och tellur. Medan jod karaktäriseras av många oxidationstillstånd och växelverkan med andra ämnen samt negativa hälsoeffekter vid inhalation i den akuta fasen av ett svårt haveri, bidrar cesium till långvarig kontaminering av mark och transporteras främst som en aerosol. Tellur, som har varit huvudfokus för Chalmers forskning inom APRI-11, är en flyktig fissionsprodukt som kan frigöras vid en härds smälta i betydande mängder och på kort sikt

ge ett stort bidrag till omgivningskonsekvenserna efter en reaktorolycka. Tellurisotoper upptäcktes i luft, vatten och jordprover tagna i Japan efter Fukushima Dai-ichi-olyckan. Forskningen under APRI-11 koncentrerades på att undersöka bildandet av organiska tellurider, särskilt dimetyltellurid (DMT), under haveriförhållanden. Den första studien utforskade möjligheten till bildande av organiska tellurider i inneslutningens vattenfas under gammabestrålning. Resultaten tyder på att organiska tellurider verkligen kan bildas under dessa förhållanden. Den andra studien undersökte bildandet av organiska tellurider i gasfasen under förhållanden som förväntas råda i primärkretsen under haveriförhållanden. Även om resultaten indikerar en ökad transport av tellur i gasfasen, finns det i sammanhanget kvarstående osäkerheter kring bildandet av organiska tellurider. Den tredje studien bedömde DMT:s stabilitet under kraftig gammastrålning, vars resultat indikerar att nedbrytningen beror på sammansättningen av vattenfasen. Radikalfångare kan där påverka DMT-stabiliteten avsevärt. I den sista studien utforskades interaktionen mellan DMT och aktivt kol från andningsskyddsfiltre. Det kunde visas att aktivt kol effektivt filtrerar DMT.

Ett av uppdragen i APRI-projektet sedan de tragiska olyckorna i Fukushima Dai-ichi, Japan, är att följa upp nya fynd, observationer och lärdomar som rapporteras från undersökningar av reaktorerna. En djupare förståelse för olyckornas förlopp och tillhörande fenomenen är relevant för APRI och svensk haverihantering eftersom de skadade reaktorerna i Fukushima också var BWR:er. Sedan APRI-10 har Tokyo Electric Power Company Holdings tillsammans med International Research Institute for Nuclear Decommissioning genomfört en undersökning i nedre primärrutrymmet i reaktor 1 i Fukushima Dai-ichi med hjälp av en undervattensrobot. Några viktiga fynd från undersökningen är:

1. Det finns sannolikt flera olika felmoder avseende tankgenombrott i reaktortanken, då vissa komponenter som styrtavshus hittades innanför pedestalerna.
2. Många av komponenterna och strukturerna innanför pedestalerna är kraftigt skadade eller oidentifierbara, medan skadorna utanför pedestalerna begränsas till området runt öppningen till pedestalerna.
3. Eroderingen av betongen till följd av betong-smältareaktioner innanför pedestalerna är cirka 1 meter hög, medan den förstärkande stålstrukturen ("inner skirt") verkar vara i huvudsak intakt.
4. Deponerat material på primärrutrymmets golv varierar i höjd från 0,2 till 1,5 meter.
5. Det finns "hyllor" som bildats av deponerat material och som har fästs vid olika strukturer som sannolikt fungerat som värmesänkor. Under hyllorna finns hålrum i det deponerade materialet.
6. Ingen signifikant termisk skada på inneslutningens stålvägg har observerats.
7. Med tanke på att det har gått över tio år sedan händelsen kan faktorer som tid, kylvattnets flöde och externa händelser (som jordbävningar) ha förändrat tillståndet för de deponerade avlagringarna.

APRI-finansiärerna angav två specifika inriktningar inför starten av APRI-11, vilket har beaktats i projektet: i) ökat deltagelse i internationell forskning inom området, ii) mer PWR-specifik forskning. KTH:s avdelning för kärnteknik har engagerats av APRI som teknisk rådgivare åt SSM i OECD/NEA THEMIS-projektet för att stärka APRI:s internationella engagemang. THEMIS-projektet har en handfull olika mål, varav ett är en bättre förståelse för fenomenen som är relevanta för källtermen, som skrubbing i vatten och IOx-

växelverkan med aerosoler. KTH har använt simuleringsverktyget GOTHIC för att analysera THEMIS-experimenten med hjälp av en modell av THAI-anläggningen som utvecklats inom avdelningen. För tillämpning av THAI-modellen genomförde KTH en modellvalidering mot flera THEMIS-experiment och en rimlig överensstämmelse mellan modell och experimentresultat uppnåddes. KTH genomförde också en osäkerhetskvantifiering och källtermsberäkning för nordiska kokvattenreaktorer med MELCOR.

APRI-11-projektet har, förutom de specifika resultaten som producerats av de involverade lärosätena inom APRI-11, också som indirekta resultat utvecklat och bibehållit kompetens, utbildning och infrastruktur vilket har möjliggjort för universiteten att också delta i andra nationella och internationella forskningssamarbeten. I detta sammanhang är APRI en viktig projektplattform för forskning inom svåra haverier i Sverige och i februari 2024 planeras APRI-12 att påbörjas.

## EXECUTIVE SUMMARY

This report presents the results obtained from the severe accident research activities in the APRI-11 research program. APRI is a financial collaboration between the Swedish Radiation Safety Authority (SSM) and the Swedish nuclear utilities that funds severe accident research at Kungliga Tekniska Högskolan (KTH) and Chalmers Tekniska Högskola (CTH).

The overall objective of APRI is to gain and improve knowledge in severe accident with a focus on the severe accident management as it is implemented in the current operating Swedish BWR's and PWR's and ultimately confirm the Swedish accident management as it is deployed. The focus and orientation is phenomena that is considered to of risk importance for the Swedish accident management strategy. Knowledge in this context is for instance data, models, codes, insights and methodologies and the research has in general been directed to resolutions of specific safety issues, phenomena, or accident management strategy. The APRI objective is achieved by funding specific research activities at two Swedish universities by participation in international research, and by following the findings and observations from the Fukushima accident.

The Swedish severe accident management strategy, with a deep water pool for quenching of core debris, was for a long time a rather unique approach where little knowledge and experiences could be utilised from international research in the field. The intention of this measure is to terminate the accident progression, stabilize core debris and maintain containment integrity. But this chosen strategy also comes with the potential negative effect of energetic fuel coolant interaction that could produce loads challenging the reactor containment integrity. This motivated earlier APRI programs to more specifically study and investigate the strategy and any potential challenges, and substantial research has been done at KTH Department for Nuclear Power Safety in APRI-6 to 9 to address this issues. It was found in the APRI-6 to 9 programs, with a focus on ex-vessel debris bed coolability and steam explosion that research activities in this area alone could not resolve the problem associated with the severe accident management measure of Swedish NPPs. The reason is that the ex-vessel phenomena are sensitive to the late-phase phenomena of in-vessel accident progression. That is, the corium evolution in the lower head, vessel failure mode and melt discharge behavior provides to a large degree the conditions for the quenching of core debris in the containment and the conditions for potential steam explosions. Therefore, in addition to a continuous study on ex-vessel phenomena, the research at KTH Department for Nuclear Power Safety also started to experimentally study a few in-vessel phenomena in the APRI-10 project.

In APRI-11 the work at KTH Department of Nuclear Power Safety initiated in APRI-10, with the study of a few in-vessel phenomena, continued together with the continued research on ex-vessel core debris coolability. More specifically the following five topical areas has been investigated in APRI-11: i) in-vessel debris behavior, ii) vessel failure mode, iii) melt-coolant interactions, iv) ex-vessel corium-structure interactions, v) reactor applications and safety analyses. The results are presented in this report. Some key results can be noted:

- (i) *In-vessel debris behavior*  
a pilot test has been carried out in the SIMECO-2 facility to investigate debris bed dryout and remelting phenomena. The facility features high operational temperature, transparent visualization and novel instrumentation, so it is a unique infrastructure to investigate the evolution and heat transfer of multi-composition debris bed in the lower head. In the MRSPOD facility melt infiltration has been

investigated and since the wettability of particle surface with melt appears to play a role in melt infiltration, a further study is conducted to measure the equilibrium contact angle of eutectic Sn-Bi melt on different substrates.

(ii) *Vessel failure mode*

For a number of years' simulations by coupled thermo-mechanical analyses of the lower head have been performed with the goal to develop predictive capabilities. For the vessel failure analyses in APRI-11 the thermal load of the corium relocated in the lower head is provided by MELCOR and for future perspective thermal load should be provided by the in-vessel corium behavior study. The result shows that it is the stress failure mechanism, rather than the strain failure and melt-through failure criteria, which is the dominant failure mechanism in the ANSYS analysis. Moreover, according to the simulation the vessel fails at its thinnest region.

(iii) *Melt-coolant interactions*

The main objective of this study is to gain basic understanding on fuel debris formation using the DEFOR facility. In APRI-11 the study has been oriented to metallic melt-coolant interactions. It is observed that the metallic melt with higher melting point at the same superheat (as oxides) results in stronger heat transfer with water and an enhanced fragmentation, while all the other metallic melt tests experience a rapid solidification process, resulting in incomplete breakup of the melt jet, i.e., so-called "frozen jet". On the other hand, the oxidic melt with a high melting point has less potential of solidification before jet breakup and fine fragmentation.

(iv) *Ex-vessel corium-structure interactions*

Since it is still an open question on how the structures below the reactor pressure vessel in a BWR will affect ex-vessel corium behavior and risk it was included as a research task in APRI-11. From the literature review three phenomena of interest have been identified selected – splashing of melt, ablation of structure caused by melt impingement and melt freezing, focusing on existing experimental, numerical and modelling efforts. Based on preliminary basic calculations some general observations of the melt-through time is that it decreases with increasing superheat and increases with decreasing melt discharge hole diameter. Comparing the values of melt-through time and melt-discharge time, it can be seen that in small jet cases, the melt-through time is very small in comparison to the melt-discharge time, indicating a minor effect of the radiation shield throughout the whole melt discharge process. However, in middle/large jet cases, especially when melt superheat is low, the melt-through time is comparable to the melt-discharge time.

(v) *Reactor applications and safety analyses*

The objective of this topical study is to perform reactor safety analyses through applying the research results (e.g., models, computer codes) to the Swedish nuclear power safety context. Methodologies have been developed during APRI-11 to investigate ex-vessel debris bed coolability in a Nordic BWR and ex-vessel corium risk in a Swedish PWR, respectively. For simulation of severe accidents with ex-vessel debris beds formed in the reactor cavity of a boiling water reactor, the COCOMO code has been coupled with the MELCOR code to simulate accident progression which includes quenching and stable cooling of ex-vessel debris beds. To reduce computational cost of the coupled MELCOR/COCOMO simulation, surrogate models have been developed and coupled with MELCOR to realize quick estimation of similar accident progression involving ex-vessel debris beds. Compared with MELCOR standalone, both coupled simulations of



MELCOR/ COCOMO and MELCOR/SM predict earlier pool saturation and containment venting.

Another topical field that has been a focus area in a number of APRI project are activities related to the understanding of chemical interactions of fission products during severe accident conditions in the primary system and containment which has influence on the potential source term. This research has been performed in Department of Nuclear Chemistry at Chalmers Tekniska Högskola. The Chalmers research has, since many years, focused on accident chemistry with emphasis on volatile, long-lived fission products such as iodine, cesium, and tellurium. While iodine is crucial due to its varied chemical interactions and potential for persistent internal contamination, cesium poses long-term contamination risks and is primarily transported as an aerosol. Tellurium, which has been the primary subject of Chalmers' research within APRI-11, is a volatile fission product element that can escape overheated nuclear fuel in significant quantity and have a major contribution to off-site dose rates shortly after a reactor accident. Tellurium isotopes were detected in air, water and soil samples taken in Japan after the Fukushima Dai-ichi accident. The research was concentrated on investigating the formation and persistence of organic tellurides, particularly dimethyl telluride (DMT), under accident conditions. The first study explored the possibility of organic telluride formation in containment water after a breakdown during gamma irradiation. The results suggest organic tellurides can indeed form, necessitating further safety assessments. The second study investigated organic telluride formation in the gas phase under conditions similar to those expected in the primary circuit during an accident. While results indicate increased tellurium transport in the gas phase, the certainty of organic telluride formation remains to be confirmed. The third study assessed DMT's persistence under strong gamma irradiation, with results indicating that decomposition depends on the water phase composition. Radical scavengers can significantly affect DMT stability. In the final study, researchers explored the interaction between DMT and activated carbon from respirator filters, demonstrating that activated carbon effectively filters DMT.

The APRI financiers provided two specific orientations for the APRI-11 scope of work which has been considered in the project: i) increased international involvement, ii) more PWR-specific research. These orientations have been considered in project plan for APRI-11 and KTH Nuclear Engineering Department have been engaged by APRI as technical advisor of SSM in the OECD/NEA THEMIS project to strengthen APRI's international engagement. The THEMIS project have a handful of different objectives among which is a better understanding of phenomenology relevant to the source term, such as pool scrubbing and IOx interaction with late phase typical aerosols. KTH Department of Nuclear Engineering have been using the simulation tool GOTHIC to analyse THEMIS experiments using a model of the THAI-facility developed within the department. For the use of the model KTH Department of Nuclear Engineering performed model validation against several THEMIS tests and a reasonable agreement was achieved. From the pool scrubbing experiments it was observed that the amount of particles retained in the pool is determined by pool scrubbing and drop deposition occurring at the pool/gas interface and their respective deposition rates are determined by several different mechanisms. Parametric study suggests that the condensation in the initial globule region is the dominant contributor to the pool. For drop deposition, the two most important mechanisms are thermal diffusion and diffusiophoresis, followed by gravitational settling and thermophoresis. Turbulent diffusion is important for deposition of the large particles. Particle deposition due to drop deposition occurs mainly at the pool/gas interface. KTH Department of Nuclear Engineering also performed uncertainty quantification and source term evaluation

for Nordic BWR designs in response to LOCA and SBO using MELCOR. The parameters associated with the models of particle behavior with high importance were identified and for the pool scrubbing model they are hydraulic geometries for bubbles in the swarm region and the coefficient to estimate the vent impaction in the initial globule region. For the aerosol particle dynamic model, the parameters with high importance are particle agglomeration shape factor and particle density.

One of the tasks in the APRI-project since the tragic accidents in Fukushima Dai-ichi, Japan, is a follow up of the new findings, observations and lessons learned from the accidents. A deep understanding of the accident progression and associated phenomena of the Fukushima accident has a relevance since the damaged reactors in Fukushima were BWRs, which is also the type of reactor which has been studied in the APRI-context. Since the start of APRI-10 Tokyo Electric Power Company Holdings (TEPCO) together with International Research Institute for Nuclear Decommissioning (IRID) have conducted an investigation in the drywell of reactor unit 1 in Fukushima Dai-ichi (1F1) using a submersible robot with an attached video camera. Some key findings from the investigation include:

1. There are likely multiple failure points in the reactor pressure vessel (RPV), as some components such as control rod guide housings was found inside the pedestal.
2. Much of the components in the pedestal area is damaged beyond recognition, but the damage outside is limited to near the pedestal opening.
3. The concrete erosion due to molten corium-concrete interaction in the pedestal is about 1 meter high, but the reinforcing structures are mostly intact.
4. Deposits on the drywell floor range from 0.2 to 1.5 meters in height.
5. Cavities exist below shelf deposits attached to various structures.
6. No significant thermal damage to the D/W shell has been observed.

Given that over ten years have passed since the incident, factors like time, cooling water flow, and external events (like earthquakes) could have changed the state of the materials. Future studies should focus on understanding the cause of the reactor vessel failure.

The APRI-11 project have, besides the specific results produced by the contracted research in APRI-11, also as indirect results developed and maintained competence, education capabilities and infrastructure that has allowed the universities to also involve in other national and international research collaborations. In this context APRI is and has been an important project platform for the severe accident field in Sweden, and in February 2024 APRI-12 is planned to commence with important input from the APRI-11 project.

# CONTENT

<b>SAMMANFATTNING .....</b>	<b>5</b>
<b>EXECUTIVE SUMMARY.....</b>	<b>9</b>
<b>CONTENT .....</b>	<b>13</b>
<b>1. Introduction.....</b>	<b>15</b>
1.1. Background .....	15
1.2. Project objectives .....	16
1.3. Project structure .....	16
1.4. Dissemination.....	17
<b>2. International Projects.....</b>	<b>19</b>
<b>3. KTH-NPS Research On Severe Accidents.....</b>	<b>21</b>
3.1. Research objectives and tasks .....	21
3.2. Vessel failure mode .....	33
3.3. Melt-coolant interactions.....	35
3.4. Reactor applications and safety analyses .....	51
3.5. Summary and outlook .....	59
3.6. References.....	66
<b>4. Chalmers' Severe Accident Research in APRI-11 .....</b>	<b>69</b>
4.1. Summary of the work .....	69
4.2. Organic telluride formation from paint solvents under gamma irradiation.....	71
4.3. Radiolytic degradation of dimethyl telluride .....	74
4.4. Gas-phase interactions between tellurium and organic material in severe accident-like circumstances .....	80
4.5. Study of the retention of dimethyl telluride by activated carbon.....	92
4.6. Conclusive remarks regarding Chalmer's work regarding APRI-11 and future work in APRI-12. ....	98
4.7. References.....	100
<b>5. KTH-NE Analytical support OECD/NEA THEMIS .....</b>	<b>101</b>
5.1. Background .....	101
5.2. Pool Scrubbing tests in THEMIS Project .....	103
5.3. Modeling of Aerosol Particles in GOTHIC .....	105
5.4. Model development for THEMIS experiments.....	110
5.5. Analysis of THEMIS experiments relevant to Nordic plants designs and conditions .....	120
5.6. Conclusions and Outlook .....	122
5.7. References.....	124
<b>6. Fukushima Accident Update .....</b>	<b>127</b>
6.1. Summary.....	127
6.2. Observations .....	127
6.3. References.....	138
<b>7. Conclusion and Outlook.....</b>	<b>139</b>
7.1. Conclusion .....	139
7.2. Recommendations and Outlook .....	141
<b>8. Abbreviation list .....</b>	<b>145</b>



# 1. Introduction

This report presents the results from the severe accident research that has been obtained in the APRI-11 project conducted between 2021-2023. APRI is a collaboration between the Swedish radiation safety authority and the Swedish nuclear power companies which in collaboration financially supports severe accident research activities at two Swedish technical universities.

A deep and solid understanding of the phenomena and accident progression that can occur during a severe accident is of great importance for a number of areas and issues related to reactor safety as accident management, emergency preparedness and safety analysis. The Swedish radiation safety authority SSM together with the Swedish nuclear power licensees have during more than three decades cooperated in financing and coordinating a Swedish severe accident research program. The program has been operated as "APRI", where APRI is an abbreviation for Accident Phenomena of Risk Importance. The APRI research have since the start in the early 1990's been carried out as three year projects.

The major part of the research done in the APRI context is performed at KTH Department of Nuclear Power Safety, Chalmers Department of Nuclear Chemistry and KTH Department of Nuclear Engineering. Different APRI-projects have had slightly different orientation but has at KTH been centered around the study of corium related issues as core degradation, debris bed formation and coolability, and fuel-coolant interaction. The research has involved both experiments, model development, and simulation/analysis. At Chalmers the research topics have been centered around issues related to the study of the source term and different pertinent fission products and also involved both experiments and model development.

## 1.1. Background

Since the early 1980s, the nuclear power companies in Sweden together with the nuclear regulatory authority have collaborated in the research area of severe accidents. Initially, this collaboration primarily focused on the practical implementation of accident management strategies and mitigation systems for severe accidents in the operating reactors as a response to the Three Mile Island-II accident. The corner stones in the Swedish strategy for severe accident management, that was developed in the 1980's, are i) early flooding of the containment ii) filtered venting of the containment and iii) strengthening of the containment spray by additional connections and flanges to the fire system or fire trucks. The early flooding of the containment is in the BWR's realised by opening dedicated valves to the pressure suppression pool with the objective to promote the conditions for the quenching of core debris. In the PWR's the reactor pit is flooded with primary coolant leaking from the relief tank in case of a severe accident. The extensive production of steam and non-condensable gases as hydrogen in the containment during a severe accident necessitates the venting of the containment during the accident progression. This is can be done using a dedicated scrubber system either by a rupture disc or manually. Finally, as a mean to manage the containment pressure and prolong the release time for the venting process and to scrub fission products, the containment spray system has been connected to the fire system with its own diesel pump and water source. The overall goal of the severe accident management strategy is to preserve the containment integrity as the last barrier against the release of radioactive material to the public and environment.

Since the implementation of the severe accident management strategies at the Swedish operating reactors, remaining uncertainties in the understanding of the severe accident phenomena and progression and the potential for negative effects of the chosen strategies have been identified. Further, observations from the Fukushima accident have had implications that influences the understanding of the Swedish severe accident management. This motivates further severe accident research activities.

## 1.2. Project objectives

The main objective of APRI-11, and previous APRI-projects, is to re-evaluate and confirm the chosen severe accident management strategy and to confirm that potential radiological releases in a severe accident do not exceed regulatory requirements. These high level objectives are accomplished by an increased knowledge base and understanding of identified accident phenomena of risk importance. More specifically, recommendations from APRI-10 has been input to the APRI-11 project. Further, in the definition of the scope of work for APRI-11, the APRI financiers highlighted that APRI should consider more international collaboration and increased research activities for PWR's.

To achieve the project objectives and to implement the recommendations from APRI-10 (SSM report 2022:2) the project has carried out following tasks:

- Follow the international research on severe accident and, if possible, evaluate the results and the implications for Swedish operating reactors,
- Continued financial support to severe accident research groups at KTH and Chalmers with specifically contracted the research of identified phenomena as core degradation, vessel failure mode, corium coolability and stabilisation in containment and the chemistry of specific fission products during accident conditions,
- Follow the observations and findings from the Fukushima accident.

## 1.3. Project structure

The APRI-11 project was carried out between 2021-2023 with a total budget frame of 20 MSEK. The budget contribution from SSM is one-third of the total budget and the remaining two-thirds of the budget is covered by the nuclear power companies equally shared. During this period the steering committee has had 12 meetings, visited 6 semi-annual technical meetings at KTH and 3 annual technical meetings at Chalmers.

The project was divided in five subtasks as:

- (i) *KTH-NPS*  
Studies of i) in-vessel debris behavior, ii) vessel failure mode, iii) melt-coolant interactions, iv) ex-vessel corium-structure interactions, v) reactor applications and safety analyses. Project leader at KTH was Weimin Ma.
- (ii) *CTH-NC*  
Studies of the formation and persistence of organic tellurides, particularly dimethyl telluride (DMT), under accident conditions. Project leader at CTH was Christian Ekberg.
- (iii) *KTH-NE*  
Analytical support to the OECD/NEA THEMIS project with GOTHIC simulations of pool scrubbing and drop deposition occurring at the pool/gas interface. Project leader at KTH was Pavel Kudinov.

- (iv) *Fukushima follow-up*. Responsible for this tasks has been Sevostian Bechta and Patrick Isaksson.
- (v) *International projects*. Responsible for this task has been Patrick Isaksson and Christian Linde.

#### **1.4. Dissemination**

A final APRI-11 seminar was arranged at Bergendal Conference venue in Sollentuna Stockholm February 6-7 with more than 60 participants. The objective was to share the results and current understanding of a severe accident for existing Swedish reactors and to promote both discussions and feedback for future activities in the area. The target audience was staff working in the nuclear power industry but not particularly knowledgeable of severe accidents, as control room staff or nuclear engineers in general.





## 2. International Projects

The APRI-partners from SSM have during APRI-11 been involved in five international NEA joint projects within the area of severe accidents. Potential synergies or other coordinating activities have been discussed and evaluated within the APRI-11 project. The results from the ongoing NEA projects are restricted and the results are typically released three years after the projects are finalised.

The international NEA projects with representation from APRI-partners that have been started or were on-going during APRI-11 are presented below.

- *ROSAU*  
The NEA ROSAU (Reduction of Severe Accident Uncertainties) project aims to reduce knowledge gaps and uncertainties associated with severe accident progression and mitigation. The project started in June 2019 and is planned to end by mid-2024. After the Fukushima accident, re-evaluations of examined plant responses to severe accident conditions and operator actions for coping with and terminating severe accident progression were done. Based on these analyses, gaps were identified in two areas of severe accident progression where additional knowledge was needed and uncertainties could be reduced. These areas are: 1) the spreading of core melt in the containment cavity after the reactor pressure vessel rupture and the effect of metal content in the melt on molten core-concrete interaction; and 2) in-vessel and ex-vessel core melt and debris coolability. The ROSAU Project comprises 10 tests in two areas of melt spreading and debris coolability/MCCI. The experiments are conducted at the Argonne National Laboratory (ANL) in the United States, under the co-ordination of the US Nuclear Regulatory Commission, and include five large underwater melt spreading tests (MST) with up to 300 kg of molten prototypic material in a newly designed facility and five smaller melt-core-concrete interaction (MCCI) and coolability tests (DCAM) with up to 80 kg of molten prototypic material. Tests are conducted at temperatures up to 2 500°C, with different metal and concrete contents in the melts, with different cooling water flow rates and sub-cooling. In addition to these experiments and with the support of project partners, the ANL will carry out an analytical activity to refine and validate models and codes for each test category, so as to form the technical basis needed to extrapolate experiment findings to plant conditions.
- *FACE*  
The NEA FACE (Fukushima Daiichi Nuclear Power Station Accident Information Collection and Evaluation) project is an extension of the already completed NEA projects BSAF, PreADES and ARC-F related to the Fukushima-Daiichi accident analysis and the preparation of the fuel debris retrieval operations. The project is active from July 2022 to mid 2026. The objectives for the FACE project are refining the interpretation of the Fukushima-Daiichi accident scenarios, including the effects of accident management measures in consistency with insights obtained from plant investigations. Further objective is interpreting the results of analysis for uranium-bearing particles collected on-site and determining suitable hot laboratory analysis techniques and procedures for future application to fuel debris analyses. Based on the general objectives, the project focuses on three main scopes of work. The first scope is in-depth discussions and analyses for accident progression in the damaged units and related fission product

behavior and hydrogen combustion. This scope considers technical issues identified in recent Fukushima-Daiichi plant investigations and the quantification of uncertainties in severe accident modelling. The first scope is influenced by the ARC-F project. The second scope is related to the characterisation of uranium-bearing particles and the establishment of techniques for future fuel debris analysis for decommissioning and dismantling. Scope 2 includes a study on the plausible mechanisms for the formation of uranium-bearing particles collected on-site. This will contribute to the understanding of the progression of the accident and which fuel debris analysis technology and evaluation methods may be most useful. An international round-robin analysis activity with debris simulants is also included in this scope. Scope 2 is influenced by the PreADES project. The third scope is data and information collection related to the Fukushima-Daiichi plant by Japanese organisations.

- *TCOFF-2*

The NEA TCOFF-2 (Thermodynamic Characterisation of Fuel Debris and Fission Products Based on Scenario Analysis of Severe Accident Progression at Fukushima Daiichi Nuclear Power Station) is the second phase of the joint project TCOFF and was launched in 2022 and will end in 2025. The program is based on the first TCOFF project, but with a broadened scope and includes studies on materials behavior of ATF's in severe accident conditions and is also looking at other reactor designs than the Fukushima Daiichi BWR. The objective of TCOFF-II is to improve the models describing material interactions and the role they play in the various phases of the severe accidents. The ultimate goal is the integration of such models in severe accident simulation codes to increase their accuracy. This improvement will be driven in particular by state-of-the-art knowledge of the thermodynamic properties of the relevant material systems for the description of core materials degrading through a severe accident. The project will be focusing on generating knowledge and data for analysis of severe accidents sequences going from the early stages of the fuel degradation, through the fuel relocation, the molten pool formation in-vessel, reactor pressure vessel (RPV) failure, and the interaction between the corium and the concrete during ex-vessel phases. The TCOFF-2 project will also generate knowledge and data regarding fission products behavior in severe accidents and assess how this may affect source term evaluations. Included in both TCOFF and TCOFF-2 is a distribution of funding for relevant research supporting the objectives of TCOFF through a call for proposal procedure.

## 3. KTH-NPS Research On Severe Accidents

### 3.1. Research objectives and tasks

The goal of severe accident research at KTH Nuclear Power Safety division (KTH-NPS) is to create a solid knowledge base to resolve severe accident issues which may remain or emerge in Swedish nuclear power plants (NPPs), including both BWR and PWR. Specifically, the research is focused on understanding and modeling of severe accident phenomena which have large uncertainties but play important roles in safety analyses and qualification of severe accident management (SAM) measures intended to terminate accident progression and maintain containment integrity. For instance, a crucial SAM measure widely adopted in NPPs is to flood the reactor cavity with water in the hope of arresting the core melt in the wet cavity after melt-through of the reactor pressure vessel (RPV). To qualify such a SAM measure, an extensive study on debris bed coolability and steam explosion has been carried out at KTH-NPS in the previous APRI programs (APRI-6 ~ APRI-9), since a debris bed on the cavity floor is foreseen due to molten fuel coolant interactions (FCI) in the water pool, but the FCI incurs the risk of steam explosion. The APRI research has been providing necessary knowledge (data, insights, models, codes and methodologies) for proving that ex-vessel debris beds are coolable with diminishing risk of steam explosion in case of severe accidents in Swedish NPPs. Notably, corium (debris bed) coolability and steam explosion are among the top severe accident research priorities ranked by the international community.

Nevertheless, due to the complexity and multi-faceted feature of severe accident phenomena, it was found that the previous focus on ex-vessel debris bed coolability and steam explosion alone could not resolve the problem associated with the SAM measure of Swedish NPPs, since the ex-vessel phenomena are sensitive to the late-phase phenomena of in-vessel accident progression, e.g., the corium evolution in the lower head, vessel failure mode and melt discharge condition to which little attention was paid in the previous study. Therefore, in addition to a continuous study on ex-vessel phenomena, APRI-10 research at KTH-NPS started to address a few in-vessel phenomena, such as melt infiltration in debris beds and modeling of vessel failure.

The compass of APRI-11 research at KTH-NPS is to advance the investigations on late-phase in-vessel melt/debris behavior and vessel failure mode which were initiated but unresolved in APRI-10, and to extend the scope of FCI study, as well as to perform case study for reactors chosen. Moreover, a new interest is the interactions of corium melt with below-vessel structures. Accordingly, the research tasks of KTH-NPS during APRI-11 (2021-2023) have been conceived as five topical areas as follows:

- In-vessel debris behavior
- Vessel failure mode
- Melt-coolant interactions
- Ex-vessel corium-structure interactions
- Reactor applications and safety analyses

This report summarized the key achievements in the five topical areas. More descriptions of the research outcomes can be found in the relevant publications [1]~[33], including peer-reviewed articles, doctoral dissertations and some technical presentations accomplished during APRI-11. In addition to the APRI-11 research, other severe accident research efforts at KTH-NPS include experimental and numerical studies on corium melt spreading in the reactor cavity [34]~[36] and spray cooling of the lower head [37][38].

Notably, four doctoral students [11][15][21][30] have graduated and received PhD degrees within the period of APRI-11 support.

APRI research at KTH-NPS does not only reduce knowledge gaps of severe accident phenomena of risk importance and maintain competence/expertise addressing severe accident issues, but also educate young scientists/engineers and retain experts knowledgeable of Swedish NPPs and prepared to effectively address complex reactor safety issues.

### 3.1.1. In-vessel debris behavior

The objective of this topical study is to gain insights into the complex phenomena of corium evolution in the lower head where we have poor knowledge, including:

- molten metal (with lower melting point) infiltration in oxidic debris bed;
- dynamics of multi-composition debris remelting to molten pool; and
- heat transfer of debris/molten pool to the vessel wall and penetrations.

In this regard several experiments have been carried out in SIMECO-2 and MRSPOD facilities to investigate debris remelting and melt infiltration, respectively. Furthermore, contact angles of melt-particle pairs employed in the MRSPOD experiment are measured, and the effect of melt-particle wettability on melt infiltration is quantified in a scaled-down experiment. Numerical studies on melt infiltration and molten pool convection have also been performed.

### 3.1.2. Experimental study on debris bed dryout and remelting

A pilot test has been carried out in the SIMECO-2 facility as shown in Figure 3-1 to investigate debris bed dryout and remelting phenomena [1]. The facility features high operational temperature, transparent visualization and novel instrumentation, so it is a unique infrastructure to investigate the evolution and heat transfer of multi-composition debris bed in the lower head.

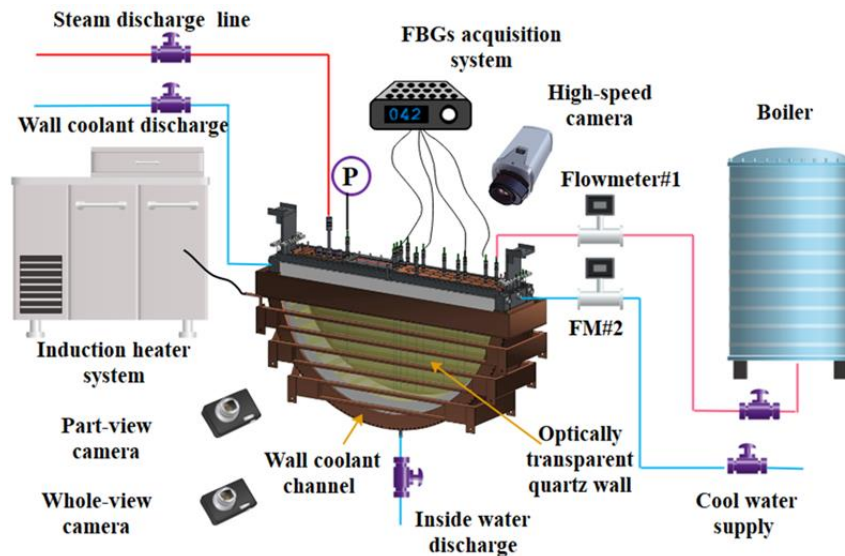


Figure 3-1: Schematic of SIMECO-2 facility.

The test section for the investigation on debris dryout and remelting in the SIMECO-2 facility is illustrated in Figure 3-2 where the numbered parts are as follows:

- (1) Water-cooled hemispherical «slice» vessel with radius of 500 mm, electromagnetically shielded by a copper screen.
- (2) Particulate debris bed with a porosity of 40% whose mass comprising 55% of carbon steel particles representing heat-generating refractory oxidic part ( $\text{UO}_2\text{-ZrO}_2$ ) of corium (dark color), and 45% of Sn-Bi particles representing fusible metallic part (Zr-Fe) of corium (grey color). Mass ratio between two components is selected based on the MELCOR simulation results of corium in the lower head of a Nordic BWR [39]. The debris bed has a maximum height of 340 mm and a thickness of 30 mm adjacent to the front quartz glass.
- (3) Three-turn inductor with high frequency generator (output power up to 150 kW, and frequency range of 200-500 kHz).
- (4) Temperature measurement sensors based on the Fiber Bragg Grating (FBG) optic fiber sensors which are not affected by induction heating.
- (5) Front and back quartz glasses and inner polycarbonate plates.
- (6) Top water level ( $\approx 40$  mm thick above debris) with continuous hot water supply from the left side.

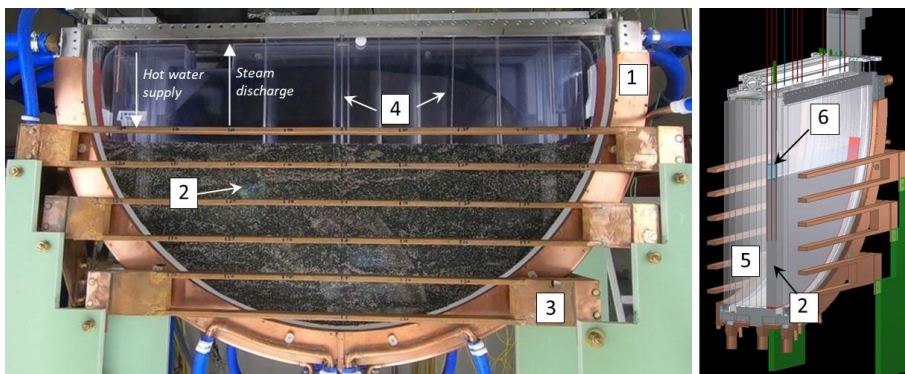


Figure 3-2: SIMECO-2 test section for the debris dryout/remelting investigation

The pre-test simulation is performed by the COCOMO code for prediction of dryout power [2]. A qualitative observation of debris bed behavior during dryout and remelting process has been observed. A detailed [1] post-test analysis of debris bed characteristics is also conducted.

In the pilot test the induction power is increased stepwise according to the diagram in Figure 3-3a. Dryout is detected by temperature increase above 100 °C (Figure 3-3b), corresponding to 14.8 kW (482 W/kg debris) of input power.

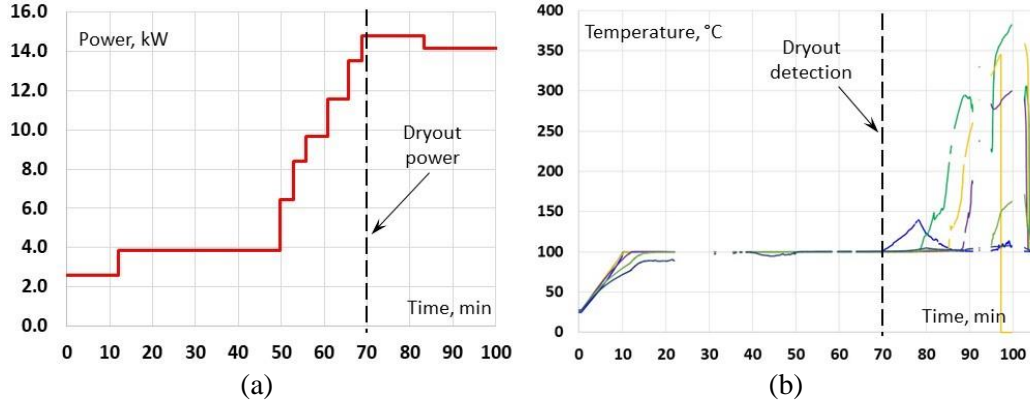
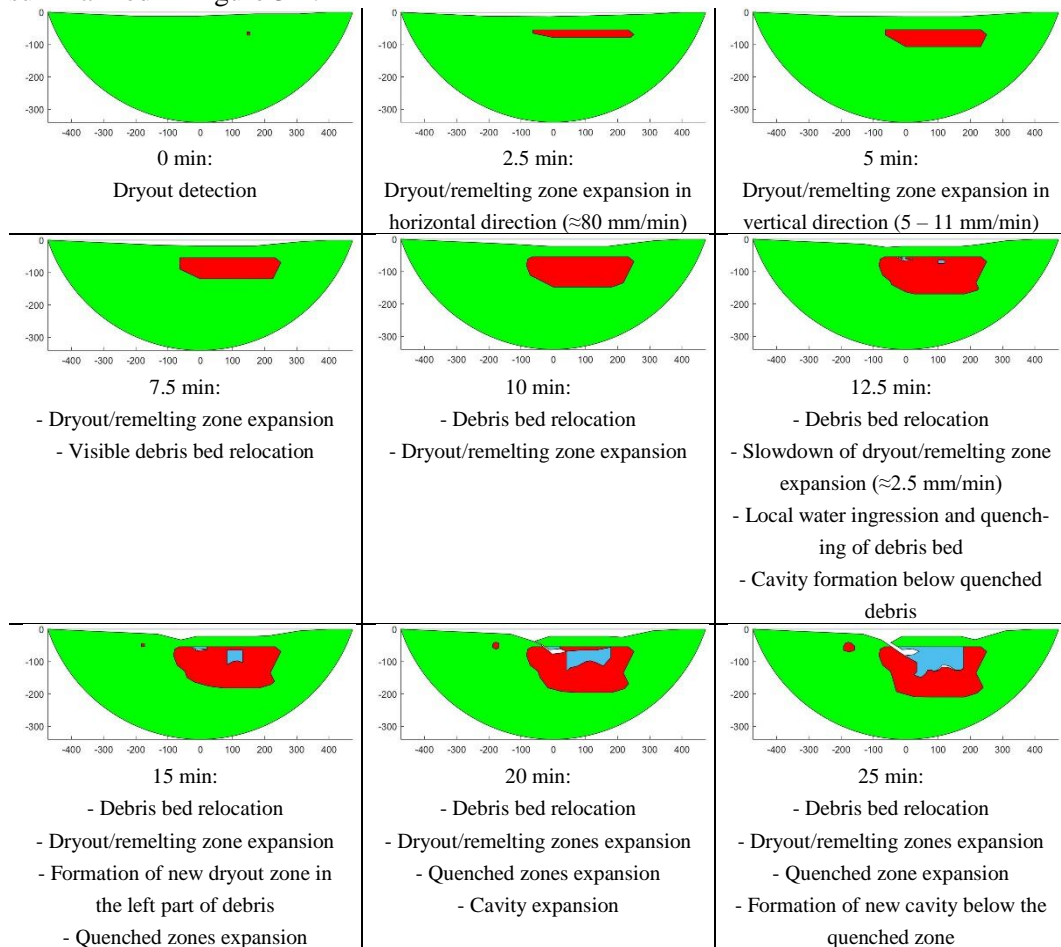


Figure 3-3: History of power increase (a) and temperature in debris bed (b).

The various stages of debris bed behavior observed in the experiment are schematically summarized in Figure 3-4.



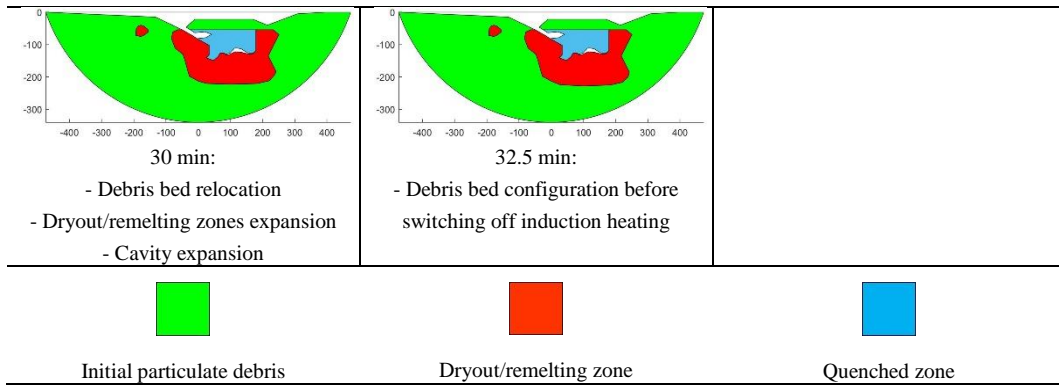


Figure 3-4: *Debris bed behavior during the dryout/remelting test with indication of time.*

The expansion of dryout zone and debris relocation are detected visually. Because of the low temperature difference between water boiling point (100 °C) and melting point of Sn-Bi alloy (139 °C), the dryout region turns to the remelting region relatively fast (in less than a minute).

Figure 3-5 illustrates a transition of wet region of the debris bed to dryout and then remelting zone. The final debris bed configuration (front view) is shown in Figure 3-6. There are four visible layers with different structure (morphology): the 1<sup>st</sup> layer with changed top debris bed profile because of material relocation consists of initial particulate debris and some solidified separated fusible material droplets; the 2<sup>nd</sup> layer includes formed cavity, solidified fusible material above and area enriched by refractory material because of relocation of all fusible material below; the 3<sup>rd</sup> layer includes main part of solidified melt of fusible material; and the 4<sup>th</sup> layer consists of initial particulate debris without visible changes.

A detailed investigation of internal structure of the post-test debris bed is performed by analyses of cross sections in different characteristic regions. Such analyses allow to make mapping of characteristic regions with their corresponding morphologies, as depicted in Figure 3-7.

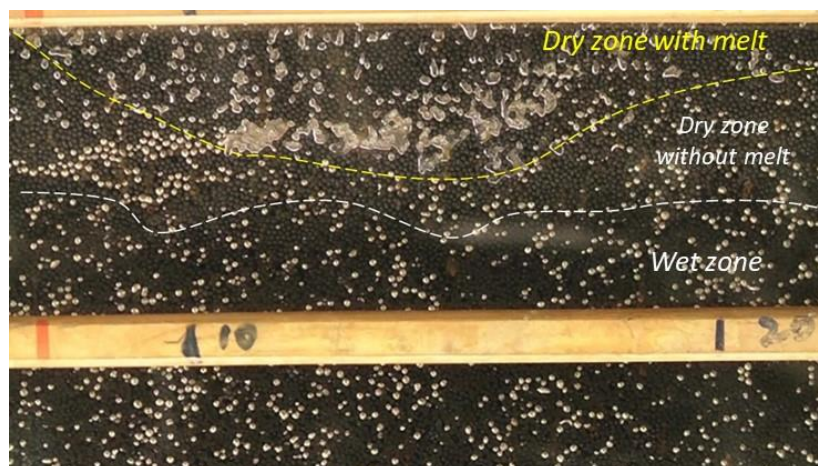


Figure 3-5: *Transition of wet zone to dryout zone and remelting zone.*

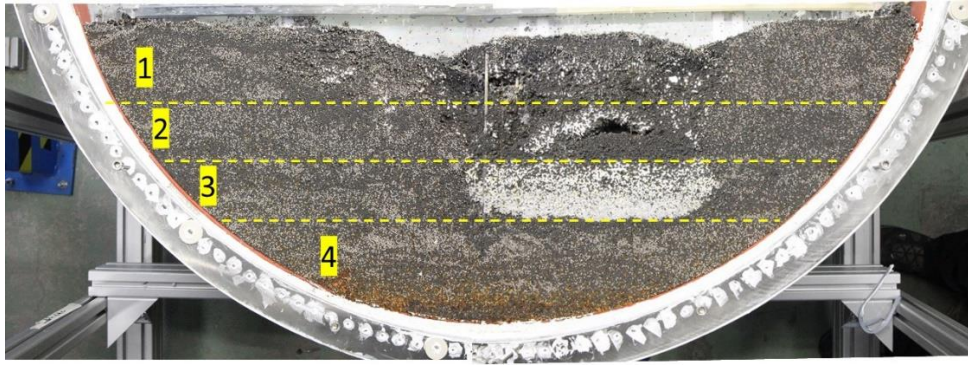


Figure 3-6: Final debris bed configuration with stratified structure.

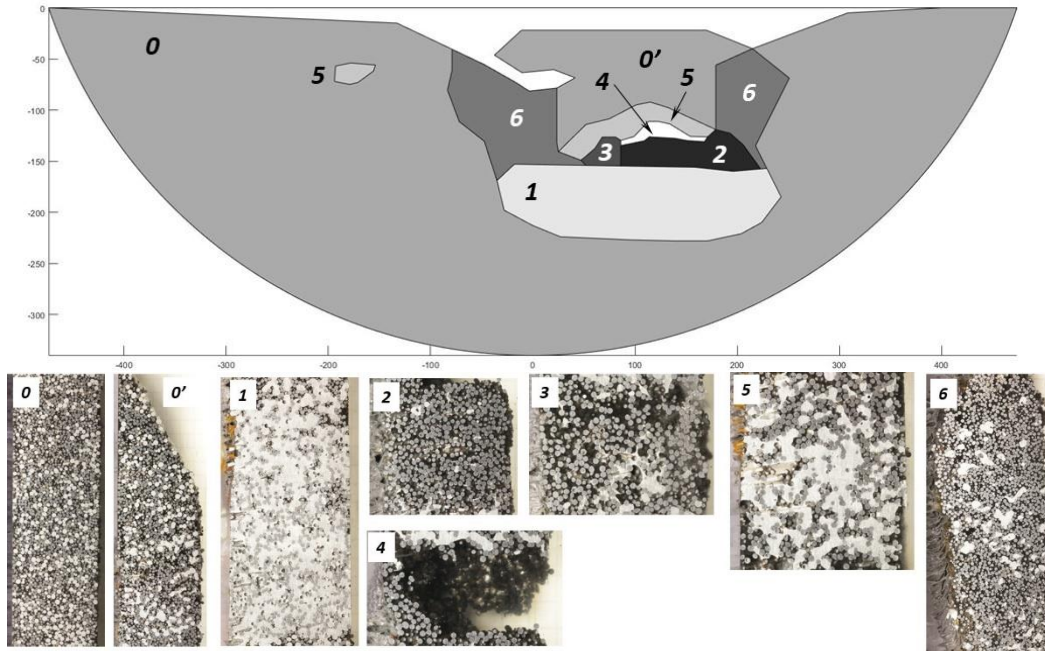


Figure 3-7: Mapping of the debris bed regions with typical morphologies.

Through image processing and analysis of the post-test debris bed, the data of porosity and material fraction in the above-mentioned regions are obtained and presented in Table 3-1. The mass fraction of melted Sn-Bi material is  $9\pm 1\%$ .

Table 3-1: Porosity and refractory material (carbon steel) mass fraction in characteristic regions

Area	Porosity, %	Carbon steel mass fraction
0 and 0'	39 – 40	55
1	3 – 5	28 – 32
2	40 – 50	> 90
3	50 – 60	> 88
4 (cavity)	100	0
5	15 – 20	33 – 38
6	35 – 40	65 – 83



A COCOMO simulation is also employed in the post-test analysis with an updated power profile from calibration. Comparison of results can be seen in Figure 3-8. The predicted dryout power is 14.5 kW which is in good agreement with the experimental value (14.8 kW). The predicted dryout location (on the right side of the debris bed) is also very close to the experimental one (cf. Figure 3-8a). It should be noted that COCOMO predicts the formation of another dryout zone on the left side of the debris bed with a larger discrepancy in location and time (Figure 3-8b). Such discrepancy between simulation and experiment can be explained by change of debris structure (Sn-Bi melting, melt and particle relocation) which happens in experiment but cannot be modelled by COCOMO. Change of debris structure leads to the redistribution of power profile with an increase of the volumetric heat release in the region with higher concentration of carbon steel, which is not modelled by the code.

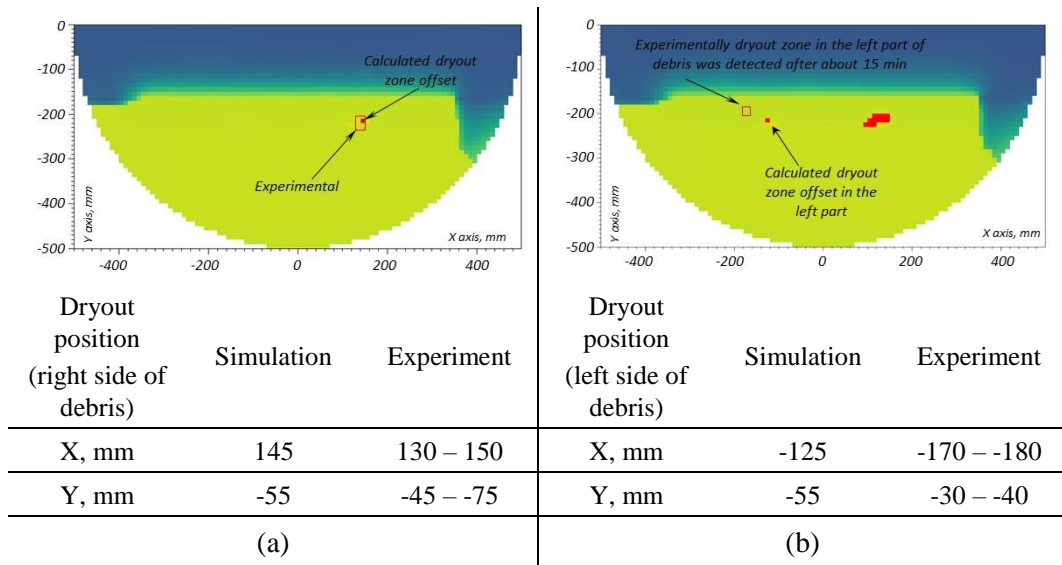


Figure 3-8: Comparison of dryout position between the COCOMO simulation and experimental observation: (a) initial dryout detection; (b) dryout extension after 2.3 min simulation time..

In summary, the transient behavior of debris bed during the pilot test reveals many important phenomena previously not addressed: formation of cavity available for water, material relocation, change of porosity, ingress of water and quenching of part of molten material, and stratification of debris structure. Such observations call for strong needs for further investigation and development of simulation capabilities.

### 3.1.3. Experimental study of melt infiltration in debris beds

The MRSPOD test facility was developed to study the thermal-hydraulic characteristics of melt penetration into debris beds. The facility places a quartz tube in a high temperature cylindrical tube furnace which can reach high temperature inside the furnace up to 1000°C. The quartz tube (120mm in diameter and 1300mm in length) is employed to accommodate a particulate bed and enable a visual property of the test section.

The recent tests in the MRSPOD facility are instrumented with thermocouples (TCs), fiber Bragg grating (FBG) sensors, laser sensor, video, and infrared cameras, which are essential in describing the overall melt infiltration and solidification behavior [3]. An eutectic Sn-Bi melt with superheat temperature between 50 and 70 °C is poured into a pre-heated particle bed consisting of 1.5-mm spherical particles made of either copper (Cu),

Sn-coated Cu, stainless steel (SS), Sn-coated SS, and/or glass beads to study the effect of thermal properties and wettability on the melt infiltration. Melt infiltrations in a single-layer, multi-layer, and two-columnar particulate beds are also performed. The measurements from TCs, FBGs, and observations from video cameras have revealed a non-linear kinetics of melt infiltration. Moreover, the extracted ingots after the experiments have shown the complex infiltration process under similar test conditions. Detailed description and results of the recent tests can be found in [3].

Since the wettability of particle surface with melt appears to play a role in melt infiltration, a further study is conducted to measure the equilibrium contact angle of eutectic Sn-Bi melt on a substrate of Cu, SS, Sn-coated SS or Sn at temperatures of 150, 200 and 250 °C using a sessile drop method [4]. The contact angles of eutectic Sn-Bi melt on Sn and Sn-coated substrates at 250 °C are not measured because the melting temperature of Sn is 230 °C.

To perform the measurement of contact angle, the molten Sn-Bi droplet is formed on a substrate in a horizontal Entech tube furnace with a quartz window for observation. Figure 3-9 illustrates representative images of two sessile drops, which are employed for determining the contact angle of eutectic Sn-Bi melt on a copper substrate.

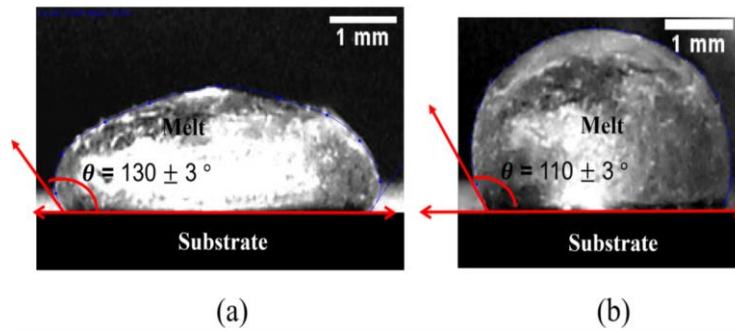


Figure 3-9: Eutectic Sn-Bi droplets on copper substrate at two distinct temperatures: (a) 200 °C and (b) 250 °C.

The results of these measurements are presented in Figure 3-10. One can see that the Cu and SS substrates are non-wettable by eutectic Sn-Bi melt at temperatures of 150, 200 and 250 °C, since at corresponding temperatures the Cu substrate has contact angles of 135°, 130° and 110°, and the SS substrate has contact angles of 119°, 119° and 100°. Conversely, the Sn and Sn-coated substrates have better wettability with eutectic Sn-Bi melt at temperatures of 150 and 200 °C, since the contact angles are 93° for Sn substrate and 92° for Sn-coated substrate at 150 °C, while they are respectively 79° and 82° at 200 °C. The measurement error is  $\pm 3^\circ$ .

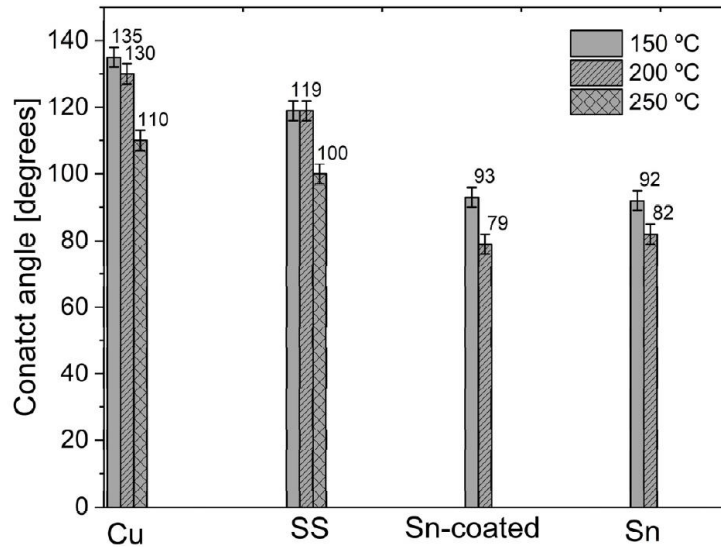


Figure 3-10: : Contact angles measured for eutectic Sn-Bi melt on substrates of copper (Cu), stainless steel (SS), tin-coated (Sn-coated), and tin (Sn) at temperatures of 150, 200 and 250 °C.

After the measurement of contact angles, four small-scale tests as shown in Figure 3-11 are conducted to investigate the infiltration phenomena of molten Sn-Bi eutectic alloy into particulate beds made of copper (Cu), 304 stainless steel (SS), stainless steel coated with Sn (Sn-coated SS), and copper coated with Sn (Sn-coated Cu), separately. The test section is a quartz tube with inner diameter of 22mm and length of 200 mm, to accommodate a particulate bed. Thus, the multi-dimensional effect observed in MRSPOD tests [3] is significantly reduced in the small-scale setup, and focus will be the impact of particle surface wettability on melt infiltration phenomena under similar test conditions.

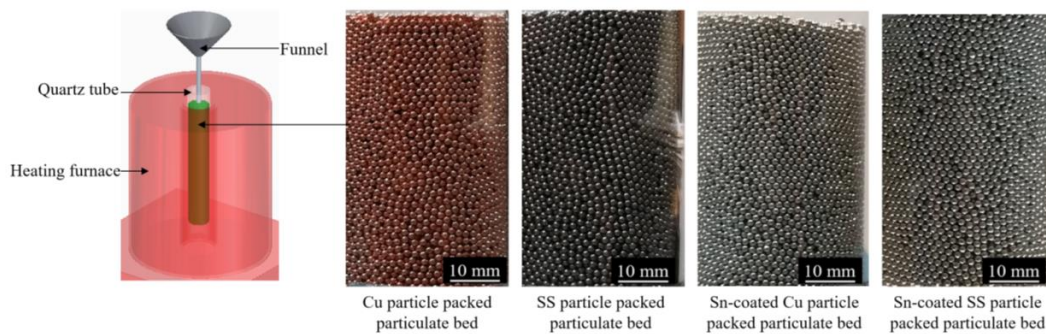


Figure 3-11: Schematic of small-scale experimental set-up and particulate beds.

The melt materials used in the experiment is Sn-Bi eutectic alloy with melting point of 139 °C and an initial temperature up to 220 °C. The melt mass is approximately 99 g, creating a ~30 mm thick molten pool overlaying the particulate bed. The diameter of the above-mentioned four spherical particles is 1.5 mm. The cylindrical particulate bed in the quartz tube has the height of 145 mm and porosity of 0.39. The bed is preheated to 200 °C before melt pouring.

Figure 3-12 plots the history of Sn-Bi melt infiltration in the four different particulate beds. The y-axis of the graph represents the leading front of melt penetrating into the particulate bed. The x-axis represents time. It is found that the melt penetrates much faster in the wettable particulate beds than in the non-wettable particulate beds. The infiltration

rates in the wettable particulate beds (19~23 mm/s) are more than double than those in the non-wettable particulate beds (8~9 mm/s).

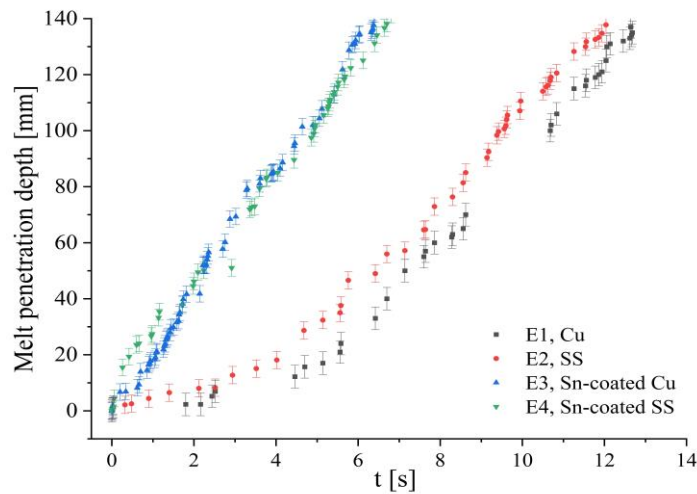


Figure 3-12: Melt penetration depth versus time for four tests of particulate beds with different spheres: E1–Cu, E2–SS 304, E3–Sn-coated Cu, E4–Sn-coated SS.

### 3.1.4. Numerical study of melt infiltration in debris beds

In addition to the experimental investigations, numerical studies are also performed to help the understanding of melt infiltration phenomena in particulate beds [5][6]. A computer code of Moving Particle Semi-implicit (MPS) method with various models representing key physics in the melt infiltration is developed and used in the simulation [5]. Moreover, the Level set method is adopted through the COMSOL Multi-physics platform to simulate melt penetration in particulate beds [6].

To validate the MPS code developed at KTH-NPS, three REMCOD tests of E08-E4, E09-C2 and E09-C4 [40] are simulated by the MPS method in the APRI-11 research program. For instance, Figure 3-13 and Figure 3-14 show the simulated melt penetration configurations of the REMCOD-E09-E4 test with respective contact angles of  $90^\circ$  and  $150^\circ$  in a comparison with experimental images. It indicates that the melt penetration front (white line for simulation and black line for experiment) is not uniform in the width's direction. A deeper penetration position appears at the center area of the test section caused by the melt solidification at the walls, which blocks the penetration channel. Obviously, most of the melt penetrates through the debris beds and is collected in the catcher. The melt mass fraction remaining in the debris beds is 10.3% in the simulation with contact angle of  $90^\circ$  and 11.1% with contact angle of  $150^\circ$ , being consistent with 12.2% in the experiment. The time for all melt to drain into the catcher is 3.92s and 4.04s in the simulation with contact angle of  $90^\circ$  and  $150^\circ$ , respectively, and 4.8s in the experiment. The difference may be attributed to the front and back wall effects in the experiment. In addition, the initial pouring effect in experiment could also contribute to such difference.

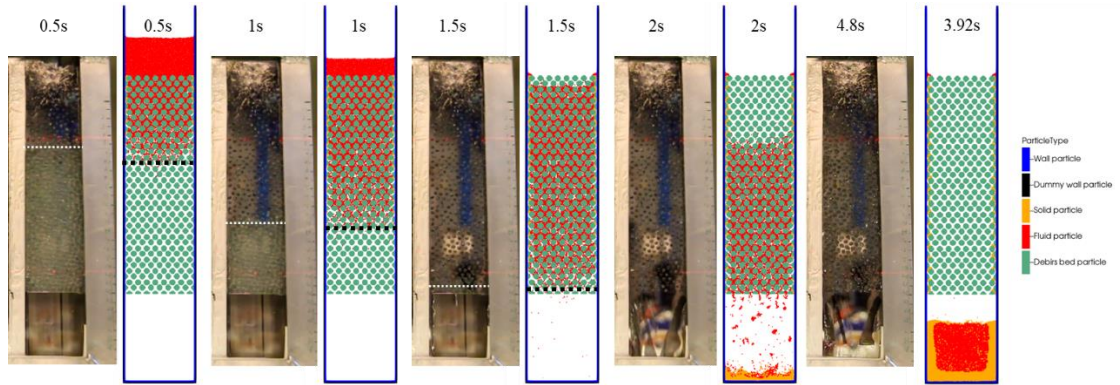


Figure 3-13: Distributions of particles for REMCOD-E09-C4 test with contact angle of  $90^\circ$ .

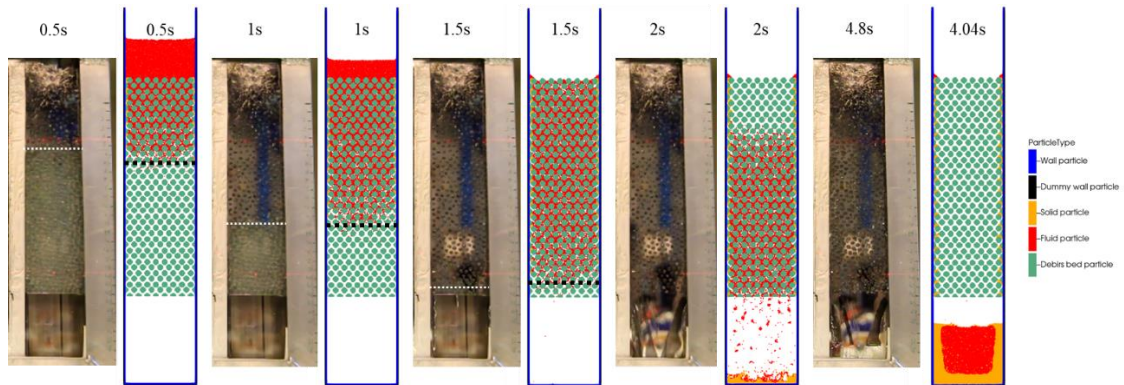


Figure 3-14: Distributions of particles for REMCOD-E09-C4 test with contact angle of  $150^\circ$ .

Figure 3-15 demonstrates the progression of the melt penetration front predicted by the MPS simulation compared with the experimental result, where the position is obtained along the center line of the compartment. The square symbols represent the results from experiment, while the green line and blue line stand for MPS results with contact angle of  $90^\circ$  and  $150^\circ$ , respectively. It is evident that higher contact angle contributes to slower penetration rate, but only slightly. This may be attributed to the large particle size and large pore size, and hence the relatively smaller capillary resistance effect. Therefore, the contact angle is set as  $150^\circ$  in the following simulations. Overall, the melt penetration process predicted by the MPS method are consistent with the experimental data.

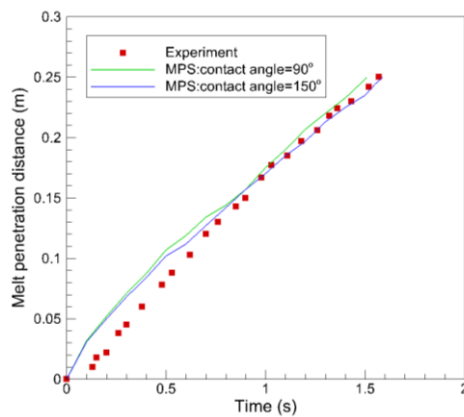


Figure 3-15: Melt penetration process with time for REMCOD-E09-C4 test.

Simulation results of the other two REMCOD tests (E08-C4 and E09-C2) can be found in [5]. In general, the comparative results show that the melt infiltration in particulate beds of the REMCOD tests can be reproduced by the MPS code.

### 3.1.5. Numerical study of melt pool convection

A stratified melt pool in the lower head has been receiving great attention in severe accident research. In the stratified molten pool there exists a pool scrubbing and drop deposition occurring at the pool/gas interface and their respective deposition rates are determined by several different mechanisms. Parametric study suggests that the condensation in the initial globule region is the dominant contributor to the pool. For drop deposition (IH) natural convection in the oxidic layer and Rayleigh-Bénard (RB) convection in the upper metallic layer.

Extensive numerical simulations have been devoted to melt pool convection and heat transfer using various methods such as various turbulence models including Reynolds Averaged Navier-Stokes (RANS) and Large Eddy Simulation (LES), effective convectivity model [41] and lumped-parameter approach [7]. To increase the fidelity of simulation, Direct Numerical Simulation (DNS) is applied to a homogeneous oxidic molten pool in a scaled-down geometry of the SIMECO-2 facility using Nek5000 – a fast and scalable high-order solver for CFD with spatial discretization based on the spectral element method and massively parallel high-performance computing. A  $\frac{1}{4}$  scaled-down SIMECO-2 test section ( $Ra=6.54\times 10^{11}$ ) is simulated by the DNS, since the original SIMECO-2 pool has  $Ra\approx 10^{15}$  which is unaffordable with the available computational resources. In addition to a DNS simulation of the IH pool, RB natural convection in a metal layer is simulated. A comparison of DNS with RANS models is also made for simulation of the BALI-Metal 8U [11]. Details of the simulation results and findings can be found in articles [8]~[10] and the doctoral thesis [11]. Below is a summary of key points.

- For the study on the natural convection of IH melt pool with three Pr values of various materials, it is found that more vigorous turbulent motion and a thicker layer of intense turbulent mixing in the upper region when the Pr is smaller [8]. The descending flow extends further down toward the bottom, creating a more intense circulation flow at the bottom with smaller Pr. Additionally, smaller Pr results in more thermal stripping structures and less stable stratification layers. Comparing the heat fluxes on the top and curved walls for different Pr cases, heat fluxes along the top boundary have higher fluctuation frequency with smaller Pr. On the other hand, the maximum heat flux to the side walls is lower with smaller Pr, although it is still significantly higher than that on the top boundary.
- The study on the IH molten pool convection in a hemispherical domain at a Rayleigh number of  $1.6\times 10^{11}$  and a Prandtl number of 0.5 [9] reveals three distinct regions within the pool: an upper region with large turbulent eddies, a nearly stagnant lower region promoting thermal stratification, and a descending flow along the curved wall enhancing heat transfer to the bottom. Heat flux distribution displays fluctuations along the top boundary due to turbulent eddies, while it shows nonlinearly increasing heat flux with the polar angle along the curved boundary, reaching a maximum at the top.
- The BALI-Metal 8U experiment is simulated by DNS and three RANS models:  $k-\omega$  SST, standard  $k-\varepsilon$ , and RSM. The simulation results are compared with experimental data to evaluate the performance of the RANS models and DNS [11]. DNS

reproduces a two-distinct region flow structure consistent with the experimental observations. Furthermore, the  $k-\omega$  SST model predicts flow patterns similar to those obtained from DNS simulation. The temperature field tends to be homogeneous in all simulations due to the mixing effect of turbulence. However, all simulations, including DNS, tend to overpredict the temperatures compared to the experimental data at measurement locations.

## 3.2. Vessel failure mode

The failure of the RPV lower head due to corium attack during a severe accident is the transition point from in-vessel to ex-vessel progression of accident. Therefore, the prediction of RPV failure is important to analysis of accident progression and assessment of severe accident mitigation strategies.

Due to its importance, KTH-NPS have been performing coupled thermo-mechanical analyses of the lower head for many years, with the goal to develop predictive capabilities which can be used to assess the vessel failure characteristics (e.g., timing and mode of the failure).

The vessel failure analyses require the thermal load of corium relocated in the lower head. In the APRI-11 research the simulations of the MELCOR code for severe accident scenarios is chosen to provide such information. In perspective the thermal load should be provided by the in-vessel corium behavior study (see the preceding section). Details of the recent progress in this research direction are documented in articles [12]~[14] and the doctoral thesis [15]. Here we briefly present an application of the developed approach to the analyses of vessel failure [14] and penetration failure [15] in a Nordic BWR during postulated severe scenarios due to station blackout (SBO) and SBO+LOCA.

### 3.2.1. Vessel failure analysis

As mentioned above, the data of corium in the lower head of a Nordic BWR are obtained from the MELCOR simulation [39]. The penetrations in the lower head of the RPV are neglected. The ANSYS model for thermo-mechanical analysis can be found in [14].

Figure 3-16 shows snapshots of the vessel ablation process for the SBO scenario, as well as the corresponding temperature distribution at specific moments. After about six hours, the vessel wall commences the ablation process, which intensifies over time, culminating in a melt-through after 7.22 hours. The melt-through region occurs at the upper surface of the RPV lower head ( $\theta = 62.5^\circ$ ), a region that consistently exhibits the thinnest cross-section of the vessel wall during all stages. A similar ablation process is observed in the SBO+LOCA scenario (not shown here), with the vessel commencing ablation and melt-through at around 6 h and 7.33 h, respectively. In that case, the melt-through region appears slightly lower, at  $\theta = 57.5^\circ$ .

Table 3-2 summarizes the results of failure analysis using ANSYS Mechanical APDL for thermo-mechanical analysis, alongside relevant information from the MELCOR simulation. It is evident that the stress failure mechanism, rather than the strain failure and melt-through failure criteria, is the dominant failure mechanism in the ANSYS analysis for both the SBO and SBO+LOCA scenarios. Moreover, the vessel fails at its thinnest regions in both accidents (i.e.,  $60^\circ\sim 63^\circ$  in the SBO case and  $55^\circ\sim 58^\circ$  in the SBO+LOCA case) at  $t = 6.8$  h and 7.1 h, respectively.

The time and region of vessel failure from MELCOR simulation have a reasonable agreement with the results obtained from ANSYS simulation. Furthermore, the failure mechanism is also identified as stress-based, consistent with the findings from the structural analysis.

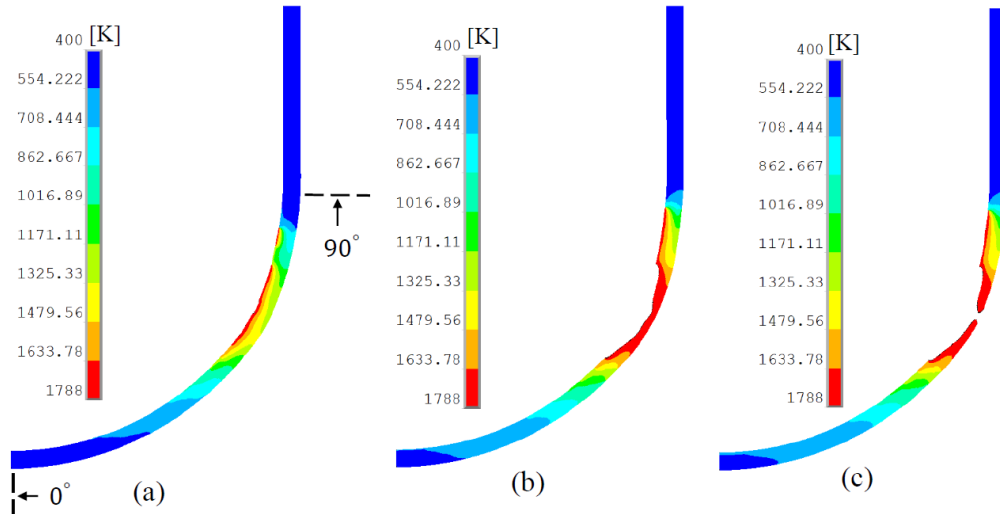


Figure 3-16: Dynamic ablation for SBO case: Temperature distribution [K] at time (a)  $t = 6$  h, (b)  $t = 7.16$  h, and (c)  $t = 7.22$  h.

Table 3-2: Data on vessel failure predicted by ANSYS and MELCOR

Accident scenario	SBO case		SBO+LOCA case	
	ANSYS	MELCOR	ANSYS	MELCOR
Failure time	$t=6.8$ hours	$t=6.7$ hours	$t=7.1$ hours	$t=6.9$ hours
Failure location	$60^{\circ}\sim 63^{\circ}$	$60.93^{\circ}\sim 63.89^{\circ}$	$55^{\circ}\sim 58^{\circ}$	$55.35^{\circ}\sim 57.88^{\circ}$
Failure mechanism	Ultimate stress	Yielding	Ultimate stress	Yielding

### 3.2.2. Penetration failure analysis

This study is to address the failure of penetrations in the lower head during a severe accident (e.g. SBO+LOCA). For this purpose, a three-dimensional model for a vessel wall incorporating a cluster of IGT structures is considered as shown in Figure 3-17 where three representative locations of IGTs are modeled. The structure of each IGT is illustrated in Figure 3-18, including a nozzle (marked in blue) and two weld joints (marked in purple). Notably, the penetration tube (marked in red) is not included in this study. This simplification is made to focus on the weld failure since it initiates IGT ejection.

An IGT ejection is caused by a failure of the top weld since it acts as the only support for the penetration tube. The IGT ejection leads to the release of molten materials into the reactor cavity. It is possible the IGT ejection is prevented by clamping if the gap between the vessel wall and the IGT is reduced to 0 mm due to deformation.

The behavior of the welds for all three IGT structures is investigated with three failure criteria (i) melt-through, (ii) stress-based failure, and (iii) strain-based failure. The simulation results show the top welds within the bottom and middle IGT structures undergo strain failure approximately at  $t = 2.2$  h and  $t = 5.8$  h, respectively. For the weld within the farthest IGT structure, apart from the strain failure at  $t = 3.2$  h, a melt-through failure



is also found at  $t = 5.5$  h. However, none of the three IGT welds exhibits stress-based failure, as the von Mises stress for all three welds consistently remains well below their ultimate stress during the entire simulation [15].

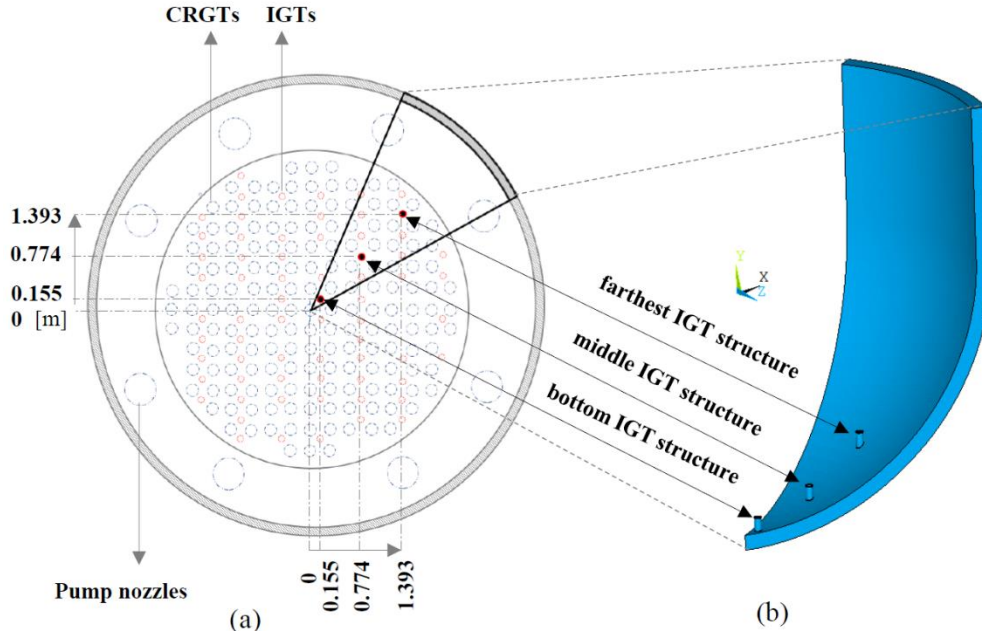


Figure 3-1: (a) Cross-section of BWR vessel lower plenum with CRGTs, IGTs, and pump nozzles, and (b) three-dimensional model of the RPV with a cluster of IGT structures. The tube is not included in the FE model.

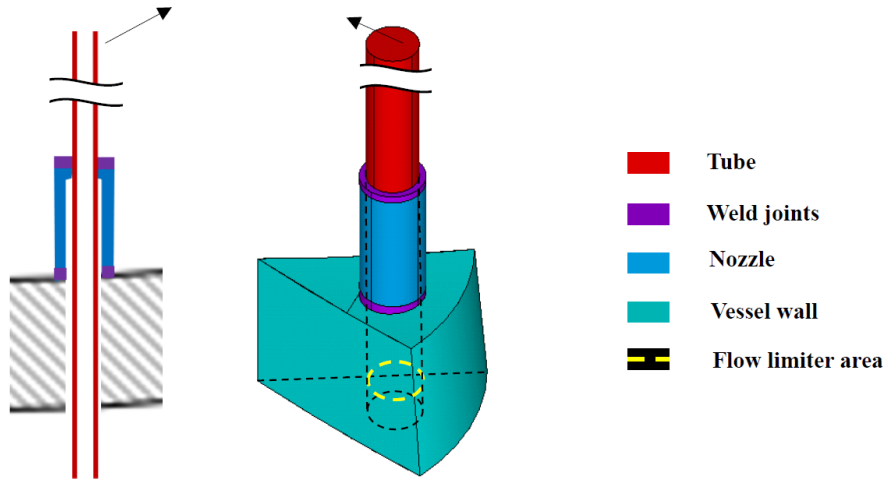


Figure 3-2: 2D and 3D schematics of the bottom IGT structure.

### 3.3. Melt-coolant interactions

The main objective of this study is to maintain the expertise in experimentation gaining basic understanding on fuel coolant interactions and steam explosion, using the DEFOR and MISTEE facilities developed at KTH-NPS during past two decades. Specifically, the study during APRI-11 is oriented to metallic melt-coolant interactions [16]~[21], as well

as single droplet quench and steam explosion in chemical solutions [22]~[26], which were not investigated in previous DEFOR and MISTEE studies.

The results have been well documented in publications [16]~[26], so below are just some highlights from the latest DEFOR and MISTEE experiments: material effect on melt-coolant interactions and steam explosion in chemical solutions.

### 3.3.1. Material effect on melt-coolant interactions

The DEFOR study [42][43] has been carried out to investigate the characteristics of debris beds by using various binary simulants (e.g.,  $\text{WO}_3\text{-CaO}$ ,  $\text{WO}_3\text{-Bi}_2\text{O}_3$ ,  $\text{Bi}_2\text{O}_3\text{-CaO}$ ) of  $\text{UO}_2\text{-ZrO}_2$  in corium. However, little attention has been paid to the metallic component (Zr/Fe) of corium in the previous DEFOR study, although it is well known that a substantial amount of metallic melt (Zr/Fe mixture) may also be available in corium, as indicated by the recent MELCOR simulation of severe accident scenarios in the Nordic BWR [39]. A configuration with oxidic debris particles submerged in a metallic melt pool may exist in the lower head upon RPV failure, resulting in metallic melt-coolant interaction at least for the initial discharge of corium from the RPV to the cavity. The different physical properties of metallic melt from oxidic melt, such as surface tension, thermal conductivity, thermal capacity and viscosity as well as chemical properties (oxidation) can have considerable influences on the melt fragmentation and debris formation.

To fill the knowledge gap in debris bed formation, a scoping study [16][17] has been carried out to gain the characteristics of metallic melt-coolant interactions and resulting debris beds, using molten Sn as a simulant of metallic melt of corium. To advance the research toward a comprehension, further studies are conducted by extending influential parameters [18] and using more simulants of metallic corium, including binary alloy Sn-Bi [19] and higher melting-point metal Zn [20]. New tests of oxidic melt-coolant interactions using  $\text{Bi}_2\text{O}_3\text{-WO}_3$  are also performed in the DEFOR facility whose crucible has been upgraded to overcome melt contamination appearing in the previous DEFOR and PULIMS studies [21].

Six tests as shown in Table 3-3 are selected to compare the effects of melt materials on melt-coolant interactions and debris bed formation. The tests M1, M2, M22 and O1 are at comparable superheat and the same subcooling conditions to delineate the effect of materials. The test O2 whose water subcooling is lower than that of O1.

Table 3-3: *Test matrix*

Parameter	M1	M2	M21	M22	O1	O2
Material	Sn	Sn-Bi	Zn	Zn	$\text{Bi}_2\text{O}_3\text{-WO}_3$	$\text{Bi}_2\text{O}_3\text{-WO}_3$
Mass fraction	-	57%-43%	-	-	43%-57 %	43%-57 %
Melt density [kg/M22]	7310	8560	7100	7100	7800	7800
Melting point [°C]	232	139	420	420	875	875
Melt temperature in nozzle [°C]	350	252	567	525	1000	1021
Melt superheat in nozzle [°C]	118	113	147	105	125	146
Melt delivery time [s]	7.1	4.7	5.7	6.6	6.1	6.7
Average flowrate [l/s]	0.58	0.50	0.5	0.43	0.44	0.41
Melt jet diameter [mm]	20					
Elevation of nozzle outlet [m]	1.73	1.73	1.75	1.75	1.75	1.75
Jet free fall height [m]	0.23	0.23	0.25	0.25	0.25	0.25
Melt volume [l]	4.1	2.34	2.82	2.82	2.56	2.56

Water pool depth [m]	1.5					
Water initial temperature [°C]	50	50	50	50	50	87
Water subcooling [°C]	50	50	50	50	50	13
Melt mass [kg]	30	20	20	20	25	25

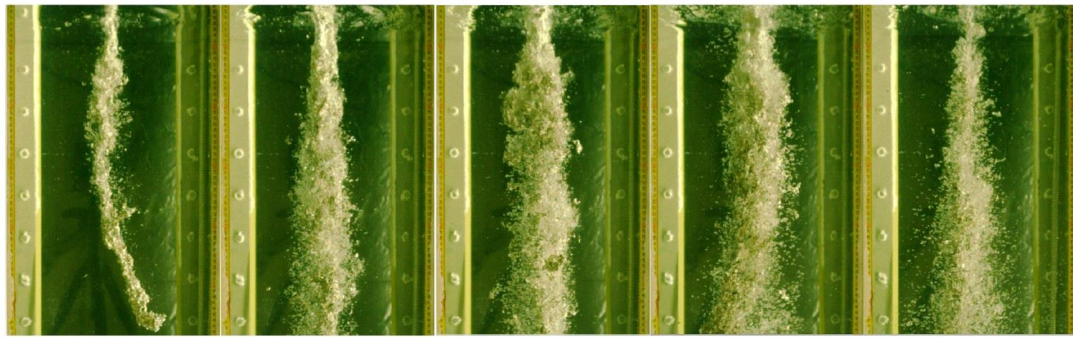
As shown in Figure 3-19, the melts are injected into the water pool and undergo considerably different processes, especially when comparing metallic and oxidic melt tests. The different background colors are the results of lighting effects, whose impact on data processing can be screened out. The snapshots gave the view of water pool from 1.5 m (water surface) to around 0.9 m, and time zero refers to the point when the melt touches the water pool surface.

The melt solidification occurs immediately upon its entry to the water pool in the test M2 with Sn-Bi melt, as shown in Figure 3-19a. After the first pour, the remaining melt jet is quenched with stripping but incomplete breakup, since the heat transfer between the melt and water is strong enough to solidify the melt before it fragments into particles. A similar solidification process is found in the test M1 with Sn as shown in Figure 3-19b, where steam explosion occurs multiple times, as marked by the red circles. However, most of the explosions are mild and located near the water surface. No steam explosion occurs in other tests. It is obvious that the melt fragmentation in the test M22 with Zn melt is stronger than those using Sn and Sn-Bi at the initial stage as illustrated in Figure 3-19c.

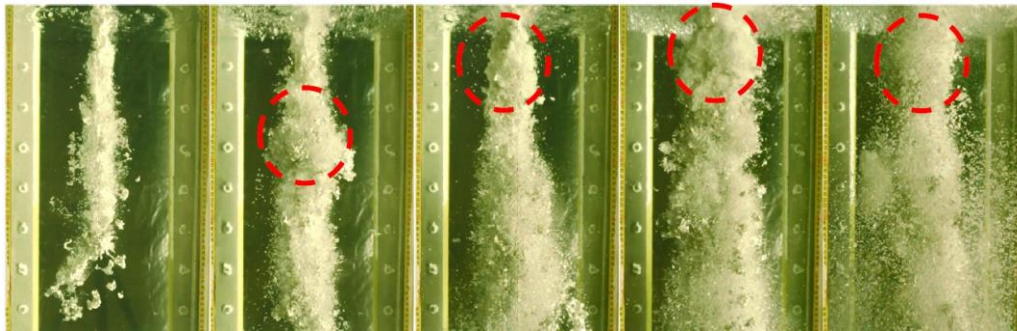
The test with Bi<sub>2</sub>O<sub>3</sub>-WO<sub>3</sub> melt show a considerable different view, as shown in Figure 3-19d. The oxidic melt jet core (red color) is covered by a vapor film at the initial stage and the stripped droplets are cooled down immediately and solidified (indicated by the black color).

In summary, it is observed that the metallic melt with higher melting point at the same superheat results in stronger heat transfer with water and an enhanced fragmentation, while all the other metallic melt tests experience a rapid solidification process, resulting in incomplete breakup of the melt jet, i.e., so-called “frozen jet”. On the other hand, the oxidic melt with a high melting point has less potential of solidification before jet breakup and fine fragmentation. The distinction may be attributed to different heat transfer modes and physical properties such as the ductility and the shear strength between oxidic melt and metallic melt.

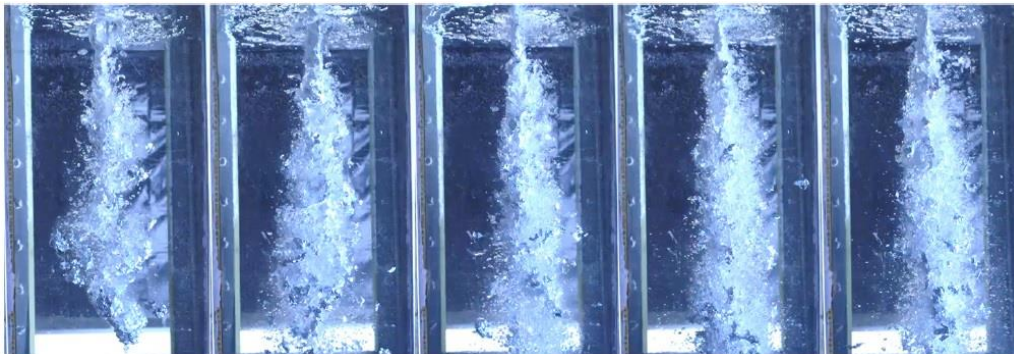
The final configuration of debris beds and particles morphology in different cases were characterized during the post-processing, shown in Table 3-4. Two types of debris bed were presented: (i) metallic debris beds are mainly composed of large, quenched chunks or large pieces of particles; (ii) oxidic debris beds are primarily composed of fine fragmented particles. It can be observed that the melt fragmentation is more intense as the melt temperature increases. In other words, the immediate solidification (formation of quenched chunks) is weaker and results in fine fragmentation (formation of small particles). Typical metallic particles are flake-like with smooth surface and large aspect ratio as the Zn case shows except the rough surface due to the covering powder in Sn case. Besides, metallic melt is usually sensitive to oxidation, especially in the Zn case where a thick oxidic layer formed on the surface of the particles, whereas particles in oxidic melt case are not in the condition of oxidation and they are spherically shaped with smooth surface and lower aspect ratio.



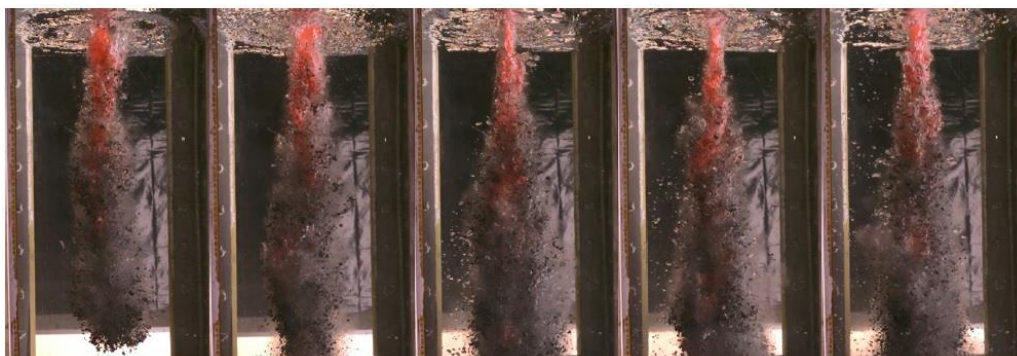
0.55 s      1.4 s      2.2 s      3.1 s      4.7 s  
 (a) DEFOR-M2 with Sn-Bi ( $T_{\text{sub}}=50\text{ }^{\circ}\text{C}$ ,  $T_{\text{sup}}=113\text{ }^{\circ}\text{C}$ ,  $T_{\text{melt}}=252\text{ }^{\circ}\text{C}$ )



0.87 s      1.4 s      2.2 s      3.1 s      5.8 s  
 (b) DEFOR-M1 with Sn ( $T_{\text{sub}}=50\text{ }^{\circ}\text{C}$ ,  $T_{\text{sup}}=118\text{ }^{\circ}\text{C}$ ,  $T_{\text{melt}}=350\text{ }^{\circ}\text{C}$ )



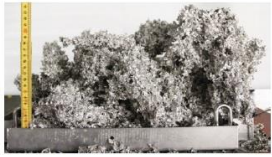










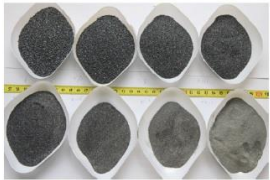
0.7 s      1.4 s      2.2 s      3.1 s      4.7 s  
 (c) DEFOR-M22 with Zn ( $T_{\text{sub}}=50\text{ }^{\circ}\text{C}$ ,  $T_{\text{sup}}=105\text{ }^{\circ}\text{C}$ ,  $T_{\text{melt}}=525\text{ }^{\circ}\text{C}$ )



1 s      1.4 s      2.2 s      3.1 s      4.7 s  
 (d) DEFOR-O1 with  $\text{Bi}_2\text{O}_3\text{-WO}_3$  ( $T_{\text{sub}}=50\text{ }^{\circ}\text{C}$ ,  $T_{\text{sup}}=125\text{ }^{\circ}\text{C}$ ,  $T_{\text{melt}}=1000\text{ }^{\circ}\text{C}$ )

Figure 3-19: Snapshots of melt water interactions with different materials.

Table 3-4: Debris bed and particle morphology in cases with different materials

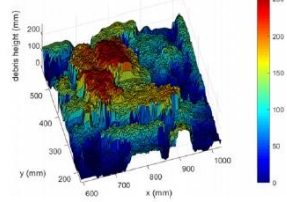

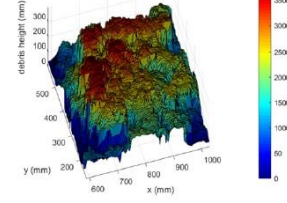

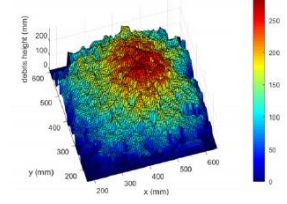
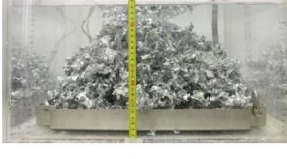
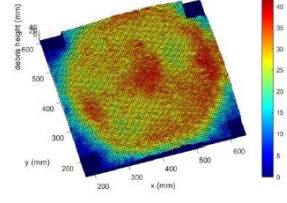
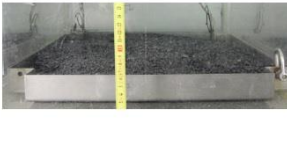
Case	Debris bed	Cross section	Particle morphology
M2 Sn-Bi $T_{sub}=50\text{ }^{\circ}\text{C}$ $T_{sup}=113\text{ }^{\circ}\text{C}$ $T_{melt}=252\text{ }^{\circ}\text{C}$			
M1 Sn $T_{sub}=50\text{ }^{\circ}\text{C}$ $T_{sup}=118\text{ }^{\circ}\text{C}$ $T_{melt}=350\text{ }^{\circ}\text{C}$			
M22 Zn $T_{sub}=50\text{ }^{\circ}\text{C}$ $T_{sup}=105\text{ }^{\circ}\text{C}$ $T_{melt}=525\text{ }^{\circ}\text{C}$			
O1 $\text{Bi}_2\text{O}_3\text{-WO}_3$ $T_{sub}=50\text{ }^{\circ}\text{C}$ $T_{sup}=125\text{ }^{\circ}\text{C}$ $T_{melt}=1000\text{ }^{\circ}\text{C}$			

Post-test analysis of the debris beds is performed to obtain the geometrical parameters and porosity of the debris beds.

Table 3-5 shows the average height, total porosity, open porosity, and closed porosity of the four debris beds with different materials. The total porosity of debris beds slightly enlarged with increasing melt temperature at almost same melt superheat. Notably, the total porosity of metallic melt case was around 90% due to the presence of huge cavity between the large chunks, while that of oxidic melt case was 50%. Besides, the closed porosity in oxidic melt cases was also smaller than that of metallic cases, which can be explained by the finer fragmentation in oxidic melt cases, providing lower chance for pore structure formation. The higher ductility and larger shear strength in metallic melt cases may also favor the generation of larger closed cavities.

In the post-test analysis, the size distribution of debris particles in each debris bed is also obtained. Based on the mass fraction of debris particles, the averaged and median sizes of particles are defined. The mass fraction of debris particles and cumulative size distribution of debris particles in the four debris beds can be found in [20]. For the fraction of debris particles from complete fragments increases with higher melt temperature at the same superheat, suggesting stronger melt-coolant interactions. The average size of metallic particles is considerably larger than that of oxidic ones. This is caused by the rapid solidification in metallic melt at medium water subcooling and stronger fragmentation in oxidic melt. In addition, the oxidic melt has lower shear strength, and therefore it is more likely to fragment into small particles.

Table 3-5: Porosity measurements in cases with different materials

Case	Debris bed scanning (3D) for $P_{total}$	Debris bed immersed in water tank for $P_{closed}$	Characteristics
M2 Sn-Bi $T_{sub}=50\text{ }^{\circ}\text{C}$ $T_{sup}=113\text{ }^{\circ}\text{C}$ $T_{melt}=252\text{ }^{\circ}\text{C}$			$h_{average} = 107.5\text{ mm}$ $P_{total} = 87.9\%$ $P_{closed} = 8\%$ $P_{open} = 79.9\%$
M1 Sn $T_{sub}=50\text{ }^{\circ}\text{C}$ $T_{sup}=118\text{ }^{\circ}\text{C}$ $T_{melt}=350\text{ }^{\circ}\text{C}$			$h_{average} = 210\text{ mm}$ $P_{total} = 91.1\%$ $P_{closed} = 9.1\%$ $P_{open} = 82\%$
M22 Zn $T_{sub}=50\text{ }^{\circ}\text{C}$ $T_{sup}=105\text{ }^{\circ}\text{C}$ $T_{melt}=525\text{ }^{\circ}\text{C}$			$h_{average} = 134.5\text{ mm}$ $P_{total} = 90\%$ $P_{closed} = 13\%$ $P_{open} = 77\%$
O1 $\text{Bi}_2\text{O}_3\text{-WO}_3$ $T_{sub}=50\text{ }^{\circ}\text{C}$ $T_{sup}=125\text{ }^{\circ}\text{C}$ $T_{melt}=1000\text{ }^{\circ}\text{C}$			$h_{average} = 26.5\text{ mm}$ $P_{total} = 55\%$ $P_{closed} = 4.8\%$ $P_{open} = 50.2\%$

### 3.3.2. Steam explosion in chemical solutions

The MISTEE (Micro-Interactions in Steam Explosion Experiments) platform was developed to pursue a basic understanding of melt-coolant interactions and steam explosion phenomena using a single molten droplet under well-controlled test conditions and applying up-to-date instrumentation.

In addition to an effort to upgrade the MISTEE facility for high-temperature operation [22], an extensive study has been carried out in the MISTEE facility to investigate single droplet quench and steam explosion in chemical solutions with additives of  $\text{H}_3\text{BO}_3$ , NaOH and  $\text{Na}_3\text{PO}_4$ , in water [23]~[24], as well as in seawater [25]. Boric acid ( $\text{H}_3\text{BO}_3$ ) is widely adopted as an additive in the coolant of light water reactors for reactivity control, and NaOH and  $\text{H}_3\text{BO}_3$  are also employed in water chemistry to adjust the pH values of reactor coolant since the  $\text{H}_3\text{BO}_3$  solution has acidity. Seawater may be utilized in extreme events such as the Fukushima accident. The quench of high-temperature spheres in a seawater pool is also investigated [26] to obtain the effect of seawater on vapor film stability

and quenching process. The description below is only limited to the effect of chemical solutions and seawater on the risk of steam explosion. More details can be found in [22][23]~[25].

The test matrix is as shown in Table 3-6 which lists five groups of tests whose concentrations of  $H_3BO_3$  vary from 0 to 3.2 wt.%. To examine the effect of  $H_3BO_3$  concentration, melt and water temperatures in all tests are fixed at 800 °C and 20 °C, respectively. To achieve the statistics of spontaneous steam explosion of a single droplet, each test under the same condition is repeated 20 times.

Table 3-6: Test matrix for  $H_3BO_3$  solution

Test ID	Coolant	Coolant temp. (°C)	Melt mass (g)	Free-fall distance (mm)	Melt temp. (°C)	Melt supeheat (°C)	Times of test (n)
DI-800-20-n	Deionized water	20	1	100	800	569	20
BA0.2-800-20-n	0.2wt.% $H_3BO_3$ solution						
BA1.2-800-20-n	1.2wt.% $H_3BO_3$ solution						
BA2.2-800-20-n	2.2wt.% $H_3BO_3$ solution						
BA3.2-800-20-n	3.2wt.% $H_3BO_3$ solution						

When a molten droplet interacts with coolant, the droplet is surrounded by a vapor film due to intense film boiling at the droplet's surface. The vapor film effectively prevents direct contact between melt and coolant. Due to deformation of droplet and continuous cooling, the vapor film becomes unstable and finally collapsed. Upon the collapse of vapor films, a direct contact between the melt and coolant occurs. As a result, the droplet is either quenched with little fragmentation or exploded with fine fragmentation. The former may be caused by solidification which has taken place before the melt-coolant contact, while the later may involve penetration of coolant into the droplet, creating more direct contact area for explosive vaporization (e.g. escalating to a steam explosion).

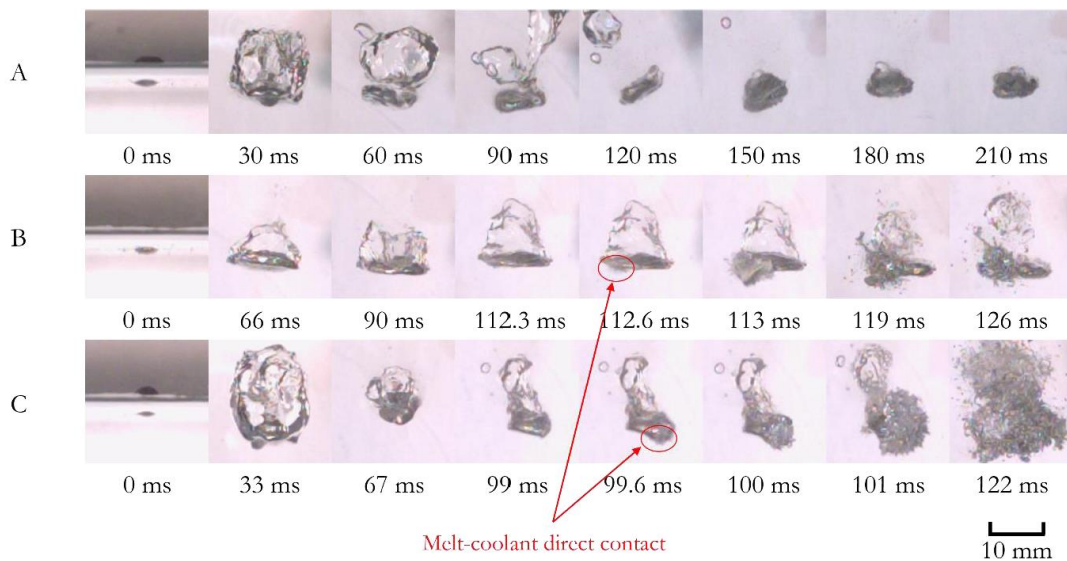


Figure 3-20: *Snapshots of three typical phenomena observed in tests (1g Sn,  $T_m=800$  °C,  $T_c=20$  °C, DI water).*

Figure 3-20 shows three typical phenomena observed in tests: Phenomena A and B have no and minor fragmentation of the droplet, respectively, while Phenomenon C involves a steam explosion. For the occurrence of Phenomenon A, the surface of the droplet should be solidified when it comes into direct contact with coolant, and therefore the droplet have no significant fragmentation. In Phenomenon B, the droplet has minor fragmentation which incurs a negligible change in pressure wave as indicated by the signal of the pressure sensor on the wall of the coolant tank. As for Phenomenon C, the molten droplet breaks up explosively, leading to an obvious peak pressure captured by the pressure sensor. Besides, the morphologies of fragments collected after tests also show a significant difference among the three phenomena. As shown in Figure 3-21, three comparable sizes of fragments from the three phenomena also have different morphologies: the surface of the fragment from Phenomenon A is smooth, while it is partly porous in the particle from Phenomenon B. Due to steam explosion, the fragments in tests with Phenomenon C are fully porous.

In both Phenomena B and C, there is a moment when the vapor film surrounding the droplet begins to rupture at a point, causing a direct contact of partial melt surface with coolant (see Figure 3-20) at 112.6 ms for Phenomenon B and at 99.6 ms for Phenomenon C). Consequently, the corresponding interface between the melt and coolant became unclear due to cloud shadow of fragments, and the criterion for differentiating Phenomenon C from Phenomenon B is the presence of a peak pressure. In Phenomenon A, the contour of the droplet is always clear throughout the quench process of the droplet. Based on the distinct features of image, dynamic pressure and debris morphology mentioned above, the three phenomena A, B and C can be effectively distinguished.



Figure 3-21: *Morphology of debris from three typical phenomena in tests.*

Figure 3-22 illustrates the probability of each phenomenon varying with  $H_3BO_3$  concentration – here the probability denotes the fraction of occurrence within 20 runs of test. Interestingly, the probability of spontaneous steam explosion decreases from 45% to 25% when the  $H_3BO_3$  concentration in the coolant increases from 0 to 1.2 wt.%, while it increases from 25% to 75% when the  $H_3BO_3$  concentration increases from 1.2 wt.% to 3.2 wt.%. Oppositely, the occurrence probability of Phenomena B (minor fragmentation) increases from 45% to 70% when the  $H_3BO_3$  concentration increases from 0 to 1.2 wt.%, and then decreases from 70% to 25% when the  $H_3BO_3$  concentration increases from 1.2 wt.% to 3.2 wt.%. In the solution of 3.2 wt.%  $H_3BO_3$  concentration, there is no occurrence of Phenomenon A, while in the other solutions there is a 5~10% probability for the occurrence of Phenomenon A.



The initially declining and then rising probability of steam explosion with increasing  $H_3BO_3$  concentration suggests that more than two competing factors are influencing spontaneous steam explosion of molten droplet as the  $H_3BO_3$  concentration increases.

If the quench depth is defined as the distance the droplet travels to the point of the first melt-contact in the coolant pool, it is found the mean quench depth in the  $H_3BO_3$  solution is smaller than that in the deionized water. Furthermore, the statistics of quench depth show the range of appearing quench depth becomes more concentrated when the  $H_3BO_3$  concentration reaches or exceeds 1.2 wt.%. This discovery demonstrates that the presence of  $H_3BO_3$  in the solution has an impact on the stability of the vapor film surrounding the droplet. Thus, the addition of  $H_3BO_3$  in coolant increases the likelihood of melt-coolant contact, particularly when the  $H_3BO_3$  concentration surpasses 1.2 wt.%.

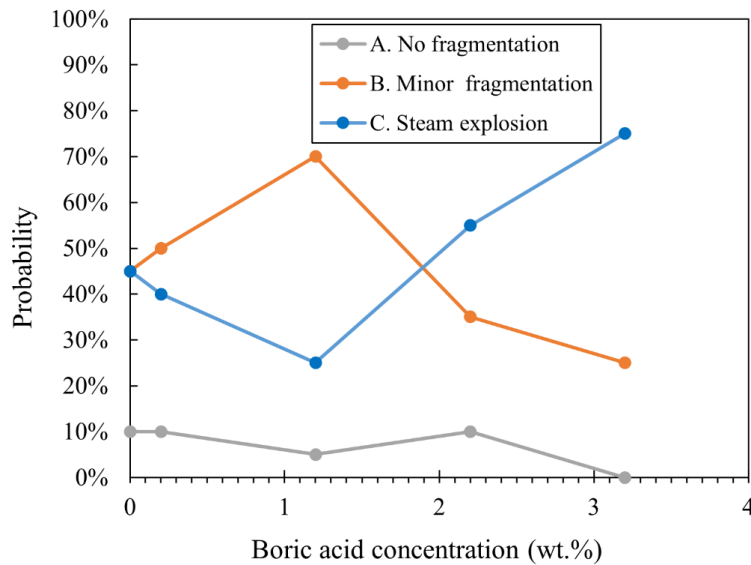


Figure 3-22: Occurrence probability of three typical phenomena against  $H_3BO_3$  concentration.

Figure 3-23 shows the lateral deformation ratio of droplet at the quench depth versus  $H_3BO_3$  concentration. One can see that the  $H_3BO_3$  concentration slightly affects both the statistical values of lateral deformation ratio and their mean (the dashed line). Given a concentration of boric acid in coolant, melt-coolant contact may occur when the lateral deformation ratio reaches a threshold. Interestingly, the lateral deformation ratio at quench depth slightly decreases initially and then increases with increasing  $H_3BO_3$  concentration.

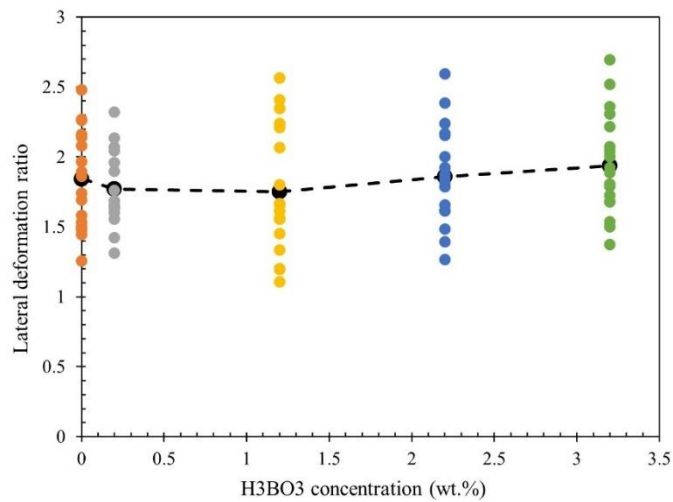


Figure 3-23: *Statistics of lateral deformation ratio at various  $H_3BO_3$  concentrations.*

The comprehension of above two parameters implies that it is more likely for the Sn droplet to deform more at the same depth in coolant as the  $H_3BO_3$  concentration increases up to a critical value (say,  $>1.2$  wt.%), thus increasing the probability of melt-coolant contact. Thus, the potential for spontaneous steam explosion is elevated with increasing  $H_3BO_3$  concentration since melt-coolant contact is a prerequisite for steam explosion. This reflects the contribution of boric acid concentration to steam explosion.

The non-monotonous trend of droplet lateral deformation ratio against  $H_3BO_3$  concentration suggest again that more than two competing factors are influencing melt-coolant interactions.

The pressure impulse is a good measure of steam explosion energetics, and it can be computed from the pressure-time curve in a steam explosion. The impulse of steam explosion is employed below to compare the influence of  $H_3BO_3$  concentration on steam explosion energetics.

Figure 3-24 shows the statistical variance of impulses generated by steam explosions in coolants with various  $H_3BO_3$  concentrations. One can see that the impulses appearing in the DI water and 2.2 wt.%  $H_3BO_3$  solution are nearly identical. However, steam explosions in 0.2 wt.%, 1.2 wt.% and 3.2 wt.%  $H_3BO_3$  solutions may produce much higher impulses. According to the results obtained in the present study, there is no apparent correlation between impulse and  $H_3BO_3$  concentration, i.e., the impulses of steam explosion do not show a trend with the change of boric acid concentration in the solution, possibly due to the randomness of steam explosion location and its distance to the pressure sensor which are not considered in impulse estimation.

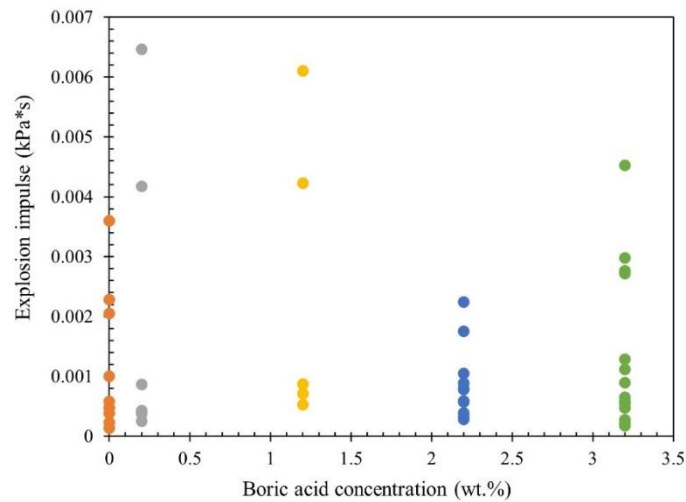


Figure 3-24: Impulse of steam explosion in solutions with different  $H_3BO_3$  concentrations.

A stronger steam explosion should result in fine fragmentation of a larger portion of droplet, and therefore the size distribution of debris particles is another measure of steam explosion energetics. Analyzing the debris size distribution in various  $H_3BO_3$  solutions can shed light on the role of  $H_3BO_3$  concentration in the occurrence of steam explosion. To observe the trend of debris size distribution in single droplet-coolant interactions, debris particles are collected from 20 runs of test under the same condition and seized.

The cumulative mass percentage of debris particles in different sizes is plotted in Figure 3-25. With other test conditions fixed, when the  $H_3BO_3$  concentration in coolant is between 0 and 2.2 wt.%, the  $H_3BO_3$  concentration has little impact on the size distribution of debris particles collected from 20 runs of test under every  $H_3BO_3$  concentration. However, a higher fraction of fine debris particles is produced from the 20 runs of test carried out in the solution of 3.2 wt.%  $H_3BO_3$  concentration. This result can be attributed to the elevated likelihood of steam explosion at high  $H_3BO_3$  concentration.

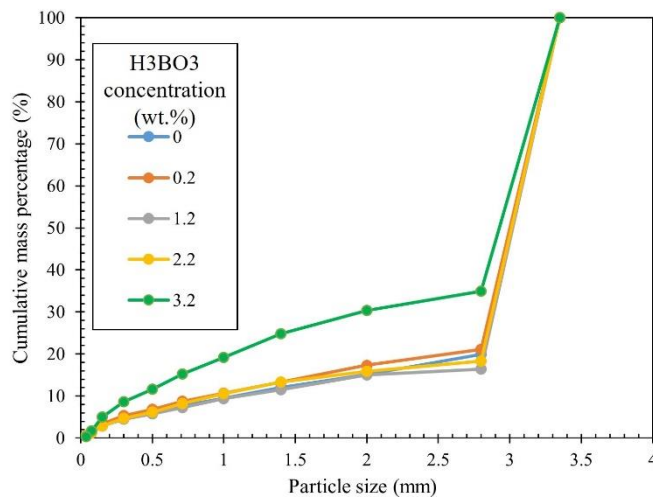


Figure 3-25: Cumulative mass percentage of debris particles in different sizes.

To obtain a neutral solution with pH value of 7 as expected in nuclear power plants, a  $H_3BO_3$  solution is carefully mixed with either  $Na_3PO_4$  solution or a NaOH solution, as

shown in Table 3-7. The mixed solution is then applied in the single drop steam explosion.

Table 3-7: Test matrix for various chemical solutions

Test ID.	Coolant	Coolant temp. (°C)	Melt mass (g)	Free-fall distance (mm)	Melt temp. (°C)	pH value (/)	Number of test (n)
DI-n	Deionized water	20	1	100	800	6.7	20
BA1.2-n	1.2wt.%H <sub>3</sub> BO <sub>3</sub> solution					4.9	
BA3.2-n	3.2wt.%H <sub>3</sub> BO <sub>3</sub> solution					4.1	
BA1.2-NP-n	1.2wt.%H <sub>3</sub> BO <sub>3</sub> +Na <sub>3</sub> PO <sub>4</sub> neutral solution					7	
BA3.2-NP-n	3.2wt.%H <sub>3</sub> BO <sub>3</sub> +Na <sub>3</sub> PO <sub>4</sub> neutral solution						
BA3.2-NH-n	1.2wt.%H <sub>3</sub> BO <sub>3</sub> +NaOH neutral solution						
BA3.2-NH-n	3.2wt.%H <sub>3</sub> BO <sub>3</sub> +NaOH neutral solution						

Figure 3-26 illustrates the probability of steam explosion in different solutions varying with boric acid concentration, where the probability denotes the fraction of steam explosion within 20 runs of test. As mentioned above, the concentration of H<sub>3</sub>BO<sub>3</sub> in the coolant increases from 0 to 1.2 wt.%, the likelihood of spontaneous steam explosion decreases from 45% to 25%. Then, further increasing the H<sub>3</sub>BO<sub>3</sub> concentration to 3.2 wt.%, the probability of steam explosion increases from 25% to 75% correspondingly. However, in the neutral solutions of H<sub>3</sub>BO<sub>3</sub> and NaOH, the steam explosion probability is only slightly affected by the concentration of boric acid (ranging from 40% to 50%). While in neutral solutions of H<sub>3</sub>BO<sub>3</sub> and Na<sub>3</sub>PO<sub>4</sub>, the steam explosion probability increases from 45% to 70% as the H<sub>3</sub>BO<sub>3</sub> concentration rises from 0 to 1.2 wt.%, but decreases from 70% to 40% with the H<sub>3</sub>BO<sub>3</sub> concentration further increasing from 1.2 wt.% to 3.2 wt.%.

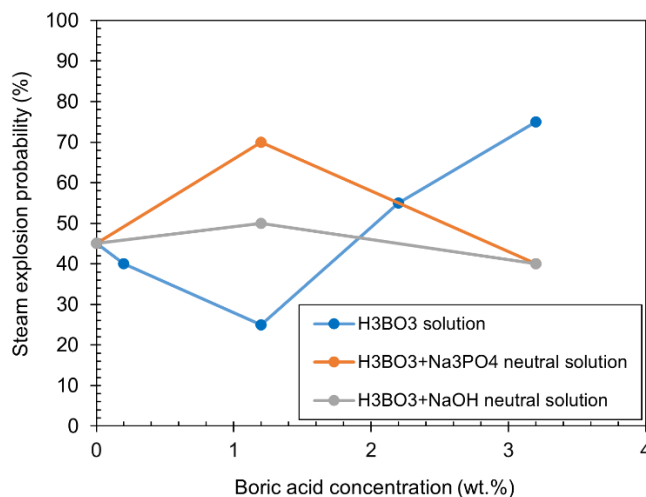


Figure 3-26: Steam explosion probability against H<sub>3</sub>BO<sub>3</sub> concentration in different solutions.

The experimental results indicate that adding NaOH or Na<sub>3</sub>PO<sub>4</sub> to the H<sub>3</sub>BO<sub>3</sub> solution significantly influences the occurrence probability of spontaneous steam explosion. Comparing the probability of steam explosion in the neutral solutions of Na<sub>3</sub>PO<sub>4</sub> and NaOH infers that the presence of PO<sub>4</sub><sup>3-</sup> and H<sup>+</sup> ions and derived ions (such as HPO<sub>4</sub><sup>2-</sup> and HBO<sub>3</sub><sup>2-</sup>) may affect steam explosion. More results from the study on single drop steam explosion in chemical solutions are documented in [24].

### 3.3.3. Ex-vessel melt-structure interactions

Previously, all studies on ex-vessel steam explosion and debris coolability were based on such an assumption that a coherent melt jet falls from the lower head of the RPV into a deep-water pool in a severe accident scenario of a reference Nordic boiling water reactor (BWR). However, it is well known that the BWR has a forest of structures (e.g., control rod driving mechanisms) and supporting plates below the lower head of the RPV. It is still an open question on how the structures below the RPV of a BWR will affect ex-vessel corium risks. Therefore, it was decided that a research task will be dedicated to this topic in APRI-11.

The first effort [27] has been focused on conducting a literature study on relevant phenomena under the scope of ex-vessel corium-structure interactions. It was found that BWR ex-vessel structures had been simplified as a combination of horizontal and vertical structures in a few previous considerations. Three phenomena of interest have been selected – splashing of melt, ablation of structure caused by melt impingement and melt freezing, focusing on existing experimental, numerical and modelling efforts. More details can be found in [27], some main remarks are included here:

- Impingement splashing: A typical experimental setup for the splashing phenomena contained a nozzle and target plate coupled with hygroscopic paper to collect splashed-off liquid. Main focuses of such kinds of study were the onset of splashing and the fraction of splashed-off liquid. One key conclusion from such studies was that the splashing phenomenon was highly related to the Weber number. A high Weber number usually results in a jet-splashing ratio of as much as 75% of the incoming fluid under certain conditions. This implies the possibility of significant splashing of melt in certain severe accident (SA) scenarios, a factor that has not been adequately addressed in most SA analysis codes and hence it represents a potential improvement orientation in research.
- Impingement ablation: Such a phenomenon is the process of structure erosion by the impinging jet whose temperature is higher than the melting point of the structure. In SA cases, two distinctive scenarios could be expected depending on whether the jet and structure are of similar composition. If the jet and structure are of materials thermally very different from each other, such as oxidic melt impinging on a metallic substrate, a crust will form and significantly influence the heat transfer and melting process. There has been extensive experimental work on such phenomenon before the year 2000, and the main focuses are the heat transfer and erosion rate at the impingement zone, towards the effect of the molten layer and crust. In recent years, such a phenomenon has been further studied and the focuses are the cavity shape evolution, transition between film and pool regime and dynamics of the liquid exit with the ultimate purpose of core catcher design. Heat transfer correlations at the impingement zone have been proposed by several researchers, which can be used for structure failure analysis during SA. However, the validity of these findings might require closer scrutiny, especially in cases of

complex geometric setups such as those involving ex-vessel structures. In recent years, there have been some numerical efforts addressing the ablation phenomenon. In general, rather “simple” processes are simulated with mesh-based methods. These methods have shown difficulties and limitations in processing fluids with large deformation and fragmentation, and high-degree of simplification is needed in most cases. Meanwhile, mesh-free methods demonstrate a higher capability to handle complex phenomena and have successfully reproduced most of the phenomena during jet impingement, indicating a potential research orientation for the current task.

- Melt freezing: The term “melt freezing” here refers more to situations where molten material is exposed to the central passage of penetrations and moves inside given the pressure difference between the primary system and containment. Extensive experimental work has been undertaken in the past, with main focus on the course of flow regimes, freezing characteristics and material deposition. The most recent studies further considered the effect of particles to address situations where debris is a mixture of molten and solidified material. Two melt freezing models have been proposed – the conduction-limited freezing model and the bulk freezing model. The mechanisms described by these two models can happen simultaneously and the two models can usually bound the range of melt penetration lengths measured in experiments. Several simulations of the freezing phenomena have been conducted in the past twenty years, and it shows a trend of transition toward the usage of mesh-free methods. Finally, coming back to the current work package, for scenarios of ex-vessel melt-structure interaction, melt freezing on (but not inside) structures should also be addressed, shedding light on possible research improvement.

The second effort [28] is focused on understanding of the ex-vessel structures configuration and on collecting relevant design data of a reference Nordic BWR. At this step, a typical Nordic BWR 3 (BWR 75 design) was chosen as the reference plant; see Figure 3-27. The RPV lower head wall is perforated by 169 control rod drive (CRD) guide tube penetrations and 72 instrument guide tube penetrations. Inside the RPV lower head, the CRD guide tubes are welded to the nozzles that are then welded to the lower head. The CRD guide tube-nozzle welds exist at the top of the nozzles, about 35 cm above the lower head. A damper-type mechanism exists near the ex-vessel end of the CRD guide tubes, providing extra support to the tubes and keeping them in place in the case of weld failure. The instrument guide tubes, on the other hand, are not supported by other measures than the in-vessel welds to the nozzle top at about 15 cm from the lower head. That’s why the ejection of guide tubes is usually expected to happen in the case of weld failure. Below the RPV lower head, there exists a radiation shield about 120 mm thick perforated by the CRD guide tubes and the instrument guide tubes. It should be pointed out that several working platforms exist below the CRD guide tubes, which will not, however, be considered for the moment. Key geometric parameters of the ex-vessel structures are summarized in Table 3-8.

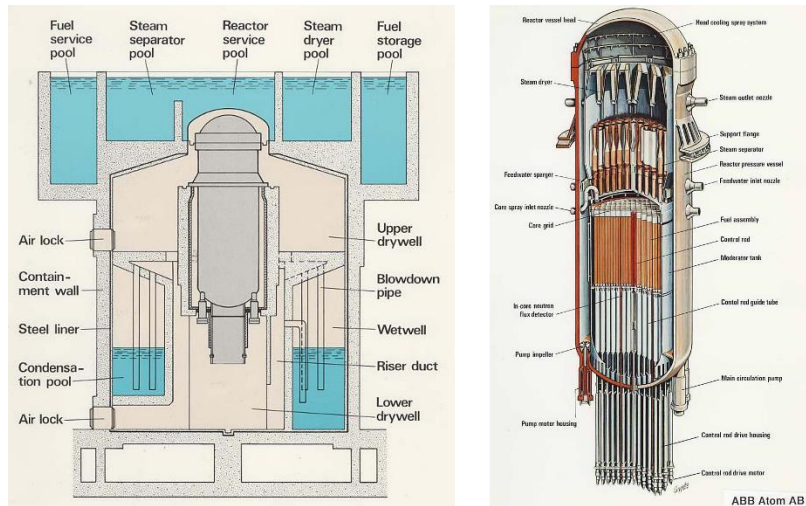


Figure 3-27: Schematic of a Nordic BWR.

Table 3-8: Key geometric parameters of ex-vessel structures

Category	Component	Parameter	Dimension (mm)	Description	Vertical distance (mm)
Vertical	CRD	Pitch	300	Bottom of vessel to radiation shield	~ 475
		Housing outer diameter (OD)	190	Radiation shield thickness	120
		Housing inner diameter (ID)	156	Bottom of radiation shield to top of dampers	~ 4500
		Motor part OD	265	Damper thickness	122
		Motor part height	800	Damper to water surface	~ 900
	IGT	Housing OD	70	Water surface to bottom of dry well	~ 7500
Horizontal	Radiation shield	Thickness	120		
		Hole diameter for CRD	220		
		Hole diameter for IGT	90.5		
	Dampers	Thickness	122		
		OD	309.5		
		ID	156		

The recent effort has been focused on conceptualizing potential research orientations. One is the analytical modelling of the relocation process and the other is experimental study on downward melt relocation by ablation of structures.

For the analytical modelling part, preliminary results have been obtained for the process of horizontal structure ablation by jet impingement. Since there is a radiation shield below the RPV lower head wall, a research interest is how this shield will affect the melt downward relocation process. The schematic is presented in Figure 3-28, physical parameters of melt jets are determined in a simplified manner with assumptions that no “pool effect” and mechanical effects are considered.

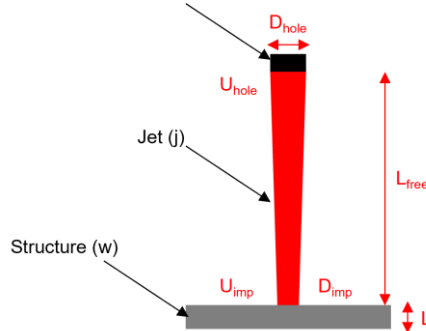


Figure 3-28: Schematic of the jet impingement scenario.

The Bernoulli's equation is applied to compute melt discharge flow rates.

$$U_{hole} = C_D \sqrt{\frac{2\Delta P}{\rho_j}} \quad (1)$$

where  $C_D$  is a discharge coefficient of value 0.6 here.  $\Delta P$  is the overpressurization of the RPV. Melt velocity at the impingement point at the structure is calculated as

$$U_{imp} = (U_{hole}^2 + 2gL_{free})^{1/2} \quad (2)$$

where  $L_{free}$  is the free fall height from the melt discharge opening to the radiation shield. Melt stream diameter impinging upon structure is calculated as

$$D_{imp} = D_{hole} \sqrt{\frac{U_{hole}}{U_{imp}}} \quad (3)$$

With the assumption of a purely energy-controlled erosion mechanism, the ablation rate of the structure is computed as

$$V_{abl} = \frac{q_{imp}}{\rho_w [H_{fusion,w} + C_{p,w}(T_{mp,w} - T_{o,w})]} \quad (4)$$

where the heat flux at the impingement point is computed as

$$q_{imp} = \begin{cases} h_{imp}(T_j - T_{mp,w}) & \text{without crust} \\ h_{imp}(T_j - T_{mp,j}) & \text{with crust} \end{cases} \quad (5)$$

The heat transfer coefficient  $h_{imp} = \frac{Nu_{imp}k_j}{D_{imp}}$  is computed from

$$Nu_{imp} = \begin{cases} 0.0152Re_{imp}^{0.92}Pr_{imp}^{0.8} & \text{metallic melt} \\ 0.0033Pe_{imp} & \text{oxidic melt} \end{cases} \quad (6)$$

Finally, the structure melt-through time and the melt-discharge time are computed as

$$\Delta t_{abl} = L/V_{abl} \quad (7)$$

$$\Delta t_{discharge} = m_{melt}/(U_{hole}S_{hole}\rho_{jet}) \quad (8)$$

A sample calculation is conducted here where the main input is shown in Table 3-9.

Table 3-9: Main inputs of the sample calculation

Parameter	Value
$D_{hole}$	5, 15, 30 cm
$\Delta P$	0.2 MPa
$L_{free}$	0.5 m
$L$	10 cm
$m_{melt}$	35 tons
Melt super heat	10, 50, 100, 150, 200, 250, 300 K
$T_{o,w}$	416 K

The structure melt-through time and the melt-discharge time given these input values are shown in Figure 3-29. A general trend of the melt-through time is that it decreases with increasing superheat and increases with decreasing melt discharge hole diameter. Comparing the values of melt-through time and melt-discharge time, it can be seen that in small jet cases, the melt-through time is very small in comparison to the melt-discharge time, indicating a minor effect of the radiation shield throughout the whole melt discharge process. However, in middle/large jet cases, especially when melt superheat is low, the



melt-through time is comparable to the melt-discharge time. In such scenarios, considerable melt will spread over the radiation protection plate. The next step in the study is to find or develop an adequate tool to address this situation.

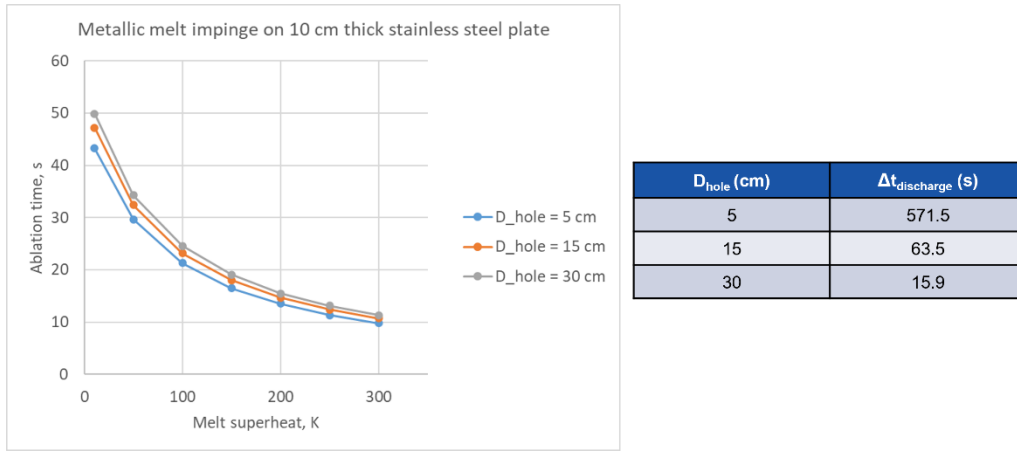


Figure 3-29: Results of the sample calculation.

The experimental part of this study is still in a conceptual phase and under development. The objective of such a study is to investigate melt relocation process within a structure such as the dense “forest” of motors and drive mechanisms for the control rods. Indeed, experiments under prototypical conditions, materially and geometrically speaking, are not feasible, and therefore geometry scaling and proper selection of simulants for both melt and structures need to be performed. Moreover, appropriate test conditions need to be specified.

### 3.4. Reactor applications and safety analyses

The objective of this topical study is to perform reactor safety analyses through applying the research results (e.g., models, computer codes) to the Swedish nuclear power safety context. Methodologies have been developed during APRI-11 to investigate ex-vessel debris bed coolability in a Nordic BWR and ex-vessel corium risk in a Swedish PWR, respectively.

#### 3.4.1. Ex-vessel debris bed coolability in a Nordic BWR

In the severe accident management strategy (SAMG) for Nordic boiling water reactors (BWRs), a flooded reactor cavity is conceived to receive corium in case of vessel failure, so that the discharged corium is expected to fragment and form a coolable particulate debris bed in the deep water pool. The MELCOR code has been selected by KTH-NPS to analyze hypothetical severe accidents of a Nordic BWR, since it has models for many accident phenomena and can integrally simulate severe accident progression of light water reactors. However, the code does not have models for thermal-hydraulics of debris beds, so it cannot predict the coolability of ex-vessel debris beds, although such predictive capability is important to assess the SAMG of Nordic BWRs.

To overcome the limitation of MELCOR, a surrogate model (SM) for estimation of debris bed coolability was developed and coupled with MELCOR [44] in the previous phase of APRI (APRI-10). The surrogate model is used to justify whether a debris bed is coolable or not under given decay power and debris bed characteristics, i.e., to estimate long-term

coolability under steady state. Since a debris bed formed on the cavity basement could be very hot at the beginning, quenching of the debris bed (a transient process) is a prerequisite step prior to the long-term coolability. To consider the precursory phase of coolability, the coupled MELCOR/COCOMO simulation has been employed to simulate quench process of ex-vessel debris beds in severe accident scenarios of a Nordic BWR [29][30]. Nevertheless, COCOMO is a mechanistic code for modeling of thermal-hydraulics in debris beds, so its calculation is much slower than MELCOR. To reduce the computational cost of MELCOR/COCOMO simulation, two surrogate models have been developed and coupled with MELCOR to realize quick estimations of the quench process of ex-vessel 1D and 2D debris beds [31][32], respectively.

For the quenching of a one-dimensional (1D) homogenous debris bed, Figure 3-30a presents the curve of energy transfer rate from the bed to the water pool predicted by a coupled MELCOR/COCOMO simulation. During the quenching process the energy transfer rate is a relatively stable and large value driven by sensible heat of the debris bed, and a peak occurs in the very beginning when the high-temperature debris bed gets initial contact with the water pool. After the debris bed is fully quenched, the energy transfer rate decreases to a relatively low level controlled by decay power. In the surrogate model of quenching the 1D debris bed, the curve of energy transfer rate is simplified as seen in Figure 3-30b and mathematically described by Eq. (9) where  $c$  and  $m$  denote specific heat capacity and mass of the 1D debris bed, respectively,  $T_i$  and  $T_f$  the initial and final temperatures of the debris bed of quenching process,  $t_{1D}$  the quench time, and  $q_d$  the decay power of the debris bed.

$$q_{1D} \approx \begin{cases} \frac{c \cdot m \cdot (T_i - T_f)}{t_{1D}} & t \leq t_{1D} \\ q_d(t) & t > t_{1D} \end{cases} \quad (9)$$

MELCOR provides mass, decay power of debris bed and initial temperature, and specific heat capacity is calculated as weighted average of the functions based on the mass percentages of debris materials. Thus, unknown quantities Eq. (9) are the final temperature and quench time of debris bed, which will be determined by a 1D surrogate model (SM) of debris bed quench. Artificial neural network (ANN) is employed in the development of the SM for prediction of the final temperature and quench time of the 1D debris bed.

Table 3-10 shows the input parameters and their ranges for the SM.

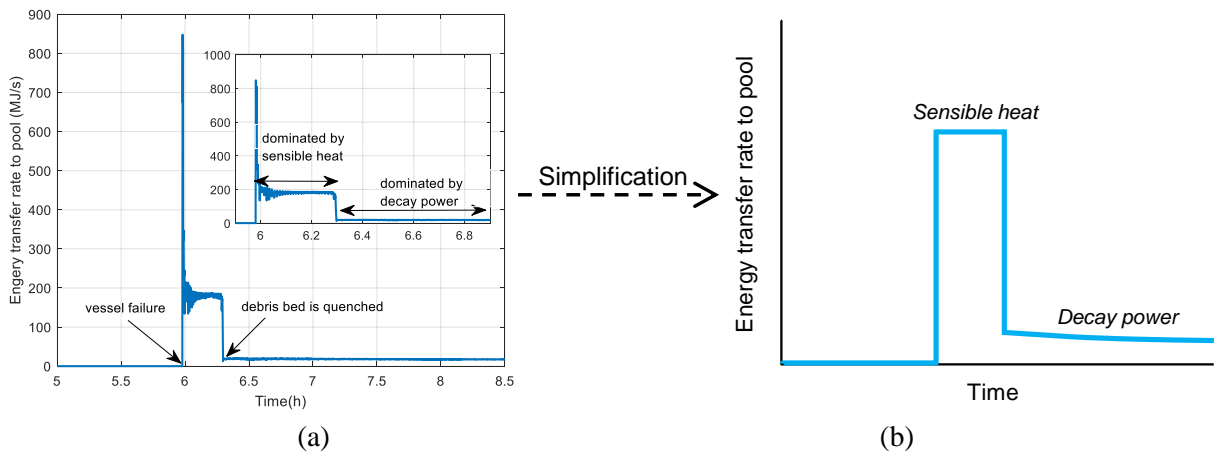


Figure 3-30: Transient curve of energy transfer rate from quenching debris bed to water pool in coupled MELCOR/COCOMO simulation for 1D debris bed (a) and its simplified curve (b).

Table 3-10: *Input parameters and their ranges for ANN training of 1D debris beds*

<b>Parameter</b>	<b>Minimum</b>	<b>Maximum</b>
Mass of debris bed (ton)	50	300
Initial temperature of debris bed (K)	1200	2000
Decay power (MW)	5	40
Porosity	0.3	0.6
Particle diameter (mm)	1	5
Pressure in cavity (bar)	1	6
Pool temperature in cavity (K)	290	330
Cavity radius (m)	4.5	6.5

Figure 3-31 illustrates the coupling of MELCOR with the SM through data exchange. The left side is MELCOR thermal-hydraulic nodes of the containment of a Nordic BWR [29]. In the lower drywell (reactor cavity) a debris bed is formed due to fragmentation of released corium after vessel failure, and consequently quenched. The right side of the picture shows the SM which consists of ANNs predicting model quench time and final temperature, and python scripts calculating the energy transfer rate with Eq. (9). The obtained energy transfer rate at each timestep is transferred back to MELCOR as an energy source term in the lower drywell.

As shown in Figure 3-32, the quench process of debris bed lasts longer in MELCOR standalone simulation because the energy transfer in MELCOR code happens only on the surface of corium layer and no water ingress is considered. Comparable results indicate that the coupled MELCOR/SM simulation can capture major features of the quench process of ex-vessel debris bed as MELCOR/COCOMO does. As for containment pressure, the water pool gets saturated earlier in coupled simulations than in MELCOR standalone simulation because of a faster energy transfer rate to from corium to water pool. Thus, the accident progression speeds up and containment venting occurs earlier in the coupled simulations. The similar containment pressure trends from two coupled simulations indicate the effectiveness of MELCOR/SM simulation for quench process of 1D debris bed.

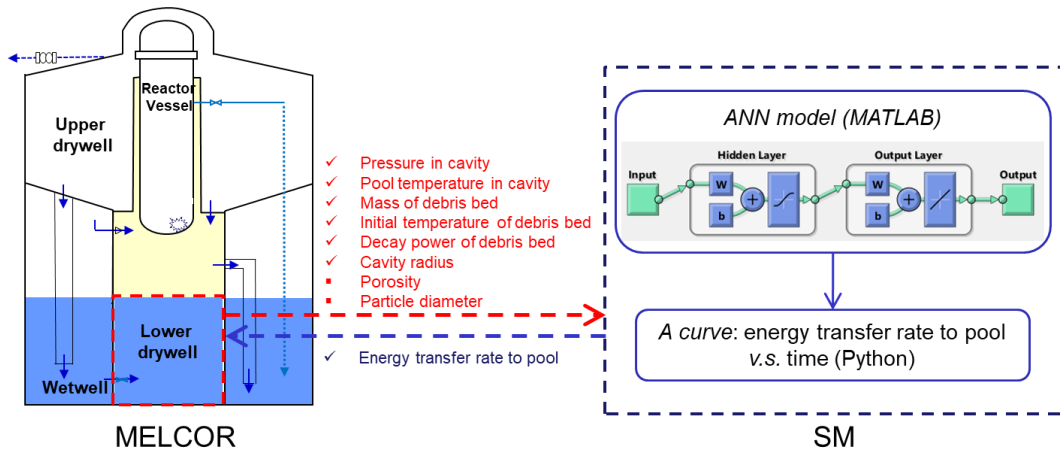


Figure 3-31: Coupled MELCOR/SM interface for 1D debris beds.

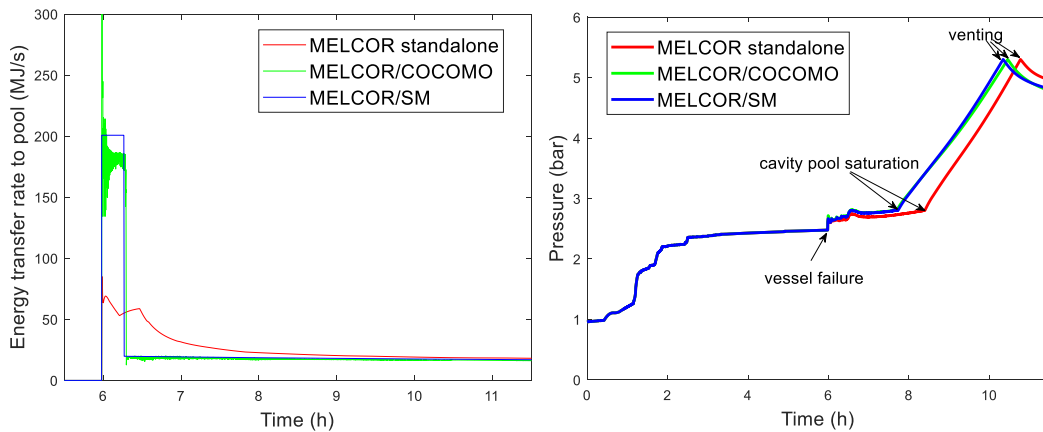


Figure 3-32: Energy transfer rate from a 1D debris bed to water pool (left) and containment pressure (right) predicted by coupled and standalone simulations.

Figure 3-33 presents energy transfer rates from debris bed to the water pool from MELCOR/COCOMO simulations for 1D debris bed and mass-equivalent 2D conical debris bed. The only difference between the two debris beds is their shape. One can see the energy transfer rate of the 2D debris bed during the quench process decreases nonlinearly and gradually to the decay power level, which is different from the sudden drop in the 1D debris bed when it is fully quenched. Table 3-11 contains quench time and final temperature of the mass-equivalent 1D and 2D debris beds. The final temperatures of mass-equivalent 1D and 2D debris beds at the time point of 2D conical debris bed being fully quenched are nearly the same. This indicates that cumulative energy transfer to water pool is supposed to be the same from the view of energy conservation. This implies that the energy transfer rate of a 2D conical debris bed can be correlated to that of mass-equivalent 1D flat debris bed.

Table 3-11: Quench time and final temperature for mass-equivalent 1D and 2D debris beds

Debris bed \ Output	Quench time (s)	Temperature at fully quenched debris beds (K)
1D	1143	418.3
2D	4870	418.6

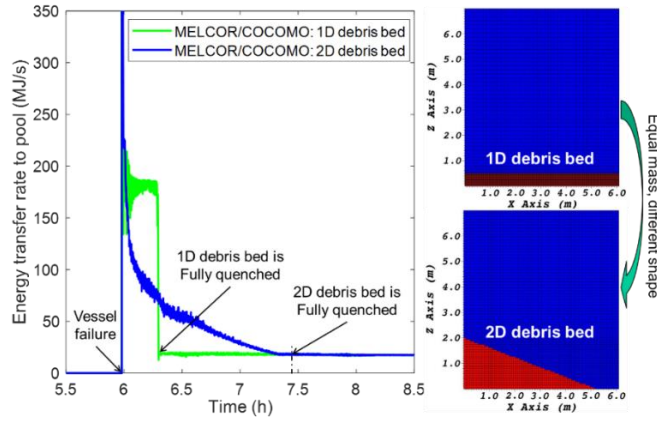


Figure 3-33: Energy transfer rates from mass-equivalent 1D and 2D debris beds in coupled MELCOR/COCOMO calculations.

A simplified energy transfer rate curve for a 2D conical debris bed can be determined by a SM expressed by Eq. (10), where  $q_{2D}$  denotes energy transfer rate from 2D debris bed to water pool,  $f(t)$  a quadratic function to capture the nonlinear decrease of energy transfer rate during the quench process,  $t_{2D}$  the quench time.

$$q_{2D} \approx \begin{cases} f(t) & t \leq t_{2D} \\ q_d(t) & t > t_{2D} \end{cases} \quad (10)$$

$f(t)$  in Eq. (10) can be determined by the continuity of the curve at  $t_{2D}$  as defined in Eq. (11) and cumulative energy transfer during quench process  $Q_{2D}$ , as defined in Eq. (12)-(13).

$$f(t_{2D}) = q_d(t_{2D}) \quad (11)$$

$$Q_{2D} \approx \int_0^{t_{2D}} q_{1D} dt = \int_0^{t_{1D}} \frac{c \cdot m \cdot (T_i - T_f)}{t_{1D}} dt + \int_{t_{1D}}^{t_{2D}} q_d(t) dt \quad (12)$$

$$Q_{2D} = \int_0^{t_{2D}} f(t) dt \quad (13)$$

In order to obtain the simplified energy transfer curve for 2D debris beds, all we need here is to predict  $t_{2D}$ , since  $t_{1D}$  and  $T_f$  are known from the SM of 1D debris beds. Table 3-12 includes input parameters and their ranges for the development of the SM predicting  $t_{2D}$ .

Table 3-12: Input parameters and their ranges for ANN training of 2 D debris beds

Parameter	Minimum	Maximum
Mass of debris beds (ton)	50	300
Initial temperature of debris beds (K)	1200	2000
Decay power (MW)	5	40
Porosity	0.3	0.6
Particle diameter (mm)	1	5
Pressure in cavity (bar)	1	6
Pool temperature in cavity (K)	290	330
Cavity radius (m)	4.5	6.5
Slope angle of debris bed (°)	0	45

Figure 3-34 shows the comparable results from simulations of the coupled MELCOR/ COCOMO, coupled MELCOR/SM and MELCOR standalone for the quench process of a 2D conical debris bed in the Nordic BWR.

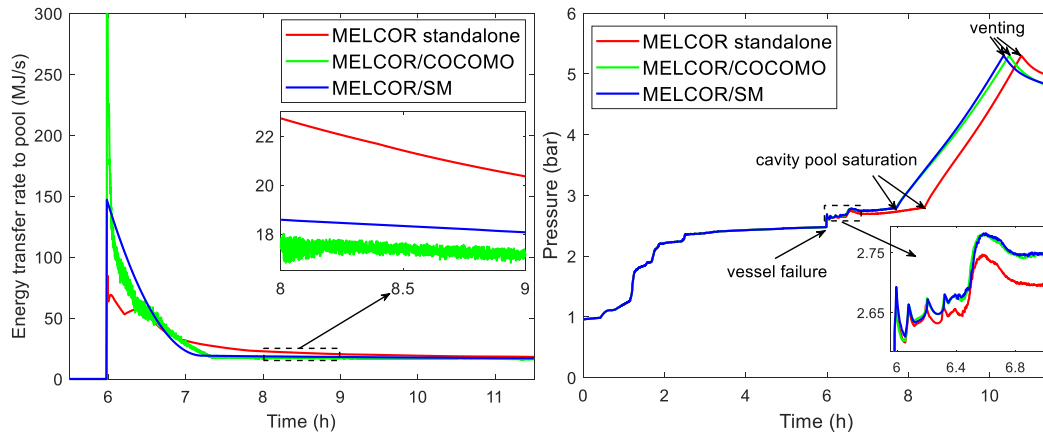


Figure 3-34: Energy transfer rate from 2D debris bed to water pool (left) and containment pressure (right) predicted by coupled and standalone simulations.

### 3.4.2. Toward assessment of ex-vessel corium risk of a Swedish PWR

In the event of a core meltdown accident in a pressurized water reactor (PWR), core melt (corium) may relocate into the lower head of the reactor pressure vessel (RPV), and finally fail the lower head due to thermal and mechanical loads. Ex-vessel corium risk comes from phenomena such as molten core concrete interactions (MCCI), fuel coolant interactions (FCI) and direct containment heating (DCH). Since different severe accident management (SAM) actions (measures) will be implemented in nuclear power plants according to the severe accident management guidelines (SAMG) for mitigating severe accident consequences, it is necessary to consider them in analyses of ex-vessel corium risks.

To estimate ex-vessel corium risk of a Swedish PWR with its SAM actions/measures, epistemic and aleatory uncertainties will be treated separately in MELCOR simulation and scenario identification, as recommended in the risk-oriented accident analysis methodology (ROAAM) [45].

We start from a TLOFW scenario in which total loss of feed water (TLOFW) occurs following a station blackout [46]. Assuming the AC power is recovered at a point of time after initiating the event, and subsequently the primary bleed and feed actions (PBF) actions can be implemented to restore core cooling. The “bleed” action is achieved by active RCS depressurization through PORVs, while the “feed” action is realized through safety injection. The major uncertainties in the SAM actions (and accident scenario) include the number of opened valves and pumps as well as safety injection timing. As an example for a preliminary investigation on the effect of aleatory uncertainty [33], only the uncertainty of safety injection timing is considered here, ranging from 3600s to 25200s with a step-wise increment of 300s.

Figure 3-35 shows the effect of safety injection timing on in-vessel and ex-vessel corium mass. According to the criteria of vessel failure and corium ejection rate, the ex-vessel corium risk can be divided into three categories: Group A (safety injection timing: 3600s–19800s) without ex-vessel corium due to no vessel failure; Group B (safety injection timing: 20100s–22200s) with rapid corium ejection upon vessel failure; Group C

(safety injection timing: 22500s–25200s) with gradual corium ejection after vessel failure. The different corium behavior in the three groups incur different ex-vessel risks. Earlier safety injection can prevent vessel failure and achieve in-vessel melt retention (IVMR). In order to acquire more valuable insights, a case study is further performed for each group to estimate epistemic uncertainties due to uncertain modeling parameters as listed in

Table 3-13. This results in three cases denoted by A, B and C with safety injection at 18000s, 21000s and 24000s, separately.

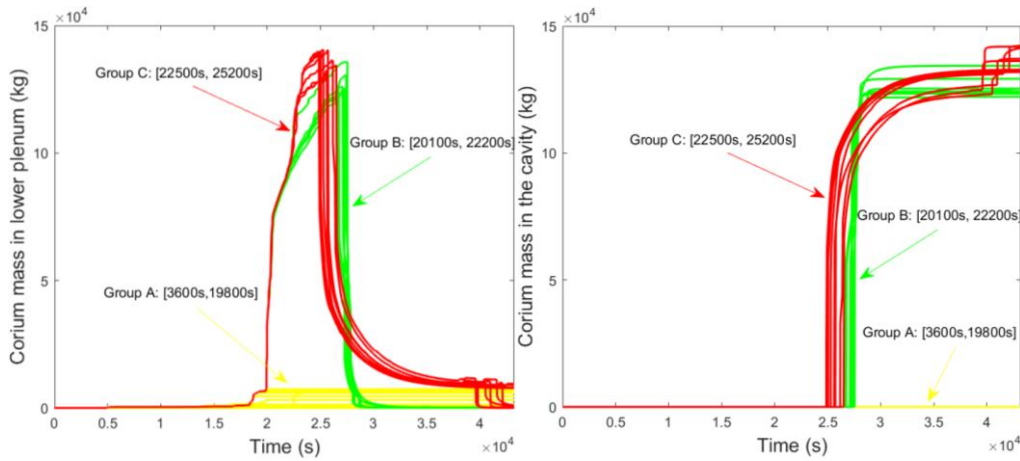


Figure 3-35: Corium mass in lower plenum (left) and in the cavity (right).

Table 3-13: Modeling parameters and their ranges.

Parameter	Range
Particulate debris porosity (PORDP)	0.3-0.5
Velocity of failing debris (VFALL)	0.01-1.0
LP Particulate debris equivalent diameter (DHYPDLP)	0.01-0.06
Oxidized fuel rod collapse temperature (TRDFAI)	2500-2650
Molten cladding (pool) drainage rate (SC11412)	0.1-2.0
Molten Zircaloy melt break-through temperature (SC11312)	2100-2540
Time constant for radial (solid) debris relocation (SC10201)	180-720
Time constant for radial (liquid) debris relocation (SC10202)	30-120
Heat transfer coefficient from in-vessel falling debris to pool (HDBH2O)	200-2000
Radiation heat transfer parameter (radial radiation exchange) (FCELR)	0.1-0.25
Radiation heat transfer parameter (axial radiation exchange) (FCELA)	0.1-0.25
Refreezing heat transfer coefficients for Zr (HFRZZR)	1000-7500
Refreezing heat transfer coefficients for SS (HFRZSS)	1000-2500

One can see from Figure 3-36 that considering uncertainties in modeling parameters in Case A might lead to vessel failure and corium ejection although Case A belongs to Group A in which vessel does not fail if only aleatory uncertainty in safety timing is considered.

Figure 3-37 indicates that considering the uncertainties in modeling parameters in Case B leads to a probability of vessel integrity which is not observed in Group B if aleatory uncertainty in safety injection timing is considered only.

As shown in Figure 3-38, considering the uncertainties of modeling parameters in Case C give rise to a high probability of vessel failure and corium ejection.

The above exercise illustrates the importance of epistemic and aleatory uncertainties in MELCOR analyses of ex-vessel corium risk of a Swedish PWR with its SAM actions. With this in mind, the ROAAM will be employed in our further study to comprehend deterministic and probabilistic results.

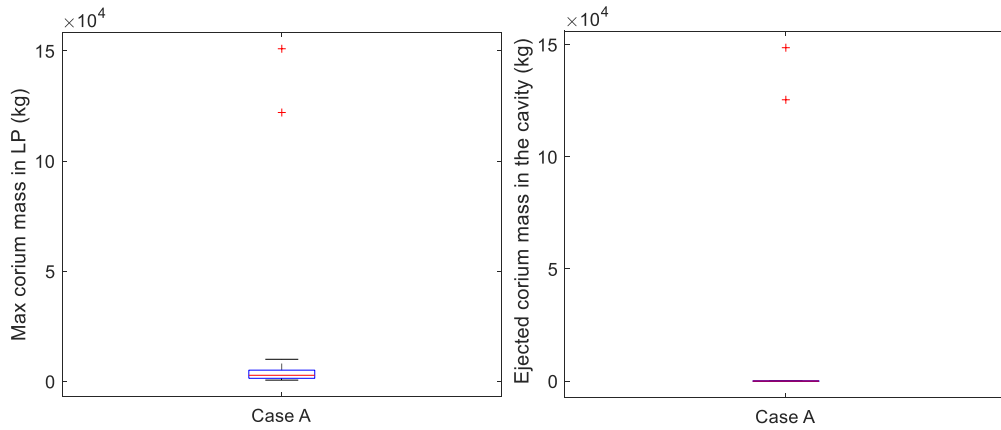


Figure 3-36: Corium mass of Case A in lower plenum (left) and in the cavity (right).

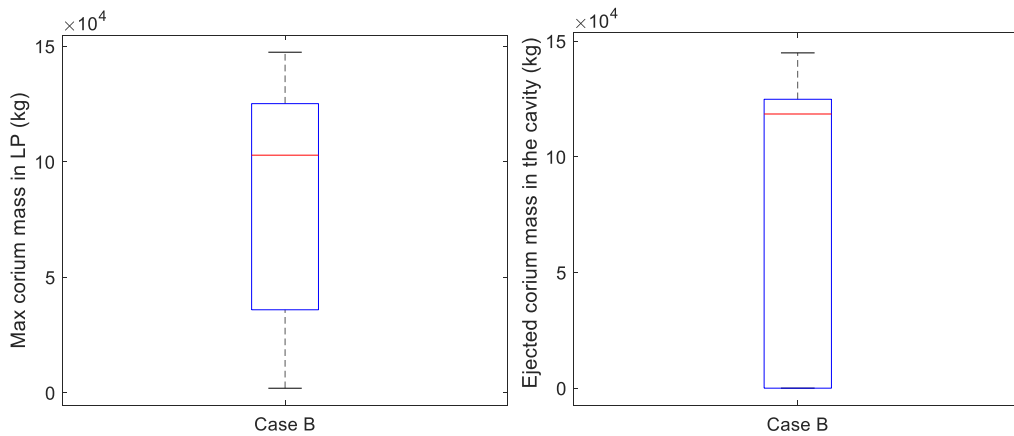


Figure 3-37: Corium mass of Case B in lower plenum (left) and the cavity (right).



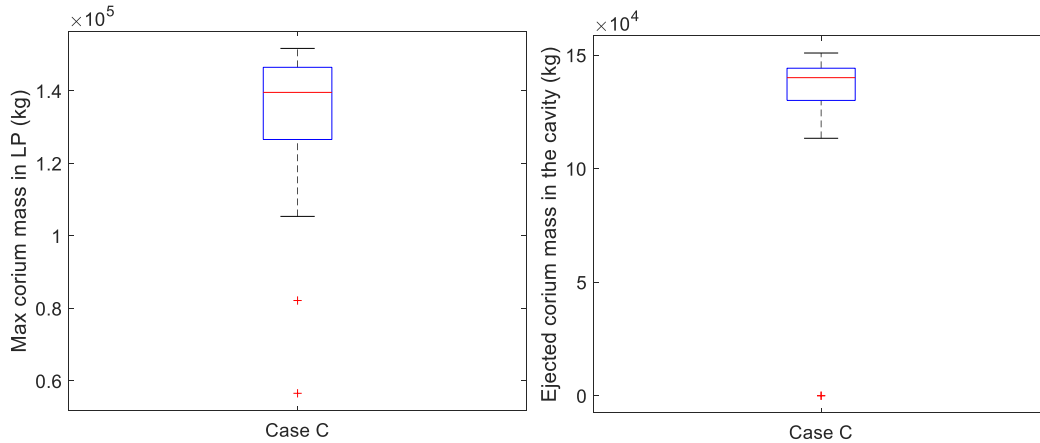


Figure 3-38: Corium mass of Case C in lower plenum (left) and in the cavity (right).

## 3.5. Summary and outlook

### 3.5.1. Summary

APRI-11 research at KTH-NPS was motivated by the resolution of remaining issues in qualification of severe accident management measures in Swedish nuclear power plants. Through the APRI-11 research, substantial knowledge (data, models, codes, insights and methodologies) has been achieved in the following topical areas: (i) in-vessel debris behaviour; (ii) vessel failure modes; (iii) melt-coolant interactions; (iv) ex-vessel corium-structure interactions; and (v) reactor applications and safety analyses.

#### In-vessel debris behavior

This study is to gain insights into the complex phenomena of corium evolution in the lower head where we have poor knowledge. The main advances and highlights are as follows:

- The SIMECO-2 test facility has been modified to perform debris bed dryout and remelting experiment [1-2], with a new test section and advanced instrumentation of Fiber Bragg Grating (FBG) optic fibers. In APRI-11 a pilot test had been conducted in the SIMECO-2 facility to provide the first-of-its-kind data on underwater dryout and melting of a debris bed composed of particles made of two materials (fusible and refractory parts of corium). The debris bed of porosity 0.4 is packed with uniform mixture of 55% of carbon steel particles representing heat-generating refractory oxidic part ( $\text{UO}_2\text{-ZrO}_2$ ) and 45% of Sn-Bi particles representing fusible metallic part (Zr-Fe) of corium. A large fraction of fusible particles was molten and penetrating in the porous media of intact particles (mainly from refractory part), resulting in a quite heterogeneous configuration.
- Tests on melt infiltration in various debris beds have been carried out in the MRSPD facility [3]. The debris beds are accommodated in a quartz tube of 120mm inside diameter for visualization of melt penetration. Eutectic Sn-Bi melt was poured to the preheated debris bed having 1.5-mm spheres made of either copper (Cu), Sn-coated Cu, stainless steel (SS), Sn-coated SS or glass to study the effects of thermal properties and wettability on melt infiltration. The temperature measurements of visual observations have revealed a non-linear kinetics of melt

infiltration. The ingots extracted from post-test analyses have also shown the complex infiltration process under similar test conditions.

- Contact angles of eutectic Sn-Bi melt with materials of particles employed in MRSPOD tests have been measured at three different temperatures using a sessile drop method [4]. A scaled-down test setup (in a quartz tube of 22mm inside diameter) of MRSPOD has been developed to investigate the effect of melt-particle wettability on melt infiltration in one-dimensional particulate beds [4]. The relation between melt infiltration kinetics and contact angle was obtained, and it was found that the melt penetrates much faster in the wettable particulate beds than in the non-wettable particulate beds.
- Numerical studies of melt infiltration in debris beds have been performed using various methods, including Moving Particle Semi-implicit (MPS) method [5], and modeling of micro-scale (pore-scale) and macro-scale transports in porous media using the COMSOL code [6]. The results not only help our understanding of relevant phenomena, but also provide the predictive capabilities for reactor case studies.
- A lumped-parameter code was developed to predict heat transfer in stratified melt pools [7]. Direct Numerical Simulation (DNS) was applied to natural convections in a bottom-heated metal layer and an internally heated oxidic molten pool ( $Ra \sim 6.54 \times 10^{11}$ ) [8-10]. The DNS results revealed some details more than RANS simulation. The BALI-Metal 8U experiment was also simulated by DNS and three RANS models:  $k-\omega$  SST, standard  $k-\epsilon$ , and RSM [11]. The results show the  $k-\omega$  SST model and DNS predict similar patterns. All simulations including DNS tend to overpredict the temperature field in experiment.

#### Vessel failure modes

This study is to provide models and tools which can be employed to predict the vessel failure mode and to perform corresponding analyses. During APRI-11 the thermomechanical approach previously developed and validated at KTH-NPS was applied to analyze the behavior of an ablated vessel wall with external cooling [12-13], and vessel breach and penetration failure of a Nordic BWR [14-15]. The main advances and highlights connected to vessel failure mode are as follows:

- For simulations of vessel breach without considering penetrations on the lower head, both MELCOR and ANSYS thermo-mechanical simulations were performed for two severe accident scenarios: station blackout (SBO) and SBO+LOCA. The MELCOR simulation also provided the thermal and mechanical loads in the ANSYS simulation. The simulation results show that the vessel failure occurs at 6.8 hours in the SBO scenario and 7.1 hours in the SBO+LOCA scenario, comparable to those of MELCOR simulations [14].
- For the thermomechanical simulation of penetration failure, three instrument guide tubes (IGT) welded in the vessel wall were considered. The results reveal strain failure occurs in all three welds much earlier than vessel failure, while melt-through failure is also observed in the weld of the farthest IGT structure earlier than vessel failure. This implies penetration failure may be dominant in vessel failure modes [15].

#### Melt-coolant interactions

This study is to maintain the expertise in experimentation gaining basic understanding on fuel coolant interactions and steam explosion, using the DEFOR and MISTEE facilities developed at KTH-NPS during past two decades. Specifically, the study was oriented to

metallic melt-coolant interactions [16-21], as well as single droplet steam explosion in chemical solutions [22-26], which were not investigated in the previous DEFOR and MISTEE studies. The main advances and highlights are as follows:

- An extensive study has been carried out to gain the characteristics of metallic melt-coolant interactions and resulting debris beds, using various simulants of metal-rich corium melt, including Sn, Zn and binary alloy of Sn-Bi. New tests of oxidic melt-coolant interactions using  $\text{Bi}_2\text{O}_3\text{-WO}_3$  are also performed for a comparison of debris bed characteristics resulting from metallic and oxidic melts. The results illustrate that the metallic melt with a higher melting point results in stronger heat transfer and enhanced fragmentation in water, while the other metallic melts with lower melting points experience rapid solidification process, leading to incomplete melt jet breakup. The oxidic melt with a high melting point has less potential of solidification before jet breakup, giving rise to a particulate bed with smaller sizes of debris particles. The distinction may be attributed to different heat transfer modes and physical properties such as ductility and shear strength between oxidic melt and metallic melt.
- For the single droplet steam explosion experiment in chemical solutions with the additives of  $\text{H}_3\text{BO}_3$ ,  $\text{NaOH}$  and  $\text{Na}_3\text{PO}_4$  which are used in the control of water chemistry of reactor coolant, as well as  $\text{NaCl}$  in seawater which may be utilized in extreme events such as the Fukushima accident. Experimental results reveal that the spontaneous steam explosion probability decreases when the  $\text{H}_3\text{BO}_3$  concentration increases from 0 to 1.2 wt.%, but it increases significantly if the  $\text{H}_3\text{BO}_3$  concentration further increases from 1.2 wt.% to 3.2 wt.% [23]. However, in the neutral solutions of  $\text{H}_3\text{BO}_3$  and  $\text{NaOH}$  the steam explosion probability is only slightly affected by the boric acid concentration [24]. Considering the neutral solutions of  $\text{H}_3\text{BO}_3$  and  $\text{Na}_3\text{PO}_4$  the steam explosion probability increases as the  $\text{H}_3\text{BO}_3$  concentration rises from 0 to 1.2 wt.% but decreases significantly with the  $\text{H}_3\text{BO}_3$  concentration further increasing from 1.2 wt.% to 3.2 wt.% [24]. The possibility of steam explosion increases with the salinity increasing from 0 to 17.5 g/kg, but the trend levels off after the salinity is higher than 17.5 g/kg [25]. A separate study on sphere quenching in various coolants confirms the specialty of film boiling in seawater [26].

#### Ex-vessel melt-structure interactions

This study is concerned with the influences of the structures below the reactor pressure vessel on corium melt discharge process after the lower head fails in a severe accident. The objective is to understand the key mechanisms and outcomes of ex-vessel corium-structure interactions, which are important to subsequent fuel coolant interactions and corium coolability in the reactor cavity. This is a new research direction just initiated in APRI-11. The main advances and highlights are as follows:

- A literature survey on relevant phenomena under the scope of ex-vessel corium-structure interactions has been conducted [27]. It is found that little attention has been paid to the below-vessel structures. In a few considerations (e.g., in MAAP code) the below-vessel structures of BWRs are simplified as a combination of horizontal and vertical structures, and lumped-parameter approaches are adopted to calculate three phenomena: splashing of melt on structure, ablation of structure caused by melt impingement and melt freezing on structure surface.
- The design data of the below-RPV structures in a reference Nordic boiling water reactor (BWR) has been collected and scrutinized [28]. The lower head wall of the

BWR is vertically penetrated by the control rod guide tubes (CRGTs) and instrument guide tubes (IGTs). Two major horizontal structures below the lower head are a radiation shield and a damper. Both are around 120mm thick and perforated by CRGTs and IGTs. There exist working platforms below the control rod driving mechanisms. Given the configuration of specific below-vessel structures, potential research orientations have been conceptualized analytically and experimentally [28].

#### Reactor applications and safety analyses

This task is intended to the applications of the research results (e.g., models, computer codes) to the Swedish nuclear power safety context. The activities consist of reactor case studies using developed tools and methodologies. The main advances and highlights are as follows:

- For simulation of severe accidents with ex-vessel debris beds formed in the reactor cavity of a boiling water reactor, the COCOMO code has been coupled with the MELCOR code to simulate accident progression which includes quenching and stable cooling of ex-vessel debris beds [29]. To reduce computational cost of the coupled MELCOR/COCOMO simulation, surrogate models (SM) are developed and coupled with MELCOR to realize quick estimation of similar accident progression involving ex-vessel debris beds [30-32]. Compared with MELCOR standalone, both coupled simulations of MELCOR/ COCOMO and MELCOR/SM predict earlier pool saturation and containment venting.
- To estimate ex-vessel corium risk of a Swedish PWR with SAM actions, a ROAAM-like approach [33] has been considered in MELCOR analyses to characterize corium discharge upon vessel failure. Preliminary results of an exercise have demonstrated the importance of combining epistemic uncertainties in physical models and aleatory uncertainties in SAM actions [33].

More detailed results of KTH-NPS research in APRI-11 can be found in the publications listed in References, including 23 peer-reviewed articles published in international journals and four doctoral dissertations.

### 3.5.2. Outlook

Extensive research activities were performed worldwide on accident phenomena of risk importance to light water reactors during past decades, including analytical and experimental studies. A substantial knowledge base has been developed, with an important contribution from KTH-NPS within the strategic APRI programs leveraging international projects (e.g. EU, ENSI) and collaborations (e.g., OECD, IAEA). The knowledge base has been instrumental in the development and improvement of various predictive capabilities and innovations in severe accident management strategies. It also helped the resolution of outstanding severe accident issues.

Nevertheless, the uncertainties in quantification of severe accident risks are still generally large due to the complex and multifaceted features of severe accident phenomena and scenarios. Therefore, a research orientation toward general understanding of severe accident phenomena seems cost ineffective. Under such circumstances, more and more severe accident research worldwide has been directed to resolutions of specific safety issues, phenomena, or accident management strategy. KTH-NPS is a pioneer in the shift of research orientation toward the quantification of phenomena which are directly relevant to

the assessment of severe accident management (SAM) measures in Swedish nuclear power plants.

For instance, for the cavity-flooding SAM measure adopted by Swedish NPPs, the research goal is to create sufficient knowledge effectively demonstrating that ex-vessel debris beds are coolable without energetic steam explosions during postulated severe accidents. For this objective, the recent focus of APRI-research at KTH-NPS has been placed on four topical areas of highest return: (i) remelting dynamics of multi-composition debris bed in the lower head, (ii) lower head failure mode and rupture dynamics, (iii) debris formation due to metallic melt-coolant interactions, and (iv) ex-vessel melt-structure interactions. The items (i), (ii) and (iv) are crucial to quantify the characteristics of corium melt which arrives at the water pool in the reactor cavity, while the item (iii) is the remaining issue in the previous DEFOR study. The melt ejection characteristics after vessel failure are the limiting conditions for ex-vessel debris bed coolability and steam explosions energetics. Therefore, it is the most cost-effective consideration for the next APRI program to continue the research activities which have been identified as priority but unfinished due to constraint of resources during APRI-11. In other words, the future work should address the unsolved problems and remaining issues of the above four topical areas as exemplified below.

#### *In-vessel debris behavior*

For the study on debris behavior in the lower head of reactor pressure vessel, the unsolved problems and remaining issues are as follows.

- The SIMECO-2 facility has been proven to be capable of investigating debris bed dryout and remelting in the pilot test carried out during APRI-11. However, the result of only one test is still quite far from comprehension and modeling of debris behavior in the lower head. Thus, a systematic study with more tests should be carried out, including dryout and melting of various debris beds, melting of multi components in debris beds, and forming of stratified molten pool behavior. Advanced experimental techniques and instrumentation also need to be developed for the more challenging tests.
- The previous MRSPOD tests were carried out at a relatively low temperature (<300°C) using eutectic Sn–Bi melt whose melting point is 139°C. The data for higher temperatures is missing. Thus, it is expected to perform a study with higher melting-point materials so as to reduce the gap between prototypical materials and simulants in the experiment, for a better understanding of molten metal (Zr/Fe) infiltration in an oxidic (UO<sub>2</sub>/ZrO<sub>2</sub>) debris bed.
- The MPS code developed during APRI-11 has been limited to melt-infiltration problems in small scales due to high demand on computational resources. Both micro- and macro-scale models of melt infiltration using COMSOL are still under refining and validation. Therefore, improvement or new development of models and simulation capabilities (tools) should be continued for either understanding of debris remelting mechanisms or analyses of reactor cases. The goal is to have mechanistic models/tools for predicting corium debris evolution in the lower head, and consequently obtaining the corium's state and dynamic loads (both thermal and mechanical) on the lower head.

#### *Vessel failure modes*

For the study on vessel failure mode and melt discharge characteristics after vessel failure, the unsolved problems and remaining issues are as follows.

- More representative penetrations (control rod guide tubes, or both CRGT and IGT) of the lower head should be considered.
- Failure hole evolution (e.g. ablation dynamics) which has not been touched in the previous APRI-studies, since this is beyond the capabilities of the thermomechanical approach developed in our previous works. A new approach is needed to predict the dynamics of failure hole, which calls for a coupling between fluid and structural mechanics.
- Melt discharge characteristics after vessel failure are still far from our reach before we can answer the preceding questions and resolve the remaining issues in the preceding topical area.

#### Melt-coolant interactions

For the study on ex-vessel fuel coolant interactions, debris bed formation and steam explosion, the unsolved problems and remaining issues are as follows.

- For the metallic melt-coolant interactions, the experimental data using Sn, Zn and binary alloy of Sn-Bi reveal some key phenomena which are different from those of oxidic melt, can be used for validation of relevant models given the known properties and well-defined test conditions. However, it is still an open question how the real metals (Zr/Fe) in corium affect the results. In particular, the oxidation of Zr/Fe and the hydrogen generation during melt-coolant interactions were reproduced in the previous tests. Thus, more experimental studies (e.g., using simulant materials with melting points close to prototypical materials) will help to narrow down the property gap of materials. Additional studies should be paid to development of models/codes which can be applied to reactor case studies.
- For the MISTEE experiment, many efforts have been spent to characterize single molten drop steam explosion. One limitation is that the used materials are different from the real metals (Zr/Fe) in corium. Another limitation is that the study of single drop only belongs to the triggering phase of a steam explosion. Hence, studies using Zr/Fe and a small melt jet rather than single drop are necessary in the future work, with upgrades of the MISTEE facility in furnace for melting Zr/Fe and in instrumentation for synchronizing photography and radiography.

#### Ex-vessel melt-structure interactions

The research plan elaborated in APRI-11 is expected to be fulfilled in the next-phase APRI.

This topical area is concerned with the interactions of the ejected melt with the structures below the reactor pressure vessel (RPV) of a BWR after the RPV lower head fails in a severe accident. To find key mechanisms and develop models in this topical area, a research plan has been conceptualized in the end of APRI-11 after an extensive literature study survey on relevant phenomena, as well as collection and scrutiny of the design data of the below-RPV structures in a reference Nordic BWR. The remaining work is to materialize and fulfil the research plan, including experimental and analytical studies.

A scaled-down structure representing the radiation shield and a unit of CRGTs and IGTs can be adopted as a test section in the DEFOR study. Melt impingement and splashing on the radiation shield as well freezing on CRGTs and IGTs can be investigated on the CoS-MUS at KTH-NPS. The analytical study will be realized through both mechanistic and parametric approaches. The mechanistic modelling of melt-structure interaction can capitalize on the development in other topical areas, such as the MPS and COMSOL models.

In addition to the research activities in the above four topical areas, it is instrumental to apply the research outcomes (e.g., models, computer codes, methodologies) to the Swedish nuclear power safety context whenever the outcomes are applicable. Such reactor application (or case study) had been conducted in previous APRI-research and should be continued in the future APRI-research, since the ultimate goal is to resolve the severe accident issues associated with the SAM measures of Swedish NPPs, as reiterated in KTH-NPS proposals to APRI. Thus, reactor application study and safety analysis are the living cases which will be advanced and updated with new knowledge and modeling capabilities acquired in the future activities.

### 3.6. References

- [1] A. Komlev, Summary of the debris dryout/remelting study in SIMECO-2 facility, *Proceeding of 57<sup>th</sup> MSWI Meeting*, KTH, Stockholm, November 2023.
- [2] Y. Xiang, A. Komlev, Y. Chen, W. Ma, and S. Bechta: Pre-test simulation and a scoping test for dryout and remelting phenomena of an in-vessel debris bed, *Nuclear Engineering and Design* 403: 112143, 2023.
- [3] W. Villanueva, S.M. Hoseyni, S. Bechta and A. Hotta, Experimental investigation of melt infiltration and solidification in a pre-heated particle bed, *Physics of Fluid* 34: 123326, 2022.
- [4] L. Chen, A. Komlev, W. Ma, S. Bechta W. Villanueva et al., An experimental study on the impact of particle surface wettability on melt infiltration in particulate beds, *Annals of Nuclear Energy*, under review.
- [5] L. Zhao, Y. Xiang, W. Ma and S. Bechta, Numerical simulation of melt penetration in debris beds using MPS method, *Progress in Nuclear Energy* 167: 104982, 2024.
- [6] L. Chen, A. Komlev, W. Ma, and S. Bechta, A numerical study of melt penetration into a particulate bed, Proc of the 20th International Topical Meeting on Nuclear Reactor Thermal Hydraulics (NURETH-20), Washington, D.C., USA, August 20–25, 2023.
- [7] Y. Peng and W. Ma, Development of a lumped-parameter code for efficient assessment of in-vessel melt retention strategy of LWRs, *Progress in Nuclear Energy* 139: 103874, 2021.
- [8] B. Bian, W. Villanueva and D. Dovizio, Direct numerical simulation of molten pool convection in a 3D semicircular slice at different Prandtl numbers, *Nuclear Engineering and Design* 393: 111772, 2022.
- [9] B. Bian, D. Dovizio and W. Villanueva, Direct numerical simulation of internally heated natural convection in a hemispherical geometry, *International Journal of Heat and Mass Transfer* 220: 124997, 2024.
- [10] B. Bian, J. Gong and W. Villanueva, Scalability of Nek5000 on high-performance computing clusters toward direct numerical simulation of molten pool convection, *Frontiers in Energy Research* 10: 864821, 2022.
- [11] B. Bian, CFD Study of Molten Pool Convection in a Reactor Vessel during a Severe Accident, *Doctoral Dissertation*, Royal Institute of Technology, Stockholm, October 2023.
- [12] H. Wang and W. Villanueva, Structural behavior of an ablated reactor pressure vessel wall with external cooling, *Progress in Nuclear Energy* 153: 104446, 2022.
- [13] H. Wang, W. Villanueva, Y. Chen, A. Kulachenko and S. Bechta, Thermo-mechanical behavior of an ablated reactor pressure vessel wall in a Nordic BWR under in-vessel core melt retention, *Nuclear Engineering and Design* 379: 111196, 2021.
- [14] H. Wang, Y. Chen and W. Villanueva, Vessel failure analysis of a boiling water reactor during a severe accident, *Frontiers in Energy Research* 10: 839667, 2022.
- [15] H. Wang, Thermo-mechanical Assessment of Reactor Pressure Vessels of Light Water Reactors During Severe Accidents, *Doctoral Dissertation*, Royal Institute of Technology, Stockholm, October 2023.
- [16] Y. Xiang, S. Thakre, W. Ma and S. Bechta, A scoping study on debris bed formation from metallic melt coolant interactions, *Nuclear Engineering and Design* 385: 111533, 2021.
- [17] S. Thakre, Y. Xiang, W. Ma, W. Villanueva and S. Bechta, Metallic melt jet fragmentation in a water pool: Experiments and numerical simulations, *Nuclear Engineering and Design* 396: 111876, 2022.



- [18] Y. Xiang, D. Fang, D. Liang, Y. Deng and W. Ma: Experimental investigation on ex-vessel debris bed formation from metallic melt coolant interactions, *International Journal of Thermal Sciences* 192: Part A: 108398, 2023.
- [19] Y. Xiang, Y. Deng, D. Fang, N. Zhao and W. Ma, Experimental investigation on ex-vessel debris bed formation using low melting-point melt of binary metals, *Progress in Nuclear Energy* 157:104564, 2023.
- [20] Y. Xiang, D. Liang, A. Komlev, Y. Deng, D. Fang and W. Ma, An experimental investigation on melt coolant interactions with both metallic and oxidic simulants, *Applied Thermal Engineering* 233: 121186, 2023.
- [21] Y. Xiang, Study on Metallic Melt Coolant Interactions and Debris Bed Formation in a Water Pool, *Doctoral Dissertation*, Royal Institute of Technology, Stockholm, November 2023.
- [22] Y. Deng, Q. Guo, D. Fang, Y. Xiang and W. Ma, A numerical study on the levitation system for droplet preparation in a fuel-coolant interaction experiment, *Progress in Nuclear Energy* 159: 104639, 2023.
- [23] Y. Deng, Q. Guo, D. Fang, Y. Xiang and W. Ma, An experimental study on droplet quench and steam explosion in boric acid solutions, *Progress in Nuclear Energy* 166: 104970, 2023.
- [24] Y. Deng, Q. Guo, D. Fang, Y. Xiang and W. Ma, An experimental study on the effect of chemical additives in coolant on steam explosion, *International Journal of Heat and Mass Transfer* 218: 124818, 2024.
- [25] Y. Deng, Experimental Study on Steam Explosions in Chemical Solutions and Seawater, *Doctoral Dissertation*, Royal Institute of Technology, Stockholm, February 2024.
- [26] Q. Guo, Y. Deng and W. Ma, An experimental study on quenching of metallic spheres in seawater, *Experimental Thermal and Fluid Science* 148: 110990, 2023.
- [27] D. Liang, Ex-vessel corium-structure interactions during severe accidents of boiling water reactors - literature review & research orientation, *Proceeding of 55<sup>th</sup> MSWI Meeting*, KTH, Stockholm, November 2022.
- [28] D. Liang, Investigating the effects of below-vessel structure on melt relocation in a Nordic BWR during SA – Research plan of FY2023, KTH, *Proceeding of 56<sup>th</sup> MSWI Meeting*, Stockholm, May 2023.
- [29] Y. Chen, H. Zhang and W. Ma, Coupled MELCOR/COCOMO analysis on quench of ex-vessel debris beds, *Annals of Nuclear Energy* 165: 108643, 2022.
- [30] Y. Chen, MELCOR Capability Development for Simulation of Debris Bed Coolability, *Doctoral Dissertation*, Royal Institute of Technology, Stockholm, September 2021.
- [31] W. Wang, Y. Chen and W. Ma, Development of a surrogate model for quenching estimation of ex-vessel debris beds and its coupling with MELCOR, *Annals of Nuclear Energy* 190: 109883, 2023.
- [32] W. Wang and W. Ma, Coupling of MELCOR with surrogate model for quench estimation of conical debris beds, *International Journal of Heat and Mass Transfer*, under review.
- [33] W. Wang, Toward assessment on ex-vessel corium risk of a reference Swedish PWR under its SAM measures, *Proceeding of 56<sup>th</sup> MSWI Meeting*, KTH, Stockholm, May 2023.
- [34] M. Punetha, L. Zhao, A. Komlev, A. Konlvalenko, W. Ma and S. Bechta, Recent studies of dry and wet spreading of corium simulant melt at KTH, The 11<sup>th</sup> International Conference on Multiphase Flow (ICMF-2023), Kobe, Japan, 2-7 April 2023.

- [35] L. Zhao, W. Ma and S. Bechta, Numerical study on melt underwater spreading with MPS method, *Annals of Nuclear Energy* 181: 109581, 2023.
- [36] L. Zhao, W. Ma, A. Konovalenko and S. Bechta, Simulation of melt spreading over dry substrates with the moving particle Semi-implicit method, *Nuclear Engineering and Design* 405: 112229, 2023.
- [37] D. Fang, Y. Xiang, Y. Deng and W. Ma, A numerical study of liquid film dynamics in multi-nozzle spray cooling of downward-facing surface, *International Journal of Multiphase Flow* 161: 104383, 2023.
- [38] D. Fang, Y. Deng, M. Punetha, Y. Xiang, L. Zhao and W. Ma, Experimental and numerical studies on spray cooling by a four-nozzle system, *Annals of Nuclear Energy*, under review.
- [39] Y. Chen, H. Zhang, W. Ma, W. Villanueva and S. Bechta, A sensitivity study of MELCOR nodalization for simulation of in-vessel severe accident progression in a boiling water reactor, *Nuclear Engineering Design* 343: 22-37, 2019.
- [40] Alexander Konovalenko et al., Investigation of Cooling Phenomena of High Temperature Molten Core: Phase-4, Technical Report, Division of Nuclear Power Safety, KTH Royal Institute of Technology, September 2020.
- [41] C.T. Tran and T.N. Dinh, The effective convectivity model for simulation of melt pool heat transfer in a light water reactor pressure vessel lower head, *Progress in Nuclear Energy* 51: 849-871, 2009.
- [42] A. Karbojian, W. Ma, P. Kudinov and T.N. Dinh, A scoping study of debris bed formation in the DEFOR test facility, *Nuclear Engineering and Design* 239: 1653-1659, 2009.
- [43] P. Kudinov, A. Karbojian, W. Ma, T.N. Dinh, The DEFOR-S experimental study of debris formation with corium simulant materials, *Nuclear Technology* 170: 219-230, 2010.
- [44] Y. Chen, W. Ma, Development and application of a surrogate model for quick estimation of ex-vessel debris bed coolability, *Nuclear Engineering and Design* 370: 110898, 2020.
- [45] T. G. Theofanous and T.N. Dinh, Integration of multiphase science and technology with risk management in nuclear power reactors: Application of the risk-oriented accident analysis methodology to the ESBWR design, *Multiphase Science and Technology* 20(2): 81-211, 2008.
- [46] N. Zhao, W. Ma and S. Bechta, Analysis of primary side bleed & feed actions in the severe accident management following total loss of feedwater accidents in a Swedish PWR, *Annual Nuclear Energy* 167: 108859, 2022.

## 4. Chalmers' Severe Accident Research in APRI-11

### 4.1. Summary of the work

Severe accident research involves the study of the chemical and physical processes that contribute to and affects accidents in nuclear facilities, in particular nuclear power plants. Accident chemistry is the branch of accident science that focuses on chemical conditions and processes that affect the course of the accident and its subsequent processes. It includes the study of e.g. the formation of hydrogen gas during the accident, interaction between the reactor melt and the pressure vessel or concrete, and processes related to the chemical nature of the fission products, which in turn relates to the spread of radioactive material in the environment after the accident.

Much of the type of research that forms the basis of accident chemistry models is based on observations from large international research projects such as PHÉBUS and VER-CORS among others, which generates a lot of data. Alongside these projects, much smaller projects are being carried out that aim to develop the understanding of individual details that cannot be studied effectively in large, complex studies. It can deal with e.g. specific chemical interactions that are suspected to affect the breakdown or source term of one or more fission products, or a physical process for how the reactor core is affected under a particular heating/cooling scenario. Ideally, these experimental studies are then compared with the output from the model code to ensure that the code is robust.

Chalmers' work during APRI-11 has focused on accident chemistry. During reactor operation, atomic nuclei of a fissile material are split by, in general, thermal neutrons which releases energy in the form of heat, as well as forms nuclear fragments. These fragments are called fission products and are radioactive isotopes of a large number of elements. Substances of special interest in accident chemistry tend to be volatile, long-lived and/or possess special chemical/biological/radiological properties that make them potentially harmful to humans or the environment. Volatile fission products that attract special interest are, for example, iodine, caesium, and tellurium.

Iodine is the fission product that is usually considered the most important. It is a halogen that can interact chemically in a number of ways depending on conditions. It can behave as a gas at low temperatures but also has a very rich chemistry in water. Furthermore, iodine is a necessary nutrient that is enriched in the thyroid gland of mammals. Exposure to radioactive iodine thus results in persistent internal contamination and irradiation that can result in cancer-related diseases long after exposure, something that was observed after the 1986 Chernobyl accident in present-day Ukraine.

Caesium is another fission product of interest. Chemically, it is an extremely reactive alkali metal that forms compounds with, for instance, iodine and molybdate. Its transport does not mainly take place as a gaseous species, but as an aerosol. However, this does not mean that its potential for proliferation is less than iodine; especially since a couple of its isotopes have half-lives of more than thirty years - compared to the most important iodine isotope which has a half-life of about 8 days. The contamination of caesium from the Chernobyl disaster is still present in nature, and it will remain to some extent for several hundred years to come.

Tellurium, finally, is a heavy chalcogen (i.e. it belongs to the oxygen group of the periodic table). Chemically speaking, it is a metalloid with a very multifaceted chemical character. It can exist in a total of five oxidation states (-2, 0, +2, +4 and +6) depending on the circumstances, and like oxygen it can interact with organic compounds to form organic tellurides. Fission products that form organic compounds have been known since before as iodine can interact in this way, but reactions with tellurium has mostly been an unverified curiosity in accident contexts.

The work within APRI-11 at Chalmers has been almost entirely focused on tellurium, and a large part of it has been focused precisely on whether organic tellurides can be formed under accident conditions, as well as studies on their persistence under the conditions that can conceivably prevail during an accident, as well as the existing safety systems' ability to delay and prevent this type of release. This has been handled in a total of four different projects.

The first project aims to investigate whether organic tellurides can form in the containment's water after a breakdown during gamma irradiation. The results indicate that it is entirely possible for organic tellurides to form in this way, which means that organic tellurides should not only be considered as theoretical possibilities, but that they should be studied further to assess whether they are relevant from a safety perspective.

The second study deals with the formation of organic tellurides in the gas phase under conditions similar to those that can be expected in the primary circuit during an accident. The project involved experimental work in collaboration with VTT in Espoo, just west of Helsinki in Finland, and the analysis of the results was mostly carried out at Chalmers. Neutron activation was also part of the analysis, which was arranged in Prague by "Research Center Řež, Ltd." The results indicate that under these conditions, the transport of tellurium in the gas phase increases, alternatively the transport of very small aerosols, which may indicate the formation of organic tellurides, although this cannot be said to be entirely certain at the moment.

The third work aimed to study the persistence of dimethyl telluride (the most likely organic telluride in the containment water, henceforth abbreviated DMT) under strong gamma irradiation. Although organic tellurides can form under conditions not dissimilar to those expected during an accident, it is nevertheless possible that they decay or react further so quickly that they do not pose a realistic radiological risk. The results indicate that the decay of organic tellurides strongly depends on the nature of the water phase, as the composition of different water phases strongly affects the stability of DMT. In particular, if there are radical scavengers present in the system, the dimethyl telluride concentration can persist despite high radiation doses.

The last work that has been done within APRI-11 investigates the interaction between DMT and activated carbon taken from a number of respirator filters, as well as a sample that came from the filter placed at one of Sweden's nuclear power plants. The results seem to indicate that activated carbon is an effective way to filter DMT, as a very large part of the input telluride was already captured by the very first filter layer, and the carrier gas was completely clean (no DMT could be detected) after four filters.

Additional studies have also begun, focused on studying the interaction between tellurium and boric acid. A similar study is also planned to involve iodine, tellurium and/or cesium iodide along with boric acid to investigate a more complex system where multiple fission products coexist.

## 4.2. Organic telluride formation from paint solvents under gamma irradiation

The presence of organic material in the containment in both aqueous and gaseous phase has been a source of concern due to the possible formation of volatile organic species. The organic material can originate from e.g. painted surfaces, insulator materials or resins. Organic species of iodine have been thoroughly investigated in severe accident scenarios and methyl iodide has been found to be a difficult to trap species. However, organic tellurides have not been part of severe accident research. The formation and stability of organic tellurium species was focused on in this work. The first step was to investigate whether tellurium can react with organic species in conditions relevant to accident scenarios. This was investigated by preparing samples of dissolved tellurium dioxide and paint solvents. A simulated sump solution was used as the liquid phase, which consisted of alkaline borate solution without sodium thiosulfate. Three paint solvents possibly present in the sump were selected: texanol ester alcohol, methyl isobutyl ketone (MIBK) and toluene. The samples were irradiated up to a dose of around 280 kGy and analyzed for total tellurium concentration, presence of volatile species and solid speciation.

### 4.2.1. Results and discussion

The formation of organic tellurides was analyzed by using gas chromatography mass spectrometry (GC-MS). Several volatile tellurium compounds were detected in the analyses. These species were identified by their characteristic mass patterns with the lowest mass group at around 128 mass-to-charge ( $m/z$ ). This group of masses corresponds to the most abundant isotope of tellurium, 126, 128 and 130  $m/z$ . The other signals were then compared to these masses to find the correct fractions and identify the organic groups. For the samples containing texanol, the most abundant organotelluride was identified as diisopropyl telluride,  $((\text{CH}_3)_2\text{CH})_2\text{-Te}^+$ . The mass spectrum for  $((\text{CH}_3)_2\text{CH})_2\text{-Te}^+$  is presented in Figure 4-1.

Another tellurium species was detected in the texanol samples (see Figure 4-1). This had a mass ion at 214  $m/z$ . The characteristic isotopic pattern for  $\text{Te}^+$  fractions was again found at around  $m/z$  130. The strongest signal for the 5.18 min peak is at  $m/z$  170 which likely corresponds to a species with a formula of  $\text{C}_3\text{H}_6\text{Te}$ . Although the mass is close to the  $\text{M}^+$  of the first peak at 4.26 min it does not correspond to isopropyl telluride. Instead, this fraction could be an allyl telluride with a  $\text{C}=\text{C}$  double bond. This assumption would also explain the signals at  $m/z$  210, 212 and 214 which would correspond to diallyl telluride.

Lastly, the third organic telluride species was detected with the highest mass. The structure resembles that of diisopropyl telluride with masses at around 172  $m/z$ . However, strong signals were observed at around 256  $m/z$  which indicated ditelluride,  $\text{Te-Te}$ , species. The mass spectrum for this species is presented in Figure 4-3.

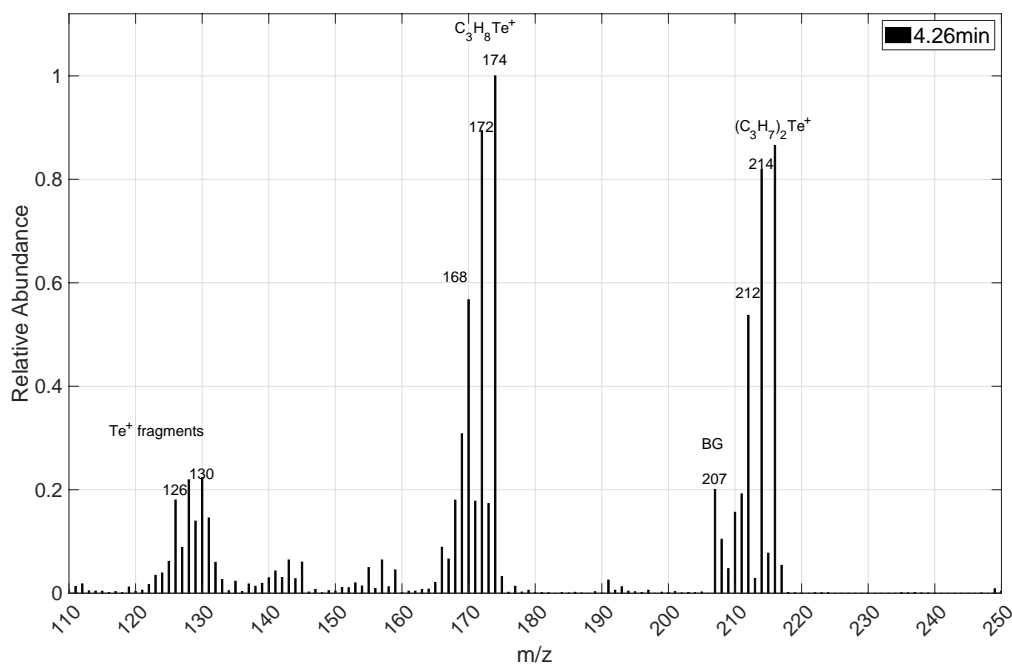


Figure 4-1: Mass spectrum for the irradiated sample containing texanol and  $TeO_2$  for a peak with retention time 4.26 minutes.

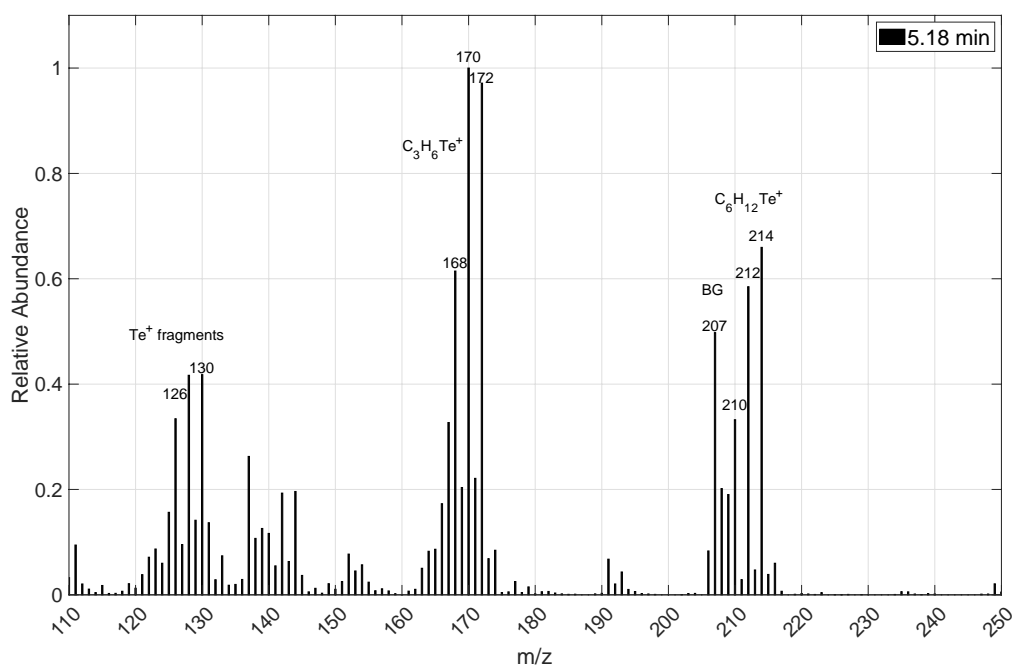


Figure 4-2: Mass spectrum for the irradiated sample containing texanol and  $TeO_2$  for a peak with retention time 5.18 minutes.

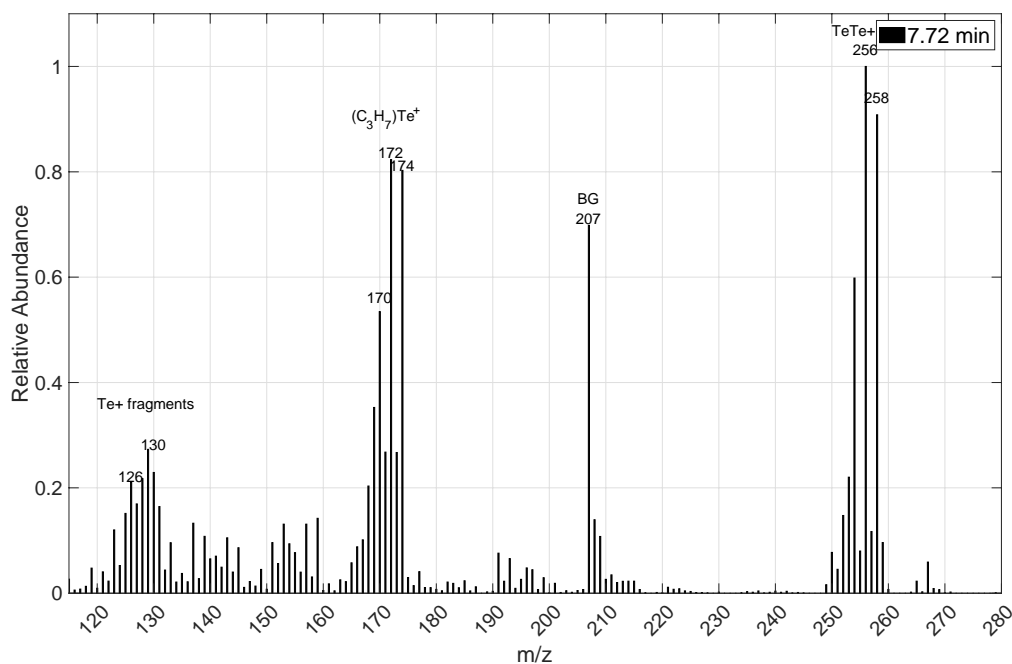


Figure 4-3: Mass spectrum for the irradiated sample containing texanol and  $\text{TeO}_2$  for a peak with retention time 7.72 minutes.

One organic telluride species was detected in samples with MIBK. As in the samples containing texanol, the irradiated MIBK sample had signals for tellurium fragments at m/z 126, 128 and 130 (Figure 4-4). In addition, there were signals for at around m/z 144 which likely correspond to methyl telluride,  $\text{CH}_3\text{Te}$  fraction. The highest mass was detected at m/z 202 with weaker signals 2 m/z apart at 198 and 200. Compared to the methyl telluride signals, the mass difference between the signals is 57 m/z, a fragment which could correspond to  $\text{C}_4\text{H}_9$ . Therefore, the organic telluride species in question could be methyl-isobutyl-telluride,  $\text{C}_4\text{H}_9\text{TeCH}_3$ . Considering the possible cleavage sites and leaving groups of MIBK, both methyl and isobutyl groups are plausible which strengthens the analysis of the telluride species.

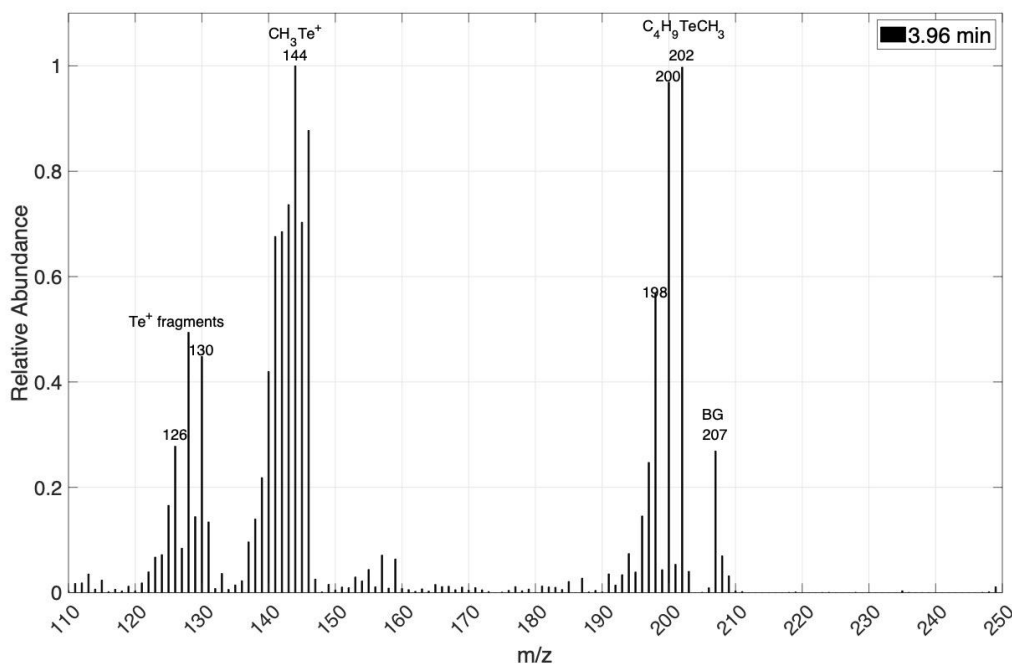


Figure 4-4: The mass spectrum of the tellurium species detected in a sample with TeO<sub>2</sub> and MIBK.

#### 4.2.2. Conclusions regarding the formation of organic tellurides from paint solvents

The formation of organic tellurides from paint solvents in a simulated water sump similar to the sump expected in case of a nuclear accidents have been investigated. The results imply that organic tellurides may form under the aforementioned conditions. Diisopropyl telluride was formed from TeO<sub>2</sub> and Texanol and was the main organic telluride observed. Decomposition of MIBK also formed another organic telluride. There is also evidence for the formation of DMT.

### 4.3. Radiolytic degradation of dimethyl telluride

The radiolytic degradation experiments were conducted to gain information on the stability of organic tellurides. In case organic tellurides decompose fast under irradiation, the probability for re-volatilization is low. The results presented here are for the radiolytic degradation of dimethyl telluride (DMT).

The degradation was studied in four different conditions to gain understanding about the radiolytic behavior and degradation mechanism. The four conditions were, aerated and deaerated water, borate buffer and sodium thiosulfate. The stock solutions were prepared by adding approximately 400 μL of liquid DMT to 400 ml of solution and mix. To minimize the possible degradation, the mixing time was kept short before preparing the samples for irradiation.

The samples were prepared by adding 10 ml of solution in a 20 ml headspace vial. The samples were then irradiated in the Gammacell 220 giving a dose rate of approximately 3.5 kGy/h at the time of the experiments. The temperature inside the Gammacell was



slightly over room temperature at around 300 K. The samples were irradiated for a time ranging from 10 minutes to 6 hours except for the deaerated aqueous samples where the irradiation was continued to 8 hours. After irradiation, the samples were taken out and analyzed with GC-MS for volatile tellurium species and with ICP-MS for total tellurium concentration. ICP-MS samples were prepared by oxidizing the remaining DMT with hydrogen peroxide to avoid any loss during sample preparation. All samples were prepared in triplicated for statistical significance.

#### 4.3.1. Results and discussion

##### Analysis with ICP-MS

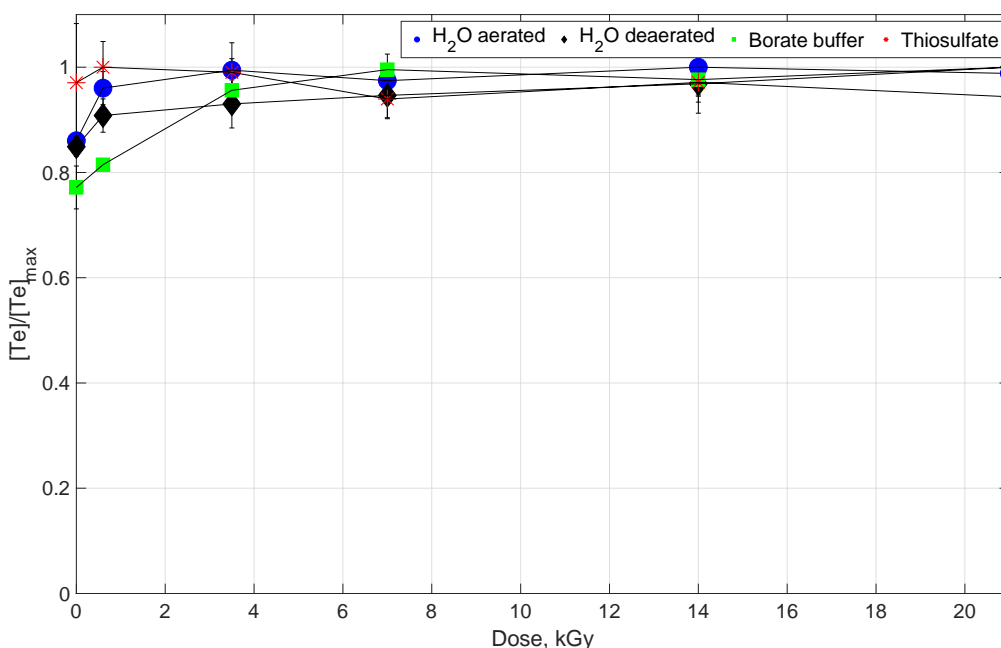


Figure 4-5: The normalized total tellurium concentration as a function of radiation dose.

The total concentration of tellurium was analyzed using ICP-MS. This was done to determine whether the loss of volatile tellurium was only due to degradation and not a result of volatilization or any other processes. The results for the concentration of tellurium normalized to the highest value as a result of irradiation dose in the four aqueous solutions are presented in Figure 4-5. Overall, the concentration stayed constant throughout the experiments. Some variation was observed in the first samples which is likely due to inhomogeneity of the stock solution. As the dimethyl telluride, when added to the aqueous solution, sank to the bottom of the flask, the concentration was likely slightly higher at the bottom which resulted in slight differences during sample preparation. However, it can be concluded that there was no loss of tellurium during the experiments.

##### Analysis with GC-MS

The degradation of dimethyl telluride was analyzed using GC-MS. The chromatograms showing the peaks for DMT are presented in Figure 4-6. The graphs A and B show the results for aerated and deaerated water, respectively. In aerated solution, the peak intensity decreased with increasing radiation dose whereas in the nitrogen saturated solution, the peak intensity stayed consistent up to 7 kGy after which the intensity decreased.

Graph C shows the results for DMT in ABS. The intensity decreased rapidly from 0 to 0.6 kGy after which the degradation is more consistent and after 21 kGy dose, the intensity is at the background level. Lastly, the results for DMT in sodium thiosulfate solution are shown in graph C. There, the intensity decreases fast in the first sample but then stays relatively consistent throughout the rest of the experiment.

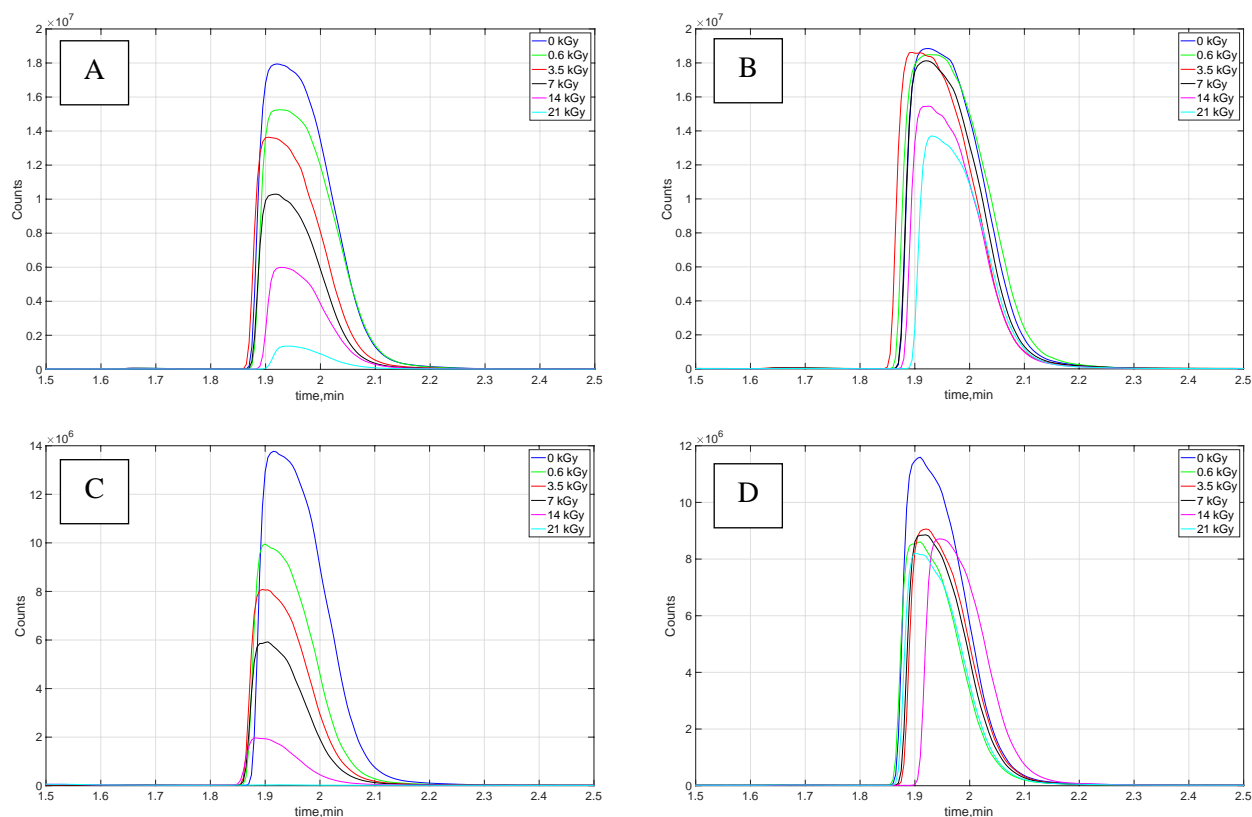


Figure 4-6: Chromatograms for dimethyl telluride degradation in A. aerated water and B. deaerated water C. ABS D. sodium thiosulfate solutions.

The results obtained from the GC-MS measurements were normalized to the highest value and are shown as a function of normalized intensity as a function of irradiation dose. Figure 4-7 presents the results for aerated and deaerated water as well as for the borate buffer. The results for sodium thiosulfate are presented separately in Figure 4-8. The intensity of DMT in aerated water decreased down to 6 % of the initial value after 21 kGy. The degradation is relatively linear and follows zero-order kinetics with a more rapid rate in the first 0.6 kGy after which the rate is relatively linear. A similar behavior was observed in the borate buffer. There, a rapid degradation was observed in the beginning after which the trend followed that of pure aerated water. In the absence of oxygen, DMT only degraded down to 60 % of the initial value. The degradation in the deaerated solution also follows zero-order kinetics but with a slower rate compared to the two aerated solutions. The differences likely originate from the amount of oxygen present in the solutions. Oxygen in the aqueous solutions leads to scavenging of reducing radicals which facilitates the oxidation in the solution but also consumes the oxygen with long irradiation times. The oxygen is also consumed via reactions with organic material which further decreases the dissolved oxygen concentration.

In addition to the oxygen effect, the most unexpected results were observed in the sodium thiosulfate solution (Figure 4-8). There, DMT degraded rapidly within the first 10 minutes of irradiation to about 73 % and only slightly decomposing during the rest of the irradiation. After 21 kGy, only about 60 % of the initial DMT was left. This behavior was surprising and unexpected, but likely relates to the complex radiolysis behavior of thio-sulfate ion.

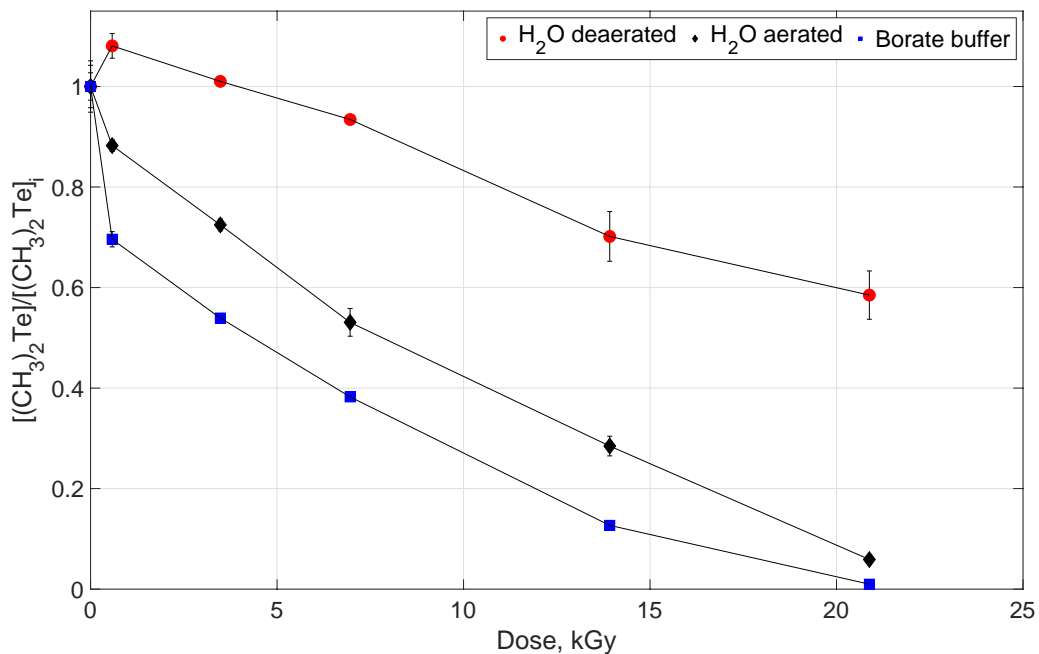


Figure 4-7: The normalized intensity of DMT in aerated (black) and deaerated (red) water and ABS (blue) as a function of irradiation dose.

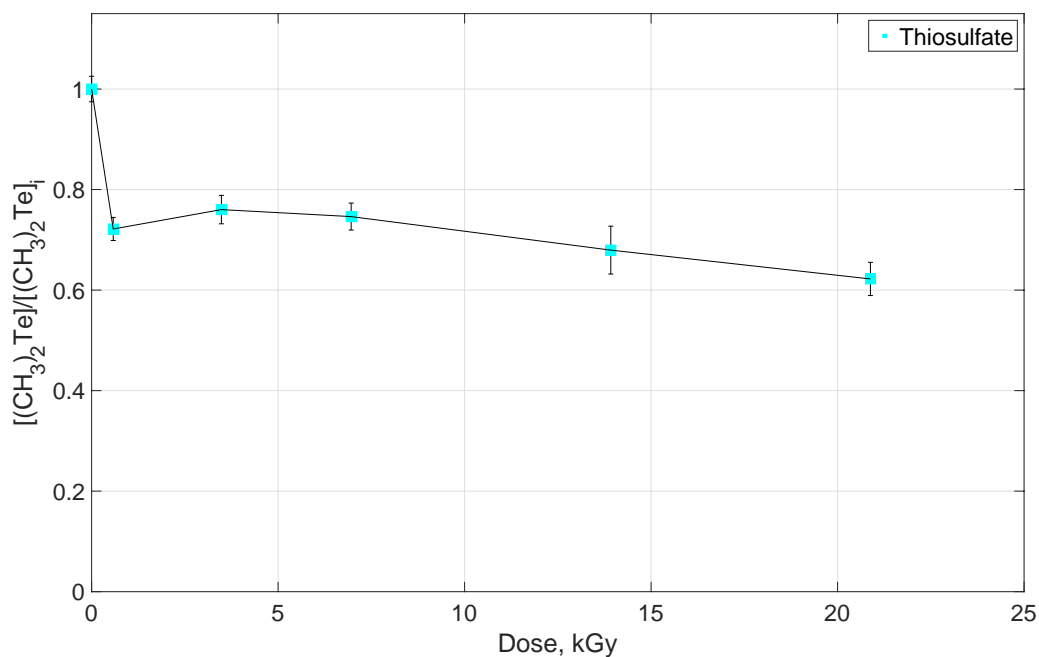
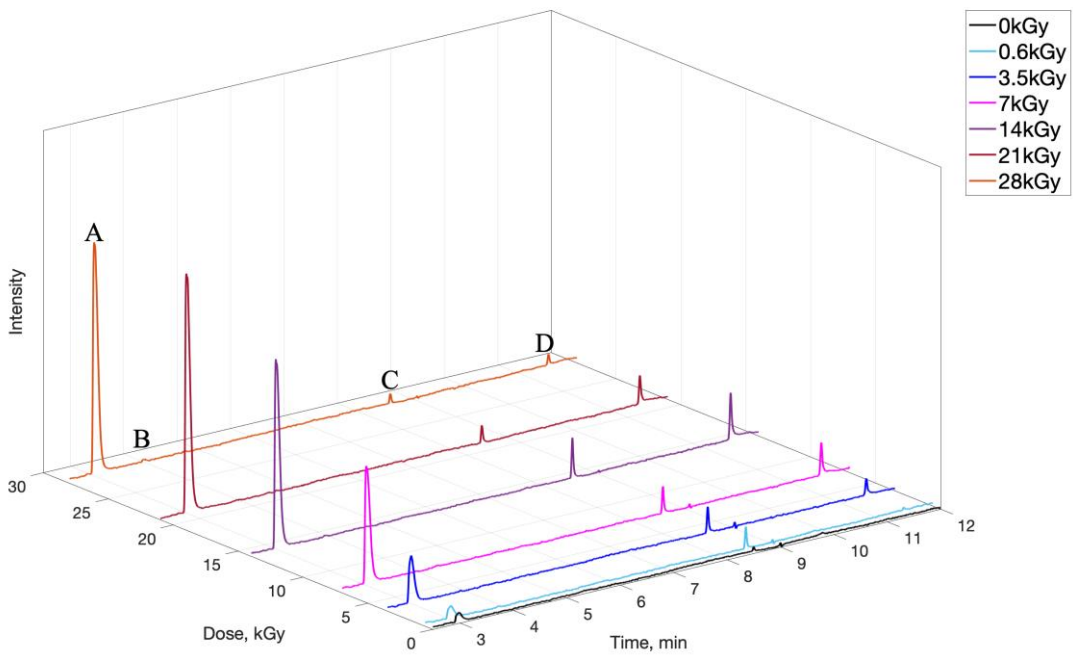
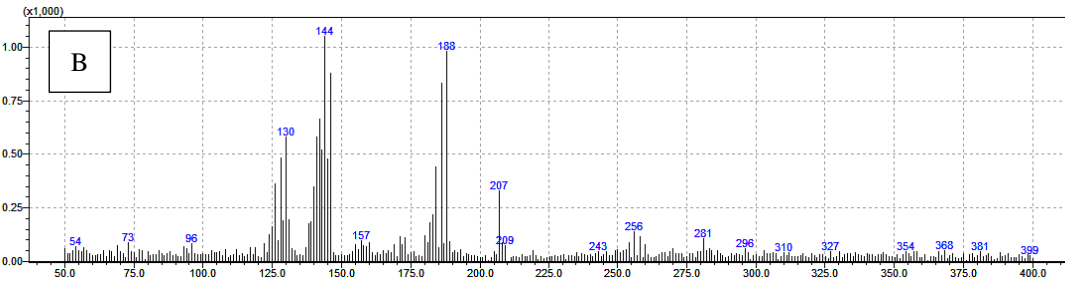
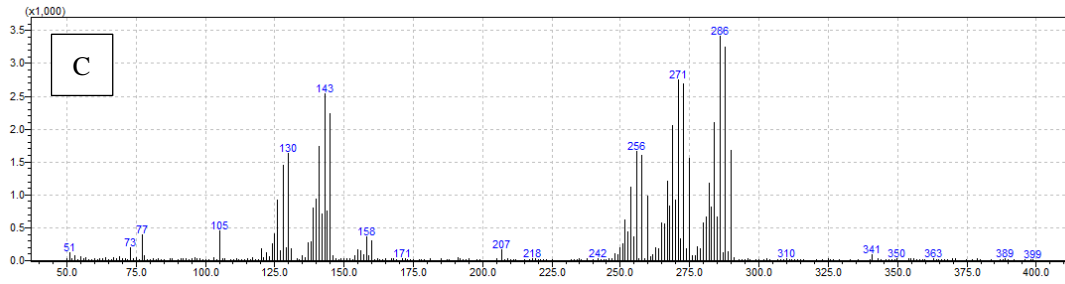
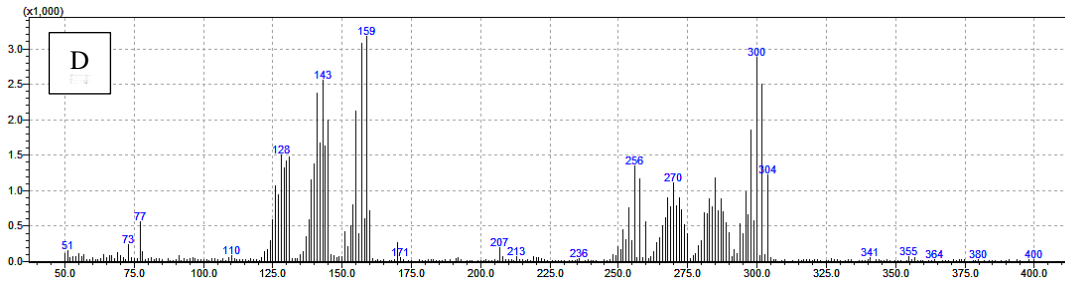


Figure 4-8: The normalized intensity of DMT in aqueous sodium thiosulfate as a function of irradiation dose.

Another phenomenon observed during the experiments was the formation of new higher mass organic species. This was a result of two reactions; lengthening of the carbon chain and dimerization of tellurium atoms forming ditellurides. Four new species were detected in the GC-MS. The chromatograms and the corresponding mass spectra are presented in Figure 4-9. The first peak was observed at around 3 minutes. The corresponding mass spectrum A was used to identify the species as methyl ethyl telluride. Further lengthening of the carbon chain to form the methyl propyl telluride was also observed (mass spectrum B).

Two species with Te-Te bonds were detected at 8.5 and 11.5 minutes (C and D). The peak at 8.5 minutes had a mass ion at 286 m/z and was identified as dimethyl ditelluride,  $CH_3TeTeCH_3$ . The last species had even higher mass at 304 m/z. In addition, it had a complete mass spectrum for dimethyl telluride between 126 and 160 m/z. This species is a dimethyl ditelluride dimer,  $(CH_3)_2TeTe(CH_3)_2$ .



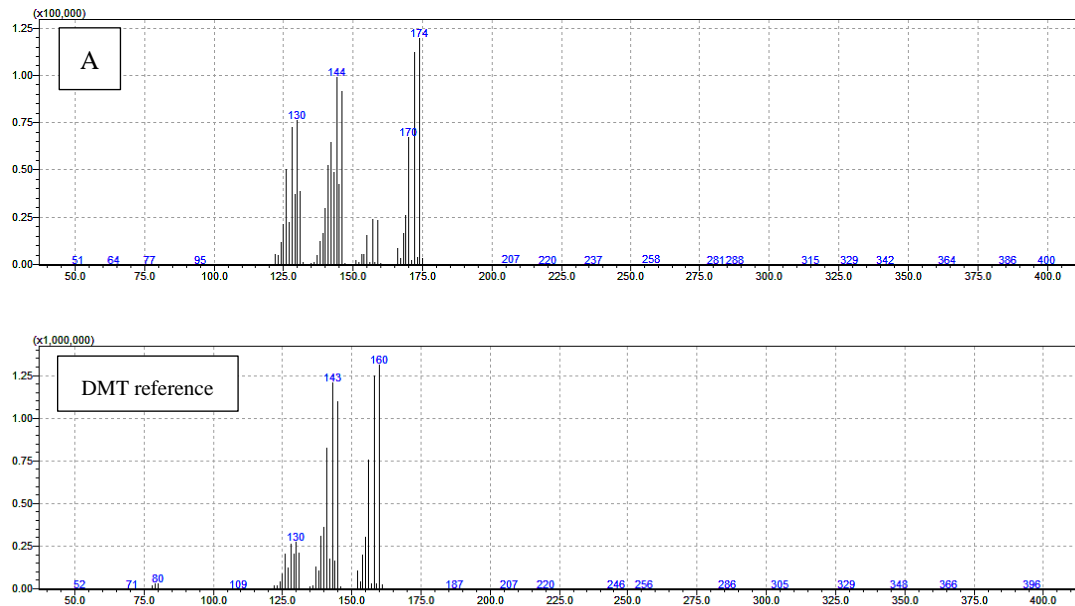


Figure 4-9: Chromatograms of the irradiated DMT solution in deaerated conditions and the corresponding mass spectra A. Methyl-ethyl telluride B. Methyl-propyl telluride C. Dimethyl ditelluride D. Dimethyl ditelluride dimer.

#### 4.3.2. Conclusions regarding the radiolytic degradation of DMT

The purpose of this study was to investigate the stability of DMT in aqueous solutions under conditions similar to those expected in case of a severe nuclear accident. The results imply that DMT is relatively stable in such conditions. The rate of degradation depends on the presence of competing species, and of oxygen. The degradation occurs through an oxidation reaction; hence the presence of oxygen serves to hasten the degradation. Without oxygen, dimerization occurs instead, leading to new volatile tellurium species.

#### 4.4. Gas-phase interactions between tellurium and organic material in severe accident-like circumstances

Tellurium is a substance that, in its pure form, melts at 450 °C and boils at 990 °C. It is thus possible that under accident conditions there may be tellurium in the gas phase, either as a gas or as aerosols. Furthermore, in and near the reactor containment there exist organic materials in the form of paints, cables, gaskets and the like. Previous studies at Chalmers have investigated the chemical inventory of the type of paint used in Swedish nuclear power plants, and it was concluded that it mostly consists of epoxy resin and polyamides [1]. A total of three types of paint were examined, and a number of substances that could dissolve in the reactor sump were detected. Methyl isobutyl ketone is one such substance that was detected in all three types of paints tested, as was acetone that was detected in two types. Of course, organic materials are likely to break down into simpler structures in the event of an accident. It is difficult, if not impossible, to determine with certainty what form they will take under accident conditions. What can be said, however, is that the organic materials are not dismissed as irrelevant to the chemistry of an accident, and their

interaction with tellurium at temperatures relevant to the primary circuit is of interest to study. There are several organic tellurides, but one of the simplest and most likely to form under breakdown conditions is dimethyl telluride, with a boiling point of 82 °C.

#### 4.4.1. Experiment

The experiments were carried out in a tube furnace with a steel tube. One gram of tellurium in its metallic form was placed in a crucible of aluminum oxide which was placed in the center of the heating section of the furnace. The temperature during the experiment was 540 °C to melt the tellurium and create a constant vapor pressure and relatively slow vaporization throughout the experiment.

A carrier gas with a flow of 3 litres per minute was connected to this furnace and was controlled by a mass flow control unit. The mixture of the carrier gas and the tellurium aerosols was fed via a three-way junction to another furnace of the same layout as the previous one. Via the three-way junction, the organic component was also supplied, which consisted of an aqueous solution with added acetone or 2-propanol, alternatively a gas flow consisting of 5% methane in argon. The gas flow through this line was 3 litres per minute, resulting in a total flow of 6 litres per minute through the second furnace, called the reaction furnace. This oven had a temperature of 300 °C.

After the second furnace, 1 litre of gas per minute was diverted and the resulting 5 litres per minute passed through a filter to capture all formed aerosols with a diameter greater than 5 µm. Beyond the filter, finally, there was a liquid trap consisting of 100 ml of 0.1 M NaOH to trap gaseous species or very fine aerosols.

The diverted gas is diluted with 10 liters per minute of hydrogen and sent through a number of measuring instruments that work in real time. A "differential mobility analyzer" (DMA), a "condensation particle counter" (CPC) and an "Electric low-pressure impactor" (ELPI) were all used together to count the number of aerosol particles of sizes between 1 nm and 10 µm. Furthermore, the total mass concentration of the particles in the gas stream was determined using a "tapered element oscillating microbalance" (TEOM), also in real time. Finally, the species in the gas stream could be determined using Fourier-transform infrared spectroscopy (FTIR). After the FTIR, another filter, identical to the previous one, was placed to capture the aerosols diverted from the main line. The entire system can be seen schematically in Figure 4-10.

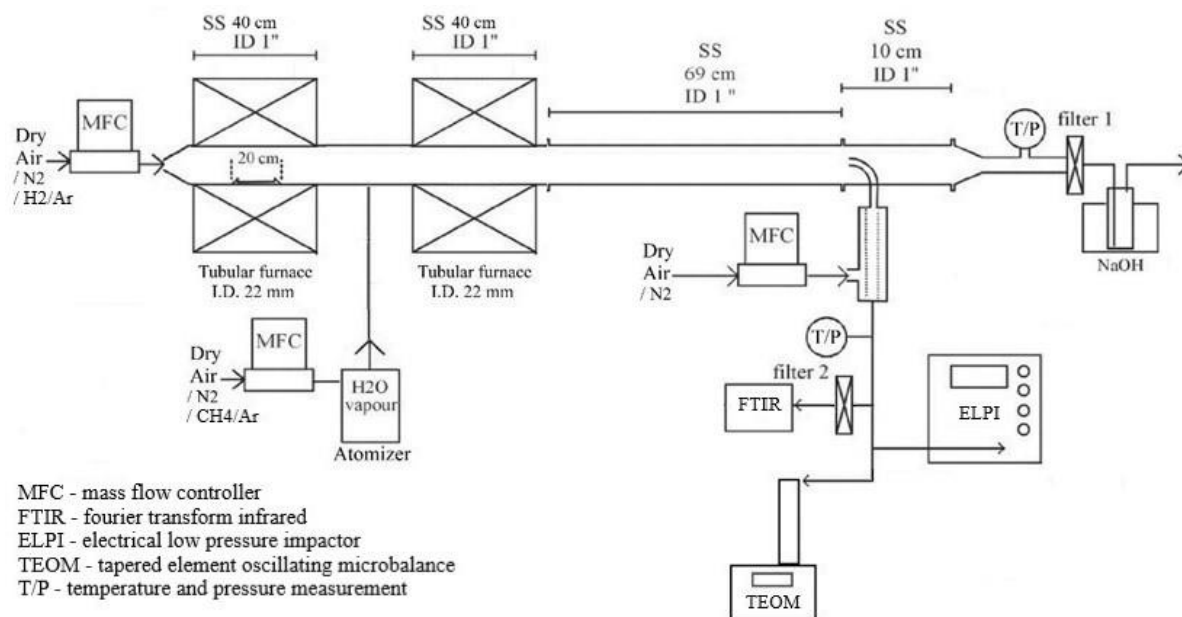


Figure 4-10: Schematic depiction of the experimental setup used in the tellurium studies.

A total of 8 experiments were performed, and they are described in Table 4-1. The experiments vary in atmosphere and in the organic species used. Only one experiment has been performed for each condition and uncertainty analysis is thus not possible.

Table 4-1: Experimental plan for the study of interactions between tellurium and organic species

Number	Precursor	Temperature, C	Atmosphere	Organic precursor
1	Te	540	Air	-
	Te	540	Air	Acetone
	Te	540	Air	1-Propanol
2	Te	540	N <sub>2</sub>	-
	Te	540	N <sub>2</sub>	Acetone
	Te	540	N <sub>2</sub>	1-Propanol
3	Te	540	H <sub>2</sub> /Ar	-
	Te	540	H <sub>2</sub> /Ar	Acetone
	Te	540	H <sub>2</sub> /Ar	1-Propanol
4	Te	540	H <sub>2</sub> /Ar	Methane
4.1	Te	540	N <sub>2</sub>	Methane

In addition to the above-mentioned analyses, ICP-MS was also performed to determine the contents of the liquid traps. However, it does not say in which chemical form the various substances exist.

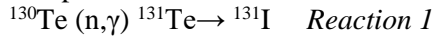
The filters were analyzed via SEM-EDX to examine their surface after the experiments and thus gain insight into the composition, shape and size of the tellurium aerosols. All filters were weighed before and after the experiments to determine the amount of material stuck to them.

Finally, the filters were examined using INAA gamma spectroscopy, which involves placing the filters in a capsule that is sent into a nuclear reactor, irradiating it with a known neutron flux, and then extract it. The radioactive material can then be measured by



gamma spectroscopy to determine the amount of material that was present on the sample. Note that after this analysis the radioactive samples must be discarded, so further analysis of them is not possible.

The process is based on the core reaction described in Reaction 1:



I.e.  $^{130}\text{Te}$  absorbs a neutron and forms  $^{131}\text{Te}$ , which decays to  $^{131}\text{I}$ .  $^{131}\text{I}$ , in turn, has a half-life of 8.03 days, and its decay can be measured i.a. gamma spectroscopy. The process thus measures iodine, rather than tellurium.

#### 4.4.2. Results and discussion

##### Contents of the liquid traps

Figure 4-11 depicts the results of the ICP-MS measurements of the liquid traps for experiments 1, 2 and 3.

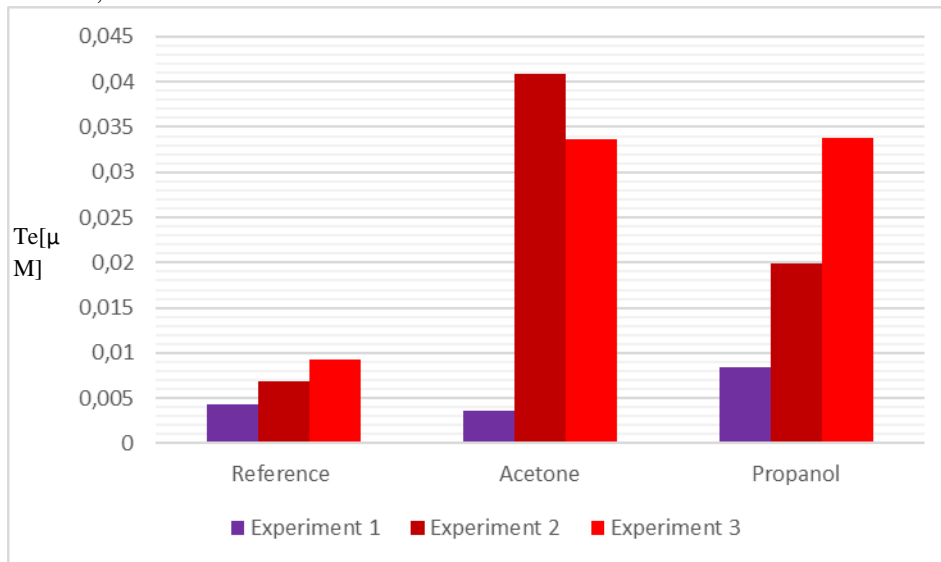


Figure 4-11: Amount of tellurium detected in the liquid trap after each experiment (names in the figure refers to Table 4-1). The addition of organic gives a noticeable increase in the tellurium concentration in the liquid traps.

Compared to the reference state for each atmosphere, the increase in tellurium concentration in the liquid trap is clearly seen when organic species are added. In the reference experiment, no organic species are used; the only thing in the system during those experiments is the carrier gas and tellurium. At the temperatures handled during this series of experiments, there are no known gaseous tellurium species that can form from tellurium and oxygen/nitrogen/hydrogen. One can thus assume that the tellurium found in the liquid trap after the reference experiments comes from very fine aerosols that can penetrate the filter.

Possibly, the fact that experiment 3 (reducing atmosphere) has the highest tellurium concentration in the reference could be related to the formation of  $\text{TeH}_2$ , which is a gas, but that species is not stable even at 300 °C [3], and the temperature in the line between the furnace and the liquid trap is even colder than that, so the contribution from the possible formation of  $\text{TeH}_2$  should be low, if it even exists; it is quite possible that the increase in

reducing environments is random, as only one experiment was performed in each environment.

The experiments performed in the presence of organic species see a clear increase in the tellurium concentration for both inert and reducing atmospheres, while for the oxidizing environment no major difference is seen. The result for the oxidizing atmosphere can be explained by the formation of tellurium dioxide early in the experiment. The way the system has been built, tellurium comes into contact with oxygen already in the first furnace at 540 °C, and tellurium dioxide is formed. Tellurium dioxide has a melting point of around 730 °C, so as the tellurium in the crucible oxidizes, there will be very little tellurium in the gas stream that can reach the filter. Obviously, the presence of organics does not matter in this scenario because the tellurium disappears from the system even before the organic species can play a role.

For inert and reducing atmospheres, we see a sharp increase of tellurium in the liquid traps. It probably means that under these conditions either very small aerosols are formed that can get through the filter, or that volatile species with such a low boiling point are formed that they are in the gas phase and can get through the filter. Organic tellurides could meet those requirements.

Without uncertainty analysis it is difficult to say, but at least under reducing conditions there does not appear to be much difference between the two organic species as both gives the same concentration of tellurium in the liquid traps. A possible explanation is that acetone is reduced by the hydrogen gas to 2-propanol, which should behave in a similar way to 1-propanol. However, that theory assumes that a ketone (acetone) is reduced to an alcohol by hydrogen alone, a reaction that is generally not possible [4]. The reaction also takes place at a high temperature and in the vicinity of an AISI316-L steel tube. The steel tube contains small amounts of nickel, so a catalysed reduction is possible, in theory.

Another possibility is pyrolysis of the organic components during the formation of radical organic species, which could react with tellurium and form organic tellurides. However, the pyrolysis of acetone does not appear to involve radical species, making that explanation less likely [6]. Pyrolysis of 1-propanol at higher temperatures (570-621°C) appears to give the end products acetaldehyde and a polymeric material [7]. However, the proposed reaction appears to involve several radicals as intermediate species, including  $\text{CH}_3\text{-CH}_2\cdot$ ,  $\cdot\text{CH}_2\text{-OH}$  and the hydrogen radical [7]. The temperature for which this is reported is higher than in the performed study, but it should be pointed out that the distance between the two furnaces is in the order of 10 cm, so it is quite possible that the temperature at the inlet of the reaction furnace is higher than 300 °C. However, the exact temperature is unknown.

Experiments 4 and 4.1 utilized methane gas as the organic species. These experiments were not performed in an oxygen-rich atmosphere due to the fire risk, but only in a reducing and inert atmosphere. The results from the liquid traps can be seen in Figure 4-12.

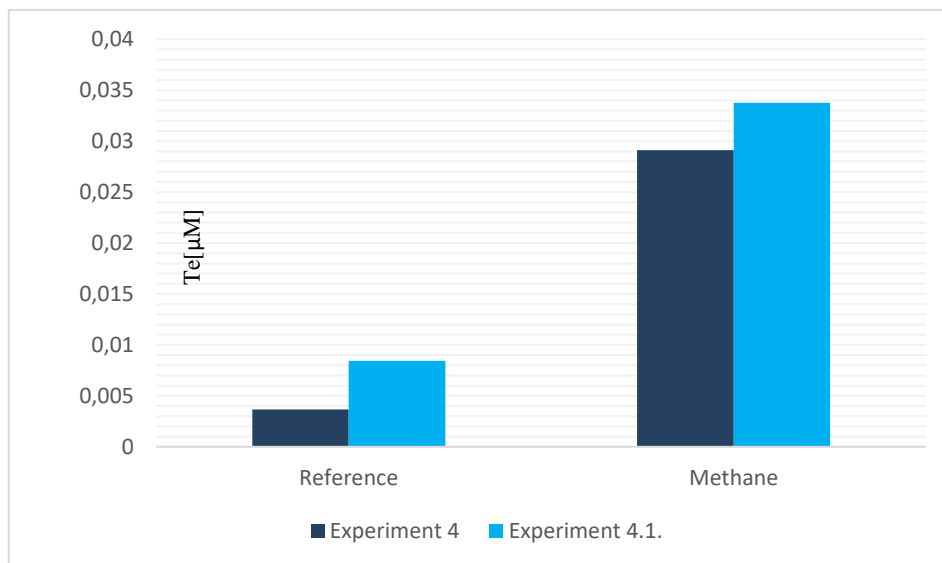


Figure 4-12: Amount of tellurium detected in the liquid traps after experiment 4 and 4.1 (the names refer to Table 4-1). Here too the organic additions to the gas stream gives a higher concentration of tellurium in the liquid traps.

Just as in the previous cases with reducing and inert atmospheres, the addition of organic species results in an increase of tellurium in the liquid traps compared to the reference conditions. As before, it is not possible to determine the species responsible for the increase. Pyrolysis of methane in an oxygen-poor atmosphere produces solid carbon and  $\text{H}_2$ , and tellurium has been reported to have been used to catalyse that pyrolysis [5]. However, that experiment was performed at a much higher temperature (827-977 °C) and with the method of bubbling methane gas through a column of liquid tellurium. Under these conditions and a residence time of 12 seconds, 30% pyrolysis was achieved. In the experiment conducted for this project, both the methane and the tellurium were diluted in the carrier gas, the residence time is less than 12 seconds, and the temperature is much lower. If pyrolysis takes place in the same way, it is therefore likely that it takes place to a relatively small extent. On the other hand, the formation of  $\text{H}_2$  and solid carbon could explain why the two conditions in experiments 4 and 4.1 are so similar. If hydrogen is formed through this reaction, the two atmospheres would become increasingly reducing.

#### 4.4.3. Filter appearance and SEM

The filters before the experiments are white discs of polytetrafluoroethylene. After the experiments, they essentially have two appearances; either they are black, or they are white. Furthermore, there are a couple of things in between, such as gray or pale beige. Examples can be seen in Figure 4-13.



Figure 4-13: *The two main appearances of the filters following the experiments.*

The white filters came mainly from experiment 1, i.e. from experiments performed in synthetic air. The white color can therefore be safely said to be tellurium dioxide. It is white and is formed when tellurium is heated in an oxygen-rich atmosphere. The most common filters are the black ones. All "main filters" i.e. filters placed before the liquid trap for the experiments in reducing and inert atmosphere were black in color. The color comes from tellurium in metallic form, which looks just like a black powder. There were also gray filters, mainly among the FTIR filters, which is also assumed to be only tellurium, but in such a small amount that the white filter shines through.

The surface of the filters was examined with SEM-EDX. Pictures of the morphology of the different filters can be found in Figure 4-14:

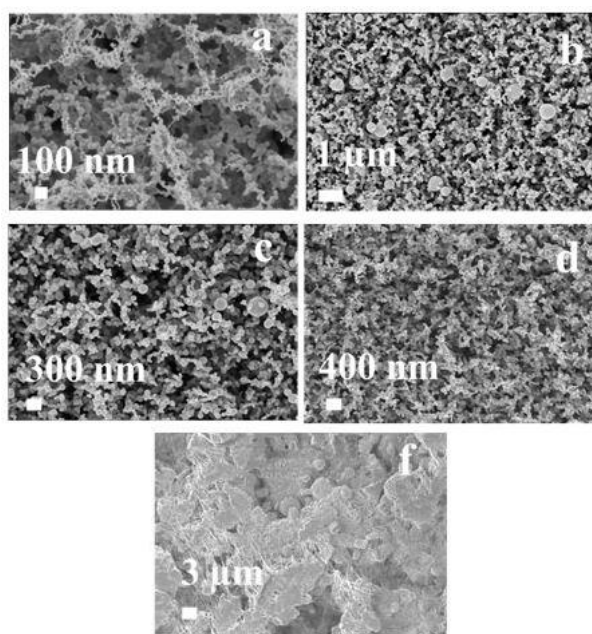


Figure 4-14: *SEM-images of the filter surfaces Micrograph "a" is of a filter subjected to oxidizing conditions, "b" is from inert conditions and "c" is from reducing conditions. "d" is from a filter in reducing conditions with methane added to the gas stream, and filter "e", finally, is of an unused filter.*

Most filters have similar surfaces, with particles of different sizes covering them regardless of the conditions the filters have been exposed to. The different scales in the images mean that there is uncertainty in the conclusions that can be drawn from the images, but it can be noted that at least images b, c, and d look relatively similar, as they mostly appear to consist of (more or less) spherical particles, potentially linked in chains. The same cannot be said for certain regarding image a, which rather appears to consist of thinner fiber-like networks. However, since the aerosols look so similar across all images, it does not seem likely that any one condition produces much smaller aerosols than another, so the explanation that organic species would cause a reduction in aerosol size cannot be considered supported by the SEM images.

#### 4.4.4. Neutron activation analysis

A total of 31 samples were measured using INAA. 22 samples were measured along with 2 standards, a blank filter, and six iron monitors. The iron monitors were placed at intervals of 6 "regular" samples and served to control and correct for the difference in the neutron flux on different parts of the irradiation capsule.

The mass of the nuclide  $^{131}\text{I}$  per filter that was calculated based on the neutron activation is presented in Table 4-2, and a more detailed description of the underlying method is described in an article by Jan Kučera et.al.[2]. Note that as each condition studied resulted in two filters, and they were basically very similar to each other, only the results for the main filters are presented.

Table 4-2: Result from the neutron activation analysis

Experiment	Sample conditions	Measurement geometry [Cm]	Concentration of $^{131}\text{I}$ [ $\mu\text{g/g}$ filter]	Combined uncertainty [ $\mu\text{g/g}$ filter; 1 std. dev.]	Relative combined uncertainty [%]
-	Blank Filter	20	4.62	0.135	0.73%
-	Standard-1	20	126	0.906	0.72%
-	Standard-2	20	124	0.905	0.73%
1	Reference, Air	20	23571	138.669	0.59%
1	Acetone, Air	20	77	1.035	1.35%
1	Propanol, Air	20	80	0.739	0.93%
2	Reference, $\text{N}_2$	45	181000	1294.439	0.71%
2	Acetone, $\text{N}_2$	20	2213	13.139	0.59%
2	Propanol, $\text{N}_2$	20	170	1.249	0.74%
3	Reference, $\text{H}_2/\text{Ar}$	45	124000	882.481	0.71%
3	Acetone, $\text{H}_2/\text{Ar}$	20	10849	63.825	0.59%
3	Propanol, $\text{H}_2/\text{Ar}$	20	5898	34.702	0.59%
4	$\text{CH}_4$ , $\text{H}_2/\text{Ar}$	45	127000	903.908	0.71%
4.1	$\text{CH}_4$ , $\text{N}_2$	20	3025	17.958	0.59%

There is apparently a large variation in measured iodine among the samples, corresponding to an equal variation in the tellurium concentration on the different filters, the highest concentration being more than a thousand times as high as the lowest.

In general, the INAA results appear to be consistent with what was seen in the liquid traps. The reference samples gave by far the largest amount of iodine on the filter, which is exactly the opposite of what is seen in the liquid traps, where the references had a comparatively small concentration of tellurium. The logic behind this could be that the more tellurium that sticks to the filter, the less can penetrate the filter; a line of reasoning that seems consistent with the results. Unfortunately, it is not possible to do a full mass balance over this experiment because a lot of tellurium crystallizes in the colder parts of the furnace or is diverted to the real-time measurements.

Experiment 1 refers to the experiment carried out in oxidizing atmosphere and shows a very low concentration of tellurium on the filter. The explanation given earlier also holds for this; oxidation of the tellurium metal in the crucible prevents it from vaporizing at all.

Very little tellurium can reach the filter (or liquid trap) and that is exactly what the analysis shows.

Based on the results from the filters, 1-propanol appears to be the more reactive of the two organics as it tended to give a lower concentration of tellurium on the filters. The exception is for the experiment that was performed in air, but in that case the concentration of tellurium on the filter is extremely low in both cases, and almost equal. It is not possible to draw any definite conclusions from that result. The fact that 1-propanol appears to give a lower concentration of tellurium on the filters could mean that 1-propanol has a (greater) tendency to form volatile species that can pass through the filter, but that explanation is not entirely satisfactory, since the content in the liquid traps does not fully correspond to that hypothesis. In the inert state, on the contrary, acetone gives a higher concentration of tellurium, and in the reducing state the concentration of tellurium is almost the same for both acetone and 1-propanol.

Finally, it is worth mentioning that the concentration of tellurium on the filter is relatively high in both cases where methane is used as an organic component. The concentration in the liquid traps is also relatively high in that case, comparable to the concentration of the other organic components. In that case, that result would mean that methane in particular provides a high volatility for tellurium, both in the form of a volatile substance (which is visible in the liquid trap) and in the form of aerosols (which we see on the filter). However, the process behind these observations is uncertain.

The experimental uncertainty looks stable, with only one experiment having a relative combined uncertainty above 1%. The background to, and the mathematical calculation underlying these calculations must be determined individually for each laboratory performing the work, but three major sources of error that should be considered are uncertainties related to sample preparation for the process (e.g. packaging and placement in the irradiation pod), uncertainties related to the irradiation process itself (depending on e.g. local variations in the neutron flux) and/or uncertainties related to the gamma spectroscopy (e.g. variation in the measurement geometry required to compensate for the different activity of the samples). These uncertainties have been determined and published previously for the laboratory that performed the neutron activation and gamma spectroscopy [8], and the details will not be reproduced here. The relative uncertainty has been taken as 0.5% for all calculations.

The individual spectrum of the different samples has been analysed. All samples were based on natural tellurium, so to some degree the gamma lines related to the isotopes that can be formed from nuclear reactions from them are found. In addition to tellurium and iodide isotopes, some contamination of caesium (observed in the form of  $^{134}\text{Cs}$ ) and iridium (observed in the form of  $^{194}\text{Ir}$ ) was also detected. None of these substances were used during the project. Caesium, which was observed for a few samples, could be a contamination from previous studies at VTT regarding volatile fission products, as caesium is of interest in that type of research, and previous work in the same lab has involved caesium iodide along with tellurium. However, iridium cannot be explained that way because it is not relevant to accident research. Since it was present in several samples, it is more likely that the contamination arose from the handling of the samples after the experiments, possibly in connection with the irradiation.

#### 4.4.5. Mass concentration in the carrier gas

The mass concentration in the gas stream was measured online, including TEOM, and the results for the first three experiments can be seen in Figure 4-15.

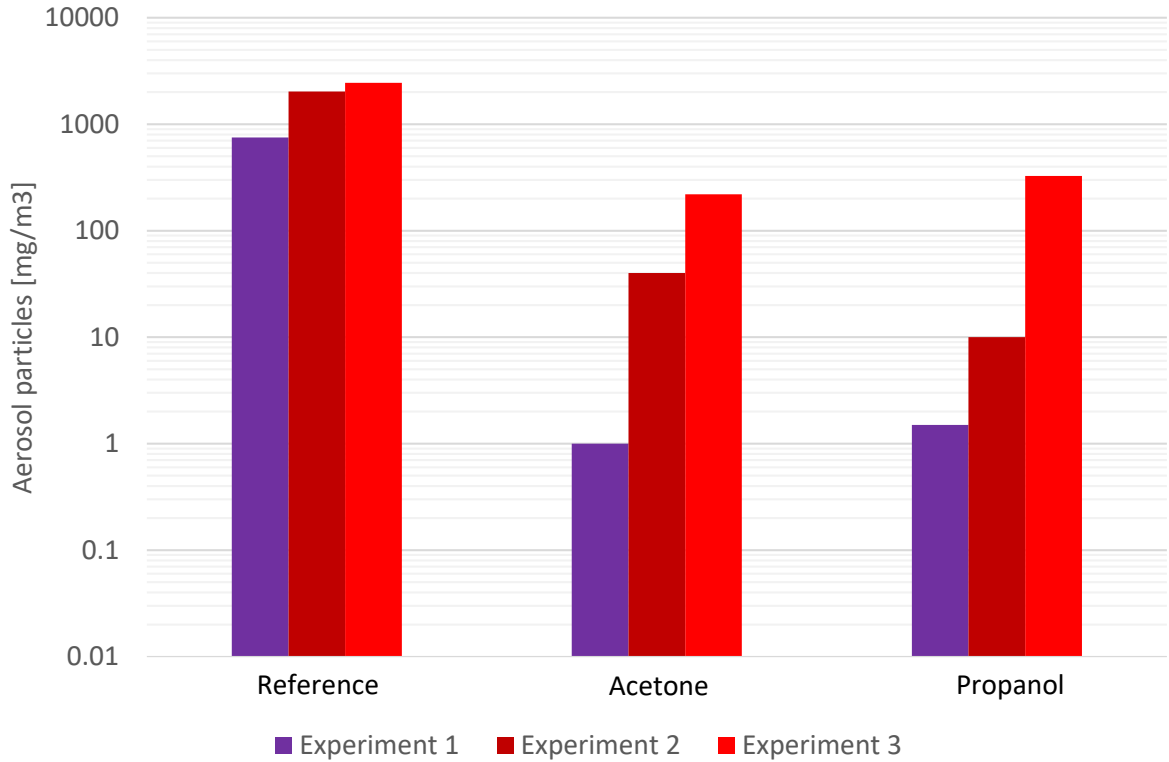


Figure 4-15: Impact of the different organic additives on the mass concentration of tellurium in the carrier gas compared to the reference cases without organics.

From a mass perspective, it looks like the addition of organic substances has an impact on the aerosols. In all experiments with organic additives, there is a decrease in the total aerosol mass. It is especially clear in the case of an oxidizing atmosphere (experiment 1 in Figure 4-16), where the mass concentration decreases by almost a factor of 1000 upon addition of acetone or 1-propanol. The other atmospheres also see a more modest decline; 20 to 100 times for inert atmospheres and about 10 times for reducing atmospheres.

Similar measurements have been performed for methane (for reducing and inert environments). These results are illustrated in Figure 4-16.

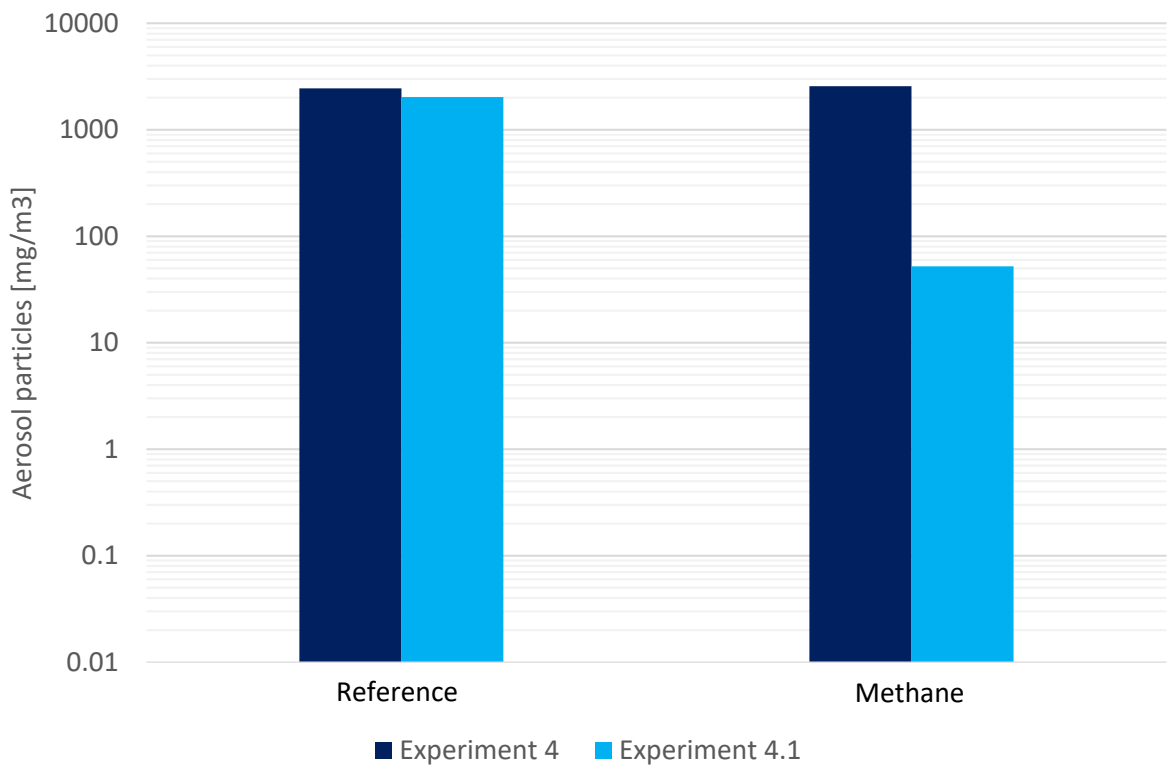


Figure 4-16: *Impact of methane on the mass concentration tellurium in the carrier gas, compared to the reference case without methane.*

The reducing atmosphere does not appear to have any influence on the mass concentration as it is almost unchanged from the reference case. The inert atmosphere shows a concentration drop of 20-40 times when methane gas is added. The total volume of carrier gas sent through the system was comparable across all cases, so the absolute mass of aerosols transported through the system will be similar to the distribution presented in Figures 4-15 and 4-16.

The reason for the reduction in mass concentration when organic species are added is uncertain. A partial explanation could be that the organic species are added together with water, which during heating causes further dilution of the gas stream, which reduces the concentration. The total amount of gas fed into the system has not been measured, so the magnitude of this effect cannot be estimated. Furthermore, it is possible that the addition of water causes condensation on the inside of the pipes in the colder parts of the system, which traps and prevents measurement of the aerosols.

A similar experiment is described in the literature [9] and uses the same equipment. Here it can be seen that the mass concentration of tellurium decreases with time, especially for the experiments carried out in an oxidizing environment. It seems to indicate that the average mass concentration is also affected by how long the measurement time is, especially in oxidizing conditions, when there is relatively little tellurium available overall due to oxidation.

The TEOM measurements point to a decrease in mass concentration upon addition of organic components, which could indicate consumption of tellurium for the formation of a gaseous species. The results from the ICP-MS and the liquid traps, on the other hand, do not support that theory. If it were the case that a new volatile species was formed to a



greater extent, it should mean that the experiments with a high tellurium content in the liquid traps would correspond to a gas stream with a low mass concentration, which is not the case. It is clearly noticeable in experiment 2 (which was carried out in inert atmosphere), where the mass concentration is the highest in the reference case, less when acetone is added, and least in the presence of propanol. The content of the liquid traps, on the other hand, is highest in the presence of acetone, less in the presence of propanol, and lowest in the reference case.

It is likely that the formation of an organic telluride reduces the mass concentration in the gas stream, but it does not appear that its eventual formation can be detected by the TEOM experiments alone; especially not considering the dilution of the gas due to the water additive.

#### 4.4.6. Conclusions regarding gas-phase interactions between tellurium and organic species in severe accident-like conditions

The goal of this study was to determine whether organic tellurides can form in the gas phase under conditions similar to those expected in the event of a severe accident.

The question still cannot be answered with certainty, but the presence of organic species in the gas phase did have an impact on the volatility of tellurium. The ICP-MS measurements of the liquid traps showed an increase in tellurium after organic species were added to the system for both inert and reducing atmospheres. In the oxidizing atmosphere, however, no increased volatility was seen, due to the oxidation to tellurium dioxide, which is not volatile at the studied temperatures.

The mass of tellurium on the filters, determined with INAA showed that the mass of tellurium on the filters used to be highest at the respective reference group, i.e. without the addition of organic substances. It appears that the addition of the organic species prevents tellurium from reaching the filter. There are several possible explanations for that.

The mass concentration of tellurium in the carrier gas generally decreases with the addition of organic species. It can be interpreted as more tellurium appearing in gas phase, rather than in aerosol form, alternatively that the tellurium interacts with the water in the system and sticks to the inside of the pipes due to condensation when the temperature drops.

One explanation for these results is the formation of organic tellurides, which are transported in the gas phase and get past the filter. This would also explain the increase in tellurium concentration in the liquid trap when organic components are added, and, at least in principle, be part of the explanation for the reduced mass concentration in the carrier gas. However, it should be pointed out that the reduction of tellurium in the carrier gas cannot be explained solely by an increased formation of gaseous species, as the reduction in mass concentration for a given experiment is not always matched by an increase in tellurium concentration in the liquid trap.

It has not been explicitly proven that organic tellurides can form under the conditions that have been investigated, but there are strong indications that point to it, and what can be considered certain is that the addition of organic matter to the atmosphere results in an increased volatility of tellurium.

## 4.5. Study of the retention of dimethyl telluride by activated carbon.

Based on the studies that Chalmers has carried out in connection with APRI-11, there is reason to continue to consider organic tellurides in accident research.

Filters based on activated carbon are used, in a nuclear context, within the containment ventilation system [10], sampling instruments [11] and in the respirators used by emergency workers [12]. These respirators have been tested and shown to be effective for a number of radioactive compounds, including organic iodides; in particular in dry environments [13].

However, the filters have not been tested for organic tellurides, which is the goal of this project. Furthermore, the adsorption mechanism of organic tellurides on activated carbon is studied.

### 4.5.1. Method and experiments

The activated carbon filters under study are referred to as "Carbon A-D". Carbon A comes from a 3M (60928) respirator, "Carbon B" from a Dräger (X-plore 6000) respirator, "Carbon C" from a Scott Pro 2000 (CF32 ABEK2) respirator, and "Carbon D", finally, comes from a filter module used in a Swedish nuclear power plant.

The experimental setup used is shown in Figure 4-17. A glass tube was filled with 8 pads of activated carbon weighing  $250 \pm 1$  mg. The pads were separated by glass wool. In total, the filters and the glass wool occupied a distance of about 10 cm in the glass tube. The flow through the tube consisted of nitrogen gas and was measured by a flow meter. Organic telluride was injected i.a. a syringe through a septum. The outlet of the filter tube was led down into a liquid trap filled with 1%  $H_2O_2$  to capture any organic tellurides that did not stick to the carbon filters.

The flow through the system was  $1 \text{ Lmin}^{-1}$  (corresponding to a flow rate of about 20 cm/s). About 80  $\mu\text{L}$  of DMT was injected about 10 cm from the first carbon pad. The gas flow was kept constant for 30 minutes.

For "Carbon A" both measurement time and flow rate were varied in a series of separate experiments.

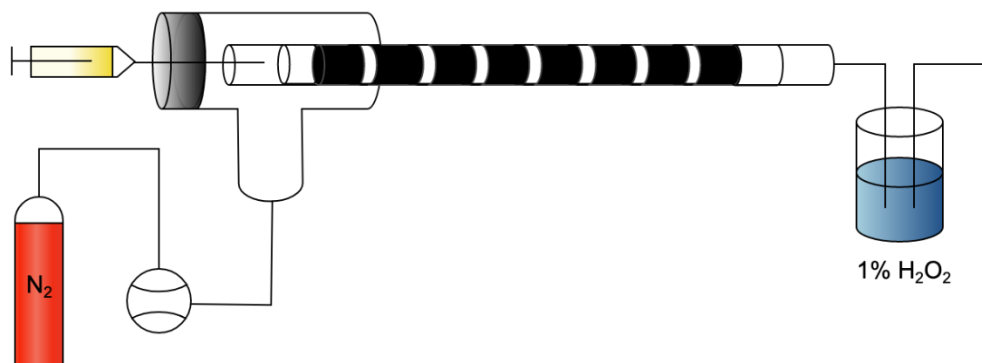


Figure 4-17: Schematic image of the experimental setup.

After the experiment, the carbon pads were separated into 20 ml glass jars, and the glass wool was also collected for analysis. 10 ml of 0.6% H<sub>2</sub>O<sub>2</sub> in 0.1 M NaOH was added to each jar to leach out the tellurium stuck to the pads. The samples were lightly mixed and left for about an hour. Samples were also taken from the liquid trap and from the liquid used to wash the glass tube. All liquid samples were diluted to appropriate concentrations for analysis by ICP-MS.

To investigate the ability to leach tellurium from the carbon samples, batch-by-batch reference experiments were performed. 50 mg of each carbon sample was weighed and 10 µL of DMT was added. A blank experiment consisted of adding 10 µL of DMT to an empty container. The samples were left for 1 hour to equilibrate with the carbon, after which 2 ml of 0.6% H<sub>2</sub>O<sub>2</sub> in 0.1M NaOH was added to each vial and mixed. H<sub>2</sub>O<sub>2</sub> was chosen to oxidize the tellurium to a soluble, non-organically soluble form and to facilitate the leaching process. The concentration is kept low due to the risk of its decomposition and its strong reaction with carbon. After one hour of leaching, a sample was taken which was diluted and analyzed in ICP-MS. All samples were taken in triplicate.

The carbon surfaces were examined with SEM-EDX to determine morphology and chemical composition. The specific surface area of the carbon particles was determined, i.a. Brunauer, The Emmett Teller Method (BET Method). An "Atmospheric Solids Analysis Probe" was used for the measurement and nitrogen gas at a temperature of 77 °K was used for the absorption. The carbon particles were dried for 25 hours at 100 °C before the BET study. One type of carbon had been investigated previously, and in that case the value from that study is used [13].

## 4.5.2. Results

### Surface analysis and SEM

All filter materials had a porous structure when examined with SEM-EDX, which can be seen in Figure 4-18. the carbon particles were irregular with sizes of a few hundred micrometers up to 2 millimeters. Carbon D in particular had larger particles than the other filters. Cracks and larger pores could also be seen in some particles.

The substances observed with EDX for the different carbon types, and the surface area measured with BET are presented in Table 4-3. The weight of carbon sample in each pad was constant, but as the grain size and structure differ between different carbon samples, the packing density is slightly different for the different samples. Carbon D had the largest carbon grains, and thus the lowest packing density, while Carbon C had the smallest grains and the highest packing density. In general, the surface area is large for all the carbons tested; between 680-780 m<sup>2</sup>/g. The surface area comes mainly from micropores on the carbon grains.

*Table 4-3: Specific surface area and elemental analysis for the investigated carbon filters*

Carbon	A	B	C	D
Origin	Respirator	Respirator	Respirator	Filter module
Specific surface area [m <sup>2</sup> g <sup>-1</sup> ]	781 ± 45	754 ± 45	686 ± 40	705 ± 45
Packing density, [g/cm <sup>3</sup> ]	0.354	0.354	0.398	0.318

Trace elements according to EDX	Si, Al, Mg	Zn, Cl	Zn, Cl	Si, K, Mg
---------------------------------	------------	--------	--------	-----------

The activity of carbon particles can be improved by activation with other substances, such as metals. The analysis indicates that the carbon here is based on wood because silicon and potassium are detected. Carbons B and C contain traces of zinc and chlorine, indicating that they have been activated with zinc chloride. Since the study [13] it is known that carbon A has not been activated by any metal.

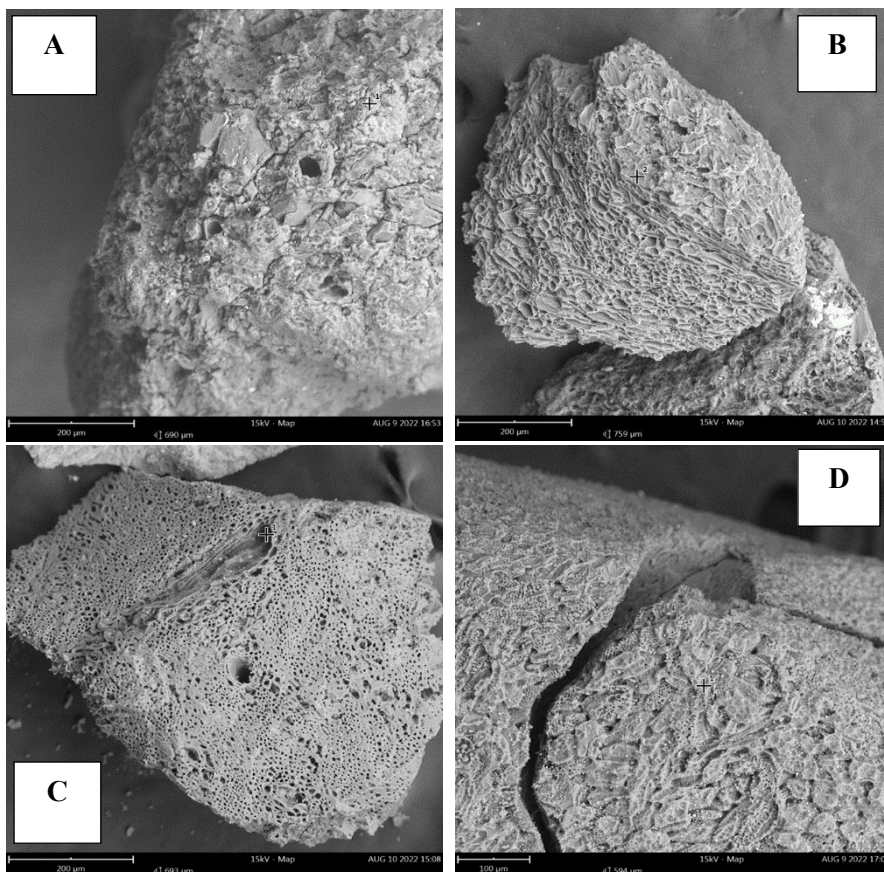


Figure 4-18: SEM micrographs of the different carbons.

The average portion of tellurium that could be leached from the carbon samples is presented in Table 4-4, with standard deviations.

Table 4-4: Portion of tellurium that could be leached from the carbon samples

Carbon type	Percentage leached from the carbon [%]	Percentage leached from the vial [%]
A	106.6 ± 14.7	1.6 ± 0.7
B	56.3 ± 11.1	1.7 ± 0.3
C	53.8 ± 9.2	1.4 ± 0.9
D	52.7 ± 8.2	2.0 ± 0.9

The results were calculated by comparing the tellurium recovery with the concentrations measured in the samples without any carbon. For carbon samples B, C, and D, the results are quite similar; recovered tellurium is about 55% with standard deviations of about 10%. Thus, the leaching efficiency, with respect to recovered tellurium gas, is low, but the possibility of reproducing and comparing the results is achieved. It is also possible that sequential extraction and/or longer leaching time results in a higher tellurium recovery.

Carbon A has a much greater recycling tendency; average tellurium recovery is over 100% with 15% uncertainty. The recovery is thus double compared to other filters. The difference probably comes from a different activation mechanism, and differences in the filter's pore structure.

The proportion of tellurium remaining in the vials after leaching was also measured and can be seen in table 4-4. The proportions are between 1.4–2% with relatively high uncertainties. Most of the added dimethyl telluride was thus absorbed on the carbon sample, rather than the vial itself.

Comparison of the different carbon filters' interaction with organic tellurides

The different filter materials were exposed to the same conditions for 30 minutes and their efficiency with respect to adsorption of DMT was compared. The adsorption results are presented in Figure 4-19 as the percentage of tellurium found in each pad. For all carbon types, the adsorption followed first-order kinetics, and between 58-68% of DMT was already adsorbed at the first carbon pad. The highest percentage was absorbed by carbon B. Pad number two absorbed between 23-33%, and for this pad carbon C was the most effective, and carbon B the least effective. Only small proportions were found at pad three, and no measurable tellurium contamination could be detected at the later carbon pads.

All four carbon types were able to adsorb DMT. The variations between the carbons come because of their individual structure; pore size and structure, as well as packing density probably affect the interaction with DMT. All carbon types were able to completely adsorb the added dimethyl telluride, and no tellurium could be detected in the liquid traps.

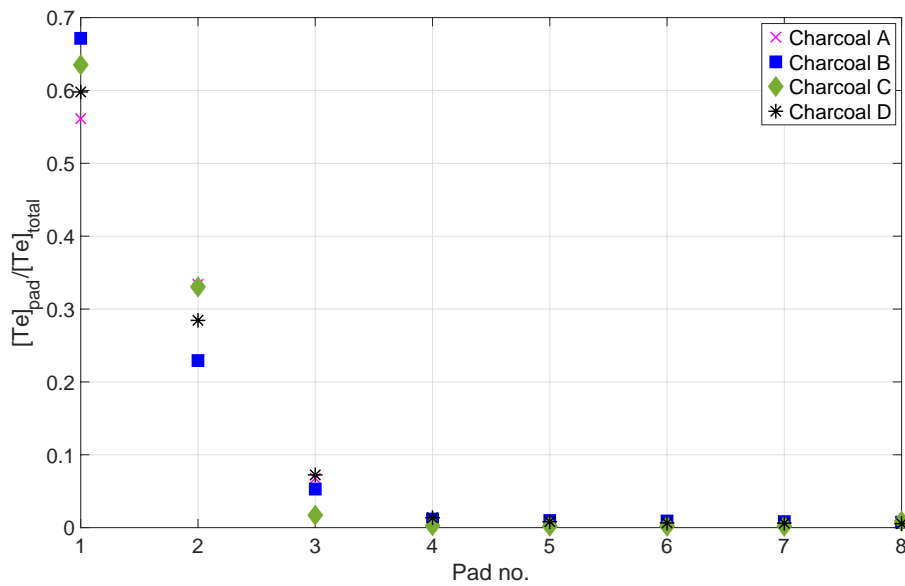


Figure 4-19: Share of the tellurium found at each carbon pad for the different filters.

To determine the rate constant of the adsorption process, the fraction of tellurium presented in Figure 4-19 was converted to a logarithmic scale based on mass and considered as a function of the distance in the column. The difference in the packing densities is taken into account here with the distance. Since no tellurium could be detected after three pads, only the first four pads are used to determine an exponential function for the result. These can be seen in Figure 4-20.

The slope of the curve versus the natural logarithm of the mass of tellurium in the carbon, plotted against distance gives the rate constant  $k_A$  divided by the linear flow rate  $VL$ .  $VL$  is about 20 cm/s, and with a void fraction of 0.7 in the tube, it carries about 30 cm/s in the packed column. This gives slopes on the different adsorption curves between -0.13 and -0.24 for all carbons.

Carbon type C has the steepest curve, again probably due to packing density and structural differences. All adsorption rate constants and correlation coefficients are tabulated in table 4-5.

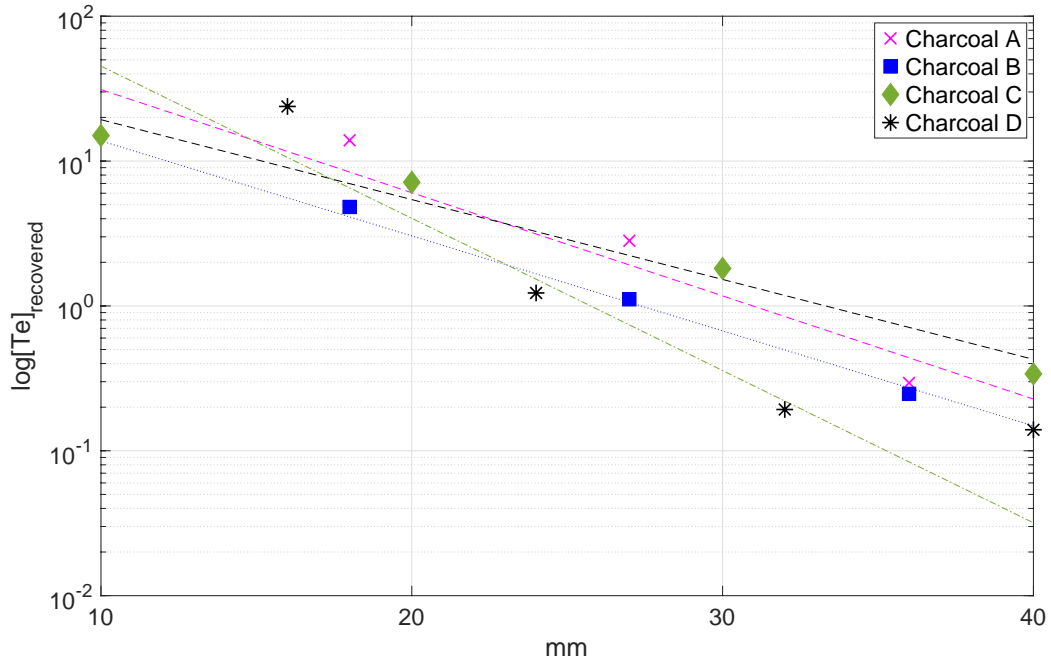


Figure 4-20: Adsorption of DMT as  $\ln(\text{Te})$  plotted against the distance in the column (mm) for the first four pads of the different carbon types.

Table 4-5: Adsorption rate constants for the different carbon types.

Carbon type	Proportionality constant, $\ln[\text{Te}]$ against distance (mm)	$R^2$	Adsorption rate constant ( $\text{s}^{-1}$ )
A	-0.164	0.86	49
B	-0.151	0.99	45
C	-0.242	0.85	73
D	-0.127	0.96	39

### 4.5.3. Diffusion of DMT in carbon type A

Carbon type A was selected for further study and exposed to longer flow times. The result of the subsequent leaching can be seen in Figure 4-21. The longer exposure times resulted in a wider distribution of the tellurium contamination in the column. With an exposure of 5 minutes, almost 70% of all adsorbed tellurium was observed in the first pad; about 6 percentage points more than with 30 minutes of exposure.

As the exposure time was extended, the proportion of tellurium detected in the first pad decreased. After a 330-minute exposure, only 18% of the total tellurium was recovered in the first pad, and the remaining tellurium had diffused further down the column. Traces of tellurium were found on all pads 1-6. In this experiment. This indicates that the adsorption process on activated carbon with DMT is reversible, but the eight pads with a total of 250 mg carbon in each were still enough to completely prevent DMT from reaching the liquid trap.

Methyl iodide, another organic species relevant in accident contexts, has been shown to move extremely slowly on activated carbon [14], unlike DMT, which can apparently remobilize after adsorption.

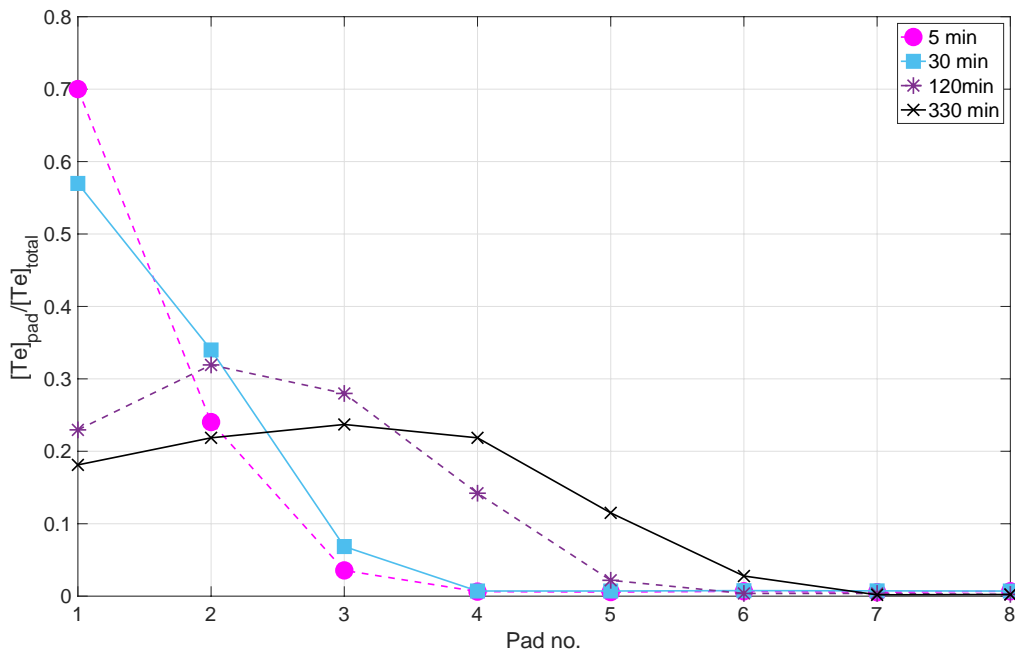


Figure 4-21: Distribution of DMT in the pads for carbon type A with different exposure.

### 4.5.4. Impact of flow rate on the absorption of DMT

Carbon type A was also exposed to different flow rates. The results from these experiments can be seen in Figure 4-22. The flow rates used were 0.5, 1 and 2 l/min. The increase in flow rate resulted in DMT penetrating deeper into the carbon bed, especially when the flow rate was doubled (to 2 L/min) the difference was clear. For the two slower flow rates, adsorption follows first-order kinetics, and DMT adsorbs on the first three carbon pads. For the increased flow rate, tellurium is also detected up to pad 6. These results

indicate that the adsorption process is strongly dependent on kinetics, and that the mechanism may be more complex than an irreversible adsorption.

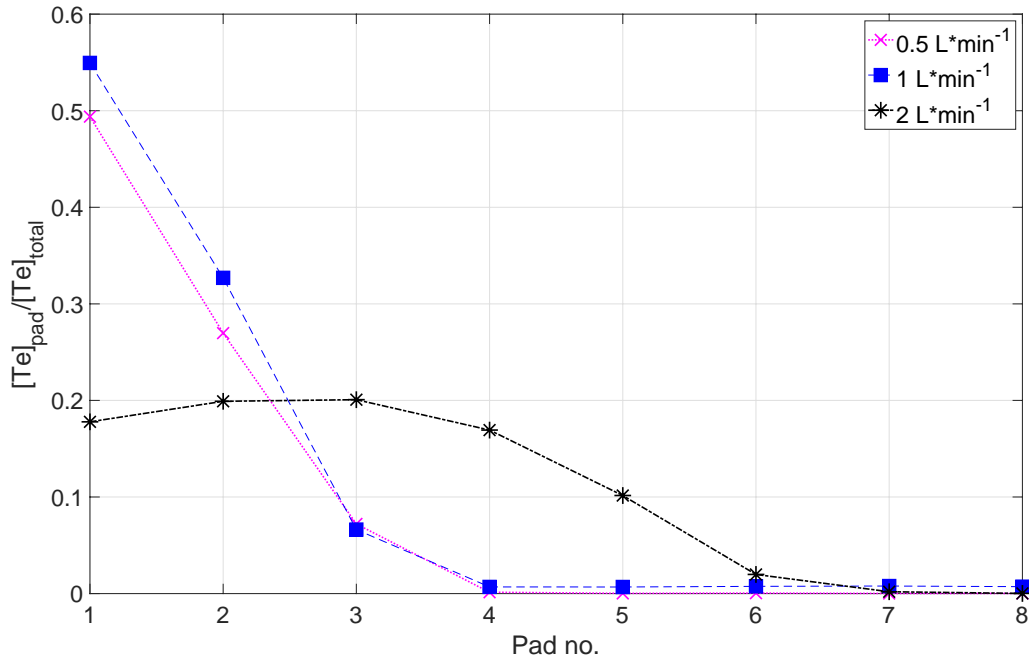


Figure 4-22: Share of tellurium found in the different pads for different flow rates of the carrier gas.

#### 4.5.5. Conclusions

The efficiency of filtering DMT, among others activated carbon has been investigated. Four types of activated carbon from respirators and from the filter module of a Swedish nuclear power plant were investigated, and all were found to be effective at adsorbing DMT. Some differences were observed for the different carbon types, probably due to the differences in structure and activation mechanism. An increase in the exposure time resulted in an increased transport of DMT. One hypothesis is that the adsorption process includes both adsorption and desorption, and that the desorbed dimethyl telluride is adsorbed again at the next carbon pad. An increase in the flow rate of the carrier gas led to a similar result where DMT was detected deeper into the filter tube. The adsorption process thus appears to be a kinetically controlled process.

Activated carbon has been shown to be effective at adsorbing DMT, but there are still questions related to the adsorption mechanism that should be studied further.

#### 4.6. Conclusive remarks regarding Chalmer's work regarding APRI-11 and future work in APRI-12.

The work at Chalmers within APRI-11 has included, at the time of writing, three published articles and a couple of manuscripts, produced by two doctoral students. The work



has focused on the fission product tellurium and its interaction with organic materials, both in irradiated environments and at temperatures representative of the primary circuit/containment in the event of a breakdown. Research has also been conducted to study the persistence of the expected organic tellurides in the containment water under high irradiation.

The work has been carried out at Chalmers, and at VTT (Espoo, Finland) with which Chalmers' department for nuclear chemistry has a good collaboration. The collaboration has developed further, and another work has recently been completed at the same location. This work (which goes by the name "Project TRIO") aims to investigate the interaction of tellurium with boric acid at temperatures representative of the primary circuit, as well as the possible effect of iodine and/or caesium iodide on this system. However, this work has not yet been published, and the results are currently being analysed. The hope is that the above project will result in one or two publications, as well as a report for NKS (Nordic Nuclear Safety Research, which partially sponsors the project) which will be available for free in their archive.

In addition to this, the Gammacell 220 at Chalmers has undergone a minor modification where channels in the top of the cell have been re-opened, which enables the transport of gases in and out of the radiation field. Plans exist for a project where carrier gas is bubbled through an organic liquid and saturated, whereupon the gas is brought into contact with tellurium under irradiation. Depending on the results, the concept may be developed, among other things by varying the carrier gas (in principle, gases such as hydrogen, synthetic air or air radiolysis products such as NO<sub>x</sub> and/or Ozone could all be of interest).

Another experimental approach based on the formation of organic tellurides would be to investigate the relative formation of organic tellurides and organic iodides. With APRI-11, there is a reasonable argument that both organic iodides and tellurides can be formed. The selectivity in their formation, and whether one of these species takes the upper hand in the formation, is considered worthy of study.

## 4.7. References

- [1] S. Tietze, M. R. St J. Foreman, C. H Ekberg, B. E. van Dongen, Identification of the Chemical inventory of different paint types applied in nuclear facilities, *Journal of Radioanalytical and Nuclear Chemistry*, 295, 1981-1999, 2013, <https://doi.org/10.1007/s10967-012-2190-3>, retrieved 2022-06-13
- [2] J. Kučera, A-E. Pasi, F. Espegren, T. Kärkelä, H.V. Lerum, J.P. Omtvedt, C. Ekberg, Tellurium determination by three modes of instrumental neutron activation analysis in aerosol filters and trap solutions for the simulation of a severe nuclear accident, *Microchemical Journal*, vol 158, 2020, retrieved 2023-02-21, <https://doi.org/10.1016/j.microc.2020.105139>
- [3] F. Garisto, Thermodynamics of iodine, cesium and tellurium in the primary heat-transport system under accident conditions, IAEA, INIS vol.15, 14, 1982, retrieved 2022-08-24
- [4] J. Clayden, N. Greaves, S. Warren, *Organic chemistry*, second edition, Oxford University Press, 2012, ISBN 978-0-19-927029-3
- [5] J. Zeng, M. Tarazkar, T. Pennebaker, M.J. Gordon, H. Metiu, E.W. McFarland, Catalytic Methane Pyrolysis with Liquid and Vapor Phase Tellurium, *ACS Catalysis*, vol. 10, 2020, pages 8223-8230, retrieved 2023-03-08, <https://dx.doi.org/10.1021/acscatal.0c00805>
- [6] J. G. DAVOUD, C.N. HINSHELWOOD, Thermal Decomposition of Acetone. *Nature*, 144(3656), 909–910, 1939, doi:10.1038/144909a0, retrieved 2022-11-24
- [7] J.A. Barnard, H.W.D. Hughes, The Pyrolysis of n-propanol, *Transactions of the Faraday Society*, Volume 56, 1960, retrieved 2023-01-17, <https://doi.org/10.1039/TF9605600064>
- [8] J. Kučera, P. Bode, V. Štěpánek, The 1993 ISO Guide to the expression of uncertainty in measurement applied to NAA, *Journal of Radioanalytical and Nuclear Chemistry*, vol 245, 115-122, retrieved 2023-22-28, <https://doi.org/10.1023/A:1006760726572>
- [9] F. Espegren, T. Kärkelä, A-E. Pasi, U. Tapper, J. Kučera, H.V. Lerum, J.P. Omtvedt, C. Ekberg, Tellurium transport in the RCS under conditions relevant for severe nuclear accidents, *Progress in Nuclear Energy*, vol 139, 2021, retrieved 2023-03-15, <https://doi.org/10.1016/j.pnucene.2021.103815>
- [10] D. JACQUEMAIN et al., “Status report on filtered containment venting: OECD Nuclear Energy Agency Report NEA/CSNI/R(2014)7,” Paris, France/Boulogne-Billancourt, France (2014).
- [11] A.-P. LEPPÄNEN et al., “Artificial radionuclides in surface air in Finland following the Fukushima Dai-ichi nuclear power plant accident” (2013); <https://doi.org/10.1016/j.jenvrad.2013.08.008>.
- [12] N. SADEGHI et al., “Dose assessment for emergency workers in early phase of Fukushima Daiichi nuclear power plant accident,” *Kerntechnik* 82 5, 562, Carl Hanser Verlag (2017)
- [13] E. ANEHEIM, D. BERNIN, and M. R. S. J. FOREMAN, “Affinity of charcoals for different forms of radioactive organic iodine,” *Nucl. Eng. Des.* 328, 228, Elsevier Ltd (2018); <https://doi.org/10.1016/j.nucengdes.2018.01.007>
- [14] J. C. WREN et al., “Modeling the removal and retention of radioiodine by TEDA-impregnated charcoal under reactor accident conditions,” *Taylor Fr.* 125 1, 13, American Nuclear Society (2017); <https://doi.org/10.13182/NT99-A2929>.

## 5. KTH-NE Analytical support OECD/NEA THEMIS

### 5.1. Background

#### 5.1.1. Severe accidents and pool scrubbing

Fission Products (FP) release into the environment is major concern for assessment of severe accident consequences. The source term is characterized by the timing, fraction, and specification of FP released. Minimization of the source term should be the main aim for the design of Severe Accident Management (SAM) strategy. Validated models are needed for reliable assessment of FP transport and release from the containment.

Pool scrubbing (PS) is a process of the retention in a water pool of volatile fission products in aerosol and gaseous forms. PS is an efficient way to prevent the release of radioactive FP into the environment during severe accidents. Fission products carried by gaseous mixtures (i.e., steam and non-condensable gas) often pass through multi-hole spargers or blow-down pipes into a large water pool of Light Water Reactor (LWR) or released into the secondary loop of the steam generator during the Steam Generator Tube Rupture (SGTR) in Pressurized Water Reactor (PWR). Gas bubbles that carry the particles can pass through the water pool. The fraction of particles retained in the pool is governed by the dynamic of the gas-liquid interface and the motion of particles inside the bubbles. The efficiency of pool scrubbing is evaluated by a Decontamination Factor (DF) defined by the ratio of injected aerosols ( $\dot{m}_{in}$ ) over escaped aerosols ( $\dot{m}_{out}$ ) as shown below:

$$DF = \frac{\dot{m}_{in}}{\dot{m}_{out}} \quad (1)$$

The injection regime depends on injection geometry, gas flow rate, and liquid phase properties. So called globule regime is observed at small Weber ( $We$ ) numbers and jet regime at  $We > 10^5$ . The  $We$  number is defined as the ratio of fluid inertia force over surface tension force. For the jet injection, it is defined as [22]:

$$We = \frac{u_{vent}^2 \rho_l d_{vent}}{\sigma_l} \quad (2)$$

where  $\rho_l$  and  $\sigma_l$  are density and surface tension of the pool liquid,  $u_{vent}$  the average gas velocity and  $d_{vent}$  the vent diameter.

Model development and validation to access the DF or removal efficiency in pool scrubbing conditions requires experimental data with reliable measurement of aerosol transport as well as the hydrodynamic characteristics inducted by gaseous jet injection. Such experiments have been conducted since the 1980s and they are summarized in [1], [2].

### 5.1.2. THEMIS project

OECD/NEA launched the next phase of the THAI project called THEMIS “THAI Experiments on Mitigation measures and source term issues to support analysis and further Improvement of Severe accident management measures”. Main objectives of the project are:

- (i) Enhanced focus on severe accident “late phase”,
- (ii) Better understanding of phenomenology relevant to H<sub>2</sub>-CO combustion risk, recombination systems (PAR), source term related issues (e.g., pool scrubbing, IOx interaction with late phase typical aerosols),
- (iii) Extended experimental database for safety analysis codes model/code validation, Reactor application (incl. Scaling and Uncertainty analysis),
- (iv) Severe Accident Management optimization (code application), potential input for SAM strategy enhancement (e.g. actuation of FCVS), and risk-informed decision making.

Several items proposed in the THEMIS experiments are of direct relevance to containment and source term phenomena:

- Item 1: H<sub>2</sub>-CO combustion and flame propagation behavior.
- Item 2: PAR performance behavior in H<sub>2</sub>-CO containing atmosphere.
- Item 3a: Interaction of “nuclear background aerosol” with Iodine Oxide (IOx) particles.
- Item 3b: Stability and evolution of IOx under high temperature.
- Item 4: Fission products released from water pools under “Pool Scrubbing” conditions including the effects of pool stratification.
- Item 5: PAR interaction with IOx and nuclear aerosol in H<sub>2</sub>-CO containing atmosphere.

### 5.1.3. Motivation, goals, and tasks

Nuclear Engineering (NE) at KTH is leading the development of advanced methods for uncertainty and risk quantification relevant to severe accidents. Specifically, the focus of the research is on the risk of containment failure due to steam explosion and formation of non-coolable debris bed. Successful application of ROAAM+ for improvement of PSA-L2 has been demonstrated in [3], [4], [5].

KTH is also leading the development of the modeling approaches (so-called Effective Heat Source (EHS) and Effective Momentum Source (EMS) models) for the simulation of the thermal-hydraulic phenomena of pressure suppression pool. The aim of the EHS/EMS models is to predict the effect of steam injection conditions on the development of thermal stratification and mixing in the pool, without explicitly resolving direct contact condensation phenomena and steam-water interface. The EHS/EMS models have been implemented in GOTHIC [[20]] and CFD code Fluent for steam injection through the blowdown pipes [6], [7], [8], [9], [10] and spargers [11], [12], [13], [14], [15], [16], [17], [18], [19]. The developed approaches have been successfully applied in providing analytical support, which incorporates pre-test simulations and post-test analysis, to the international OECD projects HYMERES [11], [12], [17] and HYMERES-2 [18], [19].

The aim of this work is to provide analytical support to the OECD/NEA THEMIS project. The primary focus is THEMIS Item 4 regarding fission products released under “pool scrubbing” conditions. The outcomes of the project will help to quantify modeling uncertainty in phenomena related to the source term. Main tasks include: Task 1. To develop and

implement GOTHIC models for THAI facility; Task 2. To provide analysis for THAI experiments relevant to Nordic plant designs and conditions; Task 3. To develop guidelines for modeling the relevant phenomena and quantification of uncertainties in plant accident conditions.

## 5.2. Pool Scrubbing tests in THEMIS Project

### 5.2.1. Test configuration and procedures

Experiments conducted since the late 1980s focus mostly in globule regime featured by low  $We$  number. The experimental database of pool scrubbing under the jet regime is limited due to (i) missing dedicated focus on pool hydrodynamics induced by jet injection, (ii) lacking variation of submergence, (iii) wall effects onto the injected jet, and (iv) challenges in aerosol measurement techniques.

To extend the current database and provide data for model development and code validation, several tests with respect to pool scrubbing have been proposed and conducted in the framework of THEMIS project. The test series aimed to measure the retention of particles injected into a water pool in the transition from globule regime to jet regime and to record gas distribution below the pool surface via a high-speed camera. The test conditions of 3 tests with 4 phases are summarized in Table 5-1. Overviews of the configuration of the test facilities are illustrated in Figure 5-1. The facilities consist of a THAI Test Vessel (TTV) and a Parallel Attachable Drum (PAD) used as a reservoir for hot gases released from the TVV. The height and diameter of TVV are around 9.2 m and 3.2 m. The non-condensable gas (represented by air or nitrogen), steam, and insoluble particle ( $SnO_2$ ) was pre-mixed and then injected into the water pool through a horizontally aligned nozzle with a diameter of 15 mm (Figure 5-1). The nozzle was placed below the pool surface with a submergence ranging from 0.25~2 m depending on tests and with a distance more than 3 m to the opposite vessel wall to minimize the wall effects of the injected jet. Additionally, the air was injected to purge the gas space of TVV and increase vessel pressure during the pre-conditioning phase, and to enhance circulation of gas space during the main test procedure. It was supplied by the compressed air supply system and injected through a downward-oriented pipe at elevation  $H = 7.6$  m.

$SnO_2$  aerosol particles were generated by a PDB (Pulverdispergierer mit Bürste) in which the pre-manufactured pellet was scrubbed by a brush and the resulting particles became airborne by heated airflow.

These airborne particles were moved from the brush into a 9 mm pipe and merged with the pre-heated air and steam before entering the pool. The pellet was produced using a ~50 g  $SnO_2$  powder wetted with 18 ml water. The density of the yielded pellet is around 2700  $kg/m^3$  and it was released with a constant feed rate of 0.42  $mm/min$ , corresponding to 12.4  $mg/s$  during all test phases.

Thermal hydraulic conditions of TVV were achieved by heating the oil mantles and electrical coils filled in the gap between the inner and outer walls. Pool temperature was also adjusted by injecting air through a connection into the sump compartment at  $H = 0.9$  m during the pre-conditioning phase. According to the temperature distribution, TVV can be generally divided into 3 distinct regions where a superheated gas space above the pool surface, a well-mixed preheated region between  $H = 3 - 4$  m to the pool surface, and a rather cold region underneath.

Every test phase started with a pre-conditioning phase to adjust the test conditions as proposed. Subsequently, the main test phase started with the activation of the PDB, air, and steam supply systems to inject gaseous aerosol into the pool. Air was also supplied through a nozzle located in the gas space to enable sufficient mixing of the space above the pool surface. After around 1.5 hours, PDB was de-activated, and the jet injection was completely terminated. The mass flow rate of purge air injection was further increased to purge the vessel atmosphere and it was ended after another 1 hour.

## 5.2.2. Instrumentation

Particles were measured by varied sensors at different locations (Figure 5-1). Two particle filter holders were positioned at the TVV exhaust line to integrally collect  $SnO_2$  particles escaping from the vessel. Particle mass concentration was measured by two bulk filters. One filter was installed inside the vessel at  $H = 7.7\text{ m}$  or  $8.65\text{ m}$ ,  $\phi = 225^\circ$  according to the water level of the test (Figure 5-1). The second filter was connected to the aerosol injection pipe before it merged with steam and support air. Two low-pressure cascade impactors, which share the same sampling stations as the bulk filter, were applied to measure the particle size distribution. Additionally, a sampling spectrometer (PALAS Welas®) was installed inside the vessel at  $H = 8.4\text{ m}$ ,  $\phi = 135^\circ$  (right above the vent) to enable piecewise continuous measurements of the particle size distribution.

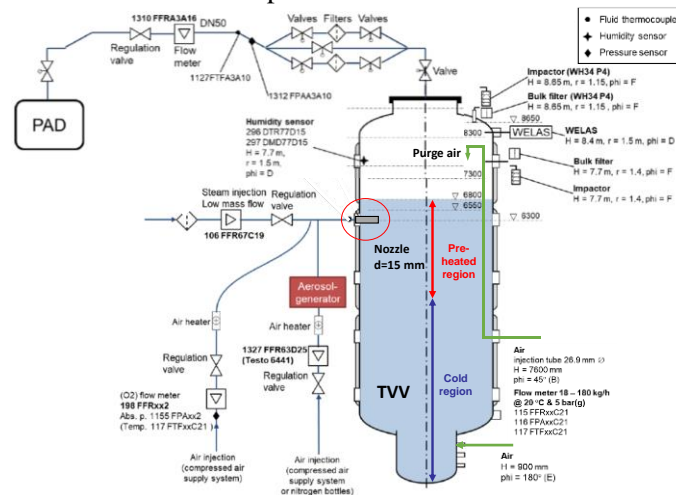


Figure 5-1: Overview of the configuration of THAI facility in pool scrubbing tests.

The mass flow rate of steam, support air in jet injection, and purge air were monitored by float-type flow meters. Piezoresistive pressure transmitters were applied to measure the pressure of the above flows and the pressure of the TVV. The relative humidity of TVV was measured by TESTO humidity sensors positioned at  $H = 7.7\text{ m}$ . Measurement of temperatures was achieved by calibrated  $1.5\text{ mm}$  ThermoCouples (TCs) (accuracy  $\pm 0.3\text{ }^\circ\text{C}$  for calibration range from  $0\sim 130\text{ }^\circ\text{C}$ ) placed at various locations, involving different heights, radii, and azimuthal angles. The hydrodynamic features of the two-phase flow were recorded via a high-speed camera. To ensure sufficient background lighting and camera positioning, these tests were conducted in a different test setup.

**Table 5-1. Test conditions as specified for the WH test series**

	$T_{vapor}$	$T_{pool}$	$Q_{steam}$	$Q_{total}$	$\alpha_{steam}$	$P_{vapor}/P_{sat}$	$H_{sub}$	$We/10^5$	$P_{vessel}$
	°C	°C	l/min	l/min	–	–	m	–	Bar, abs
WH32 varied in $P_{vapor}/P_{sat}$									
Phase1	119.8	60.9	66.6	317.3	0.210	1.3	0.5	2.00	1.23
Phase2	118.7	61.2	85.7	395.7	0.217	2.1	0.5	3.11	2.02
Phase3	115.3	60.2	73.8	382.4	0.193	2.9	0.5	2.90	3.01
Phase4	116.5	60.0	86.3	382.9	0.226	4.6	0.5	2.91	4.00
WH33 varied in We number									
Phase1	102.2	60.7	43.3	299.7	0.145	1.9	0.5	1.78	2.67
Phase2	100.9	59.8	67.5	452.1	0.149	2.1	0.5	4.05	2.67
Phase3	100.3	57.6	94.4	573.4	0.165	2.5	0.5	6.49	2.68
Phase4	100.5	56.6	185.2	806.0	0.230	3.7	0.5	12.8	2.67
WH34 varied in submergence									
Phase1	120.0	79.7	272.4	486.9	0.560	1.8	0.25	4.91	1.44
Phase2	120.2	78.9	248.8	457.8	0.543	1.8	0.5	4.33	1.45
Phase3	118.9	79.6	239.0	443.4	0.539	1.8	1	4.06	1.45
Phase4	120.3	70.8	248.1	448.2	0.553	2.7	2	4.06	1.41

### 5.3. Modeling of Aerosol Particles in GOTHIC

According to experimental investigations since the 1980s [1], [2], several Lumped Parameter (LP) codes were developed to enable the prediction of pool scrubbing efficiency, like BUSCA [23], SUPRA [24], and SPARC-90 [22]. These models are designed for the globule regime which can be characterized by the injection of gas into the pool at low or moderate velocities ( $We$  number), resulting in the formation of a large bubble that detaches from the injection orifice and subsequently breaks up into numerous small bubbles. Instead, when gas velocity increases, the surface tension between liquid and gas collapses and forms a continuous gas flow (jet regime), entraining the ambient liquid as well as small bubbles induced by strong interaction between liquid and gas. Further development of models by considering the jet regime is enabled in SPARC-B/98 [25] and SPARC90-Jet [26]. These LP codes were then integrated into several system level analysis software, for example, MELCOR with SPARC-90 [30].

In addition to LP codes, analysis of pool scrubbing can be achieved by using Computational Fluid Dynamic (CFD) codes. However, due to the considerable disparity between the small-scale interface behavior of liquid/vapor and large-scale pool circulation, simulation of the long-time transient is unaffordable. Therefore, these works have concentrated on employing CFD to explore the hydrodynamic characteristics of bubbly flow [27] and investigate particle transport, along with its underlying mechanisms within a single rising

bubble [28], [29]. These CFD studies can be later used in support of LP modeling by providing insight into local phenomena or empirical correlations.

The gap between traditional system level thermal-hydraulics (TH) codes (e.g., MELCOR, RELAP, etc.) and CFD tools can be bridged by GOTHIC [31] which is an integrated, general-purpose thermal-hydraulics code for containment analysis. For example, compared to system level TH codes which are normally limited to confined geometries, GOTHIC incorporates a comprehensive treatment of the fluid-fluid shear along with molecular and turbulent diffusion that is comparable to CFD type of codes. Collectively, these features enable GOTHIC to simulate phenomena such as stratification, and buoyancy-driven circulation of vapor or liquid in a large open region, e.g., wet, and dry wells in containment. In the latest update of GOTHIC [20], the capability of modeling pool scrubbing is enabled based on the SPARC-90 document [22] and its implementation in MELCOR [30].

### 5.3.1. GOTHIC modeling capability

This section provides an overview of GOTHIC modeling capability relevant to the phenomena of transport of aerosol particles under pool scrubbing [21]. GOTHIC uses three primary phases: vapor, continuous liquid, and drops, and three secondary phases with simplifying assumptions: mist, ice, and separate components in the liquid phase to model the transient behavior of the multiphase flow. The vapor phase consists of non-condensable gas components and steam. The continuous liquid phase represents liquid in any geometry except drops (e.g., pools, films). The continuous liquid phase is referred here as ‘liquid phase’ to distinguish from the drop phases. Droplets consist of many fields with varying sizes to cover the range of expected droplet sizes. The mass, energy, and momentum conservations are solved for a set of finite volumes for each of the three primary phases (Section 5.3.2). Interface transfer of mass, energy, and momentum between these phases and between the walls and the fluid are solved by constitutive models. Separate components in the liquid phase can be tracked in the liquid and drop phases. The component can be Solid Particles (SP) (e.g., debris, fission products), another liquid (e.g., boric acid), or dissolved gas.

A single component of a solid particle with log-norm size distribution is used to model the aerosol particles ( $SnO_2$ ). The behaviors of SP that are associated with the phenomena in THEMIS experiments are illustrated in Figure 5-2 and briefly introduced in Section 5.3.3. Drop flow containing 100% SP (called dry aerosol) within a single drop phase is mixed with vapor flow and then injected into the vessel under the pool surface. Prior to GOTHIC v8.4 [21], the drop and contained in them SP entering the pool is assumed to join the liquid phase. The pool scrubbing model implemented in GOTHIC v8.4 enables the estimation of the fraction of drop deposited in the pool (i.e., liquid phase) and the drop fraction released into the gas space. Interphase transfer (e.g., drop deposited into liquid phase, drop formation by pool entrainment) also transfers the SP component according to their mass fraction of the carrying phase. The SP in the liquid phase is either suspended or settled. The SP in the drop phase is assumed uniformly suspended. GOTHIC provides models to simulate the inter-field (within a single drop phase or multiple drop phases) transfer as agglomeration and interphase transfer as deposition and entrainment. The collection of these mechanisms leads to the change of the drop average diameter and the GSD as the transient progresses.



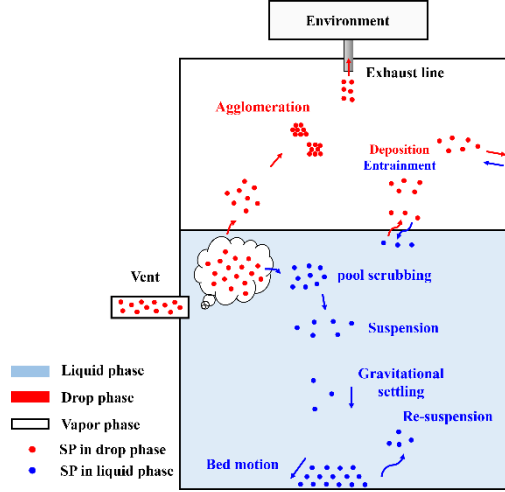


Figure 5-2: Schematic of behaviors of solid particles in GOTHIC during aerosol injection into a water pool.

### 5.3.2. Conservation equations

GOTHIC applies finite volume method to solve the conservation equations for multi-dimensional analysis. Specific modifications are made for lumped cells and junctions. Conservation equations of mass, momentum, and energy are separately solved for liquid, vapor, and each drop phase. The vapor phase hereafter refers to the mixture of steam and non-condensable gases. The (continuous) liquid phase is in the form of a pool. Drop phase can consist of many interacting drop fields and each of them is treated as a separate phase. In this work, a single drop phase is used. Conservations of momentum and energy can be found in [[21]].

$$\begin{aligned}
 & \frac{\partial}{\partial t} \int_V \Theta \alpha_\phi \rho_{\phi\zeta} dV \\
 & = - \int_{A_f} \Psi \alpha_\phi \rho_{\phi\zeta} \vec{u}_\phi \cdot \vec{n} dA + \int_{A_f} \Psi \alpha_\phi \rho_\phi D_\phi^c \vec{\nabla} \left( \frac{\rho_{\phi\zeta}}{\rho_\phi} \right) \cdot \vec{n} dA \quad (3) \\
 & + \int_{A_w} s_{\phi\zeta}^c dA + S_{\phi\zeta}^c
 \end{aligned}$$

Each term, from left to right, represents the storage, convection, diffusion, boundary source, and other sources;  $\Theta$  is the volume porosity factor of volume  $V$  and  $\Psi$  is the area porosity factor of surface  $A$ ; the subscript  $\phi$  represents the phases of  $v$  (vapor),  $l$  (liquid), and  $d_f$  (drop for field  $f$ );  $\zeta$  indicates the component of the vapor, i.e., steam, noncondensing gas mixture) and it is only applied when simulating the vapor phase;  $\alpha$  is the volume fraction,  $\rho$  density,  $\vec{u}$  velocity,  $\vec{n}$  direct vector normal to the surface;  $A_f$  is the total surface area that is in contact with the ambient fluid;  $D^c$  is the coefficient of mass diffusion, involving the effects of turbulence;  $s^c$  is the mass source per unit area flowing through or generated at

the bounding wall  $A_w$ ;  $S^c$  is the source term of mass that can be introduced by phase interaction (e.g., evaporation, condensation, drop entrainment, and deposition), safety equipment, user-defined source, etc. Non-uniformity of the drops in a drop field is represented by log-normal size distribution as:

$$\Lambda(d_i) = \frac{1}{\sqrt{2\pi}d \ln \sigma_g} \exp\left(-\frac{1}{2}\left(\frac{\ln d_i - \ln d_c}{\ln \sigma_g}\right)^2\right) \quad (4)$$

where  $d_c$  and  $\sigma_g$  are the Count Median Diameter (CMD) and Geometry Standard Deviation (GSD) of this field.

### 5.3.3. Solid particle

Transport of solid, liquid, or dissolved components can be tracked in both liquid and drop fields in GOTHIC. Two types of components are available, namely solid particle and dissolved gas. Both types are referred to as liquid components while treatment is different according to the type. In this work, aerosol particles ( $SnO_2$ ) are simulated by the solid particle as the liquid component. SP can exist in the liquid phase and drop phase where different mechanisms are modeled in each field as shown in Figure 5-2.

#### SP in liquid phase

Solid particles can be carried by the continuous liquid phase. The amount of an SP component is quantified by the volume fraction of the SP in continuous liquid, i.e., the volume of SP relative to the total volume occupied by the liquid phase. SP in each computational volume are either suspended or settled. For SP in the liquid phase, GOTHIC provides the modeling capability of settling, buoyancy, bed load (motion of settled particles), resuspension, and diffusion of suspended particles (Figure 5-2).

The momentum and energy of the solid particles (liquid components) are included in the conservation of momentum and energy equations of continuous liquid. GTOHIC assumes no-slip velocity between SP and liquid except for the z-direction where particles might move relative to the liquid phase because of buoyancy. Thermal equilibrium between particles and surrounding liquid is assumed. Effects of SP in momentum and energy equations are introduced by using effective density and heat capacity calculated according to their volume fraction. The properties of carrier liquid, i.e., viscosity, thermal conductivity, and surface tension, are not affected by the existence of the SP.

#### SP in drop phase

Solid particles can also exist in the drop phase where all particles are assumed uniformly suspended within the drops. Here we consider only a solid particle component existed in a single drop field. The volume fraction of the SP ( $\chi_{dc}$ ) is:

$$\chi_{dc} = V_{dc}/V_d \leq 1 \quad (5)$$

where  $V_{dc}$  is the volume of SP and  $V_d$  is the volume of the drop. Modeling of vaporization and condensation is inactivated when  $\chi_{dc} > 0.99$  in which the drop phase is regarded as 'dry' SP.

GOTHIC provides models to simulate the interphase and inter-field transfer as agglomeration, deposition, entrainment and breakup, pool scrubbing, evaporation, and condensation. These mechanisms leads to the change of the drop average diameter and the GSD as the transient progresses (more details in [20][21]).

#### Agglomeration

Agglomeration takes place when two drops merge together forming a single particle. These two drops can come from a single drop phase (inter-field) or from separate drop phases (interphase). Agglomeration can be categorized as thermal agglomeration when the relative motion is induced by Brownian motion or kinematic agglomeration when the motion is caused by external sources such as gravity, aerodynamics, etc.

#### Deposition

The phenomena of deposition resulting from various mechanisms, including gravitational settling, impaction, turbulent and thermal diffusion, diffusionphoresis, and thermophoresis are considered in GOTHIC. These mechanisms are assumed to operate independently, and the overall deposition rate is calculated by the summation of the deposition rates for the individual mechanisms. Deposition of flows with vapor and drop (solid particle) into a pool known as pool scrubbing is separately described below.

Generally, the drop mass deposition rate due to a specific mechanism is written as:

$$\dot{M}_{dep} = -\frac{\pi\rho_{dm}}{6} N''' \int_0^{\infty} d_i^3 K_D(d_i) \Lambda(d_i) dd_i \quad (6)$$

where  $K_D$  is the deposition kernel. Interface transfer from the drop phase to the liquid phase is mainly contributed by deposition. The amount of mass and energy sources of SP due to deposition is calculated based on the ratio of SP mass over the total mixture mass. The surface area of the drop phase can be altered due to evaporation and condensation while SP is not transferred.

#### Pool scrubbing

Pool scrubbing (PS) refers to the phenomenon of deposition of drop and its carried particles in a water pool from a submerged jet injection with vapor and drop. Modeling of pool scrubbing is enabled in the recent update of GOTHIC [21], including several deposition mechanisms according to SPARC-90 [22] and its implementation in MELCOR [30]. The models are generally consistent with the one described in SPARC-90 while some deposition factors vary because of unclear information, errors in SPARC-90 document, or different assumptions applied in GOTHIC.

From the experimental observations, the hydrodynamic of vapor flow injection through a submerged vent into the water pool is shown in Figure 5-3. Steam condenses right after it leaves the vent. In the case of the globule regime, the injected gas forms large globules initially. These globules can travel approximately 10 to 12 times their equivalent diameter at the detachment point and then break up into a swarm of smaller bubbles. The deposition during the pool scrubbing is categorized into two regions, namely (i) initial globule formation and breakup and (ii) swarm bubbles.

In the initial globule region, deposition mechanisms of inertial impaction, steam condensation, gravitational settling, centrifugal inertial impact, and thermal diffusion are considered whereas the last three mechanisms are only for sparger vents. During the swarm bubble region, gravitational settling, centrifugal inertial impact, and thermal diffusion are involved. Mechanisms within each region are assumed to operate independently and simultaneously. The deposition is consecutive as the vapor travels from the initial globule to swarm bubbles.

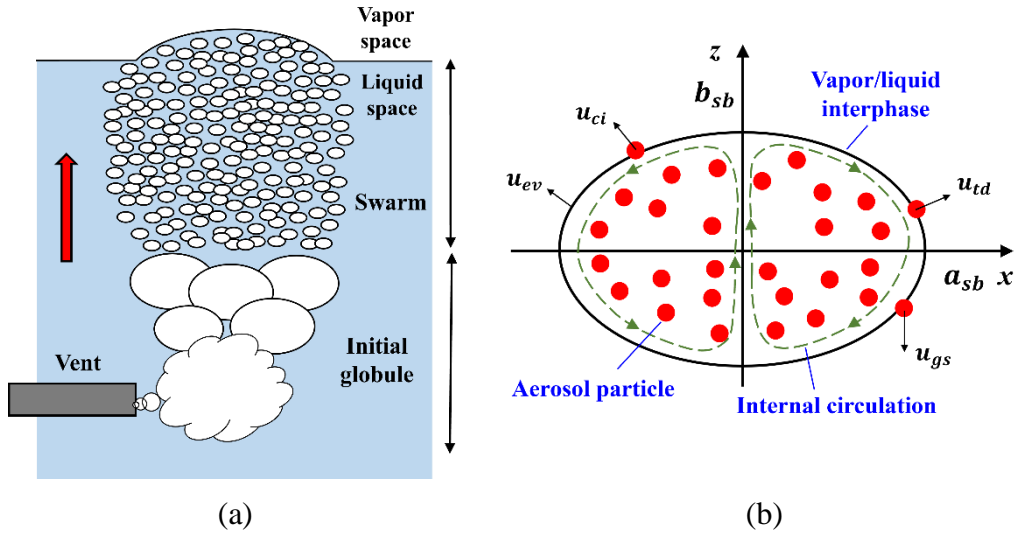


Figure 5-3: Schematic of (a) hydrodynamic of aerosol injection into a water pool under globule regime and (b) motion of aerosol particles in a swarm bubble.

The effective deposition kernel by considering all mechanisms during the entire pool scrubbing is:

$$K^{pool} = \dot{Q}_{vent} \left( 1 - \left( \frac{\dot{Q}_{s0} - K^{sw}}{\dot{Q}_{vent}} \right) \left( \frac{\dot{Q}_{ig}}{\dot{Q}_{ig} + K^{bu}} \right) \left( \frac{\dot{Q}_{ig}}{\dot{Q}_{ig} + K^{fill}} \right) \left( \frac{\dot{Q}_{vent} - K^{ig}}{\dot{Q}_{ig}} \right) \right) \quad (7)$$

where  $\dot{Q}_{vent}$  is the volumetric flow rate before entering the pool,  $\dot{Q}_{ig}$  is the volumetric flow rate at the initial globule region,  $\dot{Q}_{s0}$  is the flow rate at the beginning of the swarm region.  $K^{vent}$  is the deposition kernel due to the steam condensation and inertial impaction at the vent exit ( $K^{ig} = K_{cond}^{ig} + K_{vi}^{ig}$ ),  $K^{fill}$ ,  $K^{bu}$  are deposition kernels caused by the presence of spargers in initial globule formation and breakup region,  $K^{sw}$  is the deposition kernel due to the gravitational settling, centrifugal inertial impact, and thermal diffusion in the swarm bubbles region. The formulation of each deposition kernel can be found in [21].

## 5.4. Model development for THEMIS experiments

### 5.4.1. Model setup

The GOTHIC model and its nodalization are presented in Figure 5-4. The aerosol particles are introduced by flow boundary 1F. The volume fraction of liquid and drop flow phases are set to 1. Flow boundary 2F injects steam into a lumped volume 2 to mix with particles before entering the pool. Drop deposition is disabled for volume 2. The mixed aerosol flow is then injected into the subdivided volume 1s. Volume 1s represents the test vessel (TVV) with a height of 9.2 m and a diameter of 3.156 m. The TVV is discretized

by 3D sub-divided control volumes with a moderate resolution of  $7 \times 7 \times 10$ . The vessel contains  $6.8 \text{ m}$  of water. Flow path 3 and volume 2 are located at  $6.3 \text{ m}$  to enable a  $0.5 \text{ m}$  submergence. The pool scrubbing model is added on flow path 3 to determine the fraction of drop deposited in the pool. As suggested in [[21]], the pool scrubbing model requires liquid level located in the same cell as the injection point. The overlapping of the pool surface with the grid line should be avoided to prevent numerical oscillations. Boundary conditions from tests (Table 5-1) are applied. The density of the solid particle is set to  $2700 \text{ kg/m}^3$  and assume non-uniformly distributed with  $d_{sm} = 0.3 \mu\text{m}$  and  $GSD = 2.87$ . Injection of solid particles and vapor flow is stopped at  $100 \text{ mins}$  and  $150 \text{ mins}$ , respectively. For drop field models, the velocity equilibrium with the vapor phase is activated and vapor/drop mass transfer is deactivated. Pool entrainment is deactivated as default. The remaining parameters of models are set according to default settings.

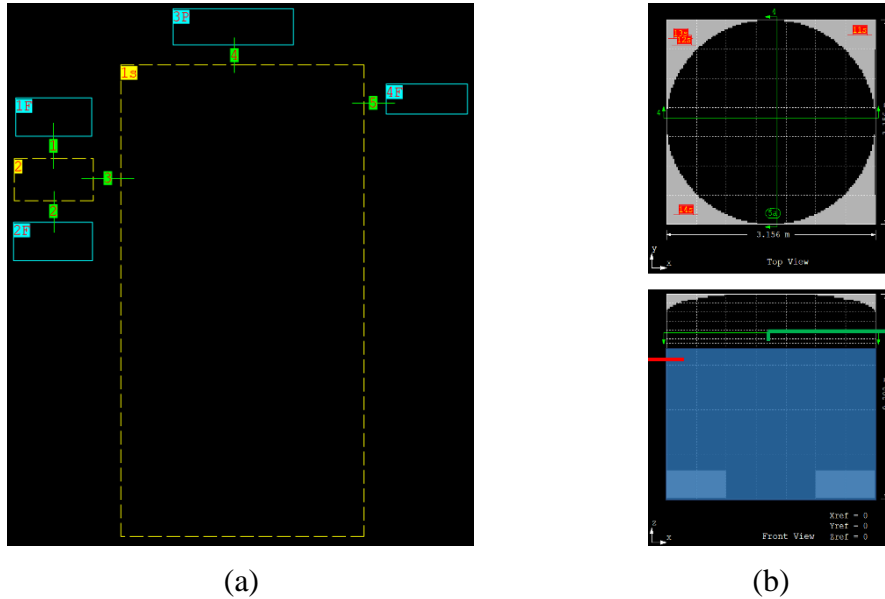


Figure 5-4: *GOTHIC* model (a) and nodalization (b) for *THEMIS* experiments.

Thermal hydraulic conditions of TVV, especially in the gas atmosphere, play an important role in determining the motion of aerosol particles. *THEMIS* experiments (Figure 5-1) applied oil mantles and electrical coils filled in the vessel wall to maintain the wall temperature and formed three distinct regions along the vertical directions. They are (i) superheated gas space above the pool surface, (ii) a preheated region with a uniform temperature distribution from the pool surface to an elevation of  $3\sim 4 \text{ m}$ , and (iii) a cold region underneath. Additionally, an air injection was installed at  $H = 7.6 \text{ m}$  to inject purge air towards the pool surface to enhance the global circulation of the gas atmosphere and to increase the particles removed from the vessel. The purge air is injected from boundary 4F through flow path 5. It should be noted that the flow path should connect the cell from the top to enable an incoming momentum directed toward the bottom of the cell. To do so, the level indicator in the elevation view should be placed near the top of the required level as shown in Figure 5-4b. Several internal thermal conductors are applied to enforce a superheated and thermally stratified gas atmosphere. The surface options of these thermal conductors are one side with a specified heat transfer coefficient with a very large value (e.g.  $1e5, \text{W/m} \cdot \text{K}$ ) and another side with a fixed temperature as desired. The injected flows and aerosols can leave the vessel through an exhaust line (flow path 4) connecting to a pressure boundary 3P with constant pressure and temperature.

### 5.4.2. Validation against WH32-P1 tests

The model developed in GOTHIC was validated against WH32 tests in which the boundary conditions summarized in Table were used. Data in the following sections, unless otherwise noted, were normalized.

#### *Pool thermal hydraulic conditions*

The measured vapor flow rates of the jet (steam + air) and purge air injections were applied to the models as input. Pressure boundary using data measured at the exhaust line was applied as the outlet in the model. The predicted vapor flow rates at the exhaust line are compared with the measurements in Figure . Good agreements are achieved for all phases of the WH32 series except for the P1. It might be caused by the deviation of temperature profiles in gas space where GOTHIC used a relatively coarse mesh so that the temperature gradients cannot be fully captured (Figure 5-6). GOTHIC seems to simply sum up the vapor mass flow rates from two inputs while measurement in WH32-1 is a little bit higher than its summation. This issue should be further studied since the flow rate at the exhaust line determines the amount of removed particles.

The comparison of temperature from GOTHIC and TCs measurements indicates the thermal conditions of the atmosphere can be reproduced by using thermal conductors with fixed temperatures. The disagreements at some elevations are induced by the coarse mesh resolution along the vertical direction.

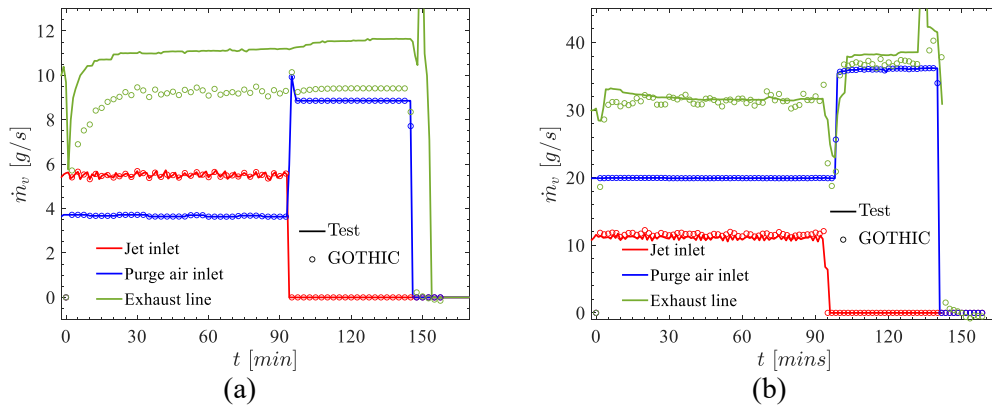


Figure 5-5: Vapor mass flow rates obtained by GOTHIC and measurements of WH32 (a) P1 and (b) P2.

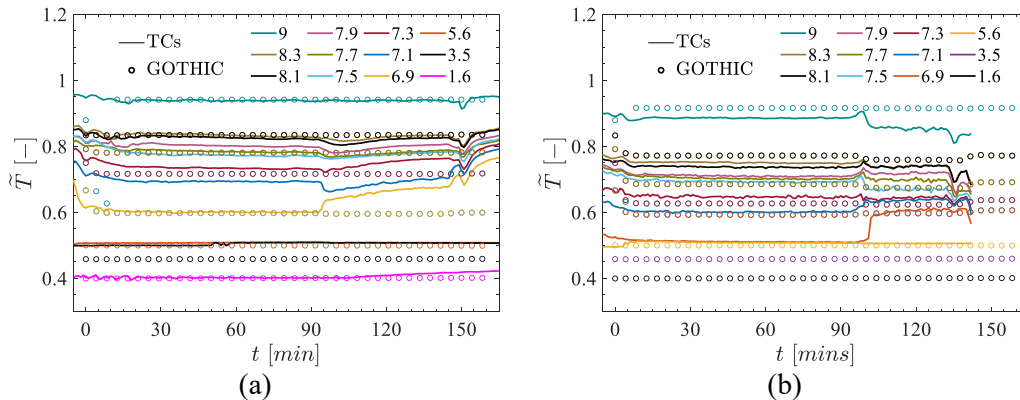


Figure 5-6: Vapor/liquid temperatures obtained by GOTHIC and measurements of WH32 (a) P1 and (b) P2.

### Transport of aerosol particles

This section presents the comparison of GOTHIC prediction of aerosol particles' concentration and size distribution with the measurements obtained in WH32-P1 test. The drop field models are set as the default settings where all agglomeration mechanisms and all deposition mechanisms except diffusionphoresis and thermophoresis are activated. All mechanisms of pool scrubbing are activated with a default multiplier of 1.0 [21].

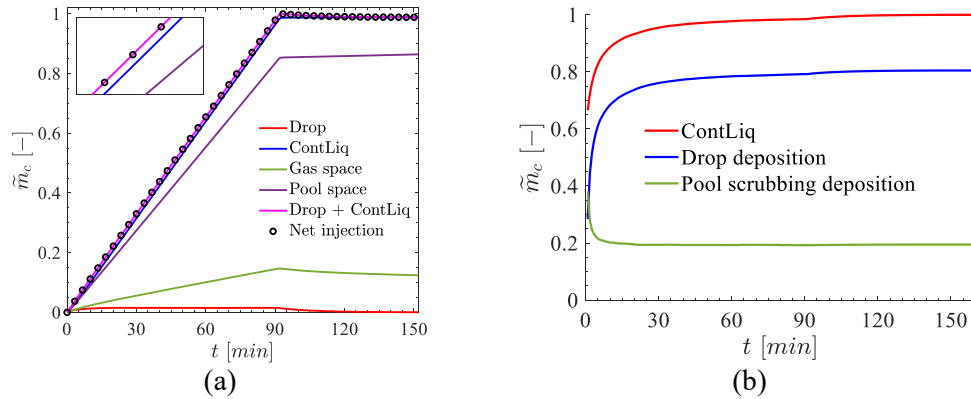


Figure 5-7: Balances of (a) SP in the vessel and (b) fractions of deposited SP (ContLiq) by drop deposition and pool scrubbing deposition for simulation of WH32-P1 test.

The integral difference between the inlet and outlet agrees well with the SP retained in the vessel (Figure 5-7a). The SP mainly exist in the liquid phase while a small fraction of SP is found in the drop phase. The SP in the drop phase are in the gas volume (Figure 5-8) while the SP in the liquid phase are distributed partly below the pool surface and partly above the pool surface. Around 20% of SP from the droplet phase are joining liquid phase due to the pool scrubbing phenomena in the cell with the vent. The remaining 80% is due to the deposition in the gas space.

The SP concentration at different elevations (Figure ) suggests that particles are accumulated in the cells near the pool surface (i.e.  $H = 5.0 - 7.0$  m) mostly in the liquid phase. The maximum deposition rate was found at the cell containing the vent and pool surface. Aerosol particles that escaped the pool still can join the pool by several drop deposition mechanisms that occur above the pool surface (Figure 5-2).

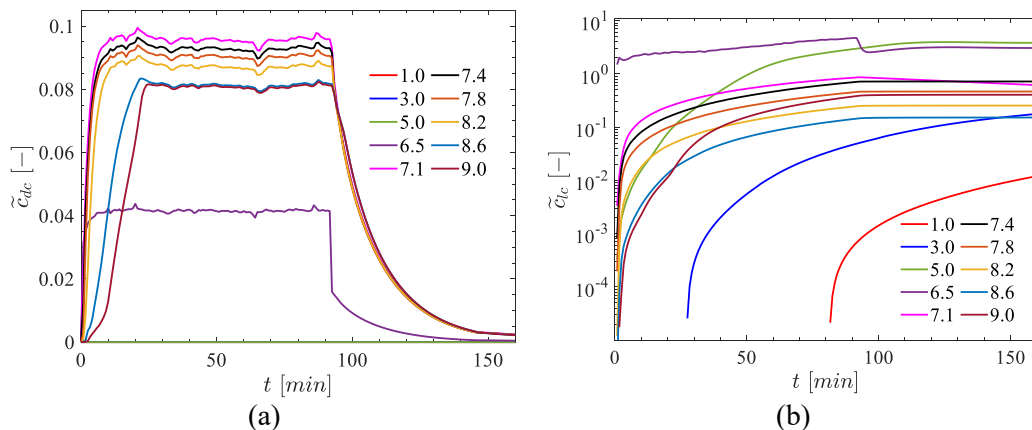


Figure 5-8: Evolution of SP concentration in (a) drop phase and (b) liquid phase along vertical direction for the simulation of WH32-P1 test.

The significant amount of particles in the liquid phase above the pool surface is due to the drop deposition into a liquid film, which is present in each cell. The liquid film (and particles) accumulate in cells and cannot be transported by vapor flow (e.g. purge air). Therefore an equilibrium is established between the cumulative particle mass and the cumulative particle deposition rate in each cell in the gas space (Figure 5-9a, c). During the aerosol injection period, the concentration of SP in the liquid phase gradually increases with an approximately constant drop deposition rate. After the stop of injection, the concentration remains unchanged due to the rapid decrease in the deposition rate.

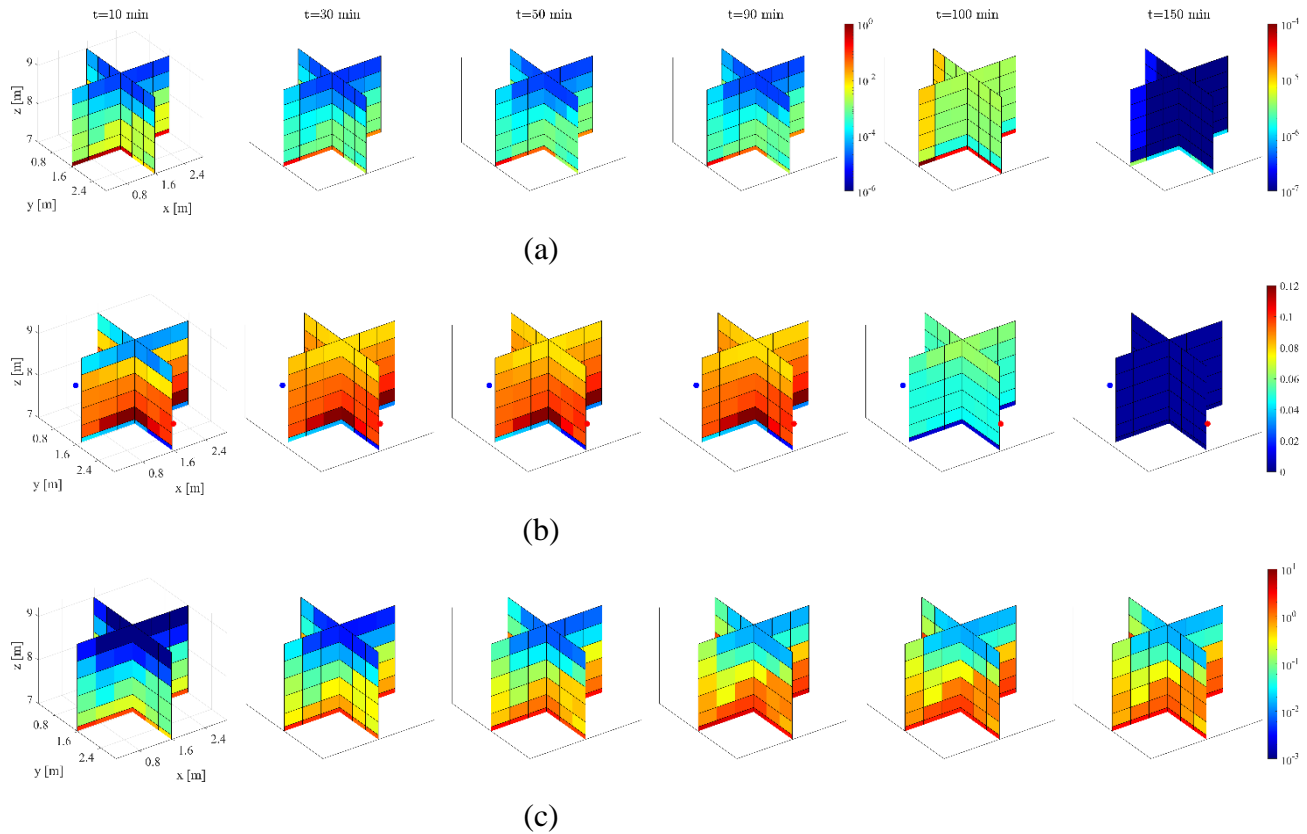


Figure 5-9: Contours of (a) SP deposition rate by drop deposition, SP concentration in (b) drop, and (c) liquid phases for simulation of WH32-P1 test. Blue and red dots represent the location of Welas and bulk sensors.

The particles in the drop phase are uniformly distributed in comparison to those in the liquid phase (Figure 5-9b). The concentration of SP in the drop phase reaches saturation after  $\sim 10$  min (Figure 5-8a) where the particles escaped from the pool are either removed through the exhaust line or deposited into the liquid phase. When the aerosol injection stops, the concentration begins to decrease by the purge air removal.

The concentration of particles predicted by GOTHIC is compared with experimental in Figure 5-10b. Two sensors (Welas, TVV bulk) are placed as shown in Figure 5-1 and Figure 5-9b. The concentration of particles in the drop phase achieves a reasonable agreement with the measurements. However, if SP in both phases are considered as the ‘particles’ that are measured by the tests, a significant deviation can be observed for the concentration at the location with the bulk impactor. Meanwhile, the total concentration (liquid phase + drop phase) predicted by GOTHIC, after injection stop, is decreased slower than in the test. This is because only particles in the drop phase are removed from the vessel. As shown in Figure



5-10a, the amount of particles removed through the exhaust line equals the product of SP concentration in the drop phase and the volumetric flow rate of vapor. The SP concentration in the liquid phase remains unchanged after 90 min. This is because the ‘liquid’ in this cell is treated as a liquid film at the bottom surface of the cell. Particles in this phase can go through the flow path only if the film thickness is larger than the distance between the flow path tip and the cell bottom, i.e. submerged flow path, which is difficult to achieve since the liquid volume fraction that determines the film thickness is extremely small.

In the experiments, purge air was used to minimize particles deposition on the vessel wall and pool surface and to enhance particle removal from the gas space of the vessel. In GOTHIC re-entrainment into the drop phase and transport by the vapor flow to the exhaust line is also modelled. However, simulations with activated pool entrainment yields an excessive entrainment rate in the cell connected to the vent. Therefore, in this work the pool entrainment was deactivated. This limitation makes interpretation of the simulation results challenging. If particles only in the drop phase are considered as ‘particles’ that were measured in the tests, then the prediction by GOTHIC underestimates the amount of particles removed from the vessel as well as the pool scrubbing efficiency since re-entrainment of the deposited particles in the simulations is disabled. On the other hand, if particles in both phases (continuous liquid and droplets) are considered, significant deviations are expected when comparing the particle concentration in the gas volume since the deposited particles are “trapped” in the cells and cannot be transported by the vapor flow. Therefore, further improvement of the modeling of pool entrainment is recommended in future work.

There are several complex interphase transfer phenomena of SP. Therefore, possible errors introduced in the pool scrubbing models can be compensated by the errors in modeling of the drop deposition and pool entrainment phenomena. Therefore, further experiments should enable separate effect study of the aerosol particles behavior both in pool and in the gas volume (e.g., particle deposition on the vessel wall, particle deposition, and re-entrainment at the pool/gas interface). It will be important for model development and validation for various mechanisms and stages starting from the vent injection to removal through the exhaust line.

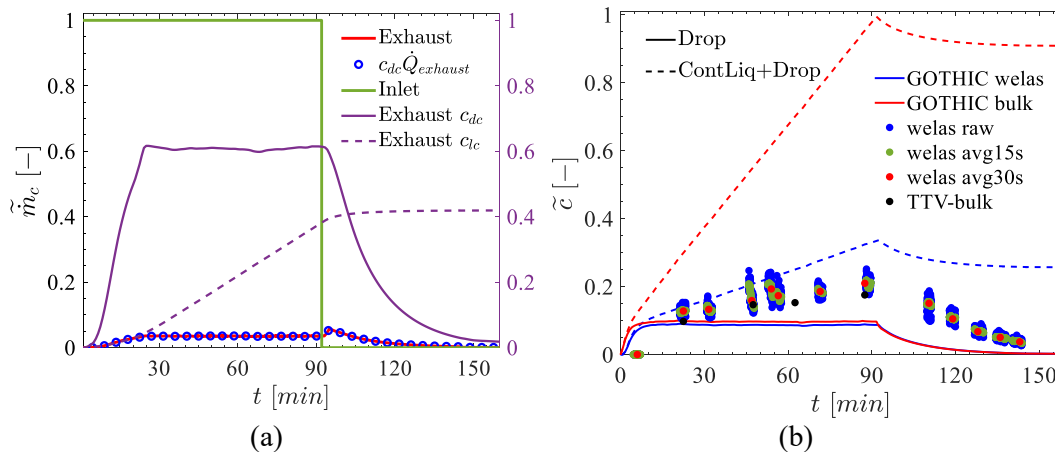


Figure 5-10: (a) SP through inlet and exhaust line, and its concentration in drop and liquid phases, and (b) comparison of SP concentration between GOTHIC prediction and test measurements.

The size distribution predicted by GOTHIC is compared with measurements by different sensors in Figure. Note that GOTHIC only evaluates the size distribution for particles in

the drop phase. It can be observed that the MMD and GSD are well captured by the simulation, indicating default drop deposition and pool scrubbing models could provide adequate prediction for particles with varied sizes.

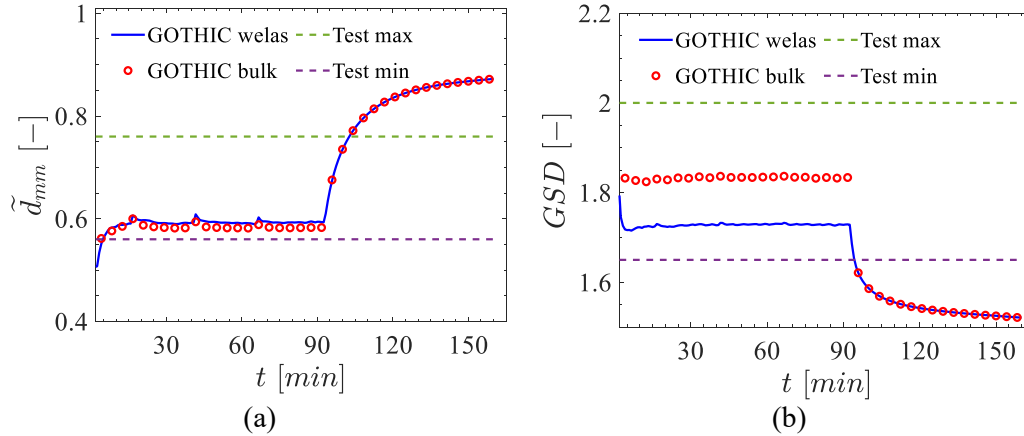


Figure 5-11: Evolution of MMD and GSD of SP for simulation of WH32-P1 test.

### 5.4.3. Parametric sensitivity study of particle deposition mechanisms

In this section, a parametric sensitivity study was performed to investigate the effects of various drop deposition and pool scrubbing mechanisms on the transport of particles. The model developed and validated in Sections 5.4.1, and 0 are used with boundary conditions from WH32-P1 test (Table 5-1). To quantify the respective contribution of each mechanism to the drop deposition, first a simulation with deactivated all drop deposition mechanisms was conducted, and then several simulations with one mechanism activated at a time.

The drop deposition rates contributed by individual mechanism and their resulting SP concentration in the drop phase are presented in Figure 5-12a. Combining all mechanisms enables the deposition of ~70-80% of particles from the injected flow. Particles are mostly retained in the vessel while predicted concentration in the drop phase is smaller than Welas measurements. Among the processes responsible for the retention, diffusiophoresis and thermal diffusion are among the dominant contributors. The thermophoresis is also important. The importance of the thermal effects can be explained by the fact that the vessel was heated during the tests. Additionally, the deposition rate can be slightly affected by the impaction while the contribution from turbulent diffusion is small (Figure 5-13). The spatial distribution of drop deposition rates by each mechanism is displayed in Figure 5-13. The mechanisms due to impaction, gravitational settling, thermal diffusion, and thermophoresis take effect on the entire pool surface while the diffusiophoresis works only in the cell with the vent.

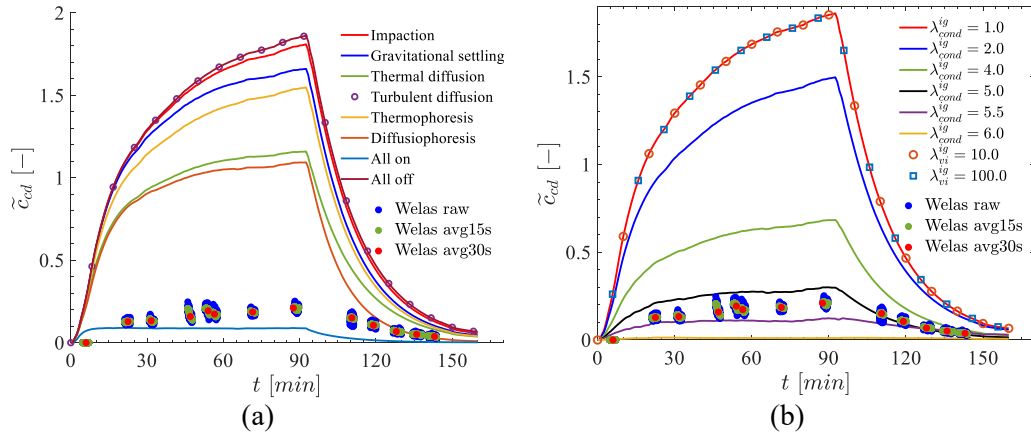


Figure 5-12: Effects of (a) drop deposition mechanisms and (b) multipliers for initial globule region on SP concentration in drop phase at the place of Welas.

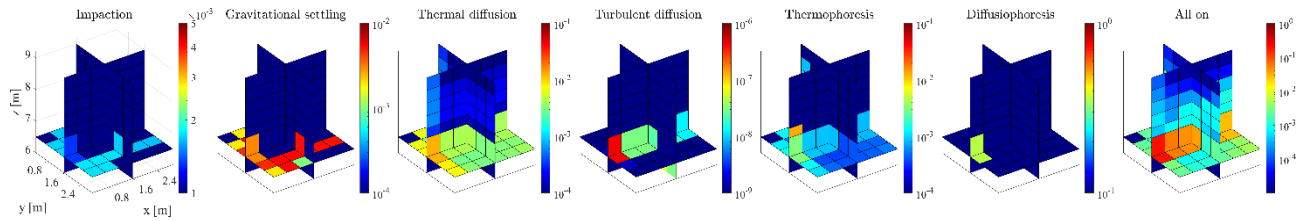


Figure 5-13: Contours of drop deposition rates induced by various mechanisms at  $t = 60 \text{ min}$ .

The study of the effect of pool scrubbing models on the SP concentration was conducted using the model with all drop deposition mechanisms deactivated. Aerosol particles after pool scrubbing would remain in the drop phase and leave the vessel without deposition. The condensation in the initial globule regime is expected to be the only dominant mechanism for aerosol injection with small diameters through a  $0.5 \text{ m}$  submerged vent. In this section, simulations were conducted with varied multipliers for condensation and impaction in the initial globule region [20].

The pool scrubbing efficiency is significantly affected by the condensation multiplier (Figure 5-12b). Variation of multipliers for impaction does not change the deposition rate due to the relatively small diameter of the particles. To evaluate the combined effect of various drop deposition mechanisms, a parametric study was performed by activating these mechanisms one by one. Simulation results are summarized in Figure 5-14,

Figure 5-15, and Figure 5-16. Unlike the results with one at a time activation of each mechanism separately, we find that turbulent diffusion becomes important in drop deposition. A rapid increase in deposition rate is observed when this option is activated. The turbulent diffusion takes effect for relatively large particles whereas agreement on MMD can be achieved only if this mechanism is applied.

Increasing the multiplier of the pool scrubbing model enhances the scrubbing efficiency and leads to a larger fraction of particles deposited in the pool. With the same mechanisms activated, the deposition rate by drop deposition is reduced because of fewer particles within the gas space. As presented in Figure 5-14, three simulations with different combinations of pool scrubbing and drop deposition models are in reasonable agreement with the experimental measurements on particle concentrations, indicating that current experimental

results do not provide the possibility to separate the fractions of particles deposited in the pool, on the vessel and in the gas volume.

Separate Effect (SE) experiments for measuring pool scrubbing efficiency with similar boundary conditions are recommended. The measured DF factors can be used as the database in support of the development of validation of pool scrubbing models. Integral Effect (IE) experiments such as THAI tests could be used to study the behavior of aerosol particles at the pool/gas interface and their transport in the gas volume with a proper instrumentation.

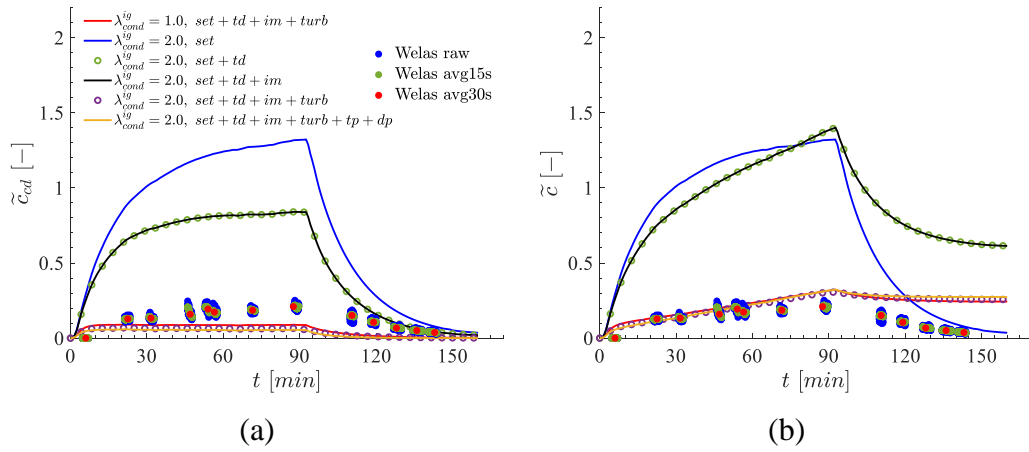


Figure 5-14: Effects of drop deposition mechanisms on SP concentration in (a) drop phase and (b) drop and liquid phases.

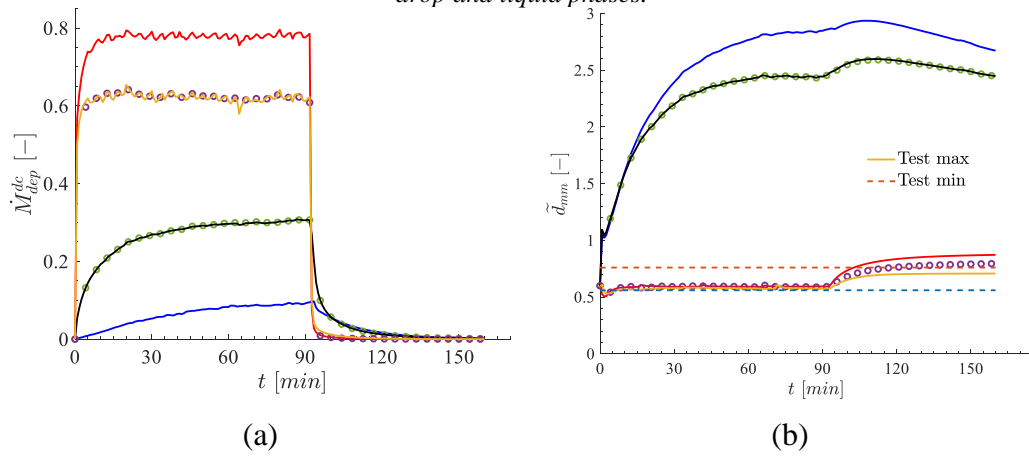
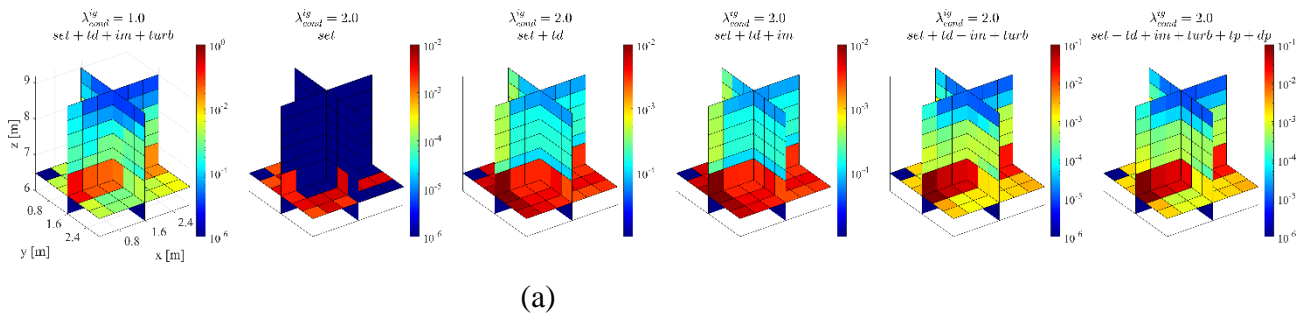


Figure 5-15: Effects of drop deposition mechanisms on (a) drop deposition rate and (b) MMD.



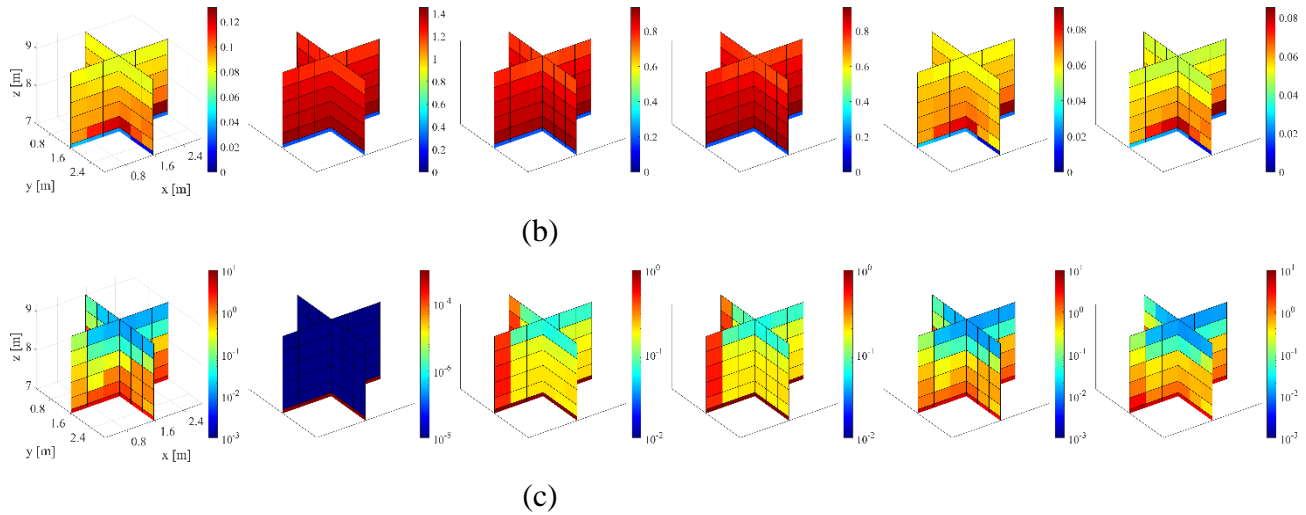


Figure 5-16: Contours of (a) SP deposition rate induced by drop deposition and SP concentration in (b) drop, and (c) liquid phases induced by different drop deposition mechanisms at  $t = 90$  min.

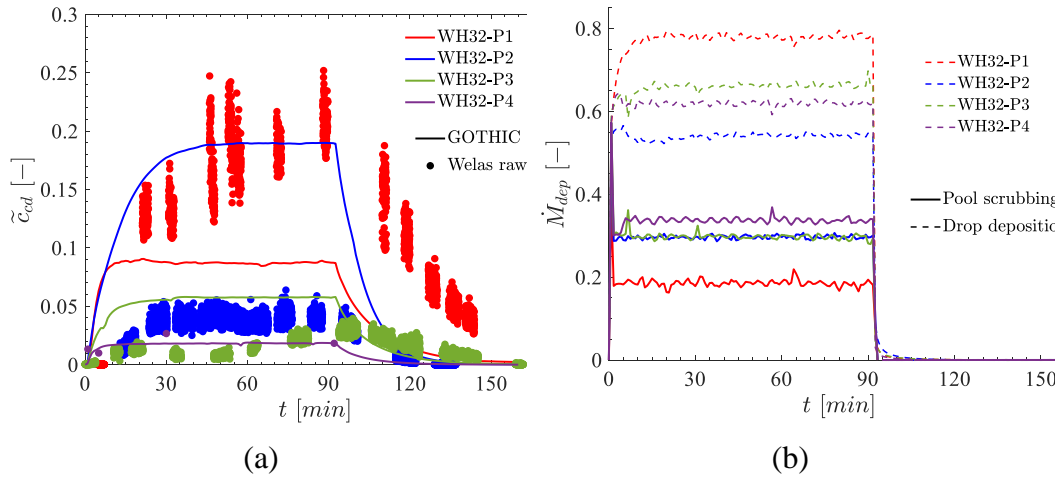


Figure 5-17: Effects of  $P_{vapor}/P_{sat}$  on (a) SP concentration in the drop phase at its comparison with measurements, and (b) deposition rates by pool scrubbing and drop deposition.

The effect of variation of the ratio between vapor pressure and steam saturated pressure  $P_{vapor}/P_{sat}$  is investigated by simulations and validated against the WH32 test series. The general trend where the particle concentration is decreased with the increase of the ratio is captured, except for the WH32-P2. This might be caused by the insufficient drop deposition in the gas space. The pool scrubbing efficiency increases with the increase of  $P_{vapor}/P_{sat}$ . SP deposit less in the gas space in P2 is compared to P3. This observation also emphasizes the significance of accessing the particle's behavior in the gas volume.

## 5.5. Analysis of THEMIS experiments relevant to Nordic plants designs and conditions

### 5.5.1. ROAAM+ and sensitivity study

The Risk Oriented Accident Analysis Methodology (ROAAM) was initially developed by Theofanous [33] and then developed as ROAAM+ framework to assess the effectiveness of SAM in preventing containment failure in Nordic BWRs [34]. ROAAM+ combines probabilistic and deterministic analyses to evaluate the effect of uncertainties in phenomena and scenarios.

In this work, experience of ROAAM+ development is used for the identification of the major contributors to uncertainty and risk quantification. Specifically, the approach includes:

- (i) a sensitivity analysis to identify major contributors to uncertainty,
- (ii) quantification of uncertainty is carried out and conclusions about the adequacy and potential for improvement of the models and the need for further experiments are provided,
- (iii) suggestions for future test conditions are provided in order to reduce uncertainty in the major contributors to uncertainty.

Uncertainty quantification and source term evaluation using MELCOR were performed [35][36] for two accident scenarios of Nordic BWR designs, namely (i) large break Loss of Coolant Accident (LOCA) and Station BlackOut (SBO) that lead to containment failure due to ex-vessel phenomena at reactor pressure vessel melt-through. The results of the study provide insights into the impact of MELCOR models, modeling parameters, and sensitivity coefficients on code predictions with a special focus on the fission product release. The parameters that are phenomenally important in code prediction of fission product release are summarized in [36].

### 5.5.2. Parametric study for important variables

The parameters that are associated with models of aerosol particles are investigated in this section. They are (i) SC71521, SC71531 and SC71542, which determine the hydraulic geometry of the bubbles in the swarm region, (ii) SC71551 and SC71555, which estimate the deposition rate by vent impaction in the initial globule region, (iii) RHONOM which is the nominal aerosol density. The aerosol agglomeration shape factor GAMMA is used in MELCOR but not in GOTHIC. The mechanisms of agglomeration and their effect on the transport of particles are planned to be investigated in future work. Detailed descriptions of each parameter can be found in [30].

The effect of vent impaction in the initial globule regime can be found in Figure 5-12b. The difference in pool scrubbing deposition predicted by various multipliers of vent impaction is not observed. This is because the injected particles in THEMIS experiments are relatively small, with an averaged MMD of  $\sim 0.5 \mu m$  in which impaction can be ignored. The shape of the bubbles in the swam region affects the deposition kernel and integrated DF factors [21]. Simulations were carried out to investigate the deposition mechanisms in the swarm region. Since the development of the swarm bubble region requires sufficient

submergence, the elevation of the pool surface was lifted to 8.3 m, and boundary conditions of WH34-P4 (Table 5-1) were applied. The variation of multipliers for mechanisms in the swarm region only slightly influences the pool scrubbing deposition rate as shown in Figure 5-18. This is attributed to the distance from the vent to the elevation at which the swarm region is expected to develop ( $\sim 2.0$  m) is identical to the submergence of the vent, suggesting that this region could be ignored for current test conditions.

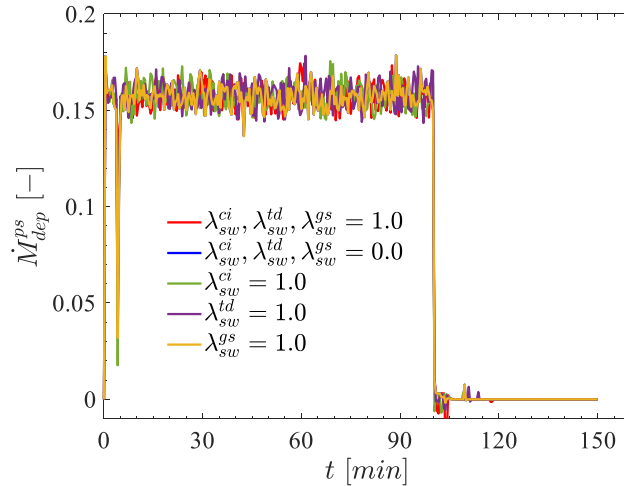


Figure 5-18: Effects of multipliers for swarm bubble region on pool scrubbing deposition rate.

Increasing aerosol density enhances the drop deposition within the gas space and therefore reduces the concentration of SP in the drop phase (Figure 5-19). The pool scrubbing efficiency is not affected by the density variation since condensation is the only important factor during this process. However, for vent injection with large submergence where the swarm region can develop, several deposition kernels associated with particle density would be influenced and consequently affect the scrubbing efficiency.

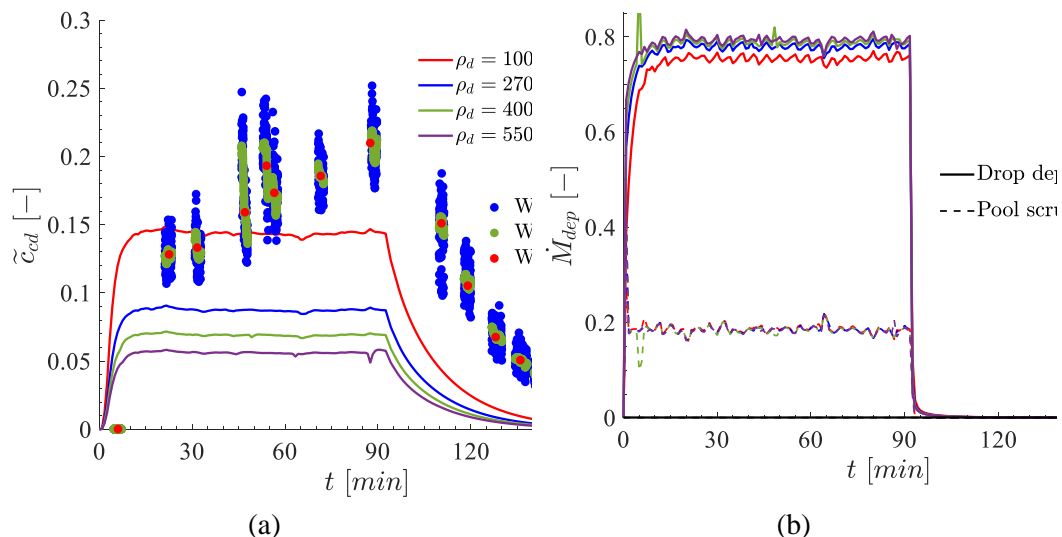


Figure 5-19: Effects of particle density on (a) SP concentration in drop phase at the place of Welas and (b) deposition rates.

## 5.6. Conclusions and Outlook

Pool scrubbing characterized by a process of the retention of fission products into a water pool is an efficient way to prevent the release of FP into the environment during accident scenarios. Evaluation of the magnitude of fission products released is crucial for the assessment of the consequences of severe accidents. The design of the strategy of severe accident management requires validated models for the analysis of source terms of FP. The next phase of the OECD/NEA THAI project called "THEMIS THAI Experiments on Mitigation measures and source term issues to support analysis and further Improvement of Severe accident management measures" was aiming to provide additional data for the model development. Within the project, several experiments were performed focusing on the FP released under pool scrubbing conditions.

This report summarizes the analytical support to the THEMIS pool scrubbing experiments. GOTHIC which is an integral, general-purpose thermal-hydraulics code for containment analysis was applied for modeling of THAI facility. Model validation was performed against several THEMIS tests and reasonable agreement was achieved. The guidelines for modeling of the relevant phenomena and quantification of different particle deposition mechanisms are detailed. Analysis results of THEMIS experiments are provided.

Solid particles are used in GOTHIC to simulate the aerosols and they can be tracked in the drop and liquid phases. Modeling of transport of SP from vent to vessel exhaust line by GOTHIC involves several models of pool scrubbing, drop deposition in gas space, re-entrainment, and agglomeration. The amount of particles retained in the pool is determined by pool scrubbing and drop deposition occurring at the pool/gas interface and their respective deposition rates are determined by several mechanisms. Parametric study suggests that the condensation in the initial globule region is the dominant contributor to the pool scrubbing under WH32 conditions. For drop deposition, the two most important mechanisms are thermal diffusion and diffusiophoresis, followed by gravitational settling and thermophoresis. Turbulent diffusion is important for deposition of the large particles. Particle deposition due to drop deposition occurs mainly at the pool/gas interface.

The particles above the pool surface can also be deposited on the vessel wall or in the cells without any surface by drop deposition, forming a liquid film with a very small amount of volume fraction occupying the volume. These particles are all suspended in the liquid film and can be re-entrained into the drop phase through pool entrainment. Activation of pool entrainment yielded an abnormal entrainment rate and therefore it was not used in this work. Particles only in the drop phase can be removed from the vessel because the film thickness in the cell connecting the exhaust pipe is too thin. Model validation against THEMIS experiments achieves a reasonable agreement on particle concentration in gas space. However, there is a possibility for the compensation of errors given that the concentration is determined by the balance between inflow of particles escaped from the pool and particles those that left the vessel.

Uncertainty quantification and source term evaluation for Nordic BWR designs in response to LOCA and SBO were performed using MELCOR and the parameters associated with the models of particle behavior with high importance were identified. For the pool scrubbing model, they are hydraulic geometries for bubbles in the swarm region and coefficient to estimate the vent impaction in the initial globule region. For the aerosol particle dynamic model, they are particle agglomeration shape factor and particle density. Parametric study in GOTHIC using THEMIS boundary conditions indicates the aerosol concentration is also sensitive to the variation of particle density. The effects of all mechanisms in the swarm region are negligible because of the relatively small submergence in THEMIS experiments.



The effect of particle agglomeration and modeling of particle re-entrainment is planned to be investigated in future work. Separate Effect (SE) experiments for measuring pool scrubbing efficiency with similar boundary conditions are recommended. Further experiments in THAI facility could focus more on the behaviors of aerosol particles at the pool/gas interface and their transport in the gas volume.

## 5.7. References

- [1] L. E. Herranz., F. Sánchez., S. Gupta. Validation Matrix for Pool Scrubbing Models, Nuclear Technology. (2022)
- [2] L. S. Lebel., A. C. Morreale., M. Freitag., et al., “Aerosol Experiments and Measurement Techniques on Pool Scrubbing-Related Source Term Issues,” NURETH-19, Brussels, Belgium, (2022).
- [3] Galushin, S., Grishchenko, D., Kudinov, P. “Implementation of framework for assessment of severe accident management effectiveness in Nordic BWR,” Reliability Engineering and System Safety, 203, art. no. 107049 (2020)
- [4] Grishchenko D., Galushin S., Kudinov P., “Failure domain analysis and uncertainty quantification using surrogate models for steam explosion in a Nordic type BWR”, Nuclear Engineering and Design, Volume 343, 2019, Pages 63-75, ISSN 0029-5493, 2019.
- [5] P. Kudinov, S. Galushin, D. Grishchenko, S. Yakush, “Development of Risk Oriented Accident Analysis Methodology (ROAAM+) for Assessment of Ex-Vessel Severe Accident Management Effectiveness,” 18th International Topical Meeting on Nuclear Reactor Thermal Hydraulics (NURETH-18), Portland, OR. August 18-23, 2019.
- [6] Li H., Villanueva W., and Kudinov P., “Approach and development of effective models for simulation of thermal stratification and mixing induced by steam injection into a large pool of water,” Science and Technology of Nuclear Installations, Article ID 108782, 2014.
- [7] Li H., Villanueva W., Puustinen M., Laine J. and Kudinov P., “Validation of effective models for simulation of thermal stratification and mixing induced by steam injection into a large pool of water,” Science and Technology of Nuclear Installations, vol. 2014, Article ID 752597, 18 pages, 2014.
- [8] Villanueva W., Li H., Puustinen M., Kudinov P., “Generalization of Experimental Data on Amplitude and Frequency of Oscillations Induced by Steam Injection into a Subcooled Pool,” Nuclear Engineering and Design, Volume 295, 15 December 2015, Pages 155–161, 2015.
- [9] Li H., Villanueva W., Puustinen M., Laine J., Kudinov P., “Thermal stratification and mixing in a suppression pool induced by direct steam injection,” Annals of Nuclear Energy, 2017.
- [10] Gallego-Marcos I, Villanueva W, Kudinov P. “Modelling of Pool Stratification and Mixing Induced by Steam Injection through Blowdown Pipes.” Annals of Nuclear Energy, 112, 624-639. 2018.
- [11] Gallego-Marcos, I., Kudinov P., W. Villanueva, et al. “Pool stratification and mixing during a steam injection through spargers: analysis of the PPOOLEX and PANDA experiments”. Nuclear Engineering and Design, 337, 300-316. 2018
- [12] Gallego-Marcos, I., Kudinov, P., Villanueva, W., et al. “Pool Stratification and Mixing Induced by Steam Injection through Spargers: CFD modelling of the PPOOLEX and PANDA experiments,” Nucl. Eng. Des, 347, 67-85, 2019.
- [13] Gallego-Marcos, I, Pavel Kudinov, Walter Villanueva, Markku Puustinen, Antti Räsänen, Kimmo Tielinen, Eetu Kotro, “Effective momentum induced by steam condensation in the oscillatory bubble regime,” Nuclear Engineering and Design, Volume 350, 2019, Pages 259-274. 2019.
- [14] Gallego-Marcos I., Grishchenko D., Kudinov P., Thermal stratification and mixing in a Nordic BWR pressure suppression pool. Annals of Nuclear Energy, Volume 132, October 2019, Pages 442-450, 2019.

- [15] Estévez-Albuja S., Gallego-Marcos I., Kudinov P., Jiménez G., “Modelling of a Nordic BWR containment and suppression pool behavior during a LOCA with GOTHIC 8.1,” *Annals of Nuclear Energy*, Volume 136, 2020, 107027, 2020.
- [16] Wang, X., Grishchenko, D., Kudinov, P. “Development of Effective Momentum Model for Steam Injection Through Multi-Hole Spargers Using a Condensation Region Approach.” *ICONE-2020*. Virtual, Online. August 4–5, 2020.
- [17] Wang, X., Grishchenko, D., Kudinov, P. “Simulation of Jets Induced by Steam Injection through Multi-hole sparger using Effective Heat and Momentum Models,” *Nucl. Eng. Des.*, 405, 112222, 2023.
- [18] Wang, X., Grishchenko, D., Kudinov, P. “Pre-test analysis for definition of steam injection tests through multi-hole sparger in PANDA facility,” *Nucl. Eng. Des.*, 386, 111573, 2022.
- [19] Kudinov, P., Wang, X., Feng, Y., et al., “Thermal Hydraulic Phenomena of the Suppression Pool”. NKS-THEOS Report, NKS-465, 2022.
- [20] “GOTHIC containment analysis package, user manual,” Version 8.4 (QA), EPRI, 2022.
- [21] “GOTHIC containment analysis package, technical manual,” Version 8.4 (QA), EPRI, 2022.
- [22] P.C. Owczarski., K.W. Burk. “SPARC-90: a code for calculating fission product capture in suppression pools”. In: *NUREG/CR-5765 TI92 003256*. U.S. Nuclear Regulatory Commission, (1991).
- [23] S. Ramsdale., H. G. Friederichs., S. Güntay. “BUSCA JUN91: Reference Manual for the Calculation of Radionuclide Scrubbing in Water Pools” GRS, Koeln, DE, (1991).
- [24] A.T. Wassel., A.F. Mills., D.C. Bugby. “Analysis of radionuclide retention in water pools”, *Nucl. Eng. Des.* 90 (87), 87–104. (1985).
- [25] B.M. Schmitz. “Further Development of ATHLET-CD Pool Scrubbing Module SPARC-B/98 for SOPHAEROS V2mod0\_1-Model Description”, TN-SMZ-00-1, GRS, (2000).
- [26] C. Berna., A. Escrivá., J.L. Muñoz-Cobo., L.E. Herranz. “Enhancement of the SPARC90 code to pool scrubbing events under jet injection regime”, *Nucl. Eng. Des.* 300, 563–577. (2016).
- [27] Y. Liao., J. Li., D. Lucas. “Investigation on pool-scrubbing hydrodynamics with VOF interface-capturing method”, *Nucl. Eng. Des.* 390, 111713. (2022).
- [28] Z, Mei., F, Kong., X, Cheng. “Modeling of submicron particle transport based on VOF-LPT method”, *Chemical Engineering Science*, 264, 118168, (2022).
- [29] Z, Mei., X, Cheng. “Impact of bubble dynamics on aerosol transport based on CFD analysis”, *Progress in Nuclear Energy*, 161, 104723, (2023).
- [30] L.L. Humphries., et al., “MELCOR Computer Code Manuals, Vol.2: Reference Manual, Version 2.2.9541”, Technical report, Sandia National Laboratory, 2017. SAND2017-8876 O2.
- [31] J.W. Lane., T.L. George., S.W. Claybrook., et al., “Applicability of GOTHIC 8.3(QA) for non-LWR simulation, aerosol modeling & hydrogen management,” *NURETH-19*, Brussels, Belgium, (2022).
- [32] GOTHIC Condition Report for Action Item (AI) 8.4-010 / EPRI CAR 2022-0081.
- [33] T.G. Theofanous, “On Proper Formulation of Safety Goals and Assessment of Safety Margins for Rare and High-Consequence Hazards,” *Reliability Engineering and System Safety*, 54, pp. 243-257 (1996).

- [34] S. Galushin, D. Grishchenko and P. Kudinov, “Implementation of Framework for Assessment of Severe Accident Management Effectiveness in Nordic BWR”, *Reliability Engineering and System Safety*, 203, Article 107049 (2020).
- [35] G. Acharya, D. Grishchenko, P. Kudinov., et al., “Uncertainty Quantification of The Fission Product Release During Severe Accidents in Nordic BWRs”, *NU-RETH-20*, Washington, D.C., August 20-25, (2023).
- [36] G. Acharya, D. Grishchenko, P. Kudinov. “Source Term Uncertainty Analysis of Severe Accidents in Nordic BWRs”, *SCOPE-1*, Dhahran, Saudi Arabia, Nov 13-15, (2023).

## 6. Fukushima Accident Update

### 6.1. Summary

One of the tasks in the APRI-project since the tragic accidents in Fukushima Dai-ichi, Japan, is a follow up of the new findings, observations and lessons learned from the accidents. A deep understanding of the accident progression and associated phenomena of the Fukushima accident has a firm relevance since the damaged reactors in Fukushima were BWR, which is also the type of reactor which has been studied in the APRI-context. Since APRI-10 Tokyo Electric Power Company Holdings (TEPCO) together with International Research Institute for Nuclear Decommissioning (IRID) have conducted an investigation in the drywell of reactor unit 1 in Fukushima Dai-ichi (1F1) using a submersible robot with an attached video camera. Some key findings from the investigation include:

1. There are likely multiple failure points in the reactor pressure vessel (RPV), as some components as control rod guide housings was found inside the pedestal.
2. Much of the components in the pedestal area is damaged beyond recognition, but the damage outside is limited to near the pedestal opening.
3. Concrete erosion in the pedestal is about 1 meter high, but the reinforcing structures are mostly intact.
4. Deposits on the drywell floor range from 0.2 to 1.5 meters in height.
5. Cavities exist below shelf deposits attached to various structures.
6. No significant thermal damage to the D/W shell has been observed.

Given that over ten years have passed since the accident, factors like time, cooling water flow, and external events (like earthquakes) could have changed the state of the materials. Future studies should focus on understanding the cause of the reactor vessel failure.

### 6.2. Observations

Tokyo Electric Power Company (TEPCO) has conducted site investigations, as well as analyses, to understand the current status inside the Primary Containment Vessels' (PCVs) and reactor pressure vessels (RPVs) of the damaged Units 1, 2, and 3. The unit 1 reactor at Fukushima Dai-ichi (1F1) experienced the earliest onset of the severe accident after losing the isolation condenser cooling when the tsunami flooded the site. The unit 1 reactor was also without any effective core cooling for the longest period and the boundary conditions reminds of the SBO-analysis the Swedish licensee's demonstrate in the Safety Analysis Report (SAR). Due to the ineffective core cooling, the accident progression resulted in substantial core damage and relocation of molten materials into the drywell of the PCV. Only a small amounts of water is expected to have been present in the drywell at the time of the ex-vessel phase of the accident and relocation of corium from the vessel to the drywell with the potential of initiating long-term unmitigated molten core-concrete interaction (MCCI) in a dry state. With the purpose of gathering information to understand the state and conditions in the containment, investigations inside the PCV utilizing submersible remotely operated vehicles (ROVs) was conducted between December 2022 and March 2023, see [1], [2] and [3].

The high water level in the 1F1 drywell prompted use of submersible ROVs for the PCV internal investigation for the study in the wide area of the D/W annulus and pedestal area. The investigation was focused on the state of the equipment outside and inside of the pedestal area; distribution of deposits; fuel debris; and state of the pedestal wall, which supports the weight of the RPV and related structures.

### 6.2.1. Upper Pedestal Area

From the video recordings it is possible to observe that almost no parts of the control rod drive (CRD) exchange equipment could be found. This is in contrast with the findings from unit 2 and unit 3, where although the CRD equipment itself was displaced from its original position, the rails, platform, and other parts could be identified. Several tube shaped objects leaning on the pedestal wall in 1F1 was identified as CRD and In-Core Monitor housings (ICM) which had been detached and fallen from the RPV lower head, see Figure 6-1. In some cases, the flanges were in an upper position which implies that they have turned upside down during their relocation, see Figure 6-2.



Figure 6-1: Dislocated CRD housing.



Figure 6-2: CRD housing hanging upside down under the RPV.



Figure 6-3: CRD housing buried in deposits and leaning on the pedestal wall.

Further, some of the detached CRD housings remain in a suspended position by the supporting bars. The total number of confirmed relocated housings, including those suspended above water level, was more than 10. Those completely separated from all the upper support structures have been found partially buried in the deposits, see Figure 6-3. Above the water level a number of flanges belonging to the CRD and ICM housings could be observed which seems to be remaining in or near their original height. While their vertical position does not appear to be significantly changed, their horizontal position deviates from the original pitch and square grid, see. Figure 6-4.



Figure 6-4: Dislocated CRD housings above the water level.

Ripplings on the water surface in the upper drywell due to dripping of the cooling water from the damaged lower head (LH) of the RPV were observed both in the central area and in the peripheral areas of the pedestal, suggesting multiple vessel penetrations [5].

### 6.2.2. Observations in the Lower Pedestal Area

A picture of pedestal opening can be seen in Figure 6-5 together with a schematic drawing of the orientation of the pedestal opening seen in Figure 6-6. The picture in Figure 6-5 is taken in front of the pedestal personnel access entry. Concrete erosion along the entire inner circumference of the pedestal wall up to a height of approximately one meter can be observed. The vertical steel rebars are exposed due to the concrete ablation but no significant damage to the rebars themselves is apparent. In many locations where the concrete

ablation could be observed in detail, the so called inner skirt is visible. The inner skirt is a cylindrical reinforcing structure in the center of the pedestal wall reaching from the basemat up to the height of one meter from the D/W floor to support the structural integrity of the pedestal on to the basemat, see Figure 6-7. No significant deformation of the inner skirt was confirmed either, and the concrete erosion is assumed to be reaching the center of the wall with regard to its depth around the entire circumference of the pedestal inner wall.



Figure 6-5: View of the pedestal opening.

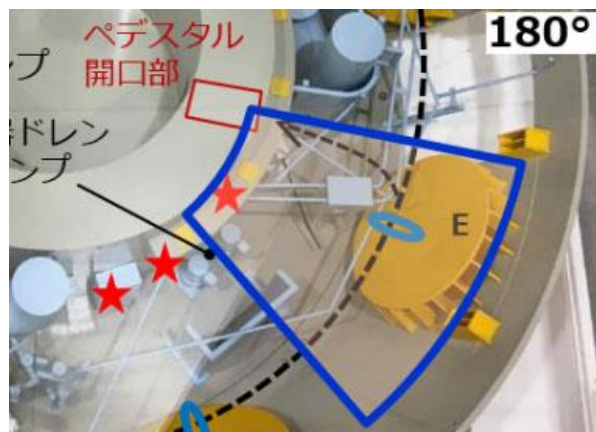


Figure 6-6: Schematic picture of the pedestal opening area.





Figure 6-7: *The inner skirt during construction.*

Above the eroded concrete, at a height about 150 centimeters, protruding deposited materials of unknown nature (referred to as shelves) were found in several places, see Figure 6-8. There is no observation of damages or irregularities on the wall concrete above the "shelf" level, except for dark-colored materials adhering to some parts of the wall and accumulating on top of some shelves. The average height of the materials deposited on the pedestal area floor is assumed to be about 60 centimeters from the normal floor level, with local maximum (in front of the pedestal opening) reaching to about one meter. No internal reactor structures, as fuel assembly shrouds, tie plates, control guide tubes etc., can be identified in the pedestal area. This is in contrast to unit 2 and 3 where the upper tie plate of the fuel assembly (unit 2) and control rod guide tubes (unit 3) was found inside the pedestal region.



Figure 6-8: *Protruding deposits above the concrete ablation area forming "shelf" structures.*

The erosion and damage done to the pedestal wall concrete during the molten corium concrete interaction could be observed in detail close to the inside of the pedestal opening, see Figure 6-9. The pedestal wall concrete was confirmed to be eroded on both sides of the wall in the opening section, up to the level slightly above the height of the inner skirt. No clear deformation of the inner skirt itself could be confirmed but the L-shaped rebars that are horizontally welded to the inner skirt to reinforce the corners of the opening were found to be bent on both the inner and outer sides of the wall on both sides of the opening, see Figure 6-10.



Figure 6-9: Molten Corium Concrete Interaction in the inside of pedestal near the opening.



Figure 6-10: Bended rebars.

On the pedestal outer wall concrete erosion and exposure of intact rebars have been confirmed. The accessibility by ROV in this region was limited due to different obstacles and thus the extent of the concrete erosion outside of the pedestal area could not be determined. A decreasing trend of the concrete erosion height was observed with increased distance from the pedestal opening, which is to be expected. Through previous PCV internal investigation efforts, where a camera was lowered to the pedestal opening area through the grating from the floor above, it was observed that significant amounts of deposits of unknown nature is present in the D/W annulus. The maximum height of deposits outside of the pedestal area and in the annulus was evaluated to be ~1.1 meter based on ultrasonic wave analysis and ~1.3 meter (on the outer edge of the pedestal opening) based on visual information. At the lowest level the deposits is estimated to be at a height of 0.2 meters. Some deposits are expected to have been distributed in jet deflectors based on height of the deposits at certain points close to the deflectors. At least in part of the investigated area, large holes or cavities exist under the surface level of the shelves that are

composed of deposits. The observed damage to the preexisting structures can be seen regarding the Reactor building Closed cooling Water system (RCW) piping and some small-sized piping located at a low height front of the pedestal opening, see Figure 6-11, 6-12 and 6-13.

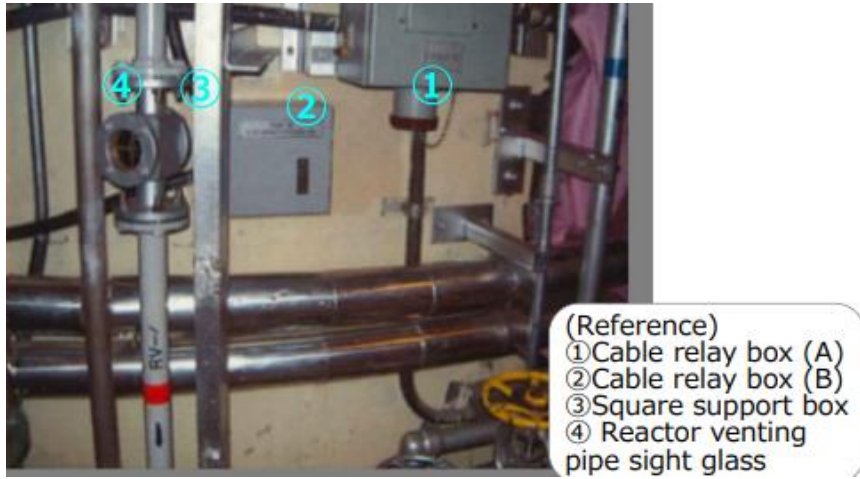


Figure 6-11: Reactor building Closed cooling Water system (RCW) piping before the accident.

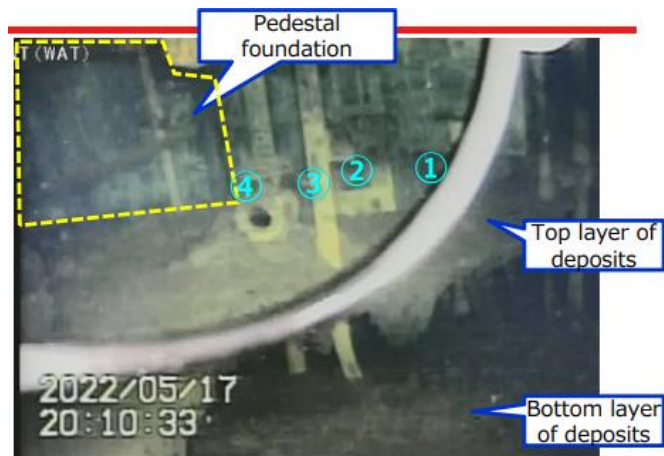


Figure 6-12: Reactor building Closed cooling Water system (RCW) piping after the accident.

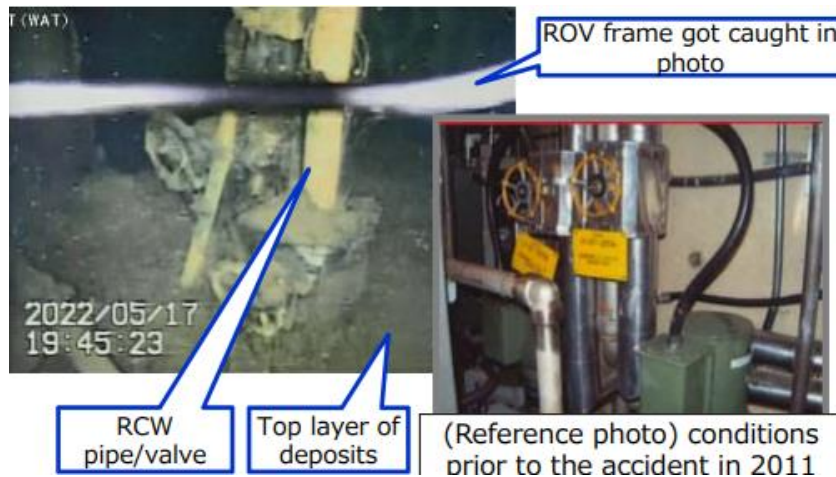


Figure 6-13: *Damage to small piping, after and before.*

No distinct deformation or melting was confirmed on the PLR piping or shielding block of the equipment drain sump pump or jet deflectors, see Figure 6-14.



Figure 6-14: *Damage on PLR piping.*

Besides the shelf deposits, other deposits of various shapes, sizes, and distributions have been confirmed, including bulky round deposits, threadlike deposits, thin layered spherical deposits resembling eggshells, and glossy glasslike deposits near the pedestal opening. Since materials of unknown nature were also found suspended on the structures high above the water level, it is expected that part of the materials currently piled on the D/W floor came from upper floors of the D/W.

### 6.2.3. Discussion of the accident progression in Unit 1

#### *Vessel failure*

Fukushima Daiichi Reactor Unit 1 was operating at full capacity when the earthquake struck on March 11, 2011, triggering an automatic shutdown. Backup diesel generators

initially maintained power, and cooling was managed through isolation condensers. However, about 40 minutes later, the first tsunami waves hit, followed by a second wave exceeding 14 meters, over reaching the power plant's tsunami walls which led to the inundation of the site area. The flooding disabled electrical systems, backup power, and monitoring equipment, forcing operators to improvise. After the power loss, operators used car batteries in an attempt to monitor key reactor parameters as water level in the core and primary circuit pressure. Attempts to operate the isolation condensers for core cooling failed leading to boil off of the water inventory in the core and primary system leading to core damage and core melt. Estimates based on simulations and recorded plant data suggest core damage began at about 4 hours after shutdown and the reactor pressure vessel failing at about 15 hours after shutdown.

Assessing how the lower head (LH) of a BWR fails is challenging due to its structure, large number of penetrations of different kind, and various materials. Often three main failure modes are considered: ejection of penetration tubes, overheating and failure of tubes, and large-scale, or global, rupture [6]. Direct observation of the LH has so far not been possible to perform due to the complicated conditions and limitations on investigating robots. Observations however suggests multiple failure points. Cooling water was seen dripping from above in several spots, and parts of the control rod drive (CRD) and in-core monitor (ICM) housings were found in the lower pedestal area, indicating structural failure. In BWR's, the CRD housing is usually prevented from full ejection by supporting structures as support plates, meaning that large debris releases are less likely. Some CRD housings appear clogged with debris, and their angled shape suggests they melted and fell after their external support structure was damaged. Unlike CRD housings, ICM housings are not held by the same support structure, so their weld failure could lead to immediate ejection, creating pathways for molten material to escape. One such detached ICM housing was found hanging above the water level in the outer pedestal area, supporting this assumption. It appears that part of the ICM housing is stuck in debris or other structures that couldn't be directly seen. Multiple CRD housings were found on top of or partially buried in debris in the pedestal area, which may indicate they rotated during the later stages of the accident. It's unclear whether some housings are fully buried or melted [5].

Another possible failure mode from molten material interaction is the RPV drain line penetration in the center of the lower head. In a case where the primary system is depressurized it could lead to a large-scale failure after the vessel dries out and debris heats up, creating a potential for molten material to move outside the vessel. The drain line thickness (0.7 cm) is much less than the vessel lower head thickness (20.0 cm) and thus, if debris relocates onto the lower head and into the drain line, the drain line may be susceptible to reaching failure temperatures more rapidly than the vessel. Further, although BWR instrument tube walls are thinner than the drain line, the drain line has a larger effective diameter for melt flow. Furthermore, the drain nozzle is directly open to corium. The position of CRD housing flanges in the upper pedestal region shows they haven't moved much vertically but are misaligned horizontally, which may indicate a larger rupture of the LH, such as vessel deformation or "unzipping." Some CRD housings were found flipped upside down, which would require substantial damage, particularly in the central area, to allow such movement. The bulky deposits found with the CRD housings are believed to be solidified debris. Due to the dense arrangement of CRD housings, molten material outside the RPV could temporarily freeze and get trapped before the housings detach. This could alter the composition of the molten material, lowering its temperature and affecting the later stages of the accident. It's still unclear which failure mechanism that allowed the rapid movement of molten material, and it's possible that several processes were happening at the same time or in sequence. More investigations in the upper

pedestal area and inside the RPV are needed for a better understanding of where and how the LH breach occurred [5].

#### *Molten Corium-Concrete Interaction*

Concrete erosion on the containment floor at Fukushima Unit 1 was expected given the severity and magnitude of the accident. The uniform height of erosion in the pedestal area suggests that molten material spread across the entire floor before significant erosion occurred, which is consistent with a rapid, high-temperature melt scenario. The erosion decreased further from the pedestal opening. As a result of this erosion support structures as rebars and the inner skirt were exposed. Surprisingly these items remain mostly intact, which is contradicting previous knowledge which suggested that the rebars would have been eroded along with the concrete. The bending of some horizontal rebars suggests that temperature dependent deterioration, rather than long-term effects like slow concrete degradation, was the main cause. The temperature wasn't high enough to melt the rebars, but it was enough to weaken them and cause them to bend under their own weight. While spallation (the breaking off of concrete chunks due to high heat) is usually seen as a minor factor in concrete erosion, the conditions at Fukushima seems to have made it a more important aspect than previously expected. Various factors like the type of concrete, moisture levels, and reinforcement could have played a role. This raises the need for further research into spalling's role in the erosion process during such accidents.

The observations in the pedestal area show that the erosion of concrete is lower than the height of shelf deposits and similar to the height of the inner skirt, with some local areas being a few centimeters higher. It's important to investigate whether the inner skirt is contributing to this concrete erosion. The inner skirt is likely to come into contact with high-temperature materials soon after the ex-vessel phase begins. One of the first contact points is expected to be at the pedestal opening, where there is no concrete covering the inner skirt. Additionally, the sump pits may see a faster spread of melting materials, as they could be about 1 meter deeper than the rest of the pedestal area, making cooling more difficult. There is a separation of about 75 cm of concrete between the edge of the sump pit and the surface of the inner skirt. This means the melting front could reach the inner skirt surface earlier in this area compared to others. The inner skirt has better thermal conductivity than concrete, allowing heat to be transferred to the pedestal wall quickly without causing melting or deformation. The heat buildup in the pedestal wall, combined with mechanical stresses from the thermal expansion of the skirt and heat transfer from the molten material, may explain the even erosion of concrete in the pedestal area. Shelves inside the pedestal could be related to a phenomenon called anchoring, which occurs when a crust of solidified material forms along the walls and prevents cooling water from reaching the molten material. Unlike what is often seen in experiments, the shelves in the pedestal do not show signs of large pieces breaking apart, indicating that the crust did not cover the entire area. Outside the pedestal, the shape of fallen fragments suggests that solidification mostly happened near structures that acted as heat sinks [5].

There are also dark materials on parts of the pedestal walls, but their origin is unclear. One theory is that they result from eruptions caused by gases interacting with melt droplets. Similarly, "icicles" found on some shelves may have formed from melt droplets solidifying as they dripped.

#### *Deposits in lower drywell*

The height of the deposits in the D/W annulus is about 1.3 meters, which is higher than the estimated 1.1 meters if all molten material was assumed to be confined to the pedestal

area. The shelves inside the pedestal appear rounded and show no signs of breaking apart, except in areas near fallen equipment, indicating that the crust did not cover the entire area. Outside the pedestal, the shape of collapsed fragments suggests that solidification primarily occurred near structures that could absorb heat, such as the drywell shell and other components. Additionally, there are dark materials on some walls inside the pedestal, but their origin is still unclear. Some dark materials found in the pedestal area might have come from “volcanic” eruptions caused by gases mixing with molten materials. Icicles on shelves could also form from melt droplets solidifying as they dripped. Although there hasn't been a full investigation into erosion on the drywell (D/W) floor, leaking water suggests there might be minor damage to the D/W shell.

After molten materials moved through the pedestal opening, the molten material could spread towards the D/W shell and other areas. Some structures in the D/W are still intact, suggesting they were not exposed to extremely high temperatures. The overall temperatures in the containment area seem to have been below the melting point of aluminum, indicating that the materials that spread likely cooled down before reaching the D/W shell.

### 6.3. References

- [1] Tokyo Electric Power Company Holdings (TEPCO)  
[2022.05.23 Implementation Status of the Unit 1 Primary Containment Vessel \(PCV\) Internal Investigation \(ROV-A2\) \(work conducted between May 17~19\)](#)
- [2] Tokyo Electric Power Company Holdings (TEPCO)  
[2023.04.04 Implementation Status of the Unit 1 Primary Containment Vessel \(PCV\) Internal Investigation \(ROV-A2\) \(work conducted between March 28~30, 2023\)](#)
- [3] Fukushima Daiichi Nuclear Power Station Unit 1 Primary Containment Vessel Internal Investigation Completion of the detailed visual investigation of the perimeter of the pedestal using submersible ROV-A2
- [4] Nuclear Regulatory Authority (of Japan)  
[www.nsr.go.jp/data/000395885.pdf](http://www.nsr.go.jp/data/000395885.pdf)
- [5] Nuclear Technology, Evaluation of Fukushima Daiichi Unit 1 Ex-Vessel Phenomenon Leveraging on Primary Containment Vessel Robotic Inspections, Michal Cibula et al, March 31 2024
- [6] NUREG/CR 5642 LWR Lower Head Failure Analysis, J Rempe et al, September 1993



## 7. Conclusion and Outlook

### 7.1. Conclusion

The research at KTH Department of Nuclear Power Safety has been focused on understanding and modeling of severe accident phenomena which have large uncertainties but play important roles in safety analyses and qualification of severe accident management (SAM) measures intended to terminate accident progression and maintain containment integrity. In APRI-11 the research at KTH-NPS advanced to include also the investigations on late-phase in-vessel met/debris behavior and vessel failure mode which were initiated but unresolved in APRI-10, and to extend the scope of FCI study, as well as to perform case study for reactors chosen. Moreover, a new interest is the interactions of corium melt with below-vessel structures. The inclusion of late in-vessel behavior was introduced since it was found that the previous focus on ex-vessel debris bed coolability and steam explosion alone could not resolve the problem associated with the SAM measure of Swedish NPPs, since the ex-vessel phenomena are sensitive to the late-phase phenomena of in-vessel accident progression. This involved processes as the corium evolution in the lower head, vessel failure mode and melt discharge condition. Hence, one of the subtasks in APRI-11 was the study of late in-vessel behavior and more specifically molten metal (with lower melting point) infiltration in oxidic debris bed, dynamics of multi-composition debris remelting to molten pool and heat transfer of debris/molten pool to the vessel wall and penetrations. For this purpose several experiments have been carried out in the SIMECO-2 and MRSPOD facilities to investigate debris remelting and melt infiltration, respectively. For developing understanding of the simulation capabilities of the in-vessel behavior in the lower plenum numerical simulations have been devoted to melt pool convection and heat transfer using various methods such as various turbulence models including Reynolds Averaged Navier-Stokes (RANS) and Large Eddy Simulation (LES), effective convectivity model and lumped-parameter approach.

The failure of the RPV lower head due to corium attack during a severe accident is the transition point from in-vessel to ex-vessel progression of accident. For this reason it has been a focus area for APRI research during APRI-10 and APRI-11. The vessel failure analyses require the thermal load of corium relocated in the lower head. In the APRI-11 research the simulations of the MELCOR code for severe accident scenarios is chosen to provide relevant information. The structural mechanical analysis has been performed with ANSYS and the results have been compared with MELCOR analysis without coupling using MELCOR mechanical models. The results demonstrates that the stress failure mechanism, rather than the strain failure and melt-through failure criteria, is the dominant failure mechanism in the ANSYS analysis for both the SBO and SBO+LOCA scenarios and the MELCOR simulation have a reasonable agreement with the results obtained from ANSYS simulation. Furthermore, the failure mechanism in the MELCOR simulations is also identified as stress-based, consistent with the findings from the structural analysis.

To study the ex-vessel phenomena and Fuel-Coolant Interaction KTH have performed an experiments in the DEFOR and MISTEE facilities. Specifically, the study during APRI-11 is oriented to metallic melt-coolant interactions in DEFOR as well as single droplet quench and steam explosion in chemical solutions in MISTEE. Regarding the experiments in DEFOR with metallic melt, it is observed that metallic melt with higher melting point at the same superheat results in stronger heat transfer with water and an enhanced fragmentation, while all the other metallic melt tests experience a rapid solidification process, resulting in incomplete breakup of the melt jet, i.e., so-called “frozen jet”. On the

other hand, the oxidic melt with a high melting point has less potential of solidification before jet breakup and fine fragmentation. The distinction may be attributed to different heat transfer modes and physical properties such as the ductility and the shear strength between oxidic melt and metallic melt.

Earlier studies on ex-vessel steam explosion and debris coolability were based on an assumption that a coherent melt jet falls from the lower head of the RPV into a deep-water pool in a severe accident scenario of a reference Nordic BWR. This is a simplified assumption and in the ambition to include the impact of the structures under the reactor vessel in a reference Nordic BWR on the release of melt from the reactor vessel, a decided research task at KTH to this topic was initiated in APRI-11. The initial effort has been focused on a literature review and it was found that BWR ex-vessel structures had been simplified as a combination of horizontal and vertical structures in a few previous considerations. Three phenomena of interest have been selected for further studies: splashing of melt, ablation of structure caused by melt impingement and melt freezing.

Yet another research task at KTH in APRI-11 was dedicated to applied reactor safety analysis. This is motivated by an effort to consolidate the severe accident research into reactor safety. KTH have used MELCOR for severe accident analysis and compared the results with MELCOR coupled with the COCOMO-code. COCOMO is a mechanistic code and in this context used to simulate ex-vessel cooling of core debris in lower dry well. Based on the models in the COCOMO code KTH has also developed surrogate models using machine learning, since the computation time of COCOMO is considerable. Two surrogate models have been developed and coupled with MELCOR to realize quick estimations of the quench process of ex-vessel 1D and 2D debris beds. Compared with MELCOR standalone, both coupled simulations of MELCOR/ COCOMO and MELCOR/SM predict earlier pool saturation and containment venting.

The Chalmers research was concentrated on investigating the formation and persistence of organic tellurides, particularly dimethyl telluride (DMT), under accident conditions. In total, four different studies were done. The first study explored the potential formation of organic tellurides in nuclear accident scenarios, focusing on interactions between tellurium and paint solvents. Using gas chromatography mass spectrometry, volatile tellurium compounds were identified in samples with texanol and MIBK solvents. Diisopropyl telluride was predominant in texanol samples, while MIBK samples showed signs of methyl-isobutyl-telluride formation. Additionally, a telluride resembling DMT was detected. The findings suggest that under simulated accident conditions, organic tellurides can indeed form from paint solvents. This underscores the importance of understanding and monitoring such reactions for nuclear safety assessments.

The second study explored the radiolytic degradation of DMT under conditions resembling a severe nuclear accident. DMT stability was assessed in aerated and deaerated water, borate buffer, and sodium thiosulfate solutions. Results, obtained through ICP-MS and GC-MS analyses, indicate DMT's relative stability in these conditions. In aerated water, degradation followed zero-order kinetics, while in deaerated water, degradation was slower. Unexpectedly, rapid degradation occurred in sodium thiosulfate solution, possibly linked to complex thiosulfate ion radiolysis. Additionally, new, higher mass organic species formed, indicating dimerization and chain lengthening reactions. Overall, DMT appears stable in simulated accident scenarios, influenced by competing species and oxygen presence.

The third study investigated gas-phase interactions between tellurium and organic materials under severe accident-like conditions. Tellurium's volatility is influenced by the pres-

ence of organic substances. Experiments, conducted with different atmospheres and organic components, revealed that the addition of organics increases tellurium volatility in both inert and reducing atmospheres. However, in an oxidizing atmosphere, tellurium dioxide formed, reducing its volatility. Mass concentration measurements suggested that organic tellurides may form, impacting gas-phase behavior. While not conclusively proven, strong indications suggest increased tellurium volatility in the presence of organic substances, emphasizing the complex interactions between tellurium and organics in severe accident scenarios.

The final study explored the retention of DMT by activated carbon filters. These filters, sourced from respirators and a nuclear power plant, are commonly used in nuclear settings. While such filters have proven effective against various radioactive compounds, their efficacy against organic tellurides, particularly DMT, remains untested. The experiment involved injecting DMT into a glass tube with activated carbon pads, assessing leaching efficiency and tellurium recovery. Results indicate varying efficiency among carbon types. The study underscores the importance of further research to understand the adsorption mechanism of organic tellurides on activated carbon.

KTH Department of Nuclear Engineering has participated as analytical support to parts of the THEMIS project and contributed to the analysis of the experiments performed in the "pool scrubbing" series of experiments, which concern studies of effects that affect the retention of fission products in water pools when gas bubbles pass through the water volume. The experiments mimic scenarios where steam or gas mixtures are blown into an aqueous phase, e.g. in a condensation basin or a scrubber. KTH has shown a good ability to carry out analytical calculation work that provides both a qualitative and quantitative understanding of the phenomena that are central to such a course of events. This applies to both transport processes in droplet and liquid phases and the behavior of particles in solution and in contact with surfaces as well as the identification of other modeling aspects that need to be handled to create a description of a complex process with many parameters that vary. KTH's contribution to THEMIS was highly appreciated by the project participants in the analytical working group. KTH participated with presentations of calculations performed with the code GOTHIC that simulated the outcome of several of the experiments. KTH also participated in exercises that included so-called blind tests where the participants calculate the outcome in advance only based on the information given about the experimental parameters before the experiment was performed. Different types of analytical exercises allow participants to exchange experiences on modeling work and to compare the performance of different codes in describing different phenomena and events. Active participation in international research contexts is therefore an important activity that promotes learning, knowledge exchange and development of the understanding of different accident phenomena.

## **7.2. Recommendations and Outlook**

The recent focus of APRI-11 research at KTH-NPS has been oriented to four topical areas: (i) in-vessel remelting dynamics of multi-composition debris bed in the lower head, (ii) lower head failure mode and rupture dynamics, (iii) debris formation due to metallic melt-coolant interactions, and (iv) ex-vessel melt-structure interactions. The items (i), (ii) and (iv) are crucial to quantify the characteristics of corium melt which arrives at the water pool in the reactor cavity, while the item (iii) is a remaining issue from the previous DEFOR studies. The melt ejection characteristics after vessel failure are the limiting conditions for ex-vessel debris bed coolability and steam explosions energetics. Therefore, it is recommended for the next APRI program to continue the research activities which have

been identified as priority during APRI-11, i.e. the work in APRI-12 should address the unsolved problems and remaining issues of the above four topical areas as exemplified below.

#### *In-vessel debris behavior*

- The SIMECO-2 facility has been proven to be capable of investigating debris bed dryout and remelting in the pilot test carried out during APRI-11. More tests should be carried out, including dryout and melting of various debris beds, melting of multi components in debris beds, and forming of stratified molten pool behavior.
- The previous MRSPOD tests were carried out at a relatively low temperature (<300°C) using eutectic Sn–Bi melt whose melting point is 139°C. The data for higher temperatures is missing. Tests with higher melting-point materials so as to reduce the gap between prototypical materials and simulants in the experiment should be carried out.
- The MPS code developed during APRI-11 has been limited to melt-infiltration problems in small scales due to high demand on computational resources. Both micro- and macro-scale models of melt infiltration using COMSOL are still under refining and validation. Therefore, improvement or new development of models and simulation capabilities (tools) should be continued for either understanding of debris remelting mechanisms or analyses of reactor cases. The goal is to have mechanistic models/tools for predicting corium debris evolution in the lower head, and consequently obtaining the corium's state and dynamic loads (both thermal and mechanical) on the lower head.

#### *Vessel failure modes*

- More representative penetrations (control rod guide tubes, or both CRGT and IGT) of the lower head should be considered.
- Penetration failure evolution (e.g. ablation dynamics) which has not been touched in the previous APRI-studies, since this is beyond the capabilities of the thermomechanical approach developed in previous works. A new approach is needed to predict the dynamics of penetration failures, which calls for a coupling between fluid and structural mechanics.

#### *Melt-coolant interactions*

- For the metallic melt-coolant interactions, the experimental data using Sn, Zn and binary alloy of Sn-Bi reveal some key phenomena which are different from those of oxidic melt, can be used for validation of relevant models given the known properties and well-defined test conditions. However, it is still an open question how the real metals (Zr/Fe) in corium affect the results. In particular, the oxidation of Zr/Fe and the hydrogen generation during melt-coolant interactions were reproduced in the previous tests. Thus, more experimental studies (e.g., using simulant materials with melting points close to prototypical materials) will help to narrow down the property gap of materials. Additional studies should be paid to development of models/codes which can be applied to reactor case studies.
- For the MISTEE experiment, much efforts have been spent to characterize single molten drop steam explosion. Limitation in previous studies are the use of simulant metals instead of Zr/Fe found in corium as well as the study of single drops. Hence, studies using Zr/Fe and a small melt jet rather than single drop are necessary in the future work, with upgrades of the MISTEE facility in furnace for melting Zr/Fe and

in instrumentation for synchronizing photography and radiography is recommended.

#### Ex-vessel melt-structure interactions

It is recommended to continue the research plan elaborated in APRI-11 into the APRI-12 project.

A scaled-down structure representing the radiation shield and a unit of CRGTs and IGTs can be adopted as a test section in the DEFOR study. Melt impingement and splashing on the radiation shield as well freezing on CRGTs and IGTs can be investigated on the CoS-MUS at KTH-NPS. The analytical study will be realized through both mechanistic and parametric approaches. The mechanistic modelling of melt-structure interaction can capitalize on the development in other topical areas, such as the MPS and COMSOL models.

- In addition to the research activities in the above four topical areas, it is instrumental to apply the research outcomes (e.g., models, computer codes, methodologies) to the Swedish nuclear power safety context whenever the outcomes are applicable. Such reactor application (or case study) had been conducted in previous APRI-research and should be continued in the future APRI-research, since the ultimate goal is to resolve the severe accident issues associated with the SAM measures of Swedish NPPs, as reiterated in KTH-NPS proposals to APRI. Thus, reactor application study and safety analysis are the living cases which will be advanced and updated with new knowledge and modeling capabilities acquired in the future activities.

Considering the source term related studies performed in Chalmers during earlier APRI programs it is recommended that Chalmers during APRI-12 investigate the interactions between tellurium and iodine in the containment sump to assess tellurium's ability to oxidize iodide to molecular iodine, impacting the iodine source term. Also, building on the APRI-11 research with organic tellurides, questions arose about the formation of organic species when tellurium, iodine, and organics coexist. Continued research will therefore examine a simplified system under various conditions to determine if one type of organic species consistently dominates, supported by theoretical analysis. In addition, a study will be done examining tellurium interactions with epsilon particles in spent fuel, with the focus to explore potential tellurium retention.

Finally, it is recommended that Chalmers during APRI-12 start examining the mechanisms behind the leaching process of a cooled and solidified core melt. The stability of fission products together with actinides and lanthanides in the corium is crucial, since leaching of radioactive materials from the corium might represent a considerable contribution to the source term. Building on their long history of performing leaching experiments for the Swedish long-term repository, Chalmers will manufacture simulant fuels and study the processes that influence the leaching behavior from such fuels under controlled conditions.



## 8. Abbreviation list

ARC-F	Analysis of Information from Reactor Buildings and Containment Vessels of Fukushima Daiichi Nuclear Power Station
ANN	Artificial Neural Network
APRI	Accident Phenomena of Risk Importance
ATF	Accident Tolerant Fuel
BALI	Bassin d'Analyse des LIquides (CEA test facility)
BIP	Behavior of Iodine Project
BSAF	Benchmark Study of the Accident at the Fukushima Daiichi Nuclear Power Station
BWR	Boiling Water Reactor
CFD	Computational Fluid Dynamics
CHF	Critical Heat Flux
COCOMO	Corium Coolability Model
CPC	Condensation Particle Counter
CRD	Control Rod Drive
CRGT	Control Rod Guide Tube
CSARP	Cooperative Severe Accident Research Program
CTH	Chalmers Tekniska Högskola
DCH	Direct Containment Heating
DEFOR	Debris Bed Formation
DF	Decontamination Factor
DHF	Dryout Heat Flux
DMA	Differential Mobility Analyzer
DMT	DiMethyl Telluride
DNS	Direct Numerical Simulation
EC	European Commission
ELPI	Electric Low-Pressure Impactor
ENSI	Eidgenössische Nuklearsicherheitsinspektorat (Swiss Federal Nuclear Safety Inspectorate)

ERMSAR	European Review Meetings on Severe Accident Research
FACE	Fukushima Daiichi Nuclear Power Station Accident Information Collection and Evaluation
FBG	Fiber Bragg Grating
FCI	Fuel-Coolant Interaction
FM	Full Model
FP	Fission Products
FTIR	Fourier-Transform InfraRed spectroscopy
GC-MS	Gas Chromatography – Mass Spectroscopy
GOTHIC	Generation of Thermal–Hydraulic Information for Containments
GSD	Gross Size Distribution
IGT	Instrumentation Guide Tube
IH	Internally Heated
IRSN	Institut de Radioprotection et de Sûrité Nucléaire
IVR	In-Vessel Retention
KTH	Kungliga Tekniska Högskolan/Royal Institute of Technology
LES	Large Eddy Simulation
LOCA	Loss Of Coolant Accident
LWR	Light Water Reactor
MCCI	Melt Corium Concrete Interaction
MELCOR	code for integral simulation of severe accident developed by Sandia National Labs on the mission from USNRC
MIBK	Methyl Isobutyl Ketone
MISTEE	Micro Interactions of Steam Explosion Energetics
MMD	Median Mass Distribution
MPS	Moving Particle Semi-implicit
MRSPOD	Multicomponent Remelting, relocation, and Solidification in Porous Debris
MSWI	Melt Structure Water Interactions
NC	Nuclear Chemistry
NE	Nuclear Engineering



NEA	Nuclear Energy Agency
NCG	Non-Condensable Gas
NPP	Nuclear Power Plant
NPS	Nuclear Power Safety
NRC	Nuclear Regulatory Commission
OECD	Organisation for Economic Co-operation and Development
PAD	Parallel Attachable Drum
PDB	PulverDispergierer mit Bürste
POMECO	Porous Media Coolability
PreADES	Preparatory Study on Analysis of Fuel Debris
PS	Pool Scrubbing
PSA/PRA	Probabilistic Safety Assessment/Probabilistic Risk Assessment
PULiMS	Pouring and Underwater Liquid Melt Spreading
PWR	Pressurized Water Reactor
RANS	Reynolds Averaged Navier-Stokes
RB	Rayleigh-Bénard
REMCOD	Remelting of Multi-Component Debris – Structure Interactions
ROAAM	Risk Oriented Accident Analysis Methodology
ROSAU	Reduction of Severe Accident Uncertainties
RPV	Reactor Pressure Vessel
SA	Severe Accident
SAM	Severe Accident Management
SAMG	Severe Accident Management Guidelines
SBO	Station Blackout
SE	Separate Effect
SEM-EDX	Single Electron Miscroscopy – Energy Dispersive X-ray spectroscopy
SGTR	Steam Generator Tube Rupture
SIMECO	Simulation of In-vessel MElt COolability

SM	Surrogate Model
SS	Stainless Steel
TEOM	Tapered Element Oscillating Microbalance
TGA	Thermo Gravimetric Analysis
THAI	Thermal-hydraulics, Hydrogen, Aerosols and Iodine
THEMIS	THAI Experiments on Mitigation measures, and source term issues to support analysis and further Improvement of Severe accident management measures
TLOFW	Total Loss Of Feed Water
TVV	THAI Test Vessel
URF	Unacceptable Release Frequency
VTT	Valtion Teknillinen Tutkimuskeskus (Technical Research Centre of Finland)
XPS	X-ray Photoelectron Spectroscopy



The Swedish Radiation Safety Authority (SSM) works proactively and preventively with nuclear safety, radiation protection, nuclear security, and nuclear non-proliferation to protect people and the environment from the harmful effects of radiation, now and in the future.

You can download our publications from [www.stralsakerhetsmyndigheten.se/en/publications](http://www.stralsakerhetsmyndigheten.se/en/publications). If you need alternative formats such as easy-to-read, Braille or Daisy, contact us by email at [registrator@ssm.se](mailto:registrator@ssm.se).

**Strålsäkerhetsmyndigheten**  
SE-171 16 Stockholm  
+46 (0) 8-799 40 00  
[www.stralsakerhetsmyndigheten.se](http://www.stralsakerhetsmyndigheten.se)  
[registrator@ssm.se](mailto:registrator@ssm.se)

©Strålsäkerhetsmyndigheten